

# Mechanical analysis of aortic aneurysms using 3D ultrasound : towards patient-specific risk assessment

**Citation for published version (APA):**

van Disseldorp, E. M. J. (2019). *Mechanical analysis of aortic aneurysms using 3D ultrasound : towards patient-specific risk assessment*. [Phd Thesis 1 (Research TU/e / Graduation TU/e), Biomedical Engineering]. Technische Universiteit Eindhoven.

**Document status and date:**

Published: 10/01/2019

**Document Version:**

Publisher's PDF, also known as Version of Record (includes final page, issue and volume numbers)

**Please check the document version of this publication:**

- A submitted manuscript is the version of the article upon submission and before peer-review. There can be important differences between the submitted version and the official published version of record. People interested in the research are advised to contact the author for the final version of the publication, or visit the DOI to the publisher's website.
- The final author version and the galley proof are versions of the publication after peer review.
- The final published version features the final layout of the paper including the volume, issue and page numbers.

[Link to publication](#)

**General rights**

Copyright and moral rights for the publications made accessible in the public portal are retained by the authors and/or other copyright owners and it is a condition of accessing publications that users recognise and abide by the legal requirements associated with these rights.

- Users may download and print one copy of any publication from the public portal for the purpose of private study or research.
- You may not further distribute the material or use it for any profit-making activity or commercial gain
- You may freely distribute the URL identifying the publication in the public portal.

If the publication is distributed under the terms of Article 25fa of the Dutch Copyright Act, indicated by the "Taverne" license above, please follow below link for the End User Agreement:

[www.tue.nl/taverne](http://www.tue.nl/taverne)

**Take down policy**

If you believe that this document breaches copyright please contact us at:

[openaccess@tue.nl](mailto:openaccess@tue.nl)

providing details and we will investigate your claim.

# MECHANICAL ANALYSIS OF AORTIC ANEURYSMS USING 3D ULTRASOUND

Towards patient-specific risk assessment

EMIEL VAN DISSELDORP

The image features a detailed anatomical illustration of the human aorta, showing its branching into the subclavian, carotid, and iliac arteries. The aorta is depicted in shades of red and blue. Overlaid on the abdominal aorta is a complex mechanical analysis, represented by a grid of red and white lines, suggesting stress or strain distribution. The background is a light, textured grey with faint, wavy lines on the left side, and a faint illustration of a hand holding a probe on the right side, indicating the use of 3D ultrasound technology.



# MECHANICAL ANALYSIS OF AORTIC ANEURYSMS USING 3D ULTRASOUND

Towards patient-specific risk assessment

A catalogue record is available from the Eindhoven University of Technology Library

ISBN: 978-90-386-4662-6

©Copyright 2018, Emiel M.J. van Disseldorp

All rights reserved. No part of this book may be reproduced, stored in a database or retrieval system, or published, in any form or in any way, electronically, mechanically, by print, photo print, microfilm or any other means without prior written permission of the author.

Cover design: Wendy Schoneveld || [www.wenziD.nl](http://www.wenziD.nl)

Printed: Proefschrift Maken || [www.proefschriftmaken.nl](http://www.proefschriftmaken.nl)

The research presented in this thesis was supported by an unrestricted educational research grant by the Dutch "Lijf en Leven" Foundation.

The publication of this thesis is financially supported by Stichting Lijf en Leven, Stichting Chirurgische Innovatie Eindhoven, Catharina Hospital Eindhoven, Chipsoft, and Rabobank Eindhoven-Veldhoven. Financial support by the Dutch Heart Foundation for the publication of this thesis is gratefully acknowledged.

The front cover is an artist impression of an abdominal aortic aneurysm and does not cover all anatomical details.

# MECHANICAL ANALYSIS OF AORTIC ANEURYSMS USING 3D ULTRASOUND

Towards patient-specific risk assessment

PROEFSCHRIFT

ter verkrijging van de graad van doctor aan de Technische Universiteit Eindhoven, op gezag van de rector magnificus prof.dr.ir. F.P.T. Baaijens, voor een commissie aangewezen door het College voor Promoties, in het openbaar te verdedigen op donderdag 10 januari 2019 om 16:00 uur

door

Emanuel Marinus Josephus van Disseldorp

Geboren op 8 juli 1990  
te Tilburg

Dit proefschrift is goedgekeurd door de promotoren en de samenstelling van de promotiecommissie is als volgt:

voorzitter: prof. dr. P.A.J. Hilbers  
1e promotor: prof. dr. M.R.H.M. van Sambeek  
2e promotor: prof. dr. ir. F.N. van de Vosse  
co-promotor: dr. ir. R.G.P. Lopata  
leden: prof. dr. T.C. Gasser (KTH Stockholm, Sweden)  
prof. dr. ir. P. Segers (Ghent University, Belgium)  
prof. dr. J.D. Blankensteijn (VUmc Amsterdam)  
prof. dr. ir. M.G.D. Geers

Het onderzoek dat in dit proefschrift wordt beschreven is uitgevoerd in overeenstemming met de TU/e Gedragscode Wetenschapsbeoefening.

# Table of Contents

<b>Summary</b>	<b>5</b>
<b>1 General Introduction</b>	<b>9</b>
1.1 Aortic aneurysms . . . . .	10
1.2 Aneurysm repair . . . . .	11
1.3 Current clinical guidelines . . . . .	12
1.4 Alternative rupture risk estimators . . . . .	13
1.4.1 Aortic volume quantification . . . . .	13
1.4.2 Wall stress analysis . . . . .	14
1.4.3 Aortic stiffness quantification . . . . .	16
1.4.4 Experimental tissue characterization . . . . .	19
1.5 Current clinical need . . . . .	20
1.6 Aim and outline of this thesis . . . . .	20
<b>2 The influence of limited field-of-view on wall stress analysis in abdominal aortic aneurysms</b>	<b>23</b>
2.1 Introduction . . . . .	25
2.2 Materials and Methods . . . . .	26
2.3 Results . . . . .	29
2.4 Discussion . . . . .	34
2.5 Conclusion . . . . .	36
<b>3 Patient-Specific wall stress analysis and mechanical characterization of abdominal aortic aneurysms using 4D Ultrasound</b>	<b>37</b>
3.1 Introduction . . . . .	39
3.2 Materials and Methods . . . . .	40
3.3 Results . . . . .	45
3.4 Discussion . . . . .	48
3.5 Conclusion . . . . .	49



<b>4</b>	<b>Quantification of Aortic Stiffness and Wall Stress in Healthy Volunteers and Abdominal Aortic Aneurysm Patients using Time-Resolved 3D Ultrasound: a Comparison Study</b>	<b>51</b>
4.1	Introduction . . . . .	53
4.2	Materials and Methods . . . . .	54
4.3	Results . . . . .	57
4.4	Discussion . . . . .	60
4.5	Conclusion . . . . .	63
<b>5</b>	<b>Wall Stress Analysis using Multi-Perspective 3D Ultrasound Imaging of Abdominal Aortic Aneurysms</b>	<b>65</b>
5.1	Introduction . . . . .	67
5.2	Materials and Methods . . . . .	69
5.3	Results . . . . .	74
5.4	Discussion . . . . .	79
5.5	Conclusion . . . . .	81
<b>6</b>	<b>A Longitudinal study on the Biomechanical properties of Abdominal Aortic Aneurysms and their Relation to AAA Growth</b>	<b>83</b>
6.1	Introduction . . . . .	85
6.2	Materials and Methods . . . . .	87
6.3	Results . . . . .	91
6.4	Discussion . . . . .	96
6.5	Conclusion . . . . .	98
<b>7</b>	<b>Reproducibility Assessment of US-Based Aortic Stiffness Quantification and Verification using Bi-axial Tensile Testing</b>	<b>99</b>
7.1	Introduction . . . . .	101
7.2	Materials and Methods . . . . .	102
7.3	Results . . . . .	111
7.4	Discussion . . . . .	115
7.5	Conclusion . . . . .	118
<b>8</b>	<b>Mechanical Characterization of Thoracic Aortic Aneurysms using 4D Ultrasound: In Vivo Findings and In Vitro Verification</b>	<b>119</b>
8.1	Introduction . . . . .	121
8.2	Materials and Methods . . . . .	123
8.3	Results . . . . .	132
8.4	Discussion . . . . .	134
8.5	Conclusion . . . . .	137

<b>9 General Discussion</b>	<b>139</b>
9.1 Motivation and main findings . . . . .	140
9.2 From evidence based to personalized medicine . . . . .	141
9.3 Limitations . . . . .	145
9.4 Future model developments . . . . .	147
9.5 Clinical perspective . . . . .	148
9.6 General conclusion . . . . .	149
<b>Bibliography</b>	<b>151</b>
<b>Dankwoord</b>	<b>169</b>
<b>Curriculum vitae</b>	<b>173</b>
<b>List of publications</b>	<b>175</b>



# Summary

## **Mechanical analysis of aortic aneurysms using 3D ultrasound: towards patient-specific risk assessment**

An abdominal aortic aneurysm (AAA) is a progressive, irreversible dilatation of the aorta with a maximum diameter of 3 cm or larger. Most AAAs are asymptomatic until rupture, which result in a life-threatening hemorrhage in 80% of all cases. Therefore, according to current clinical guidelines, surgery is recommended when the risk of rupture outweighs the risk of intervention. Large population-based studies have suggested to intervene when the maximum diameter reaches 5.5 cm, or when it grows more than 1 cm/year. Unfortunately, these thresholds do not always apply for the individual patient, since 2 – 10% of all AAAs rupture before these thresholds are reached, whereas approximately 25% of all large, but stable AAAs are currently exposed to (yet) unnecessary surgical risks due to overtreatment. Hence, a personalized approach is required.

From a biomechanical perspective, AAA wall mechanics (wall stresses, strains) and tissue properties will play an important role in growth and rupture, and may be able to distinguish between stable and more susceptible aneurysms. Model-based wall stress analysis has been introduced and successfully performed in the last two decades using finite element analysis (FEA). The method revealed that ruptured and symptomatic aneurysms have an increased peak wall stress compared to non-ruptured AAAs, indicating that peak wall stress might be a relevant criterion for patient-specific risk stratification. Despite promising results, wall stress analysis has not yet been clinically accepted. The main drawback is the use of Computed Tomography (CT) imaging for geometry assessment which suffers from exposure to radiation and nephrotoxic contrast agents, rendering the current method unsuitable for prospective, clinical validation studies.

Recently, time-resolved 3D ultrasound (4D US) had been clinically introduced, which provides multiple 3D US volumes over the cardiac cycle. AAA geometry assessment based on 4D US might be a good alternative for wall stress analysis, due to its non-invasive and harmless character. In addition, using the temporal information in the 4D US data, the arterial stiffness could be assessed simultaneously. Therefore, the aim of this thesis was to develop and verify a biomechanical model to predict the mechanical behavior of the

patient-specific AAA wall using non-invasive, 4D ultrasound imaging.

However, the use of 4D US has its limitations in terms of image quality and field-of-view, which might hinder adequate wall stress analysis. Therefore, the influence of the restricted US field-of-view on patient-specific wall stress prediction was examined in **Chapter 2**. The shoulder of the AAA revealed to be crucial for adequate wall stress analysis, and as long as these areas were in the field-of-view, US based FEA can be performed.

Afterwards, a first feasibility study was performed in **Chapter 3**, and the patient-specific stiffness of, and peak wall stresses in the aortic wall were assessed for AAA patients with a wide range of diameters. It showed that, although 4D US has a limited contrast, 4D US is applicable for AAA wall stress analysis. Moreover, verification with CT imaging revealed that US-based results were in agreement. However, to prove the clinical merit of this biomechanical model, the method should be able to distinguish between healthy and diseased arterial tissue. Therefore, the aortic stiffness and peak wall stress (PWS) of AAAs were characterized and compared with young, and age-matched healthy individuals (**Chapter 4**). Additionally, different degrees of the AAA pathology were investigated and its effect on the mechanical parameters were examined.

The study revealed significant differences in PWS and arterial stiffness between age-matched volunteers and AAA patients. Furthermore, a significant increase in aortic stiffness was measured between the age-matched volunteers and the relatively small (diameter: 30 - 39 mm) AAA patients. This suggests that the AAA pathology causes an early and significant increase in stiffness of the aorta, which further increases when the AAA wall deteriorates. This study well demonstrated the advantages of ultrasound, now including patients with diameters that would rarely be imaged with CT.

Hence, assessment of biomechanical markers might provide the physician with additional measures to estimate the state of the aortic wall. However, to perform this mechanical characterization on a large scale in a longitudinal study, automatic segmentation of the AAA geometry is required to make the pipeline more robust and less labor intensive. In **Chapter 5**, this segmentation method was developed together with a registration algorithm to merge multiple 3D US volumes to enlarge the field-of-view for AAAs with a large longitudinal length. Again, verification using CT imaging was performed.

Finally, a longitudinal follow-up study was performed in **Chapter 6**, in which the mechanical properties of the aneurysm region of 70 AAA patients were followed over a median period of 24 months, with regular follow-up intervals. Results revealed that rapidly growing AAAs have a lower aortic stiffness before AAA growth is observed, compared to stable and slow growing AAAs. Consequently, changes in arterial stiffness might have a relation with upcoming growth, which require further investigation.

In the last two chapters of this thesis, verification experiments of the arterial stiffness were performed in an experimental approach using porcine aortas, and for abdominal aneurysms after open surgery (**Chapter 7**), and in a side study for ascending thoracic aneurysms (**Chapter 8**). Furthermore, reproducibility of stiffness measurement was as-

sessed for both the *in vivo* and *ex vivo* characterization methods, and revealing overall high reproducibility.

In summary, an automatic, US-based, biomechanical modeling method was developed to assess the patient-specific aortic stiffness and wall stress distribution in the individual patient over time. The first steps towards clinical applicability have been made in thesis, and results suggest that the aortic stiffness might have diagnostic value to detect aneurysms in an early stage, and could possibly be related with upcoming growth of the aneurysms. However, further research is needed to strengthen these findings.



CHAPTER **1**

**General Introduction**



## 1.1 Aortic aneurysms

An aortic aneurysm is a localized widening of the aorta. The aorta is considered aneurysmatic, if the diameter exceeds 30 mm, or when it is 150% of the normal diameter (Moll et al., 2011). However, the size of the aorta may vary according to age, gender, body size, and the location of the aneurysm (Johnston et al., 1991). Aneurysms can occur in the complete arterial tree, although the most common site is in the abdominal aorta (Figure 1.1), known as an abdominal aortic aneurysm (AAA). Large population-based screening studies showed that the prevalence of AAAs in adults above 55 years old is 4.0 - 8.9 % in men, 0.7 - 2.2 % in women, and increases with age (Scott et al., 1995; Pleumeekers et al., 1995; Singh et al., 2001; Ashton et al., 2002). In addition to the male gender and aging, other well-known risk factors for the development of an AAA are smoking, hypertension, atherosclerosis, and a positive family history of AAA (Lederle et al., 1997; Sidloff et al., 2014).

Aortic aneurysms are generally asymptomatic, until dissection or rupture of the aortic wall occurs. A ruptured AAA results in a large, life-threatening haemorrhage, which is associated with an overall mortality rate of approximately 80%. A decline in mortality was observed over time in the subsequent years. Before 1990, the total mortality rate of ruptured AAAs was 86%, compared to 74% reported in retrospective studies since 1990 (Reimerink et al., 2013).

A ruptured AAA typically presents itself with sudden severe back or abdominal pain, a pulsating mass near the navel, and hemodynamic shock. Without clinical intervention, a ruptured AAA invariably results in death. Therefore, patients with known AAA who present with aforementioned symptoms should be referred urgently to the hospital for immediate control and repair of the aneurysm (Moll et al., 2011).

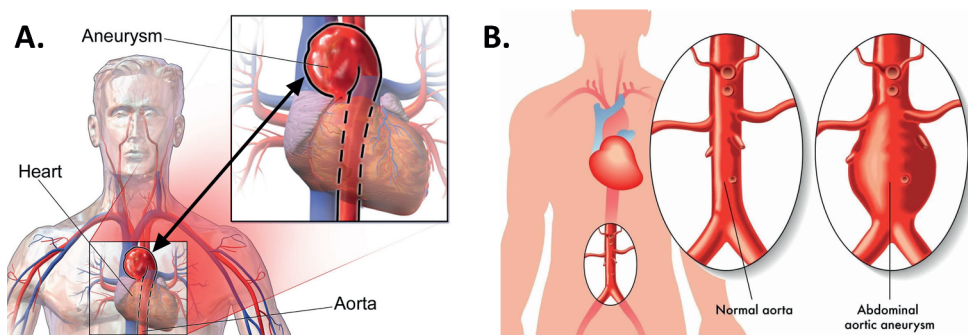


**Figure 1.1:** Graphical visualization of the two types of aortic aneurysms discussed in this thesis: **A.** ascending thoracic aortic aneurysm (Chapter 8) and **B.** abdominal aortic aneurysm (Chapters 1 - 7). Both figures adopted from [healthjade.com/aortic-aneurysm](http://healthjade.com/aortic-aneurysm).

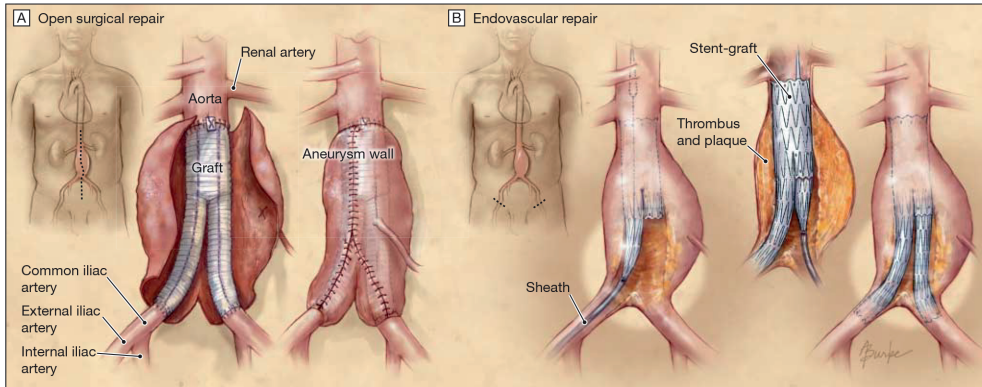


**Figure 1.2:** Two types of surgical repair of abdominal aortic aneurysms (AAAs). **A.** Open surgical repair: the abdomen and the aneurysm sac is opened anteriorly and a prosthetic graft is sutured in place. **B.** Endovascular repair: guidewires with catheter are introduced through the common femoral arteries over which a stent-graft is introduced. The stent-graft will subsequently be deployed over the aneurysmatic part of the abdominal aorta. Figure adopted from Schermerhorn (2009).

## 1.2 Aneurysm repair

In terms of treatments, two types of AAA repair are currently available: open aneurysm repair and endovascular aneurysm repair. Both methods are visualized in Figure 1.2. Open aneurysm repair is the conventional method, introduced by Dubost et al. (1952), where (using laparotomy) a tube or bifurcated prosthetic graft is sutured in the aneurysmatic part of the abdominal aorta. Open aneurysm repair is a durable solution for the management of AAAs. However, open repair involves clamping of the aorta and is regularly accompanied by substantial blood loss. As a consequence, open aortic repair is still associated with a 30-day operative mortality rate of 3.0 - 4.7% (Prinssen et al., 2004; Greenhalgh et al., 2004; Lederle et al., 2009).

As an alternative, endovascular aneurysm repair (EVAR) was first suggested by Volodos et al. (1991) and Parodi et al. (1991). During this minimal invasive approach, a small access is made in the patient's femoral arteries, through which the guidewires with catheter and the stent-graft are introduced. Under fluoroscopic guidance, the stent-graft is deployed in the dilated section of the aorta, excluding the aneurysm sac from circulation. Nowadays, EVAR is the most common procedure for treating AAAs. This is mainly due to its minimal invasive character combined with a lower 30-day mortality rate of approximately 0.5 - 1.8% (Prinssen et al., 2004; Greenhalgh et al., 2004; Lederle et al., 2009).

However, in the study by Blankensteijn et al. (2005) and later in the studies by De Bruin et al. (2010) and The United Kingdom EVAR Trial Investigators (2010) it was shown that the peri-operative survival advantage of EVAR was not sustained in the long-term. This was due to the need of secondary interventions, and endoleakage of the stent-graft which resulted

in a continued risk of aneurysm rupture. As a consequence, long-term and adequate follow-up is required for all patients treated with EVAR.

### 1.3 Current clinical guidelines

Clinical intervention for AAA patients without symptoms is recommended when the risk of rupture outweighs the risk of surgical intervention. Therefore, according to current clinical guidelines, surgery is recommended when **1)** the maximum diameter reaches 5.5 cm for men or 5.2 cm for women, **2)** when it has grown more than 1 cm/year, or **3)** when the aneurysm becomes symptomatic (Moll et al., 2011; Chaikof et al., 2018).

Current guidelines are based on necropsy and clinical studies which have shown that the risk of rupture accelerated with increasing aortic diameter (Darling, 1970; Scott et al., 1998; Lederle et al., 2002a). These studies showed that AAAs with a maximum diameter larger than 6.0 cm had a yearly rupture risk of at least 10%. Therefore, for these AAAs patients, surgical intervention is recommended. However, for AAA patients with a diameter range between 4.0 and 5.5 cm it was unclear if early surgery would be beneficial for long-term survival. Therefore, the UK Small Aneurysm Trial (The UK Small Aneurysm Trial Participants, 1998) and the American Aneurysm Detection And Management study (Lederle et al., 2002b) were conducted, and these two multi-centre randomized controlled trials showed that for AAA patients with a maximum aortic diameter up to 5.5 cm ultrasonic surveillance was safe, and early surgery did not provide a long-term survival advantage (Figure 1.3).

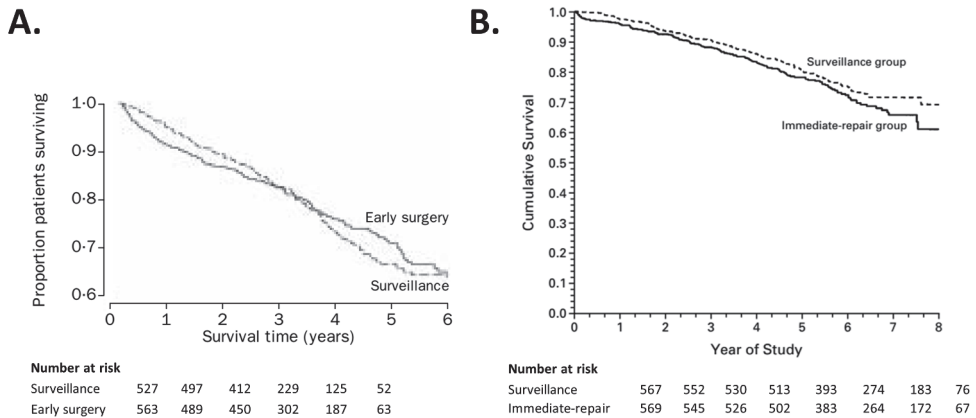


**Figure 1.3:** Kaplan-Meier curves of the overall survival by the surveillance and early surgery group in the UK Small Aneurysm Trial (A) and the American Aneurysm Detection And Management study (B). Both Kaplan-Meier estimates did not show a significant difference on the long-term. Figure adopted from The UK Small Aneurysm Trial Participants (1998) and Lederle et al. (2002b).

As a consequence of current AAA guidelines, small aneurysms prone for rupture are left untreated despite the fact that 2 – 10% of all AAAs rupture before the threshold of 5.5 cm is reached (Reed et al., 1997; Nicholls et al., 1998; Scott et al., 1998). On the other hand, some large AAAs have been known to remain stable above the current threshold and might be exposed to unnecessary surgical risks due to over-treatment (Darling et al., 1977; Conway et al., 2001; Lederle et al., 2002a). Hence, these data suggest that the maximum diameter alone is not sufficient to predict the patient-specific rupture risk of an AAA. Therefore, a more patient-specific approach is required.

## 1.4 Alternative rupture risk estimators

As an alternative, or addition to current AAA rupture risk assessment, several other methods have been proposed over the last decades. In literature, most studies focus on aortic volume measurements, (peak) wall stress analysis, and aortic stiffness quantification. The current status of these alternative or additional methods will be addressed in the following sections:

### 1.4.1 Aortic volume quantification

In contrast to maximum AAA diameter measurements during follow-up, AAA volume quantification has been proposed as alternative, and better criterion for AAA risk stratification. Several studies have determined the volume of an AAA using computed tomography (CT) data, and compared the maximum aortic diameter extracted from the volume data with manual diameter measurements. The volume measurements showed a higher intra-observer reproducibility compared to manually determined diameter measurements (Bodur et al., 2007; Kauffmann et al., 2011). Thereby, it was advocated that the AAA volume (rather than the maximum diameter) is more sensible for AAA growth (Kauffmann et al., 2012). Moreover, an aortic volume change over time does not always equate to a change in maximum diameter and could therefore provide complementary information for the clinician (Parr et al., 2011; Renapurkar et al., 2012). Despite these promising results, aortic volume measurements using CT is not implemented in current clinical practice. This is mainly due to the drawbacks in the use of CT data in these studies: **1)** it is not always part of the daily clinical work-flow for AAA patients under surveillance, **2)** it suffers from radiation exposure, and, **3)** the lack of large clinical data supporting the benefits of aortic volume quantification. Aortic volume measurements were shown to be feasible using magnetic resonance imaging (MRI), however long scan times and high costs preclude MRI from being an ideal image modality for AAA volume quantification (van 't Veer et al., 2008; Duquette et al., 2012).

Alternatively, 3D ultrasound (US) could be used to assess the volume of an AAA in a harmless manner. First attempts were made by Vidakovic et al. (2006) who used an automated bladder volume indicator (BVI) to measure the AAA volume. The volume measured

with BVI correlated closely with US and CT diameters, although the spread was considerable (Vidakovic et al., 2007). Later, in the study by Rouet et al. (2010) 3D US aneurysm data were acquired using a convex 3D mechanical probe. In this probe the transducer array is mechanically tilted in order to scan the volume. The aortic volume was obtained after semi-automatic segmentation and used to detect the optimal plane for diameter measurement. Afterwards, the segmentation method was used in a reproducibility study of the maximum AAA diameter and volume, and showed acceptable reproducibility (Long et al., 2013). In a study by Bredahl et al. (2015), it was verified that AAA volume assessed with 3D US was comparable with 3D CT volumes in 54 patients. In the latest work by Rouet et al. (2017) a segmentation approach was proposed for CT and 3D US based on implicit template deformations. Results reveal confidence intervals for diameter and volume quantifications within the acceptable limits of agreement for both modalities.

### 1.4.2 Wall stress analysis

From a biomechanical perspective, not the maximum aortic diameter or its aortic volume but AAA wall mechanics (wall stresses, strains) and tissue properties will play an important role in AAA growth and rupture risk assessment. The rationale is that AAA rupture will occur when local wall stresses exceed the strength of the aortic wall, which is a tissue property. Therefore, biomechanical analysis of the aorta can be performed, e.g., characterization of the peak stresses occurring in the vessel wall.

In a more simplified approach, aortic wall stresses can be predicted using Laplace's law (Equation (1.1)). Here, the assumption of a thin-walled cylinder is used. In this case, the circumferential wall stresses ( $\sigma_{\theta\theta}$ ) are directly proportional to the aortic pressure ( $P$ ) and diameter ( $d$ ) of the vessel, while inversely proportional to the wall thickness ( $h$ ). However, due to the complex geometry of these AAAs, a direct estimation of local wall stresses is inadequate (Elger et al., 1996; Hua and Mower, 2001).

$$\sigma_{\theta\theta} = \frac{P \cdot d}{2h} \quad (1.1)$$

To overcome these issues, a first attempt of a two dimensional AAA model was made using a finite element (FE) analysis approach by Stringfellow et al. (1987). This finite element approach has afterwards been extended to 3D, in order to include the complex, 3D shape of the aneurysm obtained most commonly from CT data. In a first clinical study by Fillinger et al. (2002) the CT-based peak wall stress was analyzed and compared between different AAA patients using 3D FE models. This study showed that ruptured and symptomatic aneurysms had an increased peak wall stress compared to non-ruptured AAAs, confirming that peak wall stress might be a relevant criterion for patient-specific risk stratification. This finding was strengthened by studies by Fillinger et al. (2003) and Venkatasubramaniam et al. (2004) who showed that peak wall stress is superior to the diameter in differentiating patients with elevated risk of rupture (Figure 1.4). Later, Truijers

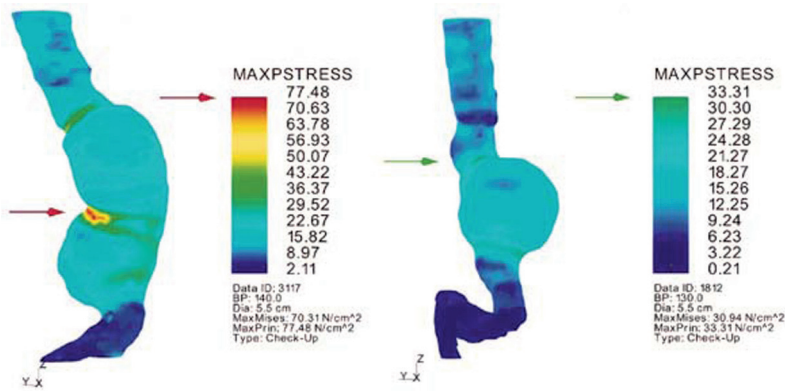


**Figure 1.4:** Wall stress distributions of two abdominal aortic aneurysms with both a maximum diameter of 5.5 cm. The peak wall stress corresponds with the red color, and the lowest wall stress is shown in blue. Figures adopted from Fillinger et al. (2003).

et al. (2007) showed that peak wall stress can detect patients with an elevated risk of aneurysm rupture including relatively small AAAs (max. diameter < 5.5 cm), which could improve the selection of patients for aneurysm repair.

Although peak wall stress was used as rupture risk estimator in all previously reported studies, the intra- and inter-operator variation in peak wall stresses were relatively high (up to 40%). This was mainly caused by small variations in geometry introduced by manual segmentation (Heng et al., 2008), affecting the resulting wall stress. As an alternative, Speelman et al. (2008) showed that not the peak wall stress but the 99<sup>th</sup> percentile wall stress might be a better risk estimator, since it is less sensitive for local inhomogeneities and thereby increases reproducibility.

Vande Geest et al. (2006a) derived a rupture potential index for AAAs based on both the peak stress and strength of the aortic wall. The region with the highest rupture potential index is considered as the peak wall rupture index (PWRI). In theory, a PWRI  $\geq 1.0$  means that the AAA will be at imminent risk of becoming symptomatic or even rupturing. Gasser et al. (2010) and Erhart et al. (2015) showed that the rupture risk predictability is higher using the PWRI instead of the peak wall stress when comparing ruptured and non-ruptured AAAs. In a large retrospective study with 243 AAA patients, Gasser et al. (2014) derived the PWRI for each individual patient and converted it into a PWRI 'equivalent' diameter, thereby facilitating a straightforward method for clinicians to interpret the biomechanical analysis. This PWRI equivalent diameter is a representative maximum diameter, which can be higher or lower than the actual diameter measured depending on the mechanical behavior of the AAA and can be used by the clinician according to the current guidelines for AAA repair.

Despite these promising results, wall stress analysis has not yet been clinically introduced (Farotto et al., 2018). The main reason is the lack of validation by prospective clinical

trials. In an ideal situation, multiple multi-center randomized clinical trials (RCT) should prove the merits of biomechanical analysis of AAAs. However, the use of CT imaging for geometry assessment hinders the current method unsuitable to perform prospective longitudinal studies. CT suffers from its drawbacks, such as radiation exposure and the use of nephrotoxic contrast agents. As a consequence, an alternative image modality is required.

Wall stress analysis using MRI has been proposed and has been shown to be feasible (de Putter et al., 2007; Merckx et al., 2009; Conlisk et al., 2017). However, long scan time and high costs will be involved when all patients in a prospective clinical trial are subjected to MRI for AAA geometry assessment. Especially, since a large number of patients is required to prove that wall stress analysis can detect patients at risk in a prospective fashion. Roughly 2 – 10% of all AAAs rupture before the current guidelines for surgery are reached (Nicholls et al., 1998), which mean that a prospective trial requires at least 100 - 1000 patients to prove the added value of MR-based wall stress analysis and rupture risk assessment.

In the 2000s, time-resolved 3D (4D) ultrasound (US) has been introduced in the clinics, which might be a good alternative for AAA geometry assessment in a non-invasive and cost-efficient matter. 3D US showed its feasibility to capture the AAA geometry for volume quantification (Long et al., 2013), yet no wall stress analysis was performed. In a first study by Kok et al. (2015), 3D US data were acquired for wall stress analysis, which was performed for eight patients and compared with corresponding CT data. This study showed that the median US-based wall stresses were in agreement with CT and good similarities between the US and CT geometries. Unfortunately, local irregularities induced by manual registration of multiple US volumes introduced high unreliable wall stress bands which prohibited the comparison of the 99<sup>th</sup> or peak wall stresses.

### 1.4.3 Aortic stiffness quantification

Besides aortic volume and wall stress analysis, aortic stiffness and compliance measurements have been proposed as alternative for current AAA risk assessment. The aortic compliance ( $C$ ) is defined as the change in volume ( $\Delta V$ ) in a segment of the aorta divided by the pressure difference ( $\Delta P$ ). In this case the pressure difference is due to the pulsatile changes in blood pressure. The aortic stiffness is inversely proportional to the aortic compliance.

$$C = \frac{\Delta V}{\Delta P} \quad (1.2)$$

The first study that measured AAA compliance and compared it with clinical outcome was by Wilson et al. (1998). In this study 112 patients were followed using US-based compliance measurements over a median time period of 7 months. It showed overall an increase in aortic stiffness (less compliant) in the non-ruptured patients, while the patients who had a ruptured AAA revealed an inverse relation to the aortic stiffness, and were more compliant. In a later multi-center study by Wilson et al. (2003) it was suggested that a

10% decrease in aortic stiffness was associated with a 28% increase in rupture risk when compared with AAAs with no change in arterial stiffness. A drawback of this method is the fact that compliance measurements can be biased by the location of the cross-section that is used to compute the area compliance, which makes comparison cumbersome.

The rationale behind these findings is that most stable, non-ruptured aneurysms increase in aortic stiffness as they increase in diameter, due to an increased wall stress (predicted by LaPlace's Law, Equation (1.1)). Presumably, as a response to the increased wall stress, the aortic wall will remodel by producing more collagen, which stiffens the vessel wall. This remodeling protects the AAA against rupture, and failure of this remodeling process might indicate an increase in rupture risk. This hypothesis supported previous findings where the ruptured AAAs had a more compliant aortic wall compared to the non-ruptured.

To evaluate these findings, Di Martino et al. (2006) performed uni-axial tensile testing on AAA wall specimens obtained after surgical repair. In total, 26 samples were obtained from patients undergoing elective repair of the AAA, while 13 specimens were resected from ruptured AAAs in an emergency setting. Results revealed a thicker aortic wall and lower wall stiffness for the ruptured aneurysms compared to the stable AAAs.

However, aortic stiffness measurements remain a controversial point, Sonesson et al. (1999) measured the aortic stiffness in a transversal 2D US plane and revealed no differences between ruptured and non-ruptured AAAs. In the work of Ganten et al. (2008) ECG-gated CT was used to measure the distensibility of AAAs to examine possible differences between large (> 50 mm) and small AAAs (< 50 mm). Although both methods were shown feasible, no significant differences between the small and large AAAs were obtained. A possible explanation for these contradictory findings could be the fact that in the aforementioned studies the aortic stiffness was measured in a single 2D cross-section of the AAA at maximum anterior-posterior diameter. Hence, it remains questionable whether the arterial stiffness at this specific location is representative for the complete AAA, i.e., to assess the AAA rupture risk. Moreover, most ruptures do not occur at the maximum diameter, but are found close to the neck of the AAA, most likely at the posterolateral side (Darling, 1970).

An alternative modality to capture AAA wall distension is using dynamic MRI. van 't Veer et al. (2008) derived segmental AAA volumes and simultaneously measured the intravascular pulsatile pressure. Subsequently, an incremental Young's modulus ( $E_{inc}$ ) was derived for each individual patient, representing a global aortic stiffness:

$$E_{inc} = \frac{\Delta P}{\Delta d} \frac{d^2(1 - \mu^2)}{2h} \quad (1.3)$$

with  $d$  representing the aortic diameter,  $h$  the wall thickness and  $\mu$  the Poisson's ratio. Since incompressible material behavior is assumed for the aortic wall, the Poisson's ratio is set to 0.5. Furthermore, Equation (1.3) can be rewritten and the Young's modulus can be



estimated using the aortic compliance by substituting Equation (1.2) in Equation (1.3):

$$E_{inc} = \frac{V_0}{C} \frac{d(1 - \mu^2)}{h} \quad (1.4)$$

Besides using the pulsatile pressure in the aorta, magnetic resonance elastography (MRE) can be used to quantify the aortic stiffness. Hence, a pneumatic driver is used which produces external mechanical waves, whose propagation was tracked in the subsequent 3D MR acquisitions. In the study by Kolipaka et al. (2016), abdominal aortic MRE was performed on AAA patients and normal individuals. Results showed similar relative differences as reported using US imaging. However, the use of MRI in a prospective study to assess the patient-specific aortic stiffness suffers from high costs and long scanning time. Therefore, MRI is not the preferred image modality to detect subject-specific differences, although this method can be used for verification purposes.

Since the introduction of ultrasound plane wave imaging (PWI), pulse wave velocity imaging (PWVI) became available, which is able to quantify the local aortic stiffness. This technique measures locally the arterial wall motion caused by the blood pressure pulse using 2D US imaging with a high frame rate. The pulse wave velocity (PWV) can directly be related to the arterial stiffness using the Moens-Korteweg equation:

$$PWV = \sqrt{\frac{E_{inc} \cdot h}{d \cdot \rho}} \quad (1.5)$$

with  $\rho$  the tissue density. In a phantom study it was shown that the Young's modulus could be measured reliably and revealed good agreement with mechanical testing (Vappou et al., 2010). Moreover, Li et al. (2013) showed that PWVI is feasible for healthy volunteers and AAA patients. However, the imaging depth is still one of the main challenges especially since the aorta for most AAA patients is located at 8 - 12 cm depth. Furthermore, the complex 3D shape of the AAA hinders accurate measurements of the PWV.

Time resolved 3D (4D) ultrasound imaging provides multiple 3D US volumes over the cardiac cycle. Using 4D US, it is possible to track the AAA geometry over time, which can be used to estimate the local vessel motion during the cardiac cycle. By capturing this dynamic motion of the aortic wall, the vessel's strains and mechanical properties of the wall can be assessed simultaneously. In the study of Karatolios et al. (2013) it was shown that 3D US speckle tracking can be used to obtain 3D strain data of the aortic wall, and offers the potential to detect differences between AAAs based on their strain patterns. Moreover, dependent on which constitutive model is used to describe the mechanical behavior of the aortic wall, different mechanical properties can be assessed quantitatively. In this thesis an isotropic geometrically non-linear model was used and applied to large patient datasets, whereas in the studies by Wittek et al. (2013, 2016), the feasibility was shown to estimate patient-specific mechanical properties of a complex fiber-reinforced material model (Gasser et al., 2006) in one healthy volunteer, and two pathological cases.

#### 1.4.4 Experimental tissue characterization

Besides *in vivo* aortic stiffness measurements using the pulsatile aortic pressure, elaborate mechanical testing on *ex vivo* aortic tissue has been performed in literature. He and Roach (1994) was one of the first who performed uni-axial tensile tests on human abdominal aneurysm tissue samples and correlated the testing results with histology. This study showed that aneurysms behaved stiffer compared to healthy aortas. Histology revealed an increase in collagen volume fractions, whereas volume fractions of elastin and muscle were lower in aneurysm tissue. Later, in a similar study by Raghavan et al. (1996), 71 aortic specimens were obtained from human organ donors or patients who underwent open aortic surgery. Using uni-axial tensile testing the longitudinal and circumferential stress-strain relations were measured. These experimental data were used in a subsequent study by the same research group to develop a two parameter, hyperelastic, isotropic, incompressible material model to capture the general material behaviour of AAA tissue from zero to systolic pressure (Raghavan and Vorp, 2000). The advantage of this well-established, population-based, material model is that it can be used to compute AAA wall stresses by finite element simulations, without knowing the patient-specific material parameters. The first 3D wall stress models of AAAs reported in literature were all based on the previous uni-axial tensile testing data (Raghavan et al., 2000; Fillinger et al., 2002, 2003; Venkatasubramaniam et al., 2004). However, Vande Geest et al. (2006b) showed that bi-axial tensile testing of AAA tissue will result in a more accurate description of the material behavior, due to the anisotropic nature of aortic tissue. In the work by Tong et al. (2011, 2013) it was suggested that a thrombus covered wall alters its mechanical behavior, and decreases its arterial stiffness. Moreover, differences in luminal wall stiffness were observed between male and female tissue samples, which might explain higher rupture risk in females. Furthermore, differences in wall stiffness were observed using different loading protocols, which highlights the anisotropic behavior of the AAA wall. Based on these observations, more complex fiber-reinforced, anisotropic, hyperelastic material models were developed to capture the general behavior of AAA tissue. Table 1.1 shows the most commonly used constitutive material models for AAA tissue behavior with increasing model complexity. The material parameters given are based on experimental mechanical testing of AAA samples by different loading protocols (e.g., O'Leary et al. (2014); Niestrawska et al. (2016); Pancheri et al. (2017)).

Despite current developments in AAA tissue characterization, it is still challenging to predict the patient-specific material behavior non-invasively. Moreover, a wide range of AAA tissue properties are reported in literature. This is mainly due to a wide range in structural differences between patients, and by the structural heterogeneity within each specific aneurysm. Structural differences are mainly caused by the presence of thrombus and calcification at different regions of the AAA (Li et al., 2008; Buijs et al., 2013). As a result, different tissue samples from the same patient may result in a wide variety of material

**Table 1.1:** Different commonly used AAA constitutive material models with their strain energy density function and material parameters. Model complexity increases from top to bottom.

Material model:	Strain energy density function ( $\Psi$ ):	Material parameters:
Neo-Hookean:	$\Psi = G(I_1 - 3)$	$G = 0.9$ MPa (Speelman et al., 2008)
Raghavan and Vorp: (Raghavan and Vorp, 2000)	$\Psi = \alpha(I_1 - 3) + \beta(I_1 - 3)^2$	$\alpha = 0.17$ Mpa; $\beta = 1.88$ Mpa (Raghavan and Vorp, 2000)
Fung four parameter model: (Sacks and Chuong, 1998)	$\Psi = b_0(e^{\frac{1}{2}b_1E_{\theta\theta}^2} + e^{\frac{1}{2}b_2E_{LL}^2} + e^{b_3E_{\theta\theta}^2E_{LL}^2} - 3)$	$b_0 = 0.14$ kPa; $b_1 = 477$ ; $b_2 = 416$ ; $b_3 = 408$ ; (Vande Geest et al., 2006b)
Gasser-Holzapfel-Ogden: (Gasser et al., 2006)	$\Psi = \mu(I_1 - 3) + \frac{k_1}{2k_2} \sum_{\alpha=1}^2 (e^{k_2 E_{\alpha}^2} - 1)$ with: $E_{\alpha} = \kappa(I_1 - 3) + (1 - 3\kappa)(I_{0\alpha} - 3)$	$\mu = 0.2$ MPa; $k_1 = 4.7$ MPa $k_2 = 1960$ ; $\kappa = 0.21$ ; $\phi = 4.6^\circ$ (Wittek et al., 2016)

properties and large uncertainties on the parameters measured.

## 1.5 Current clinical need

Over the last two decades, a large amount of knowledge and literature has been generated covering a wide variety of alternative measures to estimate the AAA rupture risk on a more individual basis. Unfortunately, none of these techniques have made it to current clinical practice yet. One of the main reasons is that these new techniques are not easy implementable in daily clinical workflow, and are lacking validation by prospective trials. Furthermore, some methods require image modalities which are not applicable for AAA screening and surveillance programs due to high costs and availability (MRI) or the exposure to radiation and contrast agents (CT).

From a clinical perspective, there is a need for an easy applicable, cost-efficient methodology to examine the benefit of additional measures to estimate patient-specific AAA rupture risk. Moreover, the ability to predict growth, or early rupture of the aneurysm before current thresholds are reached, should first be demonstrated. Finally, to prove the merit of these AAA rupture risk estimators, longitudinal prospective clinical studies should be performed.

## 1.6 Aim and outline of this thesis

In this thesis, time-resolved 3D (4D) ultrasound (US) is used as the preferred image modality to mechanically characterize the AAA wall. 4D US will be utilized to predict the patient-specific stresses and the stiffness of the aortic wall. Advantages in the use of 4D US are its non-invasive and harmless nature, it is a relative inexpensive image modality, and it is easy in use. Moreover, US is known for its high spatial and temporal resolution, which makes it

extremely suitable for cardiovascular applications. As a consequence, mechanical analysis of the AAA wall using 4D US imaging will be applicable to a large cohort of patients and can be followed over time. However, the use of US also introduces several challenges, such as the limited field-of-view and contrast of the US data.

Therefore, the objective of this thesis is:

**To develop and validate a biomechanical model of the AAA wall to characterize the patient-specific mechanical behavior using time-resolved 3D ultrasound. The method will be verified using CT data and mechanical testing *ex vivo*, while employed in a large prospective longitudinal clinical study.**

The current thesis comprises of the following chapters:

In **Chapter 2**, the influence of the limited field-of-view (FOV) of 3D US on patient-specific aortic wall stress analysis was examined. By systematically reducing the FOV, changes in wall stress and the location of peak stresses were analyzed. In addition, the necessity of assessing the aortic bifurcation for accurate wall stress analysis was studied.

In **Chapter 3**, a feasibility study was performed and patient-specific 4D US-based wall stress analysis was performed in 40 patients with a wide range of diameters. The wall stress models were calibrated using the 4D US motion data, resulting in a patient-specific material parameter, i.e., the overall stiffness of the AAA wall. For 7 out of 40 patients, CT data were available as well. Besides mechanical characterization, the AAA geometry and wall stress distributions were compared between both modalities for these patients.

In **Chapter 4**, the aortic stiffness and peak wall stresses of AAAs were characterized and compared with young, and age-matched healthy individuals with a normal aortic diameter. The relation to age, maximum diameter, and growth were assessed statistically. Moreover, different degrees of the AAA pathology were investigated and its effect on the aortic stiffness and peak wall stresses were examined.

In **Chapter 5**, a segmentation method for automated geometry assessment was developed, which was required to apply the current methodology in a robust manner and on a large scale in a longitudinal study. Multi-perspective 3D US data were acquired and used to ensure that large longitudinal AAAs that normally do not fit in a single 3D US volume could be included. The proposed method uses active deformable contour models to automatically segment the AAA geometry and a registration method to merge multiple 3D US volumes. Finally, to assess the outcome of the segmentation and registration algorithm, AAA geometries and wall stress results were verified by comparing results to CT data.

In **Chapter 6**, the mechanical properties of a large AAA patient population were followed in a longitudinal study. Patients were followed for a median period of 24 months, during regular follow-up intervals in the outpatient clinic. The aortic wall stresses and stiffness were analyzed and their relation to AAA growth and rupture were assessed.

In **Chapter 7**, final verification experiments were performed *ex vivo*. In an idealized step-up, intact porcine aortas were mechanically tested under physiological conditions in a mock loop followed by bi-axial tensile testing. Moreover, four patients who underwent open aortic surgery were included, of whom a small piece of the AAA wall was resected. The human aortic tissue was mechanically tested using again bi-axial tensile testing. Results were compared with the aortic stiffness found *in vivo*. In addition, reproducibility was assessed.

In **Chapter 8**, the method was applied to aneurysms in the ascending aorta. Mechanical characterization of ascending thoracic aortic aneurysms (ATAAs) was performed using peri-operative trans-esophageal 4D US and intra-vascular blood pressure data. The characterization methodology described in previous chapters was adapted for ATAAs, which are subjected to larger longitudinal translation and stretches due to cardiac motion. Results were verified using *ex vivo* bi-axial tensile testing on the resected ATAA tissue samples.

# **The influence of limited field-of-view on wall stress analysis in abdominal aortic aneurysms**

This chapter is based on: Influence of limited field-of-view on wall stress analysis in abdominal aortic aneurysms, **E.M.J. van Disseldorp**, K.H. Hobelman, N.J. Petterson, EN. van de Vosse, M.R.H.M. van Sambeek, and R.G.P. Lopata, In: *Journal of Biomechanics*, 2016; 49(12): pp. 2405-2412.

## Abstract

**Background:** Abdominal aortic aneurysms (AAAs) are local dilations of the aorta which can lead to a fatal hemorrhage when ruptured. Wall stress analysis of AAAs has been widely reported in literature to predict the risk of rupture. Usually, the complete AAA geometry including the aortic bifurcation is obtained by computed tomography (CT). However, performing wall stress analysis based on 3D ultrasound (3D US) has many advantages over CT, although, the field-of-view (FOV) of 3D US is limited and the aortic bifurcation is not easily imaged.

**Methods:** In this study, the influence of a limited FOV is examined by performing wall stress analysis on CT-based (total) AAA geometries in ten patients, and observing the changes in 99th percentile stresses and median stresses while systematically limiting the FOV.

**Results:** Results reveal that changes in the 99<sup>th</sup> percentile wall stresses are less than 10% when the proximal and distal shoulders of the aneurysm are in the shortened FOV. Wall stress results show that the presence of the aortic bifurcation in the FOV does not influence the wall stresses in high stress regions.

**Conclusions:** The necessity of assessing the complete FOV, including the aortic bifurcation, is of minor importance. When the proximal and distal shoulders of the AAA are in the FOV, peak wall stresses can be detected adequately.

## 2.1 Introduction

Rupture of an abdominal aortic aneurysm (AAA) lead to a fatal hemorrhage and death in 70 – 90% of all cases (Budd et al., 1989). Therefore, current guidelines suggest aortic aneurysm repair when the aortic diameter exceeds 5.5 cm, or when it has grown more than 1 cm per year (The UK Small Aneurysm Trial Participants, 1998; Moll et al., 2011). Using these evidence based guidelines, the overall risk of surgery intervention outweighs the risk of rupture. However, on a patient-specific basis these guidelines can be inaccurate for individuals and have proven to be inadequate (Nicholls et al., 1998; Valentine et al., 2000; Conway et al., 2001). Studies have shown that aneurysms may rupture below these thresholds while others remain stable even when they exceeded the threshold diameters suggested in these guidelines. Therefore, previous studies have suggested new, additional rupture risk estimators, based on the mechanical behavior of the AAA wall.

Wall stress analysis has been introduced to predict the potential rupture risk of the AAA wall, which is mostly performed using computed tomography (CT) and sparsely with magnetic resonance imaging (MRI) data. Studies have shown that the peak and 99<sup>th</sup> percentile wall stresses are related to potential rupture risk (Vorp et al., 1998; Fillinger et al., 2002, 2003; Venkatasubramaniam et al., 2004; Vorp, 2007; Speelman et al., 2008; Gasser et al., 2010, 2014; Khosla et al., 2014). In a study by Vande Geest et al. (2006a), a rupture potential index was defined, which related the local wall stress to the wall strength. In general, the patient-specific geometry is assessed from neck to bifurcation, including a small portion of the iliac arteries. Next, a uniform wall thickness, a generic and population-based material, and boundary conditions are incorporated. The boundary conditions consist of the luminal pressure, mostly derived from a pressure measurement in the upper arm, and fixation of the neck and iliac arteries.

Despite promising results, these models are not widely accepted and used in the clinical setting yet. The current approach suffers from several drawbacks, such as the use of ionizing radiation and nephrotoxic contrast agents for CT imaging, the long scanning time and high cost for MRI, and the unavailability of patient-specific material properties. Three-dimensional ultrasound (3D US) imaging overcomes abovementioned disadvantages of CT and MR, and even enables the possibility to acquire the vessel's motion during the cardiac cycle. Using the dynamic behavior of the AAA wall, finite element models can be calibrated to the vessel motion and thereby more patient-specific material properties can be derived. Also patient-specific and FEM-regularized strains (Wittek et al., 2013, 2016; Derwich et al., 2016) and wall stresses (van Disseldorp et al., 2016b) become available using 3D US. The drawbacks of 3D US are the low contrast compared to CT and MRI, but most importantly, the limited field-of-view (FOV) (Figure 2.1).

In many cases, multiple ultrasound acquisitions are required to capture the complete AAA geometry, which demands sophisticated US registration techniques to combine both US acquisitions, which is not trivial and may lead to unexpected outcomes (Kok et al.,



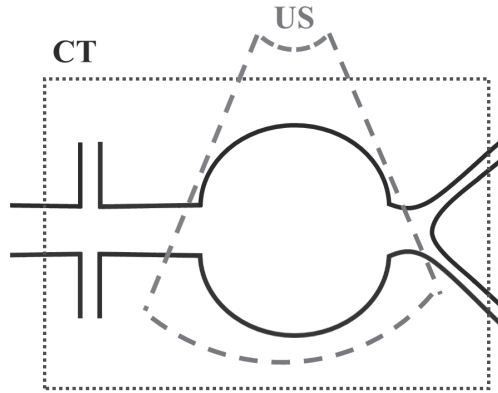


**Figure 2.1:** Graphical illustration of an abdominal aortic aneurysm (AAA) with the field-of-view of computed tomography (CT) (*black dotted line*) and that corresponding to ultrasound (US) imaging (*gray striped line*).

2015). Besides the limited FOV, the aortic bifurcation is not easily detected. The bifurcation lies deep, is small with respect to the transducer, and contrast is low, because of the dorsal angulation of the common iliac arteries. The latter is primarily the result of the fact that the ultrasound waves propagate mostly parallel to the vessel wall, resulting in a reduced signal to noise ratio. This makes proper imaging, and accurate segmentation of the bifurcation and subsequent iliac arteries (used to fixate the model) cumbersome when using ultrasound. However, the necessity of including a large portion of the iliac arteries, or even the bifurcation for that matter, has not been clearly proven or analyzed.

In this study, the influence of a limited FOV on wall stress results is examined. Wall stress analysis was performed on CT-based AAA geometries, while systematically limiting the FOV until the geometry was comparable to that obtained in a single 3D US acquisition. Thereby the conventional sites used for fixating the model, i.e., applying the boundary conditions were excluded. Changes in wall stresses and location of peak stresses were analyzed and compared to the full geometry as measured with CT.

## 2.2 Materials and Methods

### Study population

Pre-operative computed tomography angiography (CTA) scans of a random selection of 10 patients (age 60 – 82 years) were included retrospectively. The CT-data were acquired as part of the normal clinical workflow prior to endovascular aortic repair (EVAR). The maximum aortic diameter ranged from 44 to 57 mm.

## Segmentation

The CTA scans were segmented using the semi-automatic Hemodyn software package developed by Philips Medical Systems (Best, The Netherlands) and the Eindhoven University of Technology (TU/e). In this software package, the aortic lumen centerline was automatically tracked from the renal arteries to the iliac arteries. The input for this tracking were three manual selected points, one at the proximal side, and two in the distal arteries. Subsequently, a three-dimensional active object (3DAO) was formed around the centerline and inflated until the AAA lumen-wall interface was found, or, in case of thrombus, the lumen-thrombus interface. In the latter case, the 3DAO was dilated further until the layer between the thrombus and the AAA inner wall was segmented. The external forces acting on the 3DAO were based on the Hounsfield values in the CTA data, which attract the 3DAO to the lumen-wall interfaces. The internal forces were derived from the curvature and smoothness of the 3DAO. A more detailed description is found in Breeuwer et al. (2008) and Olabarriaga et al. (2004b). The segmentation results were inspected visually and manual adaptations were made when the automatic segmentation did not delineate the inner wall correctly. Finally, the outer wall of the AAA was calculated by interpolating the inner wall 2 mm into the normal direction as described by Olabarriaga et al. (2004b). Subsequently, the inner and outer surfaces were exported to MATLAB (2014b, Mathworks Inc., Natick, MA, USA).

## Reducing field-of-view

All the CT-based geometries used are shown in Figure 2.2A. The maximum anterior-posterior (A-P) diameter was detected in the CTA data using MATLAB. The position on the centerline at which the maximum A-P diameter was found was used as a center point for the field-of-view (FOV) of all AAA geometries. Subsequently, the geometry was shortened in the centerline direction with 10 mm at the proximal side and 10 mm at the distal side. This cropping procedure was repeated until the FOV of the AAA geometry was shortened to a length of 60 mm in the axial direction of the vessel. This represents a typical FOV that can be achieved with one single 3D-US acquisition. For the larger AAA geometries, fusion of two or more 3D-US acquisition is needed to achieve the complete FOV. An example of a complete series of geometries resulting from this cropping procedure is shown in Figure 2.2B. Before the geometries were converted into a volume mesh, both proximal and distal ends were elongated with 5 mm in the direction of the centerline to reduce boundary effects. Next, the geometries were exported to 3-Matic software version 5.1 (Materialise, Leuven, Belgium). Meshes were created consisting of 52.000 – 177.000 hybrid quadratic tetrahedral elements. During this meshing procedure, it was ensured that at least two elements in radial direction were present.

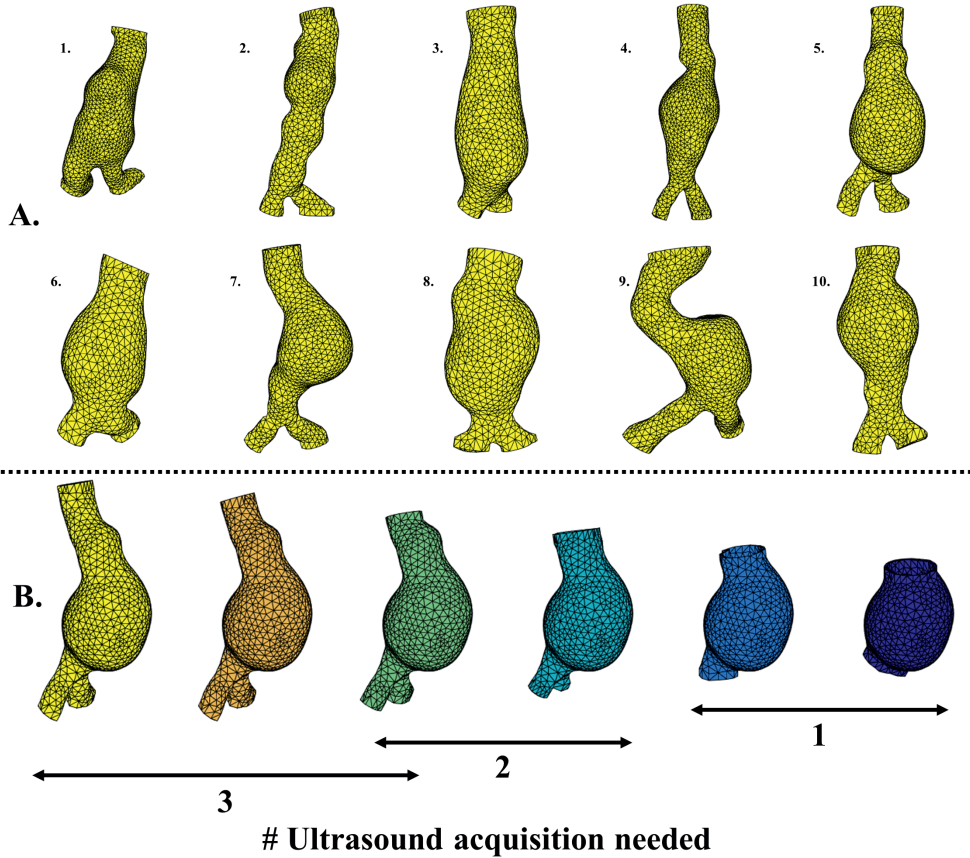


**Figure 2.2:** **A.** The geometries of all 10 included patients based on computed tomography. In **B.** an example of the shortening procedure is shown for aneurysm 5: The complete geometry of an abdominal aortic aneurysm (AAA) (*left*) is shortened 10 mm in the centreline direction at the proximal and distal. The final cropped AAA geometry (*right*) represents a typical field-of-view which can be achieved with one single three dimensional ultrasound acquisition. The larger AAA geometries (*left*) need two or more ultrasound acquisitions to capture the complete field-of-view.

## Finite Element Analysis

Finite element analysis (FEA) was executed using Abaqus 6.12 (Dassault Systèmes, Paris, France). The meshes were imported and a uniform, one-layer AAA wall model of 2 mm thickness was considered. An incompressible, reduced polynomial material model was prescribed (Yeoh, 1993), with parameters describing the AAA wall as reported by Raghavan and Vorp (2000). The strain energy density function ( $\Psi$ ) of this model is given by:

$$\Psi = \alpha(I_1 - 3) + \beta(I_1 - 3)^2 \quad (2.1)$$

with  $\alpha = 0.17$  MPa and  $\beta = 1.88$  MPa.

Next, the boundary conditions were applied. The proximal and distal side(s) were constrained in all directions. The CT-based AAA geometries were acquired during multiple heartbeats, and are therefore not stress free. It was assumed that the average blood pressure during one CTA scan was equal to the mean arterial pressure (MAP). A backward incremental method, described by de Putter et al. (2007), was prescribed until the initial stresses at MAP were derived. In this study, the MAP was set to 105 mmHg, since no patient-specific blood pressures were measured. Subsequently, a peak-systolic pressure of 140 mmHg was applied to the inner AAA wall (Kok et al., 2015). From the FEA results, the Von-Mises stresses were calculated.

### Data analysis

The 99<sup>th</sup> percentile wall stress was calculated over the complete AAA geometry for every slice of 5 mm in the axial direction, starting from the proximal AAA neck to the distal iliac arteries. Furthermore, the median wall stresses were calculated to compare the general wall stress for the complete and shortened AAA geometries. Besides the median and 99<sup>th</sup> percentile wall stresses of each slice within the geometry, high stress regions were identified and analyzed. Five regions were selected, containing the highest stresses within the complete AAA geometry, and were compared to the stresses at the same positions as found in the shortened AAA geometries. The high stress regions were defined as a 5 by 5 by 5 mm, non-overlapping, sub-volumes in which the highest stresses, i.e., the most 99<sup>th</sup> percentile to peak stresses were present. Subsequently, the corresponding Von-Mises wall stresses and their distributions were visualized. Moreover, the relative difference of the stresses in these high stress spots between each shortened and original geometry were calculated. Finally, the influence of the presence of the aortic bifurcation and iliac arteries on the final wall stress results was examined: the median Von-Mises wall stresses in the five high stress regions were compared for the shortened AAA geometry, in which the bifurcation was still present, with the subsequent, shortened geometry without a bifurcation.

## 2.3 Results

Cropping the FOV of the AAA geometries resulted in three to eight cropped geometries for the individual AAA datasets. All finite element simulations were successful, with an average computational time of one hour on a single processor core (Intel Xeon E5-2667 v3, Santa Clara, California, USA). The Von-Mises wall stress distributions for three AAA patients

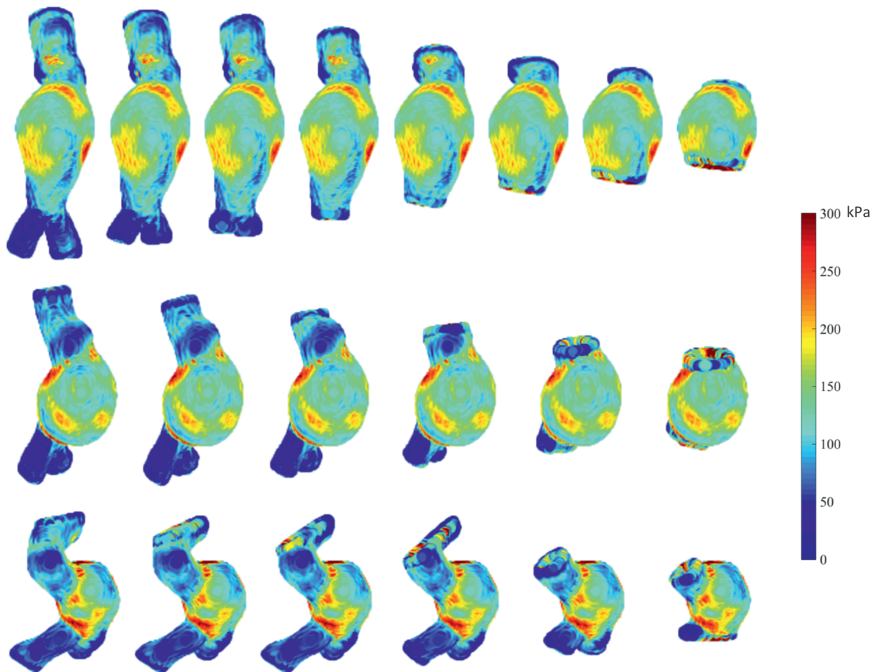


**Figure 2.3:** Von Mises wall stress distribution of aneurysm 4, 5 and 9. The most left geometry represents wall stresses for the complete AAA geometry acquired with computed tomography (CT), the most right geometry represents wall stresses from the shortest geometry, comparable the field of view of one single three dimensional ultrasound (3D US) acquisition.

are shown with the complete and each shortened FOV in Figure 2.3. It shows that regions containing the highest wall stresses are found in the areas with high curvature which are considered the shoulders of the AAA. For these three AAA geometries, the shoulders are near the maximum diameter, and still almost completely captured in the smallest FOV. Therefore, the majority of the high wall stresses are still present the smallest FOV.

### Median and 99<sup>th</sup> percentile wall stress

In Figure 2.4, the median and 99<sup>th</sup> percentile Von-Mises wall stress are shown as a function of the distance to the maximum A-P diameter. The negative values represent the distance to the maximum A-P diameter at the distal side, and the positive values are in the proximal direction. Note that at both proximal and distal ends the wall stress results were not visualized for the first 10 mm, since these results were affected by the boundary conditions and do not represent physiological wall stresses. Figure 2.4 shows no differences in the median wall stress per slice for all AAA patients when comparing the geometry of the

shortened geometries with that obtained from the complete FOV. The 99<sup>th</sup> percentile wall stress results for all AAA geometries, with the exception of geometry 8, also show similar results around the maximum diameter (distance  $\leq 15$  mm). At the proximal and distal ends, the shortest AAA geometries (dark blue) show an underestimation of the 99<sup>th</sup> percentile wall stress in four cases. In 8 out of 10 AAA geometries, a peak in the 99<sup>th</sup> percentile wall stress at the distal or proximal side is missed when the FOV is shortened maximally. However, for the geometries in which the FOV captures the proximal and distal AAA shoulder, the 99<sup>th</sup> percentile wall stresses per slice are equivalent to those found in the complete AAA geometries. For example, for patient 4, 5 and 9 (see Figure 2.2B), the light blue lines in Figure 2.4 capture all the peaks in the 99<sup>th</sup> percentile wall stresses per slice, which imply that the third shortest FOV geometry is still sufficient to capture the highest wall stresses of these aneurysms.

### High stress regions

The Von-Mises wall stress distributions of the five highest stress regions for all ten AAA patients are shown in Figure 2.5. It shows the median wall stress with its interquartile ranges, and the asterisk above the boxplots represent the presence of a bifurcation in the current shortened geometry. For patient 1 and 6 one high stress region was not present in all shortened AAA geometries. As an alternative, a subsequent high stress region was chosen and analyzed. For patient 3 and 7, respectively four and three high stress regions were not present in all limited FOV geometries.

The left boxplot of each high stress region represented the wall stress distribution corresponding to the complete, reference AAA geometry. Every boxplot rightwards shows the wall stress distribution of a subsequent, shortened geometry. This figure shows that overall the wall stress distribution in the high stress regions remain equal, even when the FOV is limited. However, in 80% of all AAA patients, the geometry with the smallest FOV underestimates ( $\geq 10\%$ ) the median wall stresses in at least one of the five high stress regions.

In Figure 2.6 the relative difference in median Von-Mises stress is shown for all shortened FOV geometries compared to the complete AAA geometry in the aforementioned, high stress regions. For visual purposes, the relative differences for only the top three high stress regions per AAA were shown. This graph shows that the median wall stress in the high stress regions for the smallest, extreme shortened FOV geometries (dark blue) differ in 7 out of 30 regions more than 10% compared to the median wall stress in the complete FOV geometries. For almost all high stress regions in the other less shortened FOV geometries (56 out of 57), the median wall stress in these regions differs less than 10% compared to the reference.

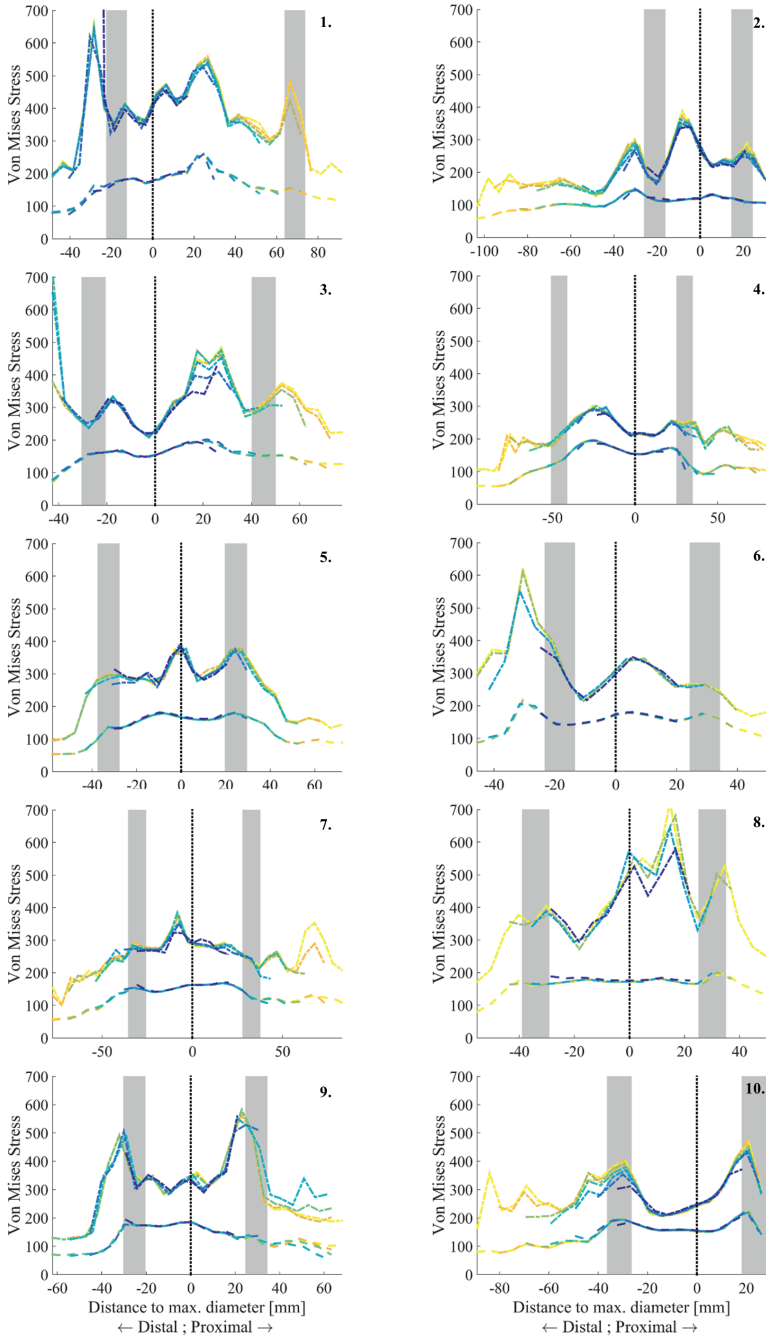


**Figure 2.4:** Median and 99<sup>th</sup> percentile Von-Mises wall stress as a function of the vessel's axial position. The axial position of the maximum anterior-posterior (A-P) diameter is indicated with the black dotted line, and the gray areas represent the proximal and distal shoulder of the aneurysm. The colors correspond to the amount of shortening as found in Figure 2.2B: yellow represents the largest FOV and dark blue the smallest FOV.

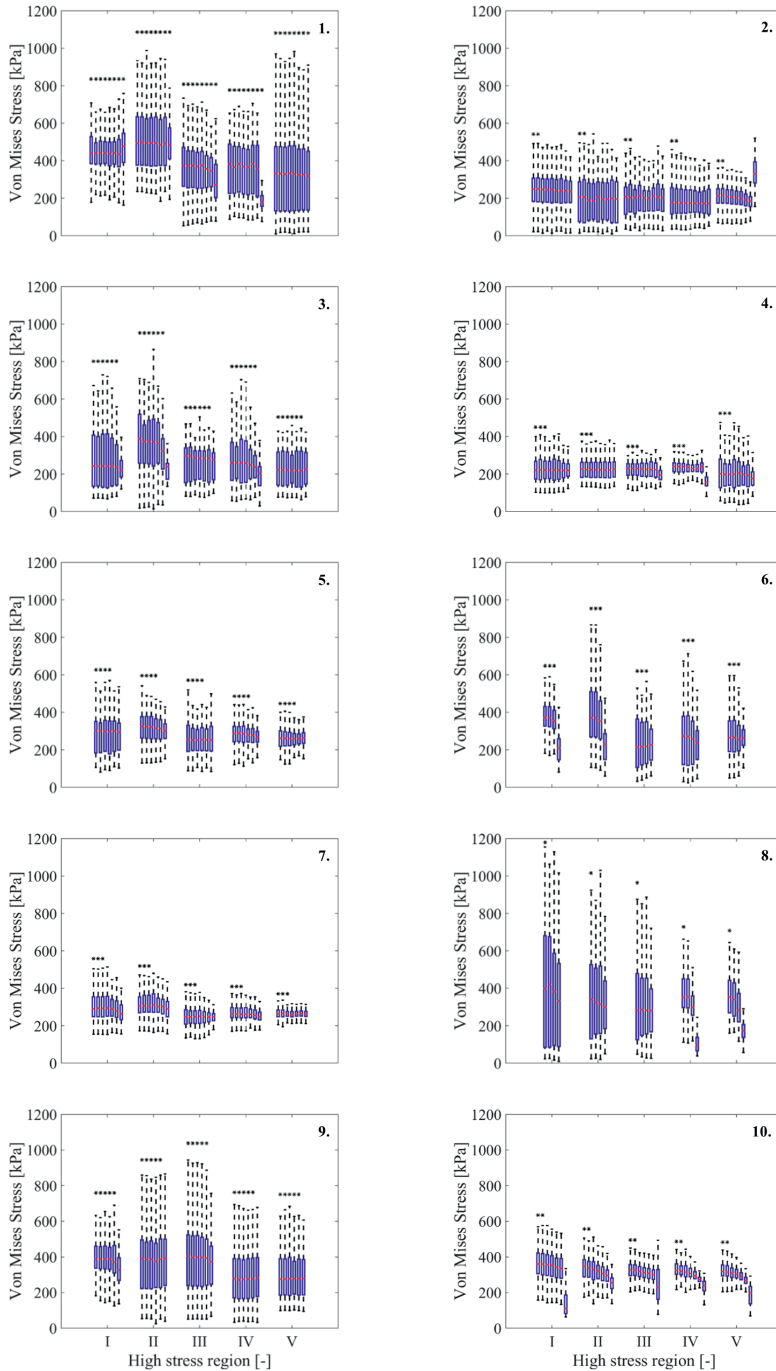


**Figure 2.5:** Distribution of the Von-Mises wall stress in the five high stress regions (I–V) found in each of the 10 AAA geometries. The asterisk represent the presence of the bifurcation in the geometry, and the extreme outliers were removed for visual proposes.



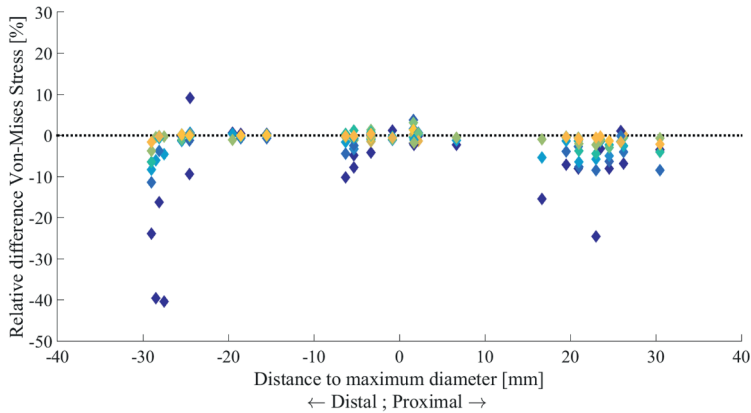


**Figure 2.6:** Relative difference in median Von-Mises wall stress of the AAA geometry with limited field-of-view (FOV) compared to the complete FOV. The results are shown for the top three high stress regions for all 10 AAAs. The colors correspond to the amount of shortening as found in Figure 2.2B: yellow represents a large FOV and dark blue the smallest FOV.

### Influence of bifurcation

For nine out of ten patients the median Von-Mises wall stresses in the high stress regions were compared between the last geometry with a bifurcation and the first without the bifurcation. Patient 1 was excluded in this analysis since the maximum A-P diameter was nearby the bifurcation ( $< 25$  mm), and therefore no geometry without bifurcation could be created. Figure 2.7 shows a scatterplot of the median Von-Mises wall stress with and without bifurcation for all data. It shows that the majority of all wall stresses are along the identity line ( $y = x$ ), representing the same median wall stress for the geometries with and without bifurcation. Only in three cases (region II in patient 3, and region I and II in patient 6), the median wall stress in the geometry with bifurcation is at least 30% higher than the geometry without bifurcation.

## 2.4 Discussion

In this study, the influence of a limited field-of-view geometry on wall stress analysis of AAAs was investigated. The influence of a limited field-of-view, and the presence of the aortic bifurcation, were examined using CT-data. Geometries were systematically shortened, and thereby also excluding the aortic bifurcation, until the FOV matches that obtained by US imaging. Results were compared to the ideal situation when the complete geometry is available.

This study shows that a limited FOV may lead to an underestimation of the higher wall stresses, or the omission of high-stress spots, but both were found in the more extreme

cases when large shortening was applied (Figure 2.6). Occasionally, high stresses were found which were artifacts caused by the cutting procedure and subsequent boundary conditions. In the majority (98%) of the less extremely shortened geometries ( $FOV \geq \max. A-P \text{ diameter} \pm 40 \text{ mm}$ ) the median wall stress in the high stress regions differ less than 10% compared to the situation when the complete geometry is available, which suggest that cropping the AAA geometry is acceptable, up to a certain limit. Next, the wall stress results in the high stress regions were compared for the geometries with and without bifurcation. The results demonstrated that the presence of a bifurcation in the geometry does not significantly affect the median wall stress in the suggested rupture risk regions.

Besides comparing the median wall stresses in the high stress regions, also the shortened and complete geometries were compared using a slice-by-slice approach. Although 10 mm at proximal and distal side were omitted in the analysis to avoid boundary effects, the median wall stress per slice showed no differences for all AAA patients. Hence, shortening of the FOV did not influence the global wall stress in the aneurysm. The 99<sup>th</sup> percentile wall stress per slice showed that peaks were missed when the shortest FOV was used for 8 out of 10 AAA patients. However, when the proximal and distal aneurysm shoulders were in the shortened FOV, the 99<sup>th</sup> percentile wall stress per slice showed equivalent results as in the reference FOV. The use of slice-by-slice data and high stress regions is favorable over analyzing only the total peak wall stress or 99<sup>th</sup> percentile wall stress of the entire aneurysm. By analyzing the stresses in these regions, the actual differences and effects induced by the reduction of the FOV can be examined on local scale, which is more accurate and illustrative. Comparing the 99<sup>th</sup> percentile or peak stress of the total geometry before and after shortening can in fact lead to a comparison of stresses found at different locations.

According to these findings, US-based FEM can lead to accurate results, even when the

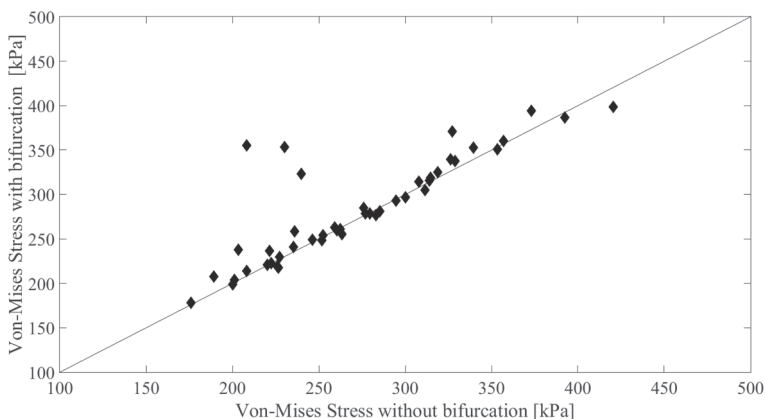


**Figure 2.7:** Scatterplot of the median Von-Mises Stress in the high stress regions of the geometry with bifurcation versus the subsequent geometry without bifurcation.

bifurcation is not visualized and therefore omitted. However, one will need to acquire multiple datasets to reconstruct a significant portion of the entire geometry to avoid underestimation or missing out on high stress regions. Obviously, in case of an aneurysm that extends to the bifurcation or iliac arteries, more data will be required. However, this is a small cohort of patients, for which wall stress analysis based on CT imaging could still be an alternative. However, US imaging in the bifurcation/iliac will be less of an issue for the aneurysms which extend to the iliac artery, since contrast and resolution will be more optimal due to the dilated vessel.

A subgroup of ten AAAs was constructed including a range of diameters. Considering the agreement of the results between different subjects, it was decided not to extend this population to higher numbers. CT-data of patients with aneurysms in or beyond the bifurcation were not considered for this study. The actual MAP was not measured during CTA imaging since this is not part of normal clinical workflow. This might have led to a bias in the residual stresses as estimated with the backward incremental method. However, for the comparison between shortened and complete AAA geometry, this bias will not be an issue. Finally, actual US data were not included in this study, and only CT-data were used as a reference. The comparison of CT and US was not the focus of this work, and has already been performed in other studies (Kok et al., 2015; van Disseldorp et al., 2016b). Limiting factors when performing US imaging, such as shadowing due to bowel gas, or high attenuation by large fat layers, were not considered and are beyond the scope of this study. In this study, local material properties such as calcification of the aortic wall and presence of intraluminal thrombus were not included, while they could have an important contribution in the local wall stresses of the AAA wall (Speelman et al., 2007; Li et al., 2008; Polzer et al., 2011). It was chosen to focus on the wall instead. In a future study, these other constituents could be included.

This study implies, that despite of the disadvantages of 3D US, it is potentially applicable for wall stress analysis of AAAs. This elicits the opportunity to perform 3D US-based wall stress analysis of AAAs over time, and thereby examine potential changes in patient-specific wall stresses and material properties.

## 2.5 Conclusion

This study showed that despite a limited field-of-view, local peak wall stresses in an aneurysm can be quantified and detected adequately. Furthermore, it was shown that the bifurcation is not necessarily needed when performing AAA wall stress analysis. Hence, some of the major drawbacks of 3D US-based wall stress analysis can be tackled, however fusion of multiple 3D US acquisitions is still needed for the majority of abdominal aortic aneurysms.

# Patient-Specific wall stress analysis and mechanical characterization of abdominal aortic aneurysms using 4D Ultrasound

This chapter is based on: Patient-specific wall stress analysis and mechanical characterization of abdominal aortic aneurysms using 4D ultrasound, **E.M.J. van Disseldorp**, N.J. Petterson, M.C.M. Rutten, F.N. van de Vosse, M.R.H.M. van Sambeek, and R.G.P. Lopata, In: *European Journal of Vascular and Endovascular Surgery*, 2016; 52(5): pp. 636-642.

## Abstract

**Background:** The aim of this study was to perform wall stress analysis (WSA) using 4D ultrasound (US) in forty patients with an abdominal aortic aneurysm (AAA). The geometries and wall stress results were compared with computed tomography (CT) in seven patients. Additionally, the WSA models were calibrated using 4D motion estimation, resulting in patient-specific material parameters which were compared between patients.

**Methods:** 4D-US images were acquired for forty patients (AAA diameter 27 – 52 mm). Patient-specific AAA geometries and wall motion were extracted from the 4D-US. WSA was performed and corresponding patient-specific material properties were derived. For seven patients, CT-data were available and analyzed for geometry and wall stress comparison.

**Results:** The 4D ultrasound-based 99<sup>th</sup> percentile wall stress ranged from 198 to 390 kPa. Regression analysis showed no significant relation between wall stress and diameter of the AAA. The similarity-indexes between US and CT were very good and ranged between 0.90 and 0.96, and the 25<sup>th</sup>, 50<sup>th</sup>, 75<sup>th</sup>, and 95<sup>th</sup> percentile wall stresses of the US and CT data were in agreement. The characterized patient-specific shear modulus had a median of 1.1 MPa (interquartile range: 0.7 - 1.4 MPa). Based on the maximum AAA diameter, the AAAs were divided in a small, medium, and large diameter group. The largest AAAs revealed an increased wall stiffness compared to the smallest AAAs.

**Conclusions:** 4D ultrasound is applicable for wall stress analysis of AAAs, and elicits the opportunity to perform wall stress analysis over time, also for AAAs who do not qualify for a CT or MRI-scan. Moreover, the patient-specific material properties can be determined, which could possibly improve risk assessment.

### 3.1 Introduction

Abdominal Aortic Aneurysms (AAAs) are localized dilations of the abdominal aorta which incidence increases with risk factors such as smoking, aging and hypertension (Lederle et al., 1997). The major complication of AAAs is rupture, resulting in a life-threatening haemorrhage and death in approximately 80% of all cases (Reimerink et al., 2013). Aortic aneurysm repair is considered when the risk of rupture exceeds the risk of a surgical intervention. Currently, the diameter is used as rupture risk estimator: when the maximum AAA diameter exceeds 5.5 cm, or has grown more than 1 cm per year, surgical repair is considered (Moll et al., 2011). However, these guidelines may not be completely reliable since smaller aneurysms can rupture below these thresholds, and some larger aneurysms remain stable above (Darling et al., 1977; Nicholls et al., 1998; Conway et al., 2001). Hence, an additional approach for rupture risk assessment is needed.

From a biomechanical point of view, aneurysms will rupture if the mechanical stress exceeds the local strength of the vessel wall. Therefore, the state of the aortic wall, i.e., the mechanical properties of the wall and stresses in the wall combined, could be a better predictor for rupture risk than AAA diameter. In previous studies, wall stress analysis has been performed widely in AAAs (Raghavan and Vorp, 2000; Gasser et al., 2010; de Putter et al., 2007), and showed its merit. Fillinger et al. (2003) and Venkatasubramaniam et al. (2004) showed that the peak wall stress could be a better predictor for rupture risk on an individual basis, and Vande Geest et al. (2006a) derived a rupture potential index for AAAs based on the wall stress and strength. In a study by Speelman et al. (2008), it was shown that the 99<sup>th</sup> percentile wall stress is less sensitive for local inhomogeneities thereby increasing reproducibility.

In most previous studies, the patient-specific geometries are obtained from pre-operative computed tomography (CT) data. Although CT is clinically used as golden standard for geometry assessment, it involves the use of ionizing radiation and nephrotoxic contrast agents. Moreover, CT does not provide temporal information, which could be used for patient-specific characterization of the mechanical properties of the AAA.

Alternatively, Magnetic Resonance Imaging (MRI) can be used to obtain both geometry and motion of the aneurysm wall. However, disadvantages of MRI are the long scanning time, relatively high costs, and the exclusion of patients with metal implants. Another alternative could be ultrasound (US) imaging, which is widely accepted as diagnostic technique for many cardiovascular applications. It combines high temporal and spatial resolution with the ability of real-time, non-invasive two-dimensional (2D) and three-dimensional (3D) imaging, and is relatively cheap.

In current clinical practice, 2D-US imaging is used to detect and determine the aortic diameter for monitoring, i.e., growth assessment. By doing so, many benefits of US imaging such as the aforementioned resolution, and the possibility to obtain time-resolved volumetric images, remain unused. Moreover, ultrasound allows longitudinal studies, also for

smaller aneurysms that are normally not imaged with CT. Time resolved 3D-US (4D-US) imaging provides the possibility to assess the differences in geometry of an AAA over time, and can be used to obtain the patient-specific geometry and vessel motion during the cardiac cycle. Karatolios et al. (2013) showed that 3D US speckle tracking can be used to obtain 3D strain data of the aortic wall, and offers the potential of characterization of AAAs by their strain patterns. In previous studies by the same group, the mechanical properties were estimated using inverse finite element analysis (FEA) of 4D-US data of the abdominal aortic wall, in five volunteers with a complex anisotropic material model (Wittek et al., 2013). In a study by Kok et al. (2015) it was shown that FEA based on 3D-US is a promising tool to predict AAA wall stresses, with comparable results as obtained by CT.

This study aims to perform patient-specific wall stress analysis of AAAs based on 4D ultrasound in a group of AAA patients with a large range of diameters. The FEA models were calibrated using the 4D-US data, resulting in one single patient-specific material parameter which represents the overall elasticity of the AAA wall. The patient-specific wall stress and elasticity could easily be followed simultaneously over time using 4D-US, and potentially be related to AAA growth or rupture. Finally, for a sub-group of patients, geometry and wall stress results were compared with the ‘golden standard’, i.e., CT.

## 3.2 Materials and Methods

### Study population

In total 40 patients were included in this study. All patients gave their informed consent prior to inclusion. This study was approved by the local ethics committee of the Catharina Hospital Eindhoven. The maximum aortic diameter varied between 27 and 52 mm. For 7 out of 40 patients, CT data were available. Patient demographics are listed in Table 3.1.

**Table 3.1:** Patient demographics

Demographics	Value
Age (mean + range)	74 (60 - 85) years
Gender (M/F)	39 / 1
Maximum AP diameter (mean + range)	40 (27 - 52) mm
Growth in 6 months (mean + range)	1 (0 - 5) mm
Blood pressure (mean DP/MAP/SP)	86 /105/144 mmHg

AP = anterior - posterior; DP = diastolic pressure;

MAP = mean arterial pressure; SP = systolic pressure

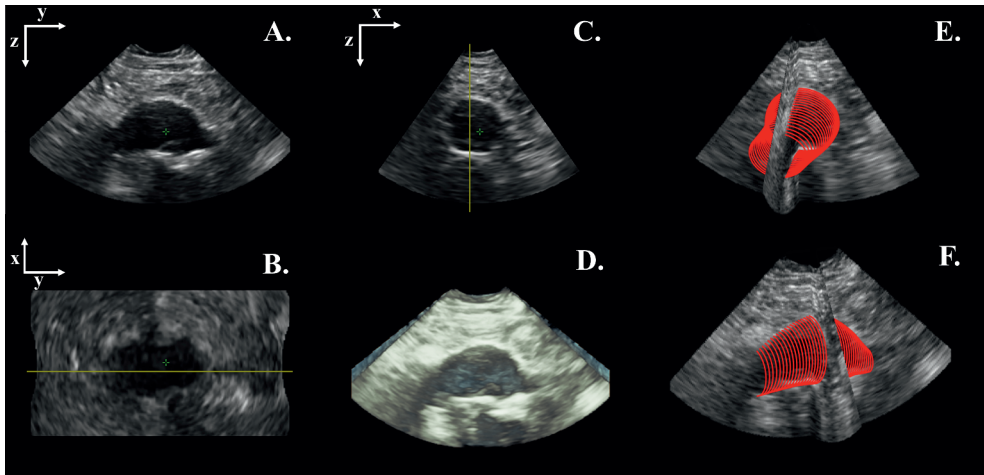


**Figure 3.1:** Example of three dimensional (3D) ultrasound data and the corresponding geometry of the abdominal aortic aneurysm (AAA). A longitudinal cross section is shown (A), with the corresponding coronal (B) and transversal plane (C). (D) A 3D render of the entire volume is visualized. (E and F) The manual segmentation of the AAA is shown (*red lines*).

### Data acquisition

Time-resolved 3D ultrasound (4D-US) data of each AAA were acquired with a commercial iU22 Philips System (Philips Medical Systems, Bothell, WA, USA) equipped with a 3D curved array X6-1 probe (center frequency = 3.5 MHz). Volume data were acquired for 5 seconds during breath-hold, with a volume acquisition rate of 4-8 Hz. The depth ranged from 6.5 – 14.6 cm and the opening angle varied between 55° and 90°.

Although field-of-view is not a limiting factor for proper analysis (van Disseldorp et al., 2016a), only patients with an AAA that could be completely captured in one single ultrasound acquisition were included in this study. Diastolic and systolic brachial blood pressure were measured in a supine position using an automatic arm cuff directly after the 4D-US acquisitions.

Computed tomography angiography (CTA) scans were made using a 256-slice CT-scanner (Philips Healthcare, Best, the Netherlands). The slice thickness was 1 mm and the CTA data were less than 6 months old compared to the US acquisitions.

### Segmentation

The 4D-US data were imported into Q-lab 10 (Philips Medical Systems, Bothell, WA, USA) where the DICOM data were converted into a Cartesian coordinate system. The y- and z-direction correspond to the length and depth of the AAA in the sagittal plane respectively (Figure 3.1A), whereas the x-direction corresponds with the width of the aneurysm in the



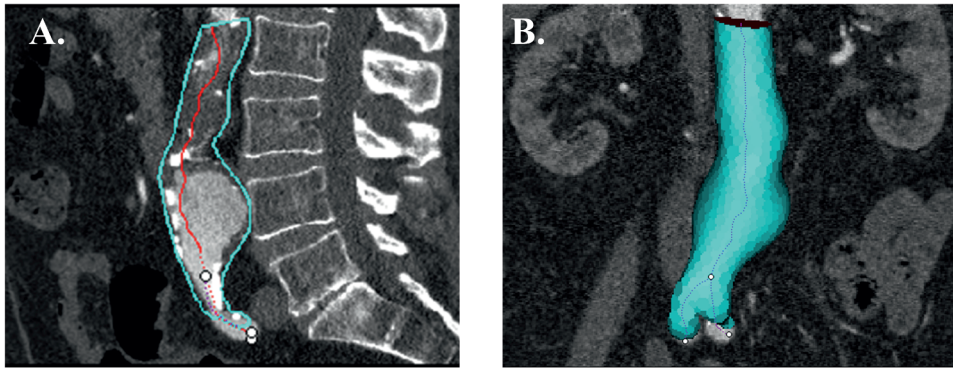


**Figure 3.2:** A sagittal (A) and coronal (B) view of the automatically segmented wall (*blue*) of an abdominal aortic aneurysm (AAA) in computed tomography data. The red solid (A) and purple dashed (B) lines represent the centerline of the AAA lumen, and the white dots visualize the bifurcation and the two distal ends.

transverse plane (Figure 3.1C). Spatial resolution of the acquired data ranged from 0.5-1.2 mm in x-direction, 0.7-1.1 mm in y-direction and 0.3-0.6 mm in z-direction.

Subsequently, the Cartesian 4D-US data were imported into Matlab (2015b, Mathworks Inc., Natick, MA, USA) and segmented manually using the transverse cross-sectional planes of the end-diastolic 3D volume of the US dataset. The end-diastolic 3D volume was denoted as the US volume with the lowest lumen volume of the AAA, derived after speckle tracking of the AAA wall in two longitudinal cross-sections. Each AAA was segmented from the proximal neck down to the bifurcation. Only the inner aortic wall was segmented since it was not always feasible to distinguish the outer wall from surrounding tissue. Each 4D-US data were segmented three times for all patients of which US and CT data were available, all others were segmented twice.

Next, the segmented AAA contours were regularized and up-sampled as described by Kok et al. (2015). An example of the resulting contours with the corresponding 3D-US data is shown in Figure 3.1E-F. The outer wall was obtained by interpolating the inner wall 2 mm in the radial direction, i.e. normal to the AAA surface (Speelman et al., 2008).

The contrast-enhanced CT-scans were semi-automatically segmented using Hemodyn, a software package developed by Philips Medical Systems (Best, The Netherlands) and the Eindhoven University of Technology (TU/e). This segmentation software is initiated by defining one proximal (neck) and two distal points (iliac arteries) (Breeuwer et al., 2008). A centerline was automatically detected, after which a three-dimensional active object was initiated around the centerline and adapted automatically until the AAA lumen-wall interface was found (Figure 3.2). Again, the wall thickness was assumed to be 2 mm for all patients.

The segmented end-diastolic AAA wall was tracked over time using 3D speckle tracking of the 4D-US data. A 3D coarse-to-fine block matching algorithm, using 3D cross correlation as a measure for similarity (Lopata et al., 2011), was adapted for aortic displacement estimation based on Cartesian DICOM data. The block matching algorithm consisted of 2 steps. First, the displacement estimation was performed in a large search window of  $12 \times 12 \times 8$  mm using a kernel of 2.0 by 2.0 by 1.5 mm to track the global motion of the AAA. Next, this procedure was repeated using a smaller search window of  $9 \times 9 \times 6$  mm and the initial displacement estimates as input to refine the displacement estimates.

### Finite element analysis

Before the AAA wall was converted into a mesh, both proximal and distal ends were elongated by 3 cm. The AAA geometry was elongated in the proximal directions warping into a vessel with a diameter of 2 mm parallel to the spine. In the distal direction, the AAA was elongated in the centerline direction. This type of elongation was applied to reduce the effects of the boundary conditions (fixation) on the stresses in the aneurysm (van Disseldorp

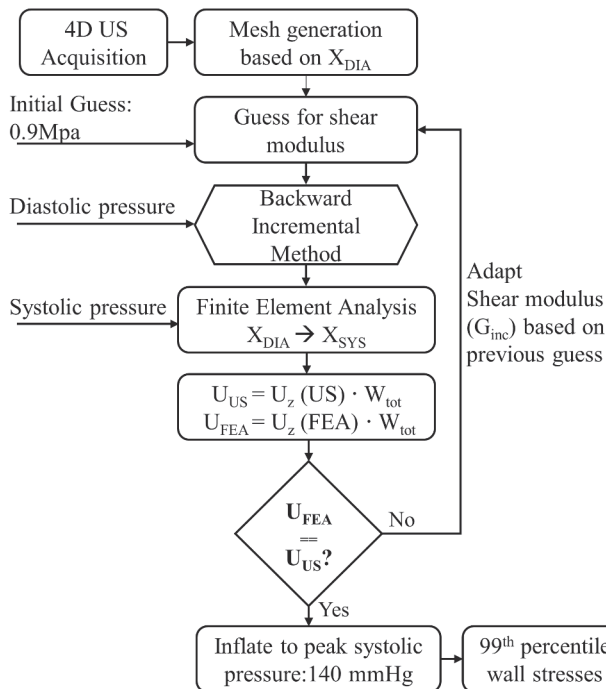


**Figure 3.3:** A graphical overview of the iterative process to determine the patient specific shear modulus and its 99<sup>th</sup> percentile wall stress.  $X_{DIA}$  and  $X_{SYS}$  represent the geometry at diastolic and systolic pressure,  $U_{US}$  and  $U_{FEA}$  the displacement in z-direction determined by ultrasound (US) and finite element analysis (FEA) and  $W_{tot}$  a weighting function.

et al., 2016a). Subsequently, a 10-node tetrahedral element mesh was created using the open-source mesh generator (Si, 2015). In total, 50.000 – 80.000 elements were used with at least two layers of elements present in the radial direction. The CT-based geometries were converted into meshes with a similar mesh density using 3 Matic version 5.1 (Materialise, Leuven, Belgium) due to the complex meshing procedure around the bifurcation.

The meshes were exported to Abaqus 6.14 (Dassault Systèmes, Paris, France) to calculate the AAA Von Mises wall stresses for both US and CT-based models. The proximal neck and the two distal iliac ends were constrained in all directions (boundary conditions). The AAA wall's mechanical behavior was described as being an incompressible Neo-Hookean material with a shear modulus of 0.9 MPa (Speelman et al., 2008), based on a linearization of the material model proposed by Raghavan and Vorp (2000) around the physiologic range.

The US-based finite element (FE) models corresponded to the AAA geometry at diastolic pressure, which are therefore not stress-free. To obtain the initial diastolic stresses in the diastolic geometry, the backward incremental method was prescribed for all FEA simulations (de Putter et al., 2007). For the CT-based FE models, not the diastolic pressure but the mean arterial pressure (MAP) was used to estimate the initial stresses in the mesh. The MAP is a better estimate of the initial load on the AAA wall, since the CT-scans were acquired during multiple heartbeats. Since no pressures were measured during the CT-scans, the MAP was based on the pressures measured directly after the US acquisition.

Next, the FE models were pressurized to a peak-systolic blood pressure of 140 mmHg, applied to the inner vessel wall of all FE models, and the Von Mises stresses were calculated. Furthermore, the 99<sup>th</sup> percentile wall stress was chosen as rupture risk estimator (Speelman et al., 2008).

### **Shear modulus characterization**

To determine the material properties of the aortic wall, the FEA model was calibrated using an iterative matching of the model output to the displacement data measured by US (Figure 3.3). In this iterative characterization method, each US-geometry at diastole was pressurized to the measured patient-specific systolic pressure. The nodal displacements were calculated in the systolic configuration and compared with the displacements estimated from the 4D-US acquisition.

Since the US displacement field is more accurately determined in the z-direction (axial) compared to the x- and y-direction, the comparison between the FEA displacements and US displacements was performed solely on the displacements in z-direction. A Gaussian-shaped weighting function ( $W_{\text{tot}}$ ) was defined and applied: regions with high displacements and/or regions where the direction of the ultrasound was perpendicular to the wall circumference were emphasized ( $W_{\text{tot}} = 1$ ), whereas regions with low axial displacements (left and right wall of the AAA) and regions where the propagation of the ultrasound was parallel to the wall's circumference were suppressed ( $W_{\text{tot}} = 0.2$ ).

The optimization procedure to estimate the incremental shear modulus ( $G_{inc}$ ) was terminated when the mean nodal displacements in the FEA and 4D-US acquisitions differed less than 1%. When the patient-specific  $G_{inc}$  was determined, the model was subsequently pressurized to the peak-systolic pressure of 140 mmHg to compare the 99<sup>th</sup> percentile stresses with those obtained with CT.

### Data analysis

The CT and US data were compared using the Dice coefficient or similarity index (SI). The SI is a measure for the percentile overlap between the two geometries, which is calculated by:

$$SI = \frac{2(P_{US} \cap P_{CT})}{(P_{US} + P_{CT})} \quad (3.1)$$

with  $P_{US}$  and  $P_{CT}$  the number of pixels in the US and CT geometry, respectively. Moreover, the 25<sup>th</sup>, 50<sup>th</sup>, 75<sup>th</sup>, 95<sup>th</sup>, and 99<sup>th</sup> percentile wall stress were calculated for all AAAs.

For the US-based FEA results, the 99<sup>th</sup> percentile wall stress was visualized as function of the maximum anterior-posterior (A-P) diameter of the AAA. Regression analysis was performed to examine a possible dependency of wall stress on diameter as shown in Speelman et al. (2008). Next, based on the 99<sup>th</sup> percentile wall stress, the patient population was equally divided into three groups. The material properties for these three groups were compared using a Wilcoxon rank sum test. Finally, the relation between the material properties and the AAA diameter was examined.

## 3.3 Results

All 40 US-based FE simulations succeeded with an average computational time of two hours on a single processor core (Intel Xeon E5-2667 v3, Santa Clara, California, USA).

### Comparison of Ultrasound vs. Computed Tomography

Figure 3.4A shows an example of the registered CT (*mesh*) and US (*solid lines*) geometry with an SI-index of 0.96. This figure shows that the field-of-view of the US geometry is smaller than the CT geometry and that the maximum diameter is captured in the US field-of-view. For each patient the three different SI-indices with their mean are shown in Figure 3.4B. For all seven matched geometries a good similarity (defined as  $SI \geq 0.7$ ) was achieved, with mean SI-indices ranging from 0.90 to 0.96. In Figure 3.4C several percentile wall stresses are shown for the US-based and CT-based geometries. It shows similar wall stress results, between US and CT, for the 25<sup>th</sup> to 95<sup>th</sup> percentile wall stresses of all seven patients. For the 99<sup>th</sup> percentile wall stress, the CT based geometry revealed higher stresses than those obtained using US in four out of seven patients.

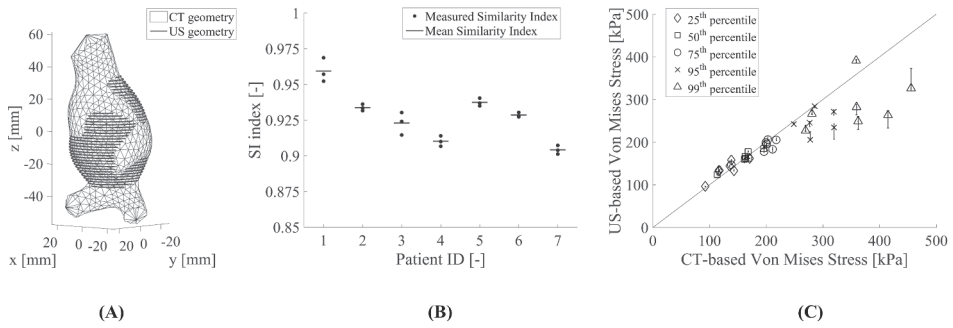


**Figure 3.4:** Segmentation obtained from computed tomography (CT) data (*mesh*) and ultrasound (US) data (*solid lines*) with a similarity index (SI) of 0.96 (A). The SIs are visualized in (B) for all patients included (*black dot*) with their mean indicated by the solid line. In (C) a comparison of the 25<sup>th</sup>, 50<sup>th</sup>, 75<sup>th</sup>, 95<sup>th</sup>, and 99<sup>th</sup> percentile wall stress for the CT and US based geometry is shown for the seven patients included. The line of equality was added as a visual aid (*solid line*).

### 99<sup>th</sup> Percentile Wall Stress

In Figure 3.5A-C a longitudinal cross-section view of three typical AAA geometries is shown. The segmented AAA geometry with its wall stress distribution is subsequently visualized in Figure 3.5D-F, whereby the elongation of the AAA geometry is represented by the mesh.

For all patients, the mean 99<sup>th</sup> percentile wall stresses of the multiple segmented AAA geometries are shown in Figure 3.6A. Regression analysis of the 99<sup>th</sup> percentile wall stress and the maximum diameter did not result in a significant linear relationship ( $R = 0.16$ ,  $p$ -value = 0.31).

Subsequently, all patients were equally divided in three groups (Figure 3.6B) and the patient-specific incremental shear moduli were visualized for each group in Figure 3.6C. No significant differences were observed when comparing these three groups. When the 99<sup>th</sup> percentile wall stress was calculated with the patient-specific shear modulus instead of the generic modulus similar stresses were obtained (mean difference  $\pm$  standard deviation:  $-2 \pm 4$  kPa).

### Patient-Specific Shear Modulus

The estimation of the patient-specific incremental shear modulus required 2 to 7 steps before the stop criterion was reached. The characterized modulus has a median of 1.1 MPa (interquartile range [IQR], 0.7 – 1.4 MPa). This modulus represents the slope of the stress-strain behavior of the AAA wall at the patient-specific blood pressure range. The patient-specific moduli were compared with the well-established model of Raghavan and Vorp (2000) at the physiological blood pressure range in Figure 3.7A. The median and IQR

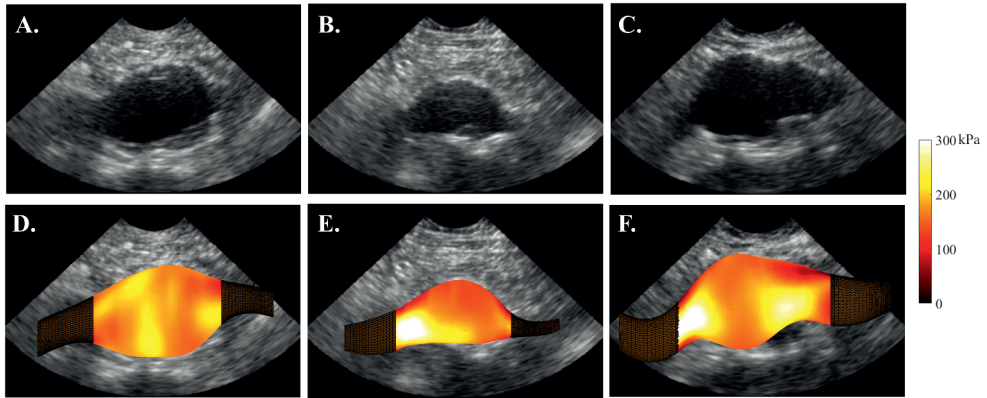


**Figure 3.5:** Longitudinal cross sectional views are shown for three typical abdominal aortic aneurysm geometries (A–C). The lower row (D–F) represents the Von Mises wall stress distribution, with the elongation of the geometry represented by the mesh.

of the patient-specific moduli are within the 95% confidence interval of the Raghavan and Vorp model.

In Figure 3.7B the mean incremental shear moduli are shown as function of the maximal AAA diameter. Subsequently, all patients were equally divided in a small, medium, and a large diameter group. The bar plot in Figure 3.7C shows that the incremental shear moduli in the small and medium diameter group do not significantly differ from each other (Wilcoxon rank sum test:  $p$ -value = 0.08), while the moduli between the small and large diameter groups are significantly different (Wilcoxon rank sum test:  $p$ -value = 0.03). The consequence of these observations is that the AAAs with a larger diameter consist of a “stiffer” aortic wall.

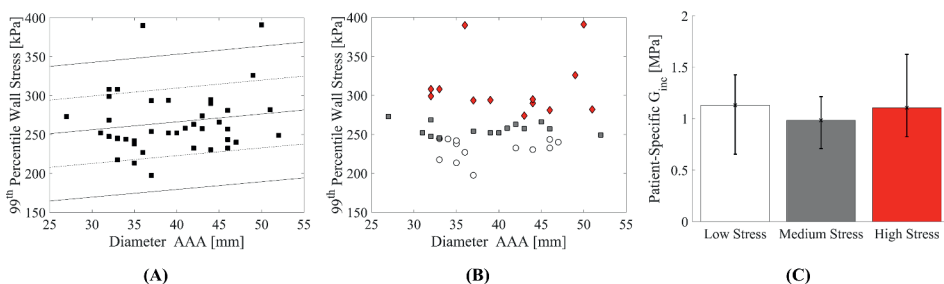


**Figure 3.6:** In (A) the regression model for the 99<sup>th</sup> percentile wall stress as a function of the aortic diameter is shown ( $R = 0.16$ ,  $p = 0.31$ ). Based on the 99<sup>th</sup> percentile wall stress, all AAAs are equally divided into a low (*white circles*), middle (*grey squares*), and high stress (*red diamonds*) group (B). In (C) the patient specific incremental shear modulus (*median  $G_{inc}$* ) is shown for the low, medium and high stress groups with its interquartile range.

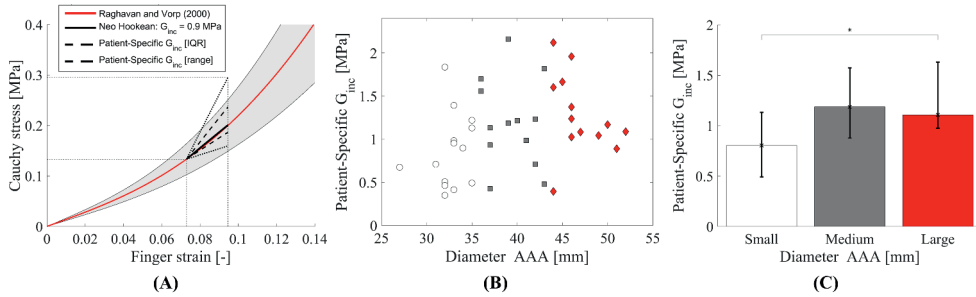


**Figure 3.7:** (A) The stress–strain curve of the Raghavan and Vorp (2000) model is shown with its 95% confidence interval (*red line with grey area*). The median and interquartile range [IQR] (*black stripped line*) of the derived patient-specific shear moduli are within this 95% confidence interval. The complete range is visualized with the black dashed line. (B) All patient specific incremental shear moduli ( $G_{inc}$ ) are shown as function of the diameter. All abdominal aortic aneurysms are equally divided into a small (*white circles*), middle (*grey squares*), and large diameter (*red diamonds*) group. (C) The patient specific incremental shear modulus (median  $G_{inc}$ ) is shown for the small, medium, and large diameter groups with its interquartile range. The median incremental shear modulus of the large diameter group is significantly higher than that obtained from the small diameter group ( $p = .03$ ), indicated by the asterisk.

### 3.4 Discussion

In this study, wall stress analysis of AAAs was performed using 4D ultrasound for the entire diameter range. The advantage of using 4D ultrasound is the ability to perform wall stress analysis on the majority of AAA patients which are under surveillance in the outpatient clinic. Besides wall stress analysis, also the patient-specific material properties were determined using the dynamic behavior of the AAA wall.

This study shows similar results for the 99<sup>th</sup> percentile wall stress as found by Speelman et al. (2008). The main differences between these studies is that in our study, patients with an AAA diameter between 27 and 52 mm are included whereas in Speelman’s CT-work the AAA diameters ranged between 44 and 57 mm. The presence of small diameter AAAs is a direct result of the use of US imaging. The difference in AAA diameter could be a possible cause for the non-significant regression between the wall stress and AAA diameter found in this study.

For a sub-group of patients, CT data were available, which showed similar results as in the corresponding 4D-US datasets. For the 99<sup>th</sup> percentile wall stresses, the CT data exceed the US data by 5-58%, possibly induced by oversmoothing of the US segmentation. In a previous study by our group, larger percentile stresses revealed a large mismatch between US and CT due to registration artifacts in the US data (Kok et al., 2015). These artifacts were caused by registering multiple US acquisitions in order to enlarge the field-of-view. In this study, only single volumes were used, thereby avoiding this issue. However, to increase

the patient inclusion rate, the registration of multiple US datasets is still an important next step.

The advantage of US-based wall stress analysis is the ability to determine the patient-specific AAA material properties. When these properties are compared with the tensile test results of Raghavan and Vorp (2000), 80% of the moduli are within their 95% confidence interval. These properties could be an important parameter in monitoring aneurysm growth and rupture risk assessment. Moreover, this study suggests that the AAA wall becomes stiffer when the diameter increases, which can potentially be an indicator for AAA growth. However, inclusion of more patients is required to strengthen this finding.

One of the limitations of 4D-US is the relatively low frame rate. Obviously, one could miss the exact peak or minimum volume, which will lead to an overestimation of the shear modulus. In a future study, a comparison between 4D-US and high(er) frame rate US techniques should be performed. Besides the frame rate of US, also the field-of-view is limited. A larger field-of-view would increase patient inclusion, although a potential solution could be the fusion of multiple 3D volume datasets. Another possible drawback can be the low image contrast due to unfavorable anatomy or considerable attenuation due to high body weight. Finally, the use of DICOM limits the precision of the displacement estimates. Especially in AAAs, where relatively small displacements are present. In those cases, the use of the raw radio-frequency data could improve the displacement estimation.

Blood pressure was only measured during the US examination, which could lead to discrepancies found between US and CT-data. Ultimately, one would desire the intravascular blood pressure, however, this would seriously increase the burden on the patient and render the whole procedure invasive.

In this study, no calcifications and intraluminal thrombus were incorporated in the wall stress simulations, which could be included in future research (Li et al., 2008). Besides adding local material properties, a more complex non-linear material model could be employed. However, introducing a more complex material model could also result in higher parameter uncertainties when determining material properties patient-specifically.

### 3.5 Conclusion

4D ultrasound provides the ability to perform wall stress analysis on AAAs ranging from small to large diameters. Results are similar as previously reported using other imaging modalities, which elicits the opportunity to perform wall stress analysis over time. Besides assessing wall stress, also the material properties representative for the specific patient could be determined. A longitudinal study should be performed to examine a possible relation with AAA growth or rupture.





# Quantification of Aortic Stiffness and Wall Stress in Healthy Volunteers and Abdominal Aortic Aneurysm Patients using Time-Resolved 3D Ultrasound: a Comparison Study

This chapter is based on: Quantification of Aortic Stiffness and Wall Stress in Healthy Volunteers and Abdominal Aortic Aneurysm Patients using Time-Resolved 3D Ultrasound: a Comparison Study, **E.M.J. van Disseldorp**, N.J. Petterson, EN. van de Vosse, M.R.H.M. van Sambeek, and R.G.P. Lopata, Accepted: *European Heart Journal: Cardiovascular Imaging*, 2018;

## Abstract

**Background:** Using non-invasive 3D ultrasound (US), peak wall stresses and aortic stiffness can be evaluated, which may provide additional criteria in abdominal aortic aneurysm (AAA) risk assessment. In this study, these measures were determined in both young and age-matched individuals, and AAA patients while its relation to age, maximum diameter, and growth was assessed statistically.

**Methods:** Time-resolved 3D-US data were acquired for 30 volunteers and 65 AAA patients. The aortic geometry was segmented, and tracked over the cardiac cycle using 3D speckle tracking to characterize the wall motion. Wall stress analysis was performed using finite element analysis. Model parameters were optimized until the model output matched the measured 3D displacements.

**Results:** A significant increase in aortic stiffness was measured between the age-matched volunteers (median 0.58, IQR: 0.48 – 0.71 kPa·m) and the small AAA patients (median 1.84, IQR: 1.38 – 2.46 kPa·m,  $p < .001$ ). In addition, an increase in aortic stiffness was evaluated between the small (30 - 39 mm) and large ( $\geq 50$  mm) AAAs (median: 2.72, IQR: 1.99 – 3.14 kPa·m,  $p = 0.01$ ). The 99th percentile wall stress showed a positive correlation with diameter ( $\rho = 0.73$ ,  $p < .001$ , and significant differences between age-matched volunteers and AAA patients).

**Conclusions:** The AAA pathology causes an early and significant increase in aortic stiffness of the abdominal aorta, even after correcting for the expected effect of ageing and differences in arterial pressure. Moreover, some AAAs revealed relatively high peak wall stress, although the maximum diameter was below the threshold for surgical repair. Using the current method, these measures become available during follow-up, which could improve AAA rupture risk assessment.

## 4.1 Introduction

An abdominal aortic aneurysm (AAA) is a progressive widening of the aorta which eventually may rupture when no medical treatment is performed. The majority of all AAAs are asymptomatic until rupture, which leads to a life threatening hemorrhage. Therefore, surgical repair is performed when the risk of rupture outweighs the risk of surgery. Current clinical guidelines suggest to perform operative repair of the aneurysm: 1) when the maximum diameter is larger than 55 mm for men and 52 mm for women, 2) if rapid growth is observed (maximum diameter > 10 mm/year), or 3) when the aneurysm becomes symptomatic (Moll et al., 2011). Although these guidelines are based on large randomized controlled trials, a population-based average is used to quantify the individual patient-specific rupture risk (The UK Small Aneurysm Trial Participants, 1998; Lederle et al., 2002b). As a consequence of current AAA management, small aneurysms prone for rupture are left untreated despite the fact that 2 – 10% of all AAAs rupture before the threshold for surgical intervention is reached (Nicholls et al., 1998; Lederle et al., 2002b). Thereby, other AAAs which are currently treated might be exposed to unnecessary surgical risks since the aneurysm could remain stable (Conway et al., 2001; Lederle et al., 2002a). These data suggest that maximum diameter evaluation alone is not sufficient to predict the patient-specific rupture risk of an AAA and a more personalized approach is needed.

From a biomechanics perspective, AAA wall mechanics plays an important role in the distinction between stable and more susceptible aneurysms. Wall stress analysis has been proposed in literature, which provides the peak stress in the aortic wall based on the AAA geometry, blood pressure, and mechanical properties of the AAA wall. The merit of these models has been shown first in the studies by Fillinger et al. (2002) and (Venkatasubramanian et al., 2004) It showed that symptomatic, and ruptured AAAs had a higher peak wall stress (PWS) compared to the asymptomatic, non-ruptured AAAs. Later, in a meta-analysis of Khosla et al. (2014) including nine consecutive studies, this finding was strengthened and remained significant when the systolic blood pressure was standardized for all patients at 120 mmHg. Finally, Gasser et al. (2014) showed in a large retrospective study with 243 patients that the peak wall stress is higher in ruptured than non-ruptured cases which could help clinical decision making. Despite the promising results, wall stress analysis has not yet been introduced in clinical workflow due to the lack of clinical validation based on prospective clinical trials. The main reason is the use of CT imaging for geometry assessment in current studies which suffer from its drawbacks, such as radiation exposure and the use of nephrotoxic contrast agents. Magnetic Resonance Imaging (MRI) has been proposed as alternative but is not easily implemented due to the long scan time and high costs (de Putter et al., 2007).

Recently, three-dimensional (3D) ultrasound has been clinically introduced and showed its feasibility in the assessment of the full 3D AAA geometry. Ultrasound (US) based wall stress analysis has been proposed and showed similar wall stress results compared to CT

imaging (Kok et al., 2015). Thereby, 3D US is relatively cheap and it does not suffer from the drawbacks of using CT or MRI imaging. Of course, 3D US has a limited field of view, but if the shoulders of the AAA, i.e., the areas with high curvature, are in the acquired image, wall stress analysis can be performed accurately (van Disseldorp et al., 2016a). Consequently, 3D US is an ideal imaging modality to calculate PWS in a prospective clinical study.

In addition, using 4D (time-resolved 3D) US imaging not only wall stress analysis can be performed. By capturing the dynamic motion of the aortic wall, the strain and mechanical properties of the AAA wall can be assessed simultaneously by fitting the displacements in the finite element model to the measured US-based 3D displacement field (Wittek et al., 2016; van Disseldorp et al., 2016b). Moreover, the use of (time-resolved) 3D US opens new opportunities to perform studies on smaller aneurysms and even healthy volunteers, which is not feasible with CT and MR due to the aforementioned drawbacks or practical issues.

The purpose of this study was to characterize the aortic stiffness and peak wall stress in young individuals, age-matched individuals, and AAA patients, and compare the results between normal aortas and aortas with different degrees of aneurysmal disease. Their relation to age, maximum diameter, and growth was assessed and statistically analyzed.

## 4.2 Materials and Methods

### Study population

Time-resolved 3D US data were acquired for 30 healthy volunteers and 65 abdominal aortic aneurysm (AAA) patients during breath hold. All participants gave informed consent to this study, which was approved by the local ethics committee. The healthy volunteers consisted of a relatively young participants group with an age < 30 years (N = 10, average age of  $24.0 \pm 2.0$  years) and a group of participants which were at least 55 years old (N = 20, average age of  $59.3 \pm 6.6$  years). All 65 AAA patients were divided in three different groups based on the maximum diameter of the aneurysm, i.e., small AAAs (diameter 30 – 39 mm, N = 25), moderate AAAs (diameter 40 – 49 mm, N = 20), and large AAAs with a diameter larger or equal to 50 mm (N = 20). Current groups were determined based on the recommended surveillance interval during outpatient follow-up. An example of the acquired US data for each group is shown in Figure 4.1, whereas demographic data are listed in Table 4.1.

### Data acquisition

All time-resolved 3D ultrasound acquisitions were obtained using a Philips iU22 (N = 86) or Philips EPIQ 7 (N = 9) system with the same transducer, a Philips X6-1 matrix curved array probe (Philips Medical Systems, Bothell, WA, USA) with a center frequency of 3.5 MHz. The ultrasound data were recorded in supine position during multiple heartbeats with an acquisition rate of 4 - 8 volumes per second, to ensure that the peak systole and

**Table 4.1:** Patient demographics for each of the five different groups

Variables	Volunteers		Abdominal Aortic Aneurysm Patients		
	Young	Age-matched	Small	Moderate	Large
Gender (M/F)	4 : 6	11 : 9	24 : 1	19 : 1	18 : 2
Age (years) <sup>a</sup>	24 (21 - 28)	58 (51 - 77)	72 (62 - 84)	76 (65 - 87)	76 (59 - 90)
Diastolic blood pressure (mmHg) <sup>b</sup>	69 (65 - 74)	83 (80 - 89)	87 (81 - 93)	81 (74 - 88)	83 (74 - 91)
Systolic blood pressure (mmHg) <sup>b</sup>	112 (107 - 133)	138 (131 - 154)	144 (135 - 163)	146 (134 - 152)	137 (123 - 148)
Max. diameter (mm) <sup>a</sup>	16 (14 - 19)	21 (13 - 29)	35 (31 - 39)	45 (40 - 49)	51 (50 - 63)
Growth (mm/year) <sup>a</sup>	N/A	N/A	0 (0 - 1)	3 (1 - 4)	4 (3 - 6)

<sup>a</sup> Values are reported as median and range; <sup>b</sup> as median and interquartile range; N/A = not applicable

end diastole was captured in the data. Brachial pressure was measured directly after the ultrasound acquisition using an automatic arm cuff.

The acquired US data were converted offline into a Cartesian coordinate system with a ranging field of view of (6 to 20) cm by (10 to 24) cm by (6 to 16) cm in width, length, and depth, respectively. The corresponding spatial resolution of the US data ranged between (0.5 to 1.3) mm x (0.4 to 1.3) mm x (0.3 to 0.7) mm.

### Data processing and biomechanical analysis

All 95 volumes were segmented in the end-diastolic phase and the aortic geometry was regularized as previously was described by Kok et al. (2015), and van Disseldorp et al. (2016b). The aortic wall was tracked over the cardiac cycle using a 3D coarse to fine block matching algorithm which was adapted for 3D displacement estimation of Cartesian DICOM data (Lopata et al., 2011). In the first step of the displacement algorithm the global motion of the aorta was tracked using a kernel size of (4.5 x 4.5 x 2.3) mm<sup>3</sup> and a search window of (14 x 14 x 12) mm<sup>3</sup>. Afterwards, the same kernel size was used to calculate the final displacements in a smaller updated search window of (10 x 10 x 7) mm<sup>3</sup> with the previous estimate as input.

The diastolic aortic geometries were elongated and converted into a hexahedral mesh with a constant wall thickness of 2 mm (Speelman et al., 2008). The geometries were together with the estimated 3D wall displacements and the measured brachial blood pressure input for an iterative finite element approach using Abaqus 6.14 (Dessault Systèmes, Paris, France). An initial value for the wall stiffness (shear modulus multiplied by the wall thickness) of 0.2 kPa·m for the healthy volunteers and 1.8 kPa·m for all AAA patients was applied (Speelman et al., 2008; van Disseldorp et al., 2016b). Optimization of the model

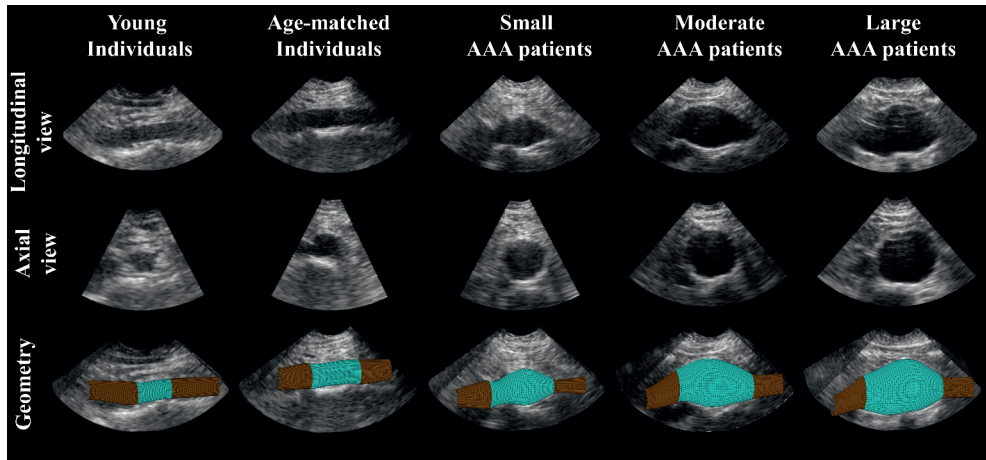


**Figure 4.1:** From left to right: examples of a longitudinal and cross-sectional view of the 3D ultrasound data for a young, and age-matched individual, and a small, moderate, and large abdominal aortic aneurysm (AAA) patient. At the bottom row the segmented geometry is shown (*blue*) with the elongation needed for correct wall stress analysis (*brown*).

was performed by changing the wall stiffness while comparing the displacements in the finite element model to the US displacements. A schematic overview of the proposed characterization method is shown for a healthy volunteer and an AAA patient in Figure 4.2.

Convergence was achieved when the estimated wall stiffness differed less than 1% with the previous estimate. Finally, in order to obtain the peak wall stresses at an equivalent pressure for each subject, the internal pressure in the aorta was increased to 140 mmHg and the peak stress distribution in the aortic wall was obtained. In this study, the 99<sup>th</sup> percentile wall stress was calculated and used as peak stress criterion for the aortic wall (Speelman et al., 2008).

### Statistical analysis

Data analyses were performed using MATLAB R2017a (Mathworks Inc., Natick, MA, USA). In order to correct for the difference in arterial pressure between each individual, the aortic stiffness was linearly scaled to a mean arterial pressure (MAP) of 100 mmHg, and expressed as mean value with standard deviation. Normality was tested by the one-sample Kolmogorov-Smirnov test. Regression analysis was performed to examine a possible dependency of aortic stiffness due to aging in the young and age-matched volunteer population. Differences between the three different groups and the volunteers were compared with the Wilcoxon rank sum test. The correlations between aortic stiffness, diameters, peak wall stress and age were evaluated using Spearman Rank correlation method. For all statistical tests a p-value below 0.05 was considered to be significant.

### 4.3 Results

For each volunteer and AAA patient the aortic stiffness and 99<sup>th</sup> percentile wall stress were calculated. For the examples shown in Figure 4.2, the wall displacements and stresses are visualized. Mechanical analysis resulted in a corresponding aortic stiffness of  $(181 \pm 2)$  kPa·m for this specific volunteers and  $(840 \pm 15)$  kPa·m for the AAA patient. A 99<sup>th</sup> percentile peak wall stress of 168 kPa and 244 kPa, were observed, respectively.

#### Aortic stiffness vs. aging

In Figure 4.3, the aortic stiffness is visualized as function of age for all young and age-matched volunteers, and AAA patients. Stiffness measurements were significantly higher for the age-matched volunteers compared to the young volunteers ( $p < .001$ ) and between

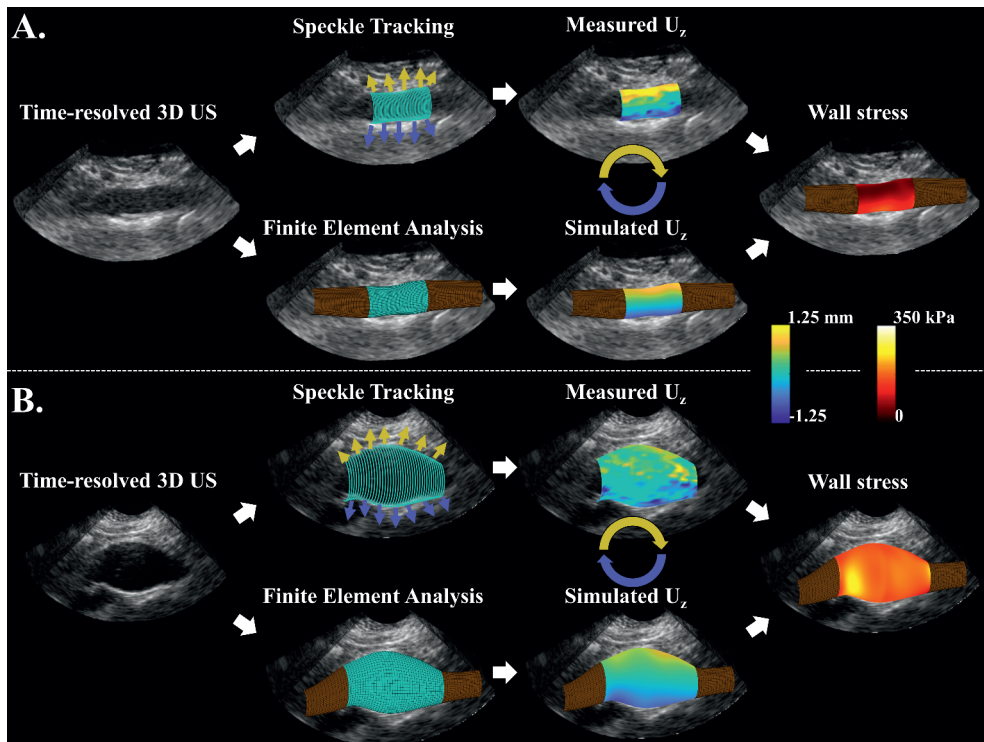


**Figure 4.2:** A schematic overview of the mechanical characterization with results for one volunteer (A) and one abdominal aortic aneurysm (AAA) patient (B). The segmented geometry was used to track the displacements using 3D speckle tracking and as input for a finite element model (please note that the displacement-arrows are illustrative, and not scaled). The measured axial displacements were fitted to the simulated displacements resulting in the subject specific aortic stiffness. Finally, the wall stress distribution at peak pressure is visualized for both cases.



the age-matched volunteers versus AAA patients ( $p < .001$ ). Correlation and regression analysis were performed to analyze the effect of arterial stiffening due to ageing. It showed a significant relation within the volunteer population ( $R^2 = 0.33$ ,  $p < .001$ ), but within the AAA patients no correlation between age and stiffness was observed ( $p = .60$ ).

### Aortic stiffness vs. aortic diameter

The aortic stiffness as function of the diameter is shown in a scatterplot in Figure 4.4A. A positive correlation between stiffness and diameter is observed in the volunteer population ( $\rho = 0.55$ ,  $p = .002$ ) and within the AAA patients ( $\rho = 0.33$ ,  $p = .007$ ). The median aortic stiffness with interquartile range (IQR) is 0.23 (0.22 – 0.29) kPa·m for the young volunteers, 0.58 (0.48 – 0.71) kPa·m for the age-matched volunteers, 1.84 (1.38 – 2.46) kPa·m for the small AAAs (diameter 31 – 39 mm), 2.04 (1.73 – 3.65) kPa·m for the moderate AAAs (diameter 40 - 49 mm), and 2.72 (1.99 – 3.14) kPa·m for the large AAAs. The grouped aortic stiffness values are visualized in a box-and-whiskers plots in Figure 4.4B. A significant difference was observed between the age-matched volunteers and all AAAs (all  $p < .001$ ), and between the small and large AAAs ( $p = .01$ ).

In Figure 4.5, the box-and-whiskers plots show the relative aortic stiffness for each of the five different groups when the arterial stiffness is corrected for the effect of ageing, i.e., the observed regression found in the volunteer group. This figure shows that the major increase in aortic stiffness between the volunteers and AAA patients is due to the aneurysm

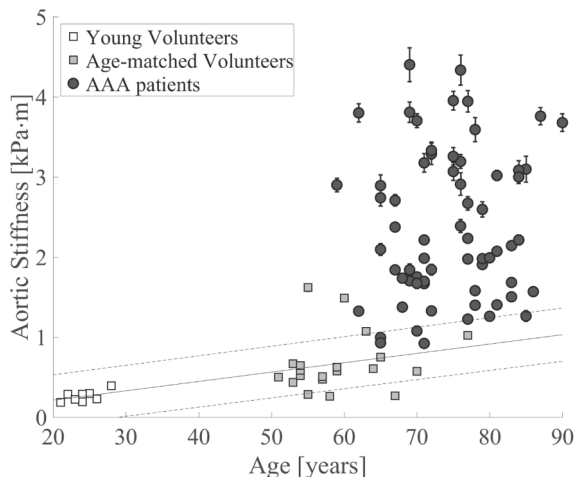


**Figure 4.3:** Measured aortic stiffness with estimated standard error to the mean as a function of age for young, age-matched volunteers, and abdominal aortic aneurysm (AAA) patients. The white and gray squares represent the young and age-matched volunteers, while the black circles show the AAA patients. The black line represents the regression line of the increase in aortic stiffness as function of age in healthy volunteers ( $R^2 = 0.33$ ,  $p < .001$ ).

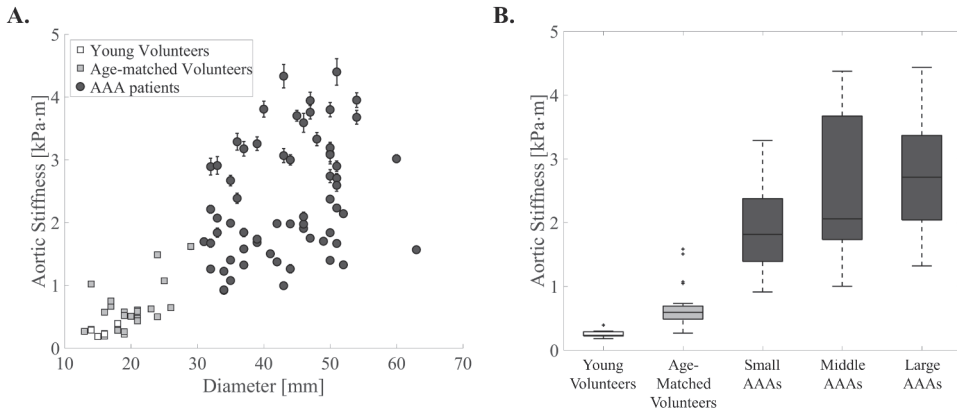


**Figure 4.4:** (A) Scatterplot of the aortic stiffness with standard deviation as function of the maximum aortic diameter for the volunteers (*gray squares*) and abdominal aortic aneurysm (AAA) patients (*black circles*) (B) Box-and-whiskers plots of aortic stiffness of the young and age-matched volunteers, and small, moderate, and large AAAs. A significant increase in stiffness is shown between the age-matched volunteers and small AAAs ( $p < .001$ ), but also between the small and large AAAs ( $p = .01$ ).

disease and is not effected by a possible relation with age.

Aortic stiffness was also correlated with AAA growth in the preceding year. Although, as expected, the maximum diameter correlated with preceding growth ( $\rho = 0.70$ ,  $p < .001$ ), no correlation was determined between aortic stiffness and growth ( $\rho = 0.10$ ,  $p = .44$ ) and between growth and 99<sup>th</sup> percentile wall stress ( $\rho = 0.13$ ,  $p = .32$ ).

### 99<sup>th</sup> percentile wall stress

Figure 4.6 shows the 99<sup>th</sup> percentile wall stress (with the 89.5<sup>th</sup> – 99.5<sup>th</sup> range as a dispersion measure) as function of the aortic diameter for all participants. Although some spread in the data is observed, a positive correlation between diameter and 99<sup>th</sup> percentile wall stress is visible ( $\rho = 0.73$ ,  $p < .001$ ). The age-matched volunteers have a significant lower 99<sup>th</sup> percentile wall stress compared to the AAA patients (all  $p < .001$ ), but no significant differences were observed when compared to the young volunteers ( $\rho = 0.22$ ). More interesting, some patients with a relatively large aortic diameter ( $> 5.0$  cm) are observed with a 99<sup>th</sup> percentile wall stress similar to healthy volunteers, while other large AAAs with an equivalent diameter have an increased, almost twice as high, 99<sup>th</sup> percentile wall stress ( $\leq 400$  kPa).

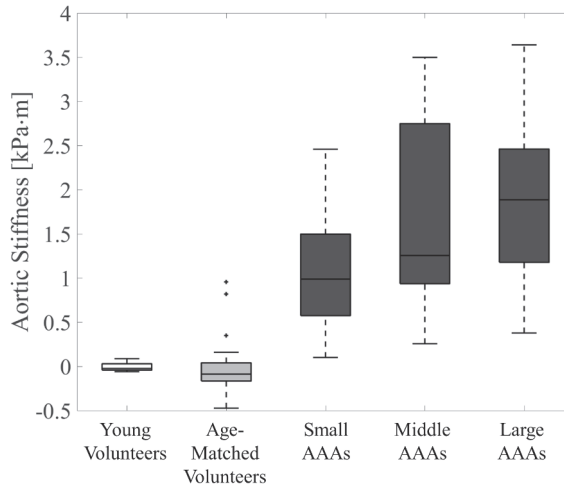


**Figure 4.5:** Box-and-whiskers plots of the aortic stiffness after the stiffness is corrected for the influence of ageing by subtracting the expected stiffness based on regression analysis. This relative aortic stiffness is shown for the young and age-matched volunteers, and the small, moderate, and large abdominal aortic aneurysm (AAA) patients.

#### 4.4 Discussion

In this study it has been demonstrated that time-resolved 3D ultrasound can be used to assess the aortic stiffness and peak wall stresses *in vivo*, which provides powerful opportunities in detecting and monitoring aneurysm disease in an early or even prior stage. The mechanical parameters were compared between young volunteers and age-matched healthy volunteers, and with AAA patients which cover the entire diameter range in follow-up. The two main findings of this study are:

1. The AAA pathology causes a significant increase in stiffness of the abdominal aorta in an early stage: local aortic stiffness was compared between healthy age-matched volunteers and AAA patients and showed significant differences, even after correcting for differences in mean arterial pressure and the expected effect of ageing.
2. Peak wall stresses assessed for volunteers and AAA patients showed a significant correlation with diameter. Moreover, AAA patients with peak stresses similar to volunteers were observed while others patients with equivalent diameters may have an increased peak wall stress, and potentially elevated rupture risk.

From a clinical perspective it would be a great value to identify those AAAs who have a high possibility of growth. This additional information could be used to personalize the follow-up management and to identify patients at risk. In a study by Raaz et al. (2015) the temporal relationship between arterial stiffening and AAA growth was assessed in a

murine model. This study showed that arterial stiffening precedes by aneurysmal dilatation, suggesting that aortic dilatation is an active process. In our current study, aortic stiffness was measured in a clinical setting during regular follow-up. It showed its feasibility and ability to detect differences in aortic stiffness between healthy volunteers and AAA patients, and within small and large AAAs. Interestingly, the aortic stiffness did not correlate with the AAA growth in the year prior to the stiffness measurements. A possible explanation is that AAA growth is the result of an increased aortic stiffness, and not vice versa (Raaz et al., 2015). To verify this hypothesis, a follow-up study could be employed using the current method to examine if this relationship is also found in AAA patients.

Few studies compared the local aortic stiffness between AAA patients and healthy volunteers, and to our knowledge this study is the first that compares both stiffness and 99<sup>th</sup> percentile peak wall stresses between volunteers and AAA patients. Current results are in good agreement with the results obtained by Li et al. (2013) using pulse wave velocity imaging (PWVI). In this study the arterial wall motion due to the blood pressure pulse wave was used to assess the regional arterial stiffness. An average pulse wave velocity of 6.03 and 10.54 m/s was measured for normal and AAA subjects, which corresponds with an aortic stiffness of 0.26 and 1.57 kPa-m, respectively (versus 0.23 and 1.98 kPa-m in current study). Derwich et al. (2016) characterized the aortic strain using 4D ultrasound between volunteers and AAA patients. Besides spatial heterogeneity in strain, also differences in mean circumferential strain were observed. These results correspond with current findings, assuming similar physiological blood pressures in both groups, an increased aortic stiffness in AAA patients will result in a decreased mean circumferential strain as

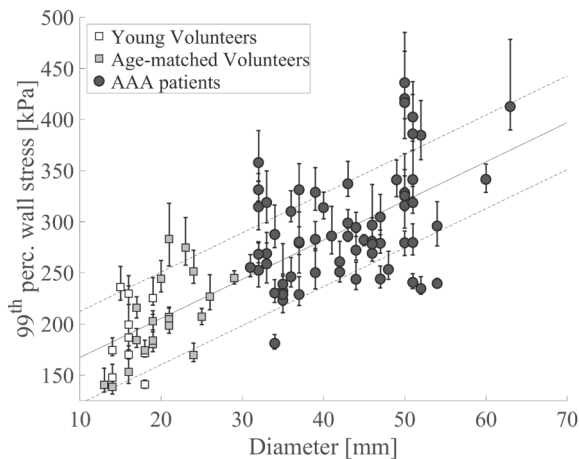


**Figure 4.6:** The 99<sup>th</sup> percentile peak wall stress as a function of the maximum aortic diameter for the volunteers (*squares*) and the abdominal aortic aneurysm patients (*circles*). Error bars represent the 89.5<sup>th</sup> – 99.5<sup>th</sup> stress range for each individual. The black line is a regression line with its standard deviation ( $R^2 = 0.57$ ,  $p < 0.001$ ).

suggested. However, strain was not part of the scope of this study. Thereby, measuring local aortic stiffness is not only limited to ultrasound imaging. Using external mechanical waves induced by a pneumatic driver magnetic resonance elastography (MRE) can be used to characterize various soft tissues. Recently, abdominal aortic MRE was performed on AAA patients and normal individuals (Kolipaka et al., 2016), and showed similar relative differences as reported in this study.

Patients with high aortic stiffness showed a larger standard deviation (SD) compared to the more compliant aortas. An explanation for this observation could be the use of DICOM data, which limits the precision of the displacement estimation. In relatively stiff AAAs the aortic displacements are small which introduces a larger uncertainty in the model calibration. In the future, the availability and use of raw frequency US data will improve the displacements estimation and thus the expected error on the parameter estimates.

The use of US-based wall stress analysis has the advantage that it is not limited to only large AAAs, as is the case with CT, but also allows the analysis of the peak wall stresses for healthy volunteers and small AAAs. Figure 4.6 showed overall higher 99<sup>th</sup> percentile wall stresses for AAA patients compared to the volunteers, and a significant correlation with diameter. However, an enlarged aortic diameter does not necessarily result in an increased peak wall stress (PWS). These findings are in line with previous CT-based studies which showed that PWS can distinguish between stable and possibly threatening AAAs. Next step in current research is to follow these patients over time to examine whether the small AAAs with high PWS are more prone to accelerated growth and rupture compared to the low PWS patients with similar diameters, how PWS evolves over time, and when large changes in aortic stiffness occur. The use of 3D ultrasound enables these future follow-up studies, however, this was beyond the scope of the current study.

One of the limitations in this current study is the use of a constant wall thickness. Since wall thickness is directly related to aortic stiffness and local variations in wall thickness, it will influence the wall stress distribution and its absolute values. However, using current ultrasound techniques it is not possible to extract the patient-specific and regional wall thickness at the specific depth of 8 – 10 cm where the majority of the aneurysm are located. Intra-vascular ultrasound could solve this issue, although it would make this technique more invasive.

In addition, good image quality is essential to obtain reliable measures for the aortic wall stiffness and PWS. For some patients with a limited echogenicity, 3D ultrasound imaging will still be challenging due to the depth of the AAA, the presence of bowel gas, or calcifications in the aortic wall leading to acoustic shadowing. Image quality might be improved using novel compounding techniques, i.e., the use of multiple ultrasound acquisitions from different angles and positions.

Ultimately, a regional stiffness map of the AAA would improve the understanding of mechanical alterations due to the AAA pathology. Calcified and more compliant regions could be detected, which subsequently also will improve the calibration of the finite ele-

ment model to predict wall stresses more accurately. However, this was beyond the scope of the present study. Finally, verification of the aortic stiffness would strengthen current findings. *In vitro* bi-axial tensile testing of corresponding AAA tissue would be an appropriate method to characterize the stiffness *ex vivo*. However, tissue samples are not available in volunteers and are limited available in patients. The majority of the AAA patients are currently treated using endovascular aortic repair, therefore only patients undergoing open surgery would yield samples for *ex vivo* validation.

## 4.5 Conclusion

Using an easy applicable and non-invasive 3D ultrasound method, aortic stiffness and peak wall stresses were calculated in healthy and aneurysmal aortas for a large range of age and AAA diameters. Results showed an early and significant increase in stiffness as a result of the AAA pathophysiology, and cases with relatively high peak wall stress despite a maximum diameter below the current threshold. These measures can provide additional criteria in AAA risk assessment in the future, especially since it is now available during follow-up using an economical and harmless imaging modality, and reference values can be established.



# Wall Stress Analysis using Multi-Perspective 3D Ultrasound Imaging of Abdominal Aortic Aneurysms

This chapter is based on: Multi-Perspective 3D Ultrasound Imaging and Geometry Assessment of Abdominal Aortic Aneurysms, **E.M.J. van Disseldorp**, J.J. van Dronkelaar, J.P.W. Pluim, M.R.H.M. van Sambeek, and R.G.P. Lopata, In revision: *European Journal of Vascular and Endovascular Surgery*, 2018;



## Abstract

**Background:** Current clinical guidelines for surgical repair of abdominal aortic aneurysms (AAAs) are primarily based on maximum diameter assessment. From a biomechanical point of view, not only the diameter but also peak wall stresses will play an important role in rupture risk assessment. These methods require the patient-specific geometry which typically utilize computed tomography (CT) or magnetic resonance imaging. Recently, wall stress analysis based on 3D ultrasound (US) has been proposed, which showed promising results. However, the major limitations in these studies were the use of manual segmentation and the limiting field-of-view of US. Therefore in this study, the AAA is imaged with multi-perspective 3D ultrasound, merged to obtain a large field-of-view, and afterwards automatically segmented. Geometry and wall stress results were validated using CT imaging.

**Methods:** 3D US and CT data were acquired for 40 AAA patients (max. diameter: 34 – 61 mm). The full US-based AAA geometry was determined using automatic segmentation, and, in case the aneurysm exceeded a single 3D volume, automatic fusion of multiple 3D US volumes was used. Wall stress analysis was performed for all AAA patients and percentile wall stresses were derived. Accuracy of the US-based geometry and wall stress prediction was measured by comparison with CT data.

**Results:** Estimated geometries showed good similarity, i.e., an overall median Similarity Index (SI) with interquartile range = 0.89 (0.87 – 0.92), whereas the median Hausdorff distances (HD), a measure for the maximum local mismatch, was 4.6 (4.0 – 5.9) mm for all AAA geometries. Thereby, the wall stress results based on merged multi-perspective 3D US data revealed a higher similarity with CT compared to single 3D US data.

**Conclusions:** This study showed that large volume geometry assessment of AAAs using multi-perspective 3D ultrasound, segmentation, and fusion is feasible in a robust and labor efficient manner.

## 5.1 Introduction

Abdominal aortic aneurysms (AAAs) are local enlargements of the abdominal aorta. The majority of AAAs are asymptomatic until rupture, which causes a large abdominal hemorrhage and results in an overall mortality of approximately 80% (Reimerink et al., 2013). Therefore, surgical guidelines suggest operative repair when the risk of rupture outweighs the risk of the surgical intervention. Currently, surgical intervention is suggested when the AAA diameter exceeds 55 mm ( $> 52$  mm for women) or in case of rapid growth (i.e.  $\geq 1$  cm/year) (Moll et al., 2011). However, small aneurysms with a maximum diameter below the threshold do rupture, while others remain stable, sometimes up to 9 or 10 cm (Darling et al., 1977; Nicholls et al., 1998; Conway et al., 2001). Hence, a more personalized rupture risk assessment is required to prevent premature rupture and overtreatment, respectively.

As an alternative, aortic wall stress analysis has been proposed, which utilize the patient-specific geometry and the blood pressure measured to calculate peak wall stresses. Results showed that high peak (or 99<sup>th</sup> percentile) wall stresses were associated with AAA rupture (Fillinger et al., 2002; Vande Geest et al., 2006a; Speelman et al., 2008). Moreover, in the study of Venkatasubramaniam et al. (2004), it was shown that the peak wall stress (PWS) was significantly higher in ruptured AAAs compared to non-ruptured AAAs. Hence, peak wall stress assessment might improve the rupture risk estimation on a more individual basis.

These biomechanical models require the patient-specific geometry, which is generally obtained from computed tomography (CT), or magnetic resonance imaging (MRI) (Merkx et al., 2009; Gasser et al., 2014). However, both image modalities have disadvantages when applied frequently, or on a large scale. CT uses ionizing radiation and has the disadvantage of requiring nephrotoxic contrast agents. Thereby, geometry assessment using MRI involves a long scanning time, high costs, and the exclusion of patients with metal implants. Despite the promising results of wall stress analysis, the aforementioned drawbacks of CT and MRI hinder large prospective, longitudinal clinical trials needed for clinical validation and the introduction in the current clinical workflow (Farotto et al., 2018).

Alternatively, 3D ultrasound (US) has been introduced recently and could be used to assess the patient-specific geometry for AAA wall stress analysis. It overcomes the disadvantages of CT and MRI, has sufficient temporal resolution, is easy in use, and is relatively cheap. The main drawbacks are the limited field-of-view and the low image contrast. Despite these challenges, geometry assessment and wall stress analysis using 3D US in selected AAAs have shown to be feasible (Kok et al., 2015; Wittek et al., 2016; van Disseldorp et al., 2018), and revealed similar results when compared to CT-based methods (Kok et al., 2015; van Disseldorp et al., 2016b). Therefore, 3D US could be an ideal image modality to perform patient-specific wall stress analysis in longitudinal studies that could aid in a better understanding or prediction of aneurysm rupture risk or growth.

However, a the major limitation is the fact that large AAAs cannot be captured in one

single 3D US volume, due to the limited field-of-view. This is the case in 40 – 45% of all patients, and in the majority of AAAs with a diameter of 5.0 cm or more (see Figure 5.1). Thereby, for wall stress analysis, the complete geometry including both shoulders needs to be available (van Disseldorp et al., 2016a). Unfortunately, the field-of-view cannot be increased effectively due to physical constraints. A workaround would be the acquisition of multiple 3D US volumes to obtain a large US field-of-view. This requires either a probe tracking system or image registration. The latter is easy to implement in clinical workflow and requires no hardware modifications.

A second limitation in the aforementioned US wall stress studies was the lack of automatic segmentation of the AAA geometry, making the segmentation process labor intensive and subjective for operator dependency. Studies on automated 3D US segmentation are sparse. In the study by Rouet et al. (2010) a semi-automatic segmentation method was proposed to assess maximum AAA diameter and volume. This method was used to study

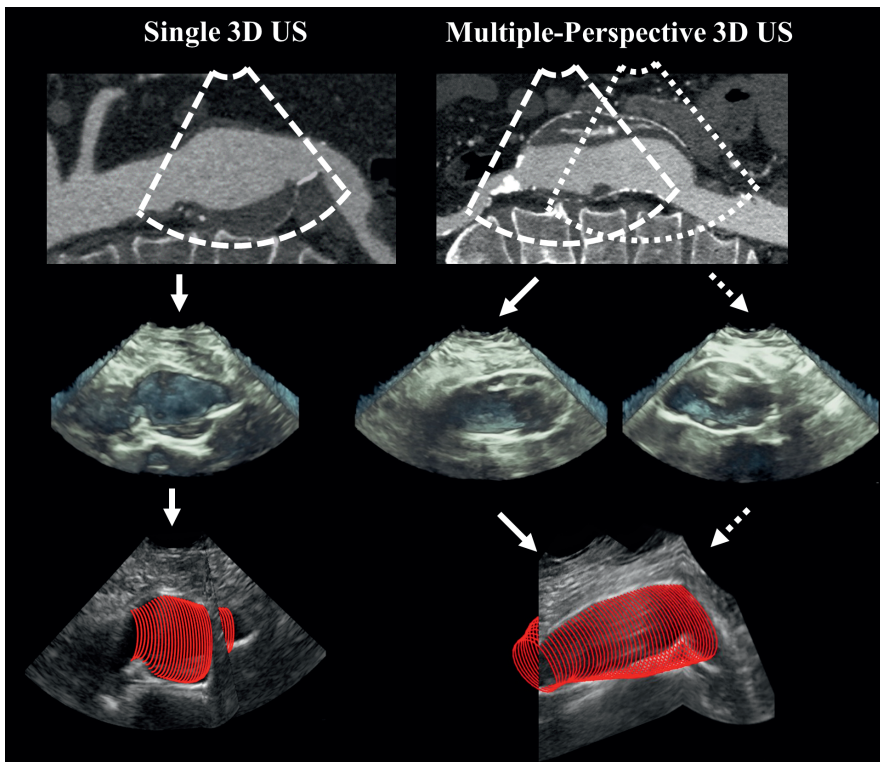


**Figure 5.1:** *Left:* Example of a relatively small abdominal aortic aneurysm (AAA), and a larger AAA (*right*). Computed Tomography data are shown (*top row*) with the field-of-view of the 3D ultrasound (US) scan in the x-z plane (*dashed white lines*), as well as the corresponding 3D US volume data (*middle row*). Finally, automatic segmentation of the US data for the single volume and the merged 3D volumes are shown (*bottom row*).

the reproducibility of assessing the maximum AAA diameter and volume (Long et al., 2013; Rouet et al., 2017), and it was verified in 54 patients that the AAA volume assessed with 3D US was comparable with 3D CT (Bredahl et al., 2015). In these studies, patient-specific wall stress analysis was not part of the study protocol, and therefore no comparison between the 3D US and CT wall stresses was made. In this study, a solution for these limitations is proposed which opens the door for longitudinal wall stress studies using 3D US. Therefore this study aims to:

1. Assess the complete geometry of both small and large longitudinal length AAAs using multi-perspective 3D US imaging and automatic segmentation (Figure 5.1). For AAAs with a larger axial length, multiple hand-held 3D US acquisitions were obtained and automatically merged into a large field-of-view before 3D segmentation.
2. Perform wall stress analysis based on the full automatically segmented 3D US-based geometry.

The performance of the US method was assessed by comparing the outcome in geometry and wall stress distribution to the gold standard: Computed Tomography.

## 5.2 Materials and Methods

### Study population

A total of 40 AAA patients were included in this study with a ranging maximum aortic diameter between 34 and 61 mm, covering the complete diameter range of patients in follow-up. All patients were selected based on the availability of Computed Tomography Angiography (CTA) data (contrast agent: 72 ml Iomeron 300 and 8 ml NaCl 0.9%), which were acquired for other diagnostic purposes, and not necessarily for the current study protocol. For each patient, an additional 3D US acquisition was performed. Patient-specific demographics are listed in 5.1. This study was approved by the local ethical committee of the Catharina Hospital Eindhoven, and all patients gave their informed consent.

### Computed tomography acquisition and segmentation

Pre-operative Computed Tomography Angiography (CTA) scans were performed with a 256 iCT scanner (Philips Healthcare, Best, the Netherlands) with a slice thickness of 3 mm and an in-plane resolution that ranged between 0.55 – 0.85 mm by 0.55 – 0.85 mm.

The CTA data were segmented semi-automatically using the previously reported software package Hemodyn (Philips Medical Systems, Best, the Netherlands) (Olabarriaga et al., 2004a,b). The segmentation required one proximal point at the neck of the AAA and two distal points in both iliac arteries. The centerline was automatically tracked throughout the AAA, after which an 3D active object was automatically adapted, based on the present image

gradients in the CTA data, until the AAA lumen-wall was detected. In case thrombus was present, the layer between the thrombus and the AAA inner layer was segmented (Breeuwer et al., 2008).

### 3D ultrasound acquisition

A commercial IU22 system (Philips Ultrasound, Bothell, WA, USA) equipped with a 3D matrix probe (type: X6-1, center frequency: 3.5 MHz) was used to acquire transabdominal 3D ultrasound acquisitions during breath hold.

For 20 AAA patients the field-of-view of one single 3D US acquisition was not sufficient to capture the complete AAA geometry (proximal neck to iliac arteries), due to the limited field-of-view of US imaging (Figure 5.1, *right*). Therefore, a proximal and a distal sub-volume were acquired. These data were used to develop and validate our multi-perspective fusion technique. The spatial resolution was 0.42 – 0.85 mm in the x-direction (width), 0.26 – 0.48 mm across the y-direction (length), and 0.17 – 0.33 mm in the z-direction (depth).

### Pre-processing

Before segmentation, the 3D US data were imported in MATLAB R2017a (Mathworks Inc., Natick, MA, USA) and converted into isometric data. In order to maintain the highest possible detail, the highest resolution of the three dimensions was maintained, whereas lower resolution pixels were up-sampled to match in resolution. Next, image filtering was performed to reduce image noise, caused by the presence of bowel gas, reverberations, and acoustic shadowing. Finally, using limited user-interaction, the start and end cross-sectional slice were selected in the cross-sectional slice where the AAA was still visible.

**Table 5.1:** Patient demographics

<b>Variables:</b>	<b>Patients with: Single 3D US acquisition</b>	<b>Patients with: Multiple 3D US acquisition</b>
Gender (M / F)	17 / 3	16 / 4
Age (years) <sup>a</sup>	72 (59 - 90)	71 (59 - 88)
Max. diameter (mm) <sup>a</sup>	50 (34 - 54)	52 (35 - 61)
Hypertensive blood pressure (%) <sup>b</sup>	55	60
Growth (mm/year) <sup>a</sup>	6 (0 - 8)	4 (0 - 8)

<sup>a</sup> Values are reported as median and range; <sup>b</sup> Hypertensive blood pressure is characterized as a systolic blood pressure of at least 140 mmHg or 90 mmHg in the diastolic phase.

## Filter analysis

In order to enhance the relevant structure in the image data, i.e., the aortic wall, an elaborate filter analysis was performed using five different filtering techniques, commonly used in US image analysis. A Gaussian, median, adaptive median, Euclidian shortening flow, and Perona and Malik filter were applied to the 3D data (Perona and Malik, 1990; Alvarez et al., 1993). Ten transversal image slices from six different AAA geometries were analyzed quantitatively. The contrast to noise ratio (CNR) was measured between the blood and the vessel wall segments, which is given by:

$$CNR = \frac{|\mu_{wall} - \mu_{blood}|}{\sqrt{\sigma_{wall}^2 + \sigma_{blood}^2}} \quad (5.1)$$

with  $\mu$  being the mean and  $\sigma$  the standard deviation of the pixel intensity in the vessel wall or blood segment, respectively. Please note that the wall and lumen were segmented manually for this filter analysis. An increase in CNR represented a better distinction between the lumen and vessel wall. The change in CNR after filtering was calculated as well as the overlap in grey values between the wall and lumen, which is an alternative measure for wall-lumen contrast (Nillesen et al., 2007).

## Segmentation and regularization

The segmentation algorithm is based on the well-established active deformable contour models or snakes as introduced by Kass et al. (1988). These active contours are energy minimizing functions that attract towards image features (in this case the aortic wall) and on the other hand are constrained by internal forces that resist deformation of the contour.

As a first step during the segmentation process, 2D deformable contours were applied slice-by-slice starting with the most proximal and distal contour. In both cases, the algorithm propagated towards the center, resulting in a full 3D segmentation of the AAA geometry. Each previously obtained contour was shrunk 2.5 mm inwards and used as an initial guess for the next 2D image plane. The contrast between the vessel wall and the lumen is limited at the proximal and distal side, due to the angle of incidence between the ultrasound waves and the vessel wall. Therefore, to correct for this limited contrast, a reduced internal force was used at the most proximal and distal 25% of 3D US volume. An example of the final slice-by-slice segmented AAA geometry is visualized in Figure 5.2.

Next, a regularization method was applied to correct for local irregularities. The AAA contours were converted into a 3D binary mask and similar to the 2D deformable contours, a 3D deformable object was inflated which was attracted to the image gradients, present in the binary image. Meanwhile, its 3D geometry was restricted by the tension and 3D curvature in the object.

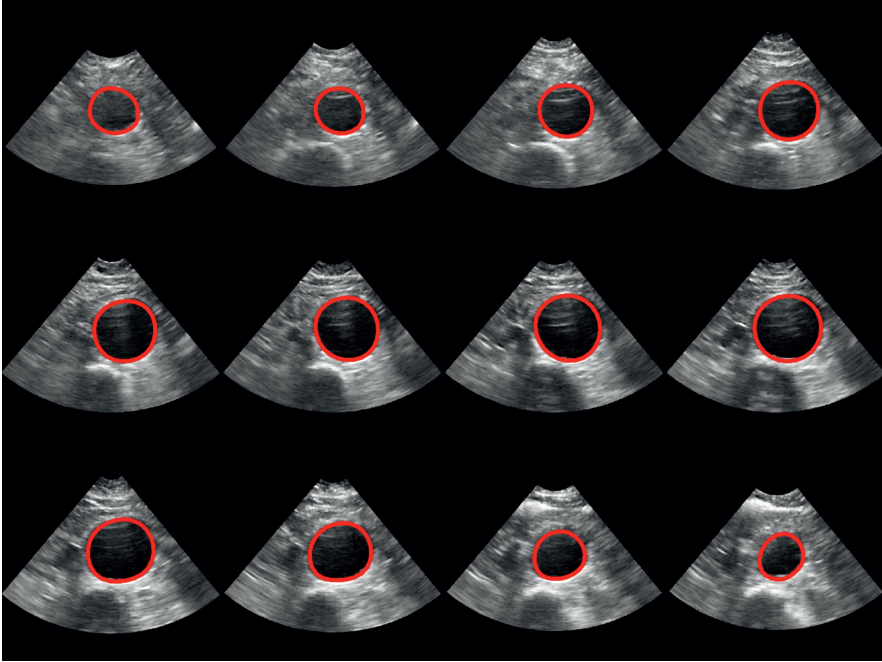


**Figure 5.2:** A Computed Tomography based representation of the segmented 3D ultrasound (US) data. The top left is the most proximal, and at the right bottom the most distal cross-sectional of the segmented 3D US data. The red lines represent the automatic segmented contour, per slice.

### Fusion of multi-perspective 3D ultrasound data

For the sub-group of patients with large AAAs extending beyond a single 3D US volume ( $n = 17$ , Figure 5.1, *right*), a rigid registration method was developed to combine the proximal and distal sub-volumes, and obtain the complete 3D volume. First, both proximal and distal sub-volume were segmented as described in the previous section. Next, the centerlines of both contours were aligned such that the first half of the distal centerline overlaps with the proximal centerline, which is visualized in Figure 5.3.

A simplified Powell method (Powell, 1964) was used to obtain the best overlap between the proximal and distal contours. The similarity index (SI) was calculated for the overlapping part of both contours, which is defined as:

$$SI = \frac{2(P_{\text{prox}} \cap P_{\text{dist}})}{(P_{\text{prox}} + P_{\text{dist}})} \quad (5.2)$$

with  $P_{\text{prox}}$  and  $P_{\text{dist}}$  in this case the number of pixels in the overlapping part of the proximal and distal segmented lumens, respectively. Next, the SI was maximized by an imposed search in all six degrees-of-freedom to estimate the optimal translation and rotation. Both sub-volumes were merged by averaging gray values in overlapping regions to obtain one

volume that includes the complete AAA geometry. This proposed fusion method was performed fully automatic using an in-house developed software program and required approximately 20 minutes of time. Finally, the combined image data were segmented using the previously described approach to obtain the final, complete, AAA geometry (Figure 5.3C).

### Wall stress analysis

The final US-based AAA geometries were converted into a tetrahedral mesh with a fixed wall thickness of 2 mm. Both proximal and distal ends were elongated to avoid the effects of the boundary conditions on the wall stresses in the aneurysm (van Disseldorp et al., 2016a). The CT-based geometries were imported in the meshing software package 3-Matic 5.1 (Materialise, Leuven, Belgium) due to the complex meshing procedure around the bifurcation. Finally, the CT-based meshes were created with similar mesh density compared to the US-based mesh. For mechanical analysis, all meshes were imported in Abaqus 6.14 (Dassault Systèmes, Paris, France) where the well-established Raghavan and Vorp material model was prescribed to simulate the mechanical behavior of the AAA wall (Raghavan and Vorp, 2000).

Both the US and CT-based geometries were acquired during one or multiple heartbeats, therefore the blood pressure in the AAA was assumed to be a constant mean arterial pressure (MAP) of 100 mmHg. Since, the aortic wall is not stress free at MAP, the initial

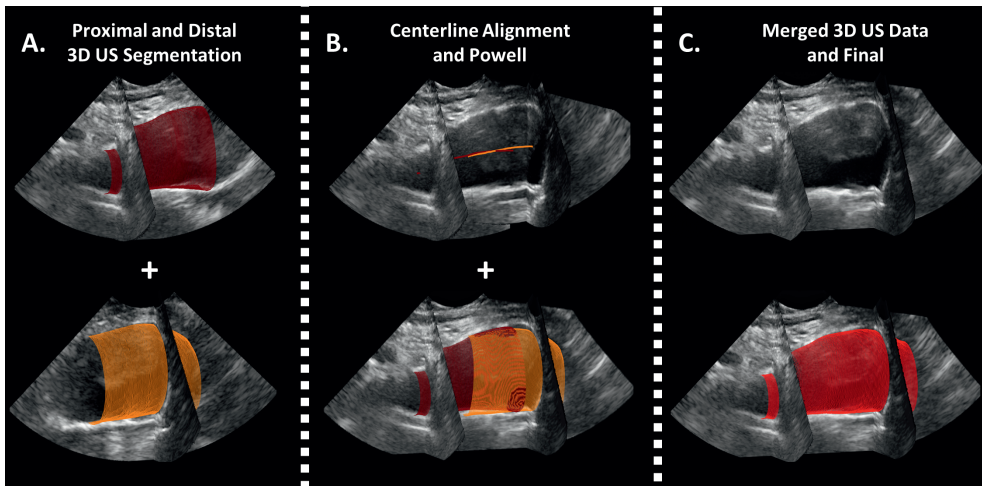


**Figure 5.3:** (A) Example of an automatic segmented proximal (*top*) and distal (*bottom*) sub-volume of the abdominal aortic aneurysm (AAA) geometry. (B) The centerlines of both sub-volumes were aligned (*top*) after which registration was performed (*bottom*). (C) The final merged 3D ultrasound data (*top*), with the complete segmented AAA geometry (*bottom*).



wall stresses were calculated using a backward incremental method (de Putter et al., 2007), while afterwards the blood pressure was increased to a peak-systolic pressure of 140 mmHg to obtain the final peak wall stresses.

## Validation

First, the automatic segmented US geometries were validated using CT contours for all single and merged 3D US segmentations. In addition, manual segmentation of the 3D US data was executed in the subgroup of AAA patients where no fusion was needed, since this data was similar to 3D US data used in previous feasibility studies (Kok et al., 2015; van Disseldorp et al., 2018).

To compare the CT-based geometries with the US contours, both modalities were registered using the same method as presented in the registration section. The agreement between the three different segmentations was quantified by the SI, a measure for agreement in geometry overlap, and the Hausdorff distance (HD), which quantifies the local deviations between the two segmented geometries (Rote, 1991). Thereby, the contrast-to-noise ratio (CNR) between the AAA wall and lumen was calculated for each acquisition.

US and CT-based wall stresses were calculated and the median, 75<sup>th</sup>, 95<sup>th</sup>, and 99<sup>th</sup> percentile wall stress were compared for all single and registered 3D US geometries with the corresponding CT-based wall stresses. Regression analysis and pairwise comparison were performed to analyze the differences in wall stress between the single and registered 3D US acquisitions. Differences between the US and CT segmentations and wall stresses were analyzed using the Wilcoxon rank sum test, whereas correlation was tested using the Spearman's rank test.

## 5.3 Results

### Filter analysis

Results of the filter analysis showed that the Euclidian Shortening Flow (ESF) filter had the largest decrease in overlap between the AAA wall versus lumen. Thereby, the contrast-to-noise ratio (CNR) increased overall with 25.6% when ESF filtering was applied, although the median filter performed slightly better. Overall, and compared to the other filters used (see Table 5.2), ESF filtering was most suited for this type of 3D US data. Therefore all 3D US data were first filtered with an ESF filter before segmentation and registration was applied.

### 3D ultrasound segmentation and validation

A representative selection of the segmented 3D US geometries (*red*), with the corresponding CT-based geometries (*orange*) are shown in Figure 5.4. In Figure 5.4A-E the AAA geometries obtained from a single 3D ultrasound acquisition are shown, whereas in Figure 5.4F-I the

**Table 5.2:** Results filter analysis. All values are given in median and interquartile range (IQR).

Type of Filter:	$\Delta$ CNR	$\Delta$ overlap wall vs. lumen:
	Median (IQR):	Median (IOR):
Gaussian:	22.2 (8.2 – 24.6) %	-38.1 (-62.8 – -15.7) %
Median:	29.7 (12.5 – 41.0) %	-43.4 (-64.4 – -21.2) %
Adaptive Median:	22.1 (11.9 – 36.6) %	-44.4 (-65.1 – -20.6) %
Euclidian	25.6 (9.7 – 42.4) %	-50.2 (-64.6 – -25.2) %
Shortening Flow:	1.1 (-3.3 – 5.7) %	-17.2 (-30.6 – -5.9) %

geometries are obtained from registration of multiple 3D US acquisitions. The medial CT slices in the coronal and sagittal plane are visualized behind the segmented geometries with the corresponding contours obtained using US and CT-based segmentation. It shows overall good quantitative similarity between automatic US and CT segmentation. Secondly, it visualizes that, although the field-of-view of 3D US is limited compared to CT, it is possible to capture the areas with high curvature ('shoulders' of the aneurysm) in most cases using multi-perspective 3D US data.

All quantitative results of the segmentation analysis are listed in Table 5.3 and visualized in Figure 5.5. The SIs range between 0.83 and 0.93 for the automatically segmented 3D US contours and CT-based AAA geometries in the single 3D US acquisitions, whereas the median HDs vary between 2.5 and 8.6 mm. For the multi-perspective US data, the SIs and HDs range between 0.82 and 0.92 and between 3.3 and 8.5 mm, respectively. The Wilcoxon rank sum test revealed lower SIs ( $p = 0.02$ ) and higher HDs ( $p = 0.04$ ) for the merged 3D US segmentations compared to the single 3D US contours.

Thereby, the automatically segmented US-based AAA geometries were compared with the manual segmented AAA contours and revealed a very good similarity with a median SI of 0.93 (interquartile range [IQR] = 0.91 – 0.94). This suggests that differences in geometry are not only caused by the different segmentation techniques used, but are also a result of the differences in image modality.

To evaluate the influence of the patient's echogenicity on the final automatic 3D US segmentation, the contrast-to-noise ratio (CNR) between the AAA wall and lumen gray values was correlated with the final SI and HD values. Analysis did not show a significant correlation between the CNR and these geometrical metrics for both the single and merged 3D US acquisitions ( $p$ -values ranged between 0.43 and 0.88).

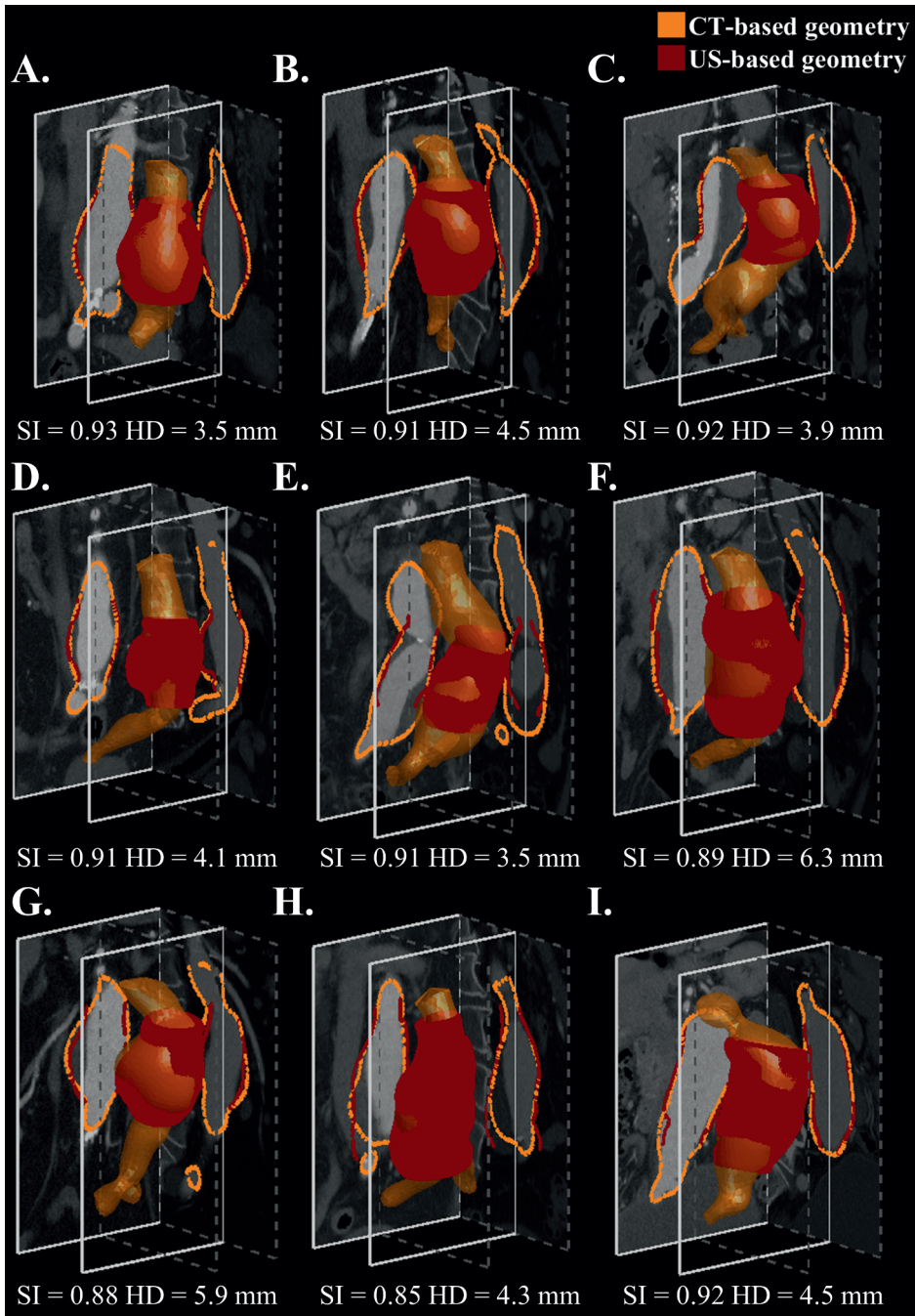


**Figure 5.4:** An overview of nine abdominal aortic aneurysm (AAA) geometries obtained from automatic segmented 3D ultrasound (US) data (*red*) with their corresponding Computed Tomography (CT) contours (*orange*). Subfigure A-E represent AAA geometries obtained from a single 3D US acquisition, whereas subfigure F-I are based on registered 3D US data. The Similarity Index (SI) and median Hausdorff distance (HD) are given for each geometry. The median coronal and sagittal CT slice are shown behind the AAA geometries, and the white solid and dashed represent the original position of the CT slices.

**Table 5.3:** Similarity Indices and Hausdorff Distances of single 3D ultrasound acquisitions using different segmentation methods and modalities.

Single 3D US acquisitions vs. CT segmentation						Multiple registered 3D US acquisitions vs. CT segmentation					
AAA ID:	Max. diameter [mm]	Similarity Index [-]	HD [mm], median (IQR)	Time between US and CT [months]	AAA ID:	Max. diameter [mm]	Similarity Index [-]	HD [mm], median (IQR)	Time between US and CT [months]		
1	52	0.93	3.5 (3.2 - 4.1)	<1	21	54	0.89	4.6 (4.0 - 6.0)	<1		
2	52	0.92	4.1 (3.1 - 5.1)	5	22	58	0.83	7.7 (6.4 - 10.1)	2		
3	41	0.89	5.3 (2.9 - 7.4)	2	23	53	0.83	7.9 (5.9 - 10.8)	<1		
4	34	0.90	5.2 (4.1 - 6.5)	<1	24	51	0.82	7.1 (5.7 - 13.6)	<1		
5	52	0.91	4.5 (3.9 - 6.2)	<1	25	55	0.87	5.0 (3.5 - 9.9)	1		
6	53	0.93	3.7 (3.1 - 5.3)	<1	26	54	0.92	4.5 (3.7 - 5.2)	<1		
7	49	0.92	3.9 (3.6 - 5.4)	<1	27	54	0.89	6.3 (3.2 - 8.9)	<1		
8	39	0.93	2.5 (1.8 - 3.1)	<1	28	48	0.87	3.6 (2.9 - 8.5)	13		
9	48	0.86	5.2 (3.5 - 12.7)	<1	29	50	0.86	4.3 (3.4 - 8.3)	<1		
10	50	0.91	4.1 (3.4 - 6.8)	12	30	52	0.85	4.3 (3.7 - 6.7)	6		
11	51	0.91	4.0 (2.9 - 5.5)	1	31	50	0.88	5.9 (4.7 - 8.0)	7		
12	54	0.83	8.6 (4.2 - 10.3)	<1	32	52	0.92	5.2 (3.7 - 6.0)	<1		
13	50	0.85	6.4 (5.1 - 10.0)	<1	33	45	0.87	8.5 (6.8 - 10.6)	12		
14	45	0.91	3.5 (3.0 - 4.1)	0	34	53	0.92	4.5 (3.1 - 5.0)	<1		
15	50	0.93	4.0 (2.3 - 5.6)	<1	35	49	0.92	3.6 (2.5 - 4.7)	<1		
16	53	0.90	3.7 (2.6 - 8.9)	<1	36	40	0.83	5.6 (3.6 - 6.6)	3		
17	47	0.88	5.9 (3.2 - 9.8)	<1	37	35	0.91	3.3 (2.5 - 3.8)	<1		
18	47	0.89	5.9 (2.8 - 11.3)	3	38	55	0.89	5.9 (4.6 - 6.9)	<1		
19	50	0.90	4.1 (2.0 - 15.0)	<1	39	53	0.87	6.3 (4.4 - 8.5)	6		
20	51	0.91	4.3 (3.2 - 7.4)	<1	40	61	0.88	7.3 (6.4 - 8.0)	<1		

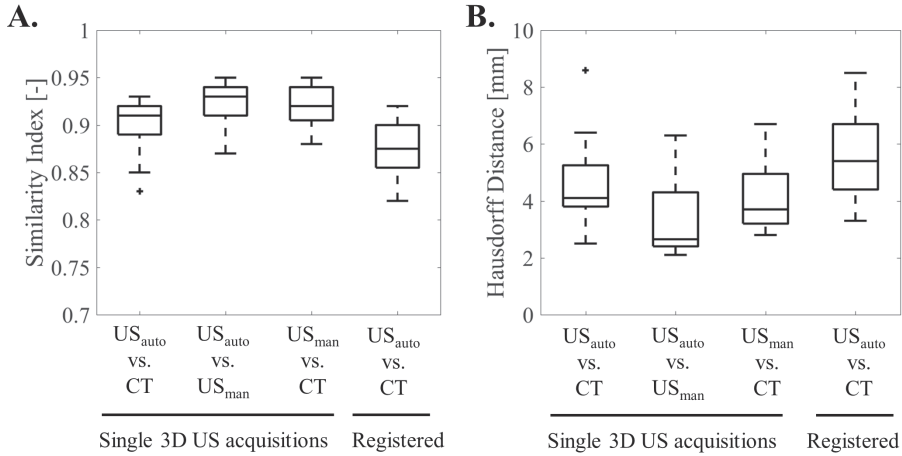


**Figure 5.5:** (A) Similarity index (SI) between automatic segmented 3D ultrasound geometry ( $US_{auto}$ ) and Computed Tomography (CT) contours,  $US_{auto}$  and manual segmented 3D ultrasound contours ( $US_{man}$ ), and the SIs of  $US_{man}$  and CT for the abdominal aortic aneurysm (AAA) geometries based on single 3D ultrasound (US) acquisitions. The most right box-and-whiskers plot shows SI between automatic segmented 3D US contours based on the registered large field-of-view data and the corresponding CT geometry. (B) The median Hausdorff distance (HD) between  $US_{auto}$  and CT contours,  $US_{auto}$  and  $US_{man}$ , and the median HD of  $US_{man}$  and CT for the AAA geometries based on single 3D US acquisitions. The median HD of the automatic segmented 3D US contours based on the registered 3D US data and the corresponding CT geometry is visualized most right.

## Aortic wall stress

In Figure 6A and B, examples of CT- and US-based AAA wall stress distributions are shown for both single and registered AAA geometries, respectively. Good similarities in geometry and wall stress are observed, although in the second example of the multi-perspective US-based geometry two high stress spots were missing in the US geometry when compared to the CT-based wall stresses.

The median, 75<sup>th</sup>, 95<sup>th</sup>, and 99<sup>th</sup> percentile wall stresses are visualized for the single and registered US-based geometries and compared with the corresponding CT geometry in Figure 5.7. It shows overall a good agreement between the US and CT-based percentile wall stresses. However, the spread in the percentile wall stress is higher for the single 3D US acquisitions compared to the merged multi-perspective acquisitions, especially in the 99<sup>th</sup> percentile wall stress comparison. Overall, the percentile wall stresses were 23% (18 – 30%) higher for the single 3D US and 10% (5 – 15%) higher for the merged 3D US geometries compared to the CT data. Finally, the time between the 3D US and CT data acquisitions did not influence the results significantly.

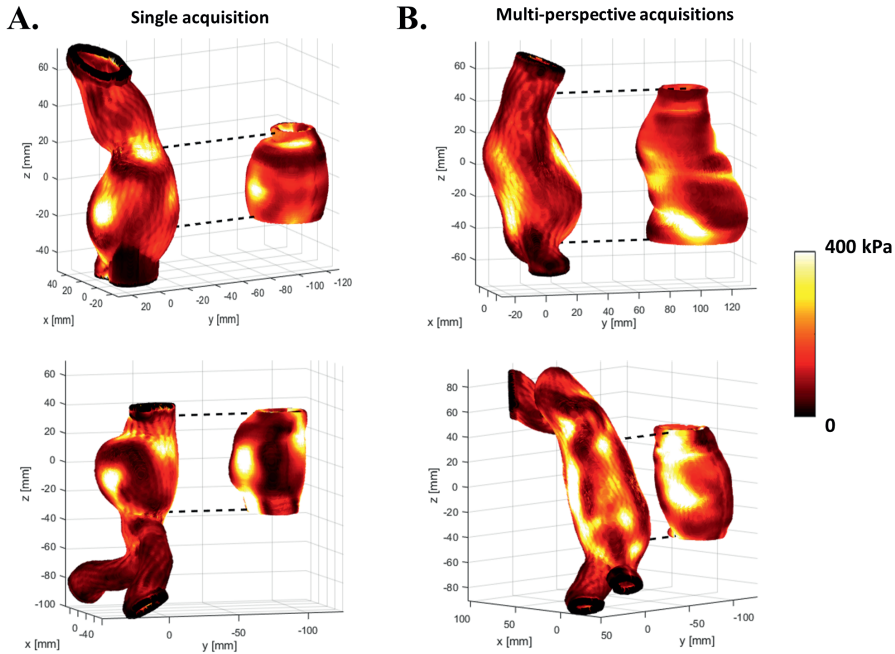


**Figure 5.6:** Wall stress distribution of abdominal aortic aneurysms (AAAs) based on computed tomography (CT) (*left*) and 3D ultrasound (US) (*right*). In **(A)** two examples are shown of the AAA wall stress based on a single 3D ultrasound acquisition. **(B)** AAA wall stress distribution based on registered 3D ultrasound data. The dashed lines represent the region in the CT data which corresponds with the US-based wall stress data.

## 5.4 Discussion

Pre-operative monitoring of abdominal aortic aneurysms using patient-specific wall stress analysis is a next step towards personalized growth and rupture risk assessment. Therefore, in this study a multi-perspective 3D US geometry assessment method was proposed to segment the AAA geometry automatically, thereby tackling issues such as limited field-of-view. These geometries were used to perform patient-specific wall stress analysis which revealed high similarity with CT-based wall stresses. Therefore, the current study is a next step forward to assess peak wall stresses of AAAs in a harmless and cost-efficient manner.

Studies that use fusion of multi-perspective 3D US data are sparse, yet in this case necessary to obtain the complete field-of-view of the aneurysm from proximal to the distal shoulder. Therefore, proximal and distal US acquisitions were merged to obtain the desired field-of-view. Wall stress results revealed that the multi-perspective 3D US geometries have not only an increased field-of-view, but also an improved agreement in percentile wall stress compared to single 3D image data (Figure 5.7). This might be initiated by an increased image quality of the overlapping part of the 3D US data, which is subsequently

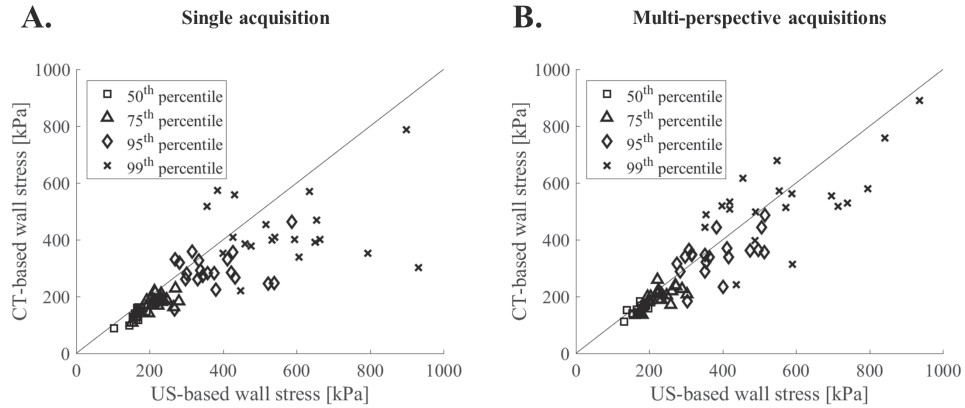


**Figure 5.7:** Comparison of the 50<sup>th</sup>, 75<sup>th</sup>, 95<sup>th</sup>, and 99<sup>th</sup> percentile wall stress calculated based on the computed tomography (CT) and 3D ultrasound (US). In (A) the percentile wall stresses are shown for the abdominal aortic aneurysm geometry acquired with a single 3D US acquisition, and in (B) using merged multi-perspective 3D US acquisitions.

coherent to a correct segmentation of the AAA geometry. To improve the accuracy of the wall stress analysis further, multi-US acquisitions from different angles can be acquired as well, and merged in order to increase the image quality in regions where the angle between sound propagation direction and the radial direction of the wall is small. However, for some patients with a limited echogenicity, US-based AAA segmentation will still be challenging due to the presence of bowel gas, the depth of the AAA, or calcifications in the aortic wall.

In this study, segmentation was performed without any post-processing or manual corrections, and was directly compared to CT. Current results showed a good similarity between all the 3D-US based AAA geometries and the geometries obtained by CT data. The SIs ranged between 0.82 and 0.93, while in general an SI higher than 0.70 is already considered as good agreement between two geometries (Bartko, 1991). Thereby, overall a median HD of 4.6 mm was measured between both AAA geometries, which is considerable although in the same range as reported in previous studies (Kok et al., 2015; Rouet et al., 2017). This local mismatch is probably caused by lower image contrast at the shoulders of the aneurysm and the lumen-thrombus border, resulting in local irregularities. These irregularities will affect the AAA wall stress distribution and thereby could explain the remaining differences in US and CT-based percentile wall stress. Smoothing of the US-based AAA geometry might reduce this local mismatch, while for some patients manual post-processing will still be necessary. Besides the differences between each segmentation method, also the influence of the maximum AAA diameter and the time between the US and CT data acquisition on the segmentation results was examined. However, no significant effect of these on the SI and HD was measured.

The merit of this study lies in the large area geometry assessment based on multi-perspective 3D US data. Besides the reduction in labor intensity and proneness for intra-observer variability expected when performing manual segmentation and registration, the current study showed significantly lower HDs as reported in Kok et al. (2015) ( $p < 0.01$ ). These differences are explained by the automated multi-perspective approach, rather than manually merging two or more segmentations leading to malformations in the geometry and inadequate high wall stress regions. In future research, the registration method could possibly be further improved by including image- and intensity features present in the overlapping part of the 3D US data. Furthermore, verification could be performed using a probe location tracking system.

Manual segmentation showed slightly higher SIs and lower HDs with respect to CT-data, compared to the automatic segmentation. In addition, patients with a relatively low SI between automatic 3D US and CT segmentation, did reveal a high SI when manual segmentation was used. A possible explanation for these differences could be a priori knowledge of the of AAA shape. A calcified thrombus can result in a bright edge in the US data which may affect the automatic segmentation approach and subsequently result in an incorrect segmentation of the aortic wall, whereas with manual segmentation this thrombus will be recognized and corrected for. Preferably, in cases where thrombus is present in the AAA geometry, not only the AAA wall but also the thrombus geometry should be automatically detected and segmented. However, thrombus segmentation in 3D US data is challenging due to the presence of different thrombus layers and its age-dependend elastic properties (Tong et al., 2011), which all will alter the echogenic properties of the thrombus.

Finally, this method is not limited to only pre-operative 3D US data of AAAs, but can also be applied to post-operative data. Post-operative 3D US data showed improvements in assessing the maximum diameter after EVAR (Bredahl et al., 2013) and the detection of endoleaks using contrast enhanced ultrasound (CEUS) (Abbas et al., 2014). Although the method presented could directly be applied to the post-operative 3D US data, this was beyond the scope of this research.

## 5.5 Conclusion

In conclusion, an automatic segmentation and fusion method of multiple 3D US acquisitions was developed in this study, which thereby avoid issues of limited field-of-view and user-dependency due to manual segmentation of 3D US data. Therefore, using the current method, wall stress studies can adequately be performed using 3D US independent of AAA length and size, which opens the door for longitudinal wall stress studies on aneurysm development and growth. Future steps will focus on improvement of contrast, segmentation of the thrombus, and longitudinal studies in patients.





# **A Longitudinal study on the Biomechanical properties of Abdominal Aortic Aneurysms and their Relation to AAA Growth**

This chapter is based on: A Longitudinal Study on the Biomechanical Properties of Abdominal Aortic Aneurysms and their Relation to AAA Growth, **E.M.J. van Disseldorp**, N.J. Petterson, F.N. van de Vosse, M.R.H.M. van Sambeek, R.G.P. Lopata, *In preparation*, 2018;

## Abstract

**Background:** Rupture of an abdominal aortic aneurysm (AAA) will result in a life-threatening hemorrhage in 80% of all cases. Current clinical guidelines for surgical repair have shown their shortcomings, and indicate that a more patient-specific method is required. In previous studies, we have demonstrated a fully automated method to characterize the mechanical properties of AAAs using 4D ultrasound (US) based finite element analysis in volunteers and AAA patients. In the current study, we report patient-specific material properties monitored over time, and investigated their possible relation with aneurysm size and growth in ruptured and non-ruptured AAAs.

**Methods:** In total 70 AAA patients (4 ruptured and 66 non-ruptured) with a diameter ranging between 30 - 58 mm were included in this study. 4D-US data were acquired using a Philips iU22 (X6-1 transducer) during breath-hold while brachial blood pressure was measured simultaneously. Afterwards, these patients were followed over a median period of 24 months (range 3 – 38 months), which resulted in 2 to 12 consecutive interval moments where repeated measurements were performed.

The aortic geometry was automatically segmented, tracked over time, and converted into mesh with a wall thickness of 2 mm. Using a previously described mechanical characterization method the arterial stiffness and the 99<sup>th</sup> percentile peak wall stress were assessed for all consecutive time moments. Finally, all patients were divided in a small (< 40 mm), moderate (40 – 50 mm), and large ( $\geq$  50 mm) AAA diameter group. Differences between slow and rapid growing AAAs were analyzed within these three groups. The aneurysms were considered to be rapidly growing when the diameter increased with at least 2 mm in 3 months time.

**Results:** Aortic stiffness and peak wall stress measurements were obtained for all patients. Rapid growing AAAs (median 1.3, IQR: 1.1 - 1.7 kPa·m) revealed a lower preceding aortic stiffness compared to slow growing AAAs (median 1.8, IQR: 1.3 - 2.6 kPa·m,  $p = 0.05$ ). This effect was predominantly visible for the moderate ( $p = 0.01$ ) to large ( $p = 0.26$ ) diameter groups. No statistical differences in aortic stiffness ( $p = 0.15$ ) and peak wall stress ( $p = 0.56$ ) were shown between the ruptured and non-ruptured AAAs, yet three out of four ruptured AAAs had a relatively low stiffness in their last measurement before rupture.

**Conclusions:** Using 4D US, the patient-specific AAA stiffness and peak wall stress can be assessed and followed over time. First results revealed that rapid growing AAAs have a lower arterial stiffness before growth, compared to slow growing or stable AAAs. A decrease in aortic stiffness might be a marker for upcoming AAA growth, however, future research is required to strengthen this finding.

## 6.1 Introduction

Abdominal aortic aneurysms (AAAs) are currently monitored using ultrasound (US). During regular surveillance the maximum anterior-posterior diameter is measured and followed over time. According to current clinical guidelines, surgical intervention is recommended when the maximum aortic exceeds 55 mm for men and 52 mm for woman, or when excessive AAA growth is observed ( $\geq 10$  mm/year) (Moll et al., 2011; Chaikof et al., 2018). These criteria are based on two multi-center randomized clinical trials which showed that the risk of rupture did not outweighs the risk of intervention below these thresholds, based on a population-based average (The UK Small Aneurysm Trial Participants, 1998; Lederle et al., 2002b).

As a consequence of current population-based guidelines, possibly vulnerable AAAs with a maximum aortic diameter below these thresholds are left untreated (Darling et al., 1977; Nicholls et al., 1998; Scott et al., 1998). Meanwhile, not all AAAs above 55 mm are prone to rupture, which result in unnecessary surgical risks for the patient and is associated costs which is a burden to the health-care systems (Conway et al., 2001; Epstein et al., 2008). Hence, an approach is required that can stratify aneurysms on an individual basis.

There is growing evidence that the mechanical behavior of the AAA wall can aid in identifying aneurysms at risk. In the first study by Wilson et al. (1998), AAA compliance was measured and revealed an overall decrease in aortic compliance with an increasing aortic diameter. These data indicated that the AAA wall remodeled and the collagen composition increased in response to the increased aortic diameter and wall tension (Hua and Mower, 2001). This remodeling process might prevent the AAA wall from rupture. Failure to increase in aortic stiffness with AAA growth might be an indicator for an increased AAA rupture risk (Wilson et al., 2001, 2003).

Besides monitoring the elastic properties of the AAA wall, aortic peak wall stress (PWS) has been extensively studied over the last two decades. The rationale behind wall stress analysis is that AAA rupture will occur when (locally) the wall stress exceeds the strength of the aortic wall. First evidence was provided by Fillinger et al. (2002, 2003) that showed that ruptured and symptomatic AAAs had an increased PWS compared to non-ruptured AAA. Later, in the study by Truijers et al. (2007), it was shown that PWS can also detect patients with an elevated rupture risk which are currently under surveillance (i.e., with a maximum diameter  $\leq 5.5$  cm). As a consequence, PWS might be superior to maximum the aortic diameter as rupture risk estimator in follow-up. In addition, Vande Geest et al. (2006a) derived a rupture potential index based on the PWS and strength of the aortic wall. The specific region with the highest rupture risk index is considered as the peak wall rupture risk index (PWRI), where a PWRI of 1 means that the AAA is at imminent risk of rupture (Gasser et al., 2010).

In a large retrospective study by Gasser et al. (2014), wall stress analysis was performed, the peak wall rupture risk index (PWRI) was calculated, and subsequently converted in an

'equivalent' aortic diameter. This equivalent diameter supports clinicians to interpret the biomechanical state (e.g., peak wall stress and strength) of the AAA, and might be higher or lower than the actual physical diameter. Recent improvements also included parameter uncertainties for a probabilistic analysis of the PWRI (Polzer and Gasser, 2015), although this additional step introduces a long computational time, which in turn might hinder clinical introduction.

Ideally, the aforementioned measures should be followed over time, on an individual basis in a longitudinal study to prove the merit of PWRI or mechanical properties as additional rupture risk estimators. However, most wall stress studies are limited to the availability of preoperative computed tomography (CT) datasets, typically one per patient. As a result, PWS and PWRI were calculated for the individual patient, but were only compared between different patients. A few studies followed the patient-specific PWS over time, and results suggested that an increased shoulder peak stress is associated with a rapid growth rate (Li et al., 2010), and that a low PWS is correlated with a slow AAA expansion rate (Speelman et al., 2010). Recently, Stevens et al. (2017) calculated the PWRI in a longitudinal study with four AAA patients each with five consecutive CT follow-up acquisitions. This study revealed fluctuations in PWRI over time and highlighted the effect of intraluminal thrombus in risk assessment. However, a possible explanation for these fluctuations is still unclear and would require more research (Stevens et al., 2017).

The main bottleneck in these follow-up studies is the use of CT imaging. CT imaging suffers from radiation exposure and the use of nephrotoxic contrast agents, which limits the patient inclusion and the ability to follow these patients for a longer time period. As an alternative, wall stress analysis based on 3D ultrasound (US) has become available in recent years (Kok et al., 2015). By using not only the AAA geometry but also the temporal information obtained from the US data, its mechanical behavior could be assessed (Wittek et al., 2016; van Disseldorp et al., 2016b). Moreover, biomechanical analysis based on time-resolved 3D US can be more easily implemented in the clinical workflow, and, due to its non-invasive nature, it can be utilized to study in a large patient group over time.

In this chapter, a longitudinal study is presented, executed in a large group of AAA patients who were followed over time using 4D (time-resolved 3D) US imaging. Biomechanical properties, i.e., the aortic stiffness and PWS, were assessed using the US data, and their relation with respect to the maximum AAA diameter and growth was examined and statistically tested. Furthermore, the mechanical properties of a small group of patients with a ruptured AAA were compared to the non-ruptured cases.

## 6.2 Materials and Methods

### Study population and design

In total, 81 AAA patients under outpatient surveillance without prior aortic surgery were enrolled in this study. US acquisition was repeated for each surveillance interval according to the European Society of Vascular Surgery AAA guidelines (Moll et al., 2011). The follow-up period was not changed for this study, and the study protocol was added to the standard surveillance program. The study was approved by the local ethics committee of the Catharina Hospital Eindhoven. The study was started on December 1, 2014 while the study period for each patient was defined as the time from enrollment with a maximum of 42 months follow-up. All patients gave written informed consent for additional 4D US acquisitions with simultaneous blood pressure measurements.

Four AAA patients were included since aortic rupture (max. diameter < 55 mm) was observed before current guidelines for surgery were achieved. In addition, 77 non-ruptured AAAs with a long period of follow-up were included to perform mechanical analysis of the AAA wall. Out of the included non-ruptured AAA patients, 11 patients were excluded since no follow-up data were available ( $n = 6$ ), or due to poor US image quality ( $n = 5$ ). In summary, 66 patients with a non-ruptured AAA and 4 with a ruptured AAA, were included with a median follow-up period of 24 months (range 3 - 38 months). A dataset with on average 4 (range 2 - 12) follow-up measurements was analyzed. This resulted in a total amount of 262 4D US datasets. The maximum aortic diameter at enrollment ranged from 30 - 58 mm, covering the complete range of AAA diameters encountered in outpatient follow-up. More patient-specific demographics are listed in Table 6.1. Furthermore, a flowchart of the patient inclusion is visualized in Figure 6.1.

**Table 6.1:** Patient demographics for the non-ruptured and ruptured AAAs

Variables:	Non-ruptured	Ruptured
Gender (M / F)	58 / 8	2 / 2
Age at enrollment (years) <sup>a</sup>	72 (53 - 86)	75 (68 - 81)
Max. diameter at enrollment (mm) <sup>b</sup>	43 (37 - 48)	44 (41 - 50)
Max. diameter end (mm) <sup>b</sup>	49 (40 - 54)	48 (42 - 52)
Growth (mm/year) <sup>b</sup>	2.1 (1 - 4.7)	1.3 (0 - 4.1)
Number of follow-up intervals (-) <sup>a</sup>	4 (2 - 12)	3 (2 - 4)
Median time in follow-up (months) <sup>a</sup>	24 (3 - 38)	13 (3 - 18)
Diastolic blood pressure (mmHg) <sup>b</sup>	83 (78 - 88)	88 (80 - 93)
Systolic blood pressure (mmHg) <sup>b</sup>	140 (134 - 155)	128 (115 - 145)

<sup>a</sup> Values are reported as median and range; <sup>b</sup> as median and interquartile range

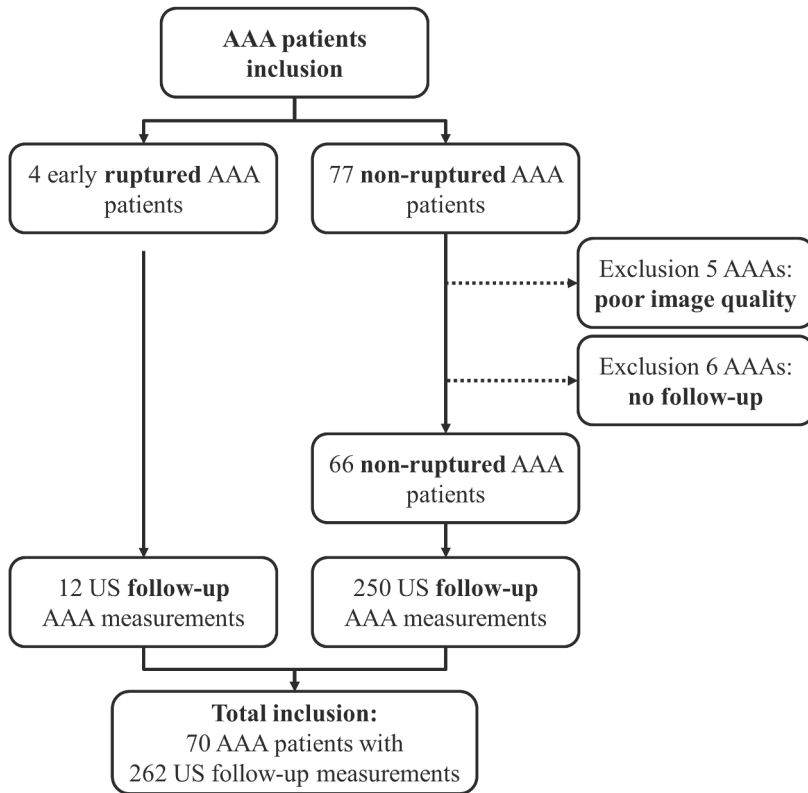


**Figure 6.1:** A graphical overview of the patient selection in the follow-up study. For each included AAA patient, at least two US measurements were acquired.

### Data acquisition and mechanical analysis

All 4D US datasets were acquired using a Philips iU22 US scanner (Philips Medical Systems, Bothell, WA, USA) equipped with a 3D matrix curved array probe (X-6-1) with a center-frequency of 3.5 MHz. While the patient was in supine position, 4D US data of the AAA were recorded during multiple heartbeats and during breath-hold. Directly after US acquisition, the brachial pressure was measured using a sphygmomanometer.

All acquired US datasets were stored off-line. Examples of the longitudinal 4D US datasets for three AAA patients, respectively, with two, four, and five follow-up time intervals, are shown in Figure 6.2. For analysis, the data were imported into Matlab (2017a, Mathworks Inc., Natick, MA, USA) and converted into a Cartesian coordinate system. First step during data analysis was to detect the diastolic and systolic phase of the cardiac cycle in the 4D US data. The middle longitudinal 2D US plane was extracted out of the 3D dataset, while the upper and lower AAA wall were tracked over the cardiac cycle using a 2D coarse to fine displacement estimation algorithm (Lopata et al., 2009). Next, the diastolic

3D US data were automatically segmented based on active deformable contours as described in Chapter 5. The automatic segmentation was followed by mesh generation with a uniform wall thickness of 2 mm, 3D tracking of the diastolic geometry over the cardiac cycle (Lopata et al., 2011), and mechanical characterization using a forward iterative finite element approach (van Disseldorp et al., 2018).

In this iterative calibration process, the arterial stiffness (shear modulus multiplied by the wall thickness) was adapted until the measured US displacements matched the predicted US displacements in the finite element model. Convergence was achieved when the aortic stiffness differed less than 1% with previous estimate.

To make an adequate comparison between the different aortic stiffness measurements for each follow-up interval, only the 3D displacement field of the middle 2 cm around the maximum diameter was used in the calibration process. By doing so, it was ensured that this region was always in the field-of-view during 4D US acquisition at each follow-up moment.

Finally, the internal pressure in the diastolic AAA geometry was increased to a peak pressure of 140 mmHg. Examples of the peak wall stress distribution are shown for three AAA patients, ranging from relatively small to large diameters, in Figure 6.2. In addition, the 99<sup>th</sup> percentile wall stress was calculated and used as measure for peak wall stress (Speelman et al., 2008).

## Statistical analysis

Statistical analyses were performed in Matlab (R2017a, Mathworks Inc., Natick, MA, USA). The estimated arterial stiffness was linearly scaled to a mean arterial pressure (MAP) of 100 mmHg (van Disseldorp et al., 2018), to correct for possible changes in pressure over time. The maximum anterior-posterior diameter measurements were performed by trained vascular technicians, using a standard 2D US protocol (Moll et al., 2011).

Normality was tested using the one-sample Kolmogorov-Smirnov test, and differences in mechanical properties between different groups were statistically analyzed with the Wilcoxon rank-sum test. The correlations between geometrical parameter, i.e., AAA growth and diameter, and mechanical parameters, i.e., aortic stiffness and peak wall stresses, were evaluated using the Spearman Rank correlation. For all statistical tests a p-value < 0.05 was considered to be significant.

Next, the AAA patients with a ruptured AAA were analyzed and the mechanical properties were compared with the non-ruptured AAAs. In this analysis, the maximum aortic diameter, AAA growth, aortic stiffness, and peak wall stresses (PWS) were estimated for each follow-up measurement. Moreover, the last 4D US dataset before rupture was compared with all prior US acquisitions.

Finally, for all patients included in the analysis, the possible relations between aortic growth and changes in arterial stiffness and PWS were statically investigated. Since, the time



between two consecutive measurements intervals varied between different AAA patients (and also within one patient), the AAA growth was normalized to a growth period of 3 months. Afterwards, the AAA patient population was divided in rapid growing AAAs with at least 2 mm growth in 3 months, and in relatively slow growing or stable AAAs (< 2 mm in 3 months). Differences in arterial stiffness and PWS between rapid and slow growing AAAs were analyzed and compared for the complete patient population, and, as function of the maximum diameter. For the latter, each group was subsequently divided in a small (30 - 39 mm), moderate (40 - 49 mm), and a relatively large ( $\geq 50$  mm) AAA diameter group.

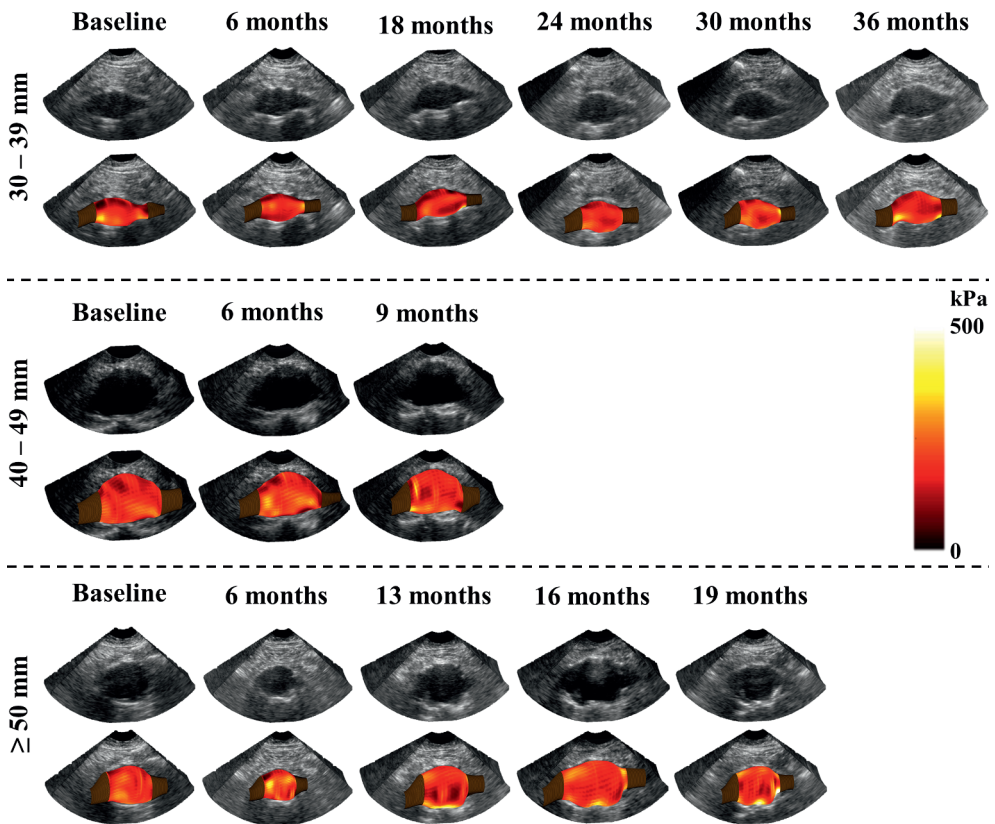


**Figure 6.2:** Three examples of abdominal aortic aneurysms (AAA) showing the US data acquired at different intervals. **Top:** a relatively small AAA is shown with six consecutive US datasets with a maximum follow-up period of 36 months. **Middle:** a moderate AAA, a maximum diameter of 48 mm at baseline, with nine months follow-up, and a large AAA (51 mm at baseline) with 19 months follow-up (**bottom**). Below each 3D US volume, the automatic segmented AAA geometry and simulated wall stress distribution are shown. The *brown* segment of the mesh is the elongated part.

## 6.3 Results

### Ruptured vs. Non-ruptured AAAs

In Figure 6.3 the aortic stiffness is shown for all patients, with each point representing the specific aortic stiffness during follow-up. The ruptured AAAs are highlighted in this figure to show their aortic stiffness over time and in contrast with the non-ruptured AAAs. Regression and correlation analysis were performed and revealed a significant relation between aortic stiffness and maximum AAA diameter ( $\rho = 0.29$ ,  $p < 0.001$ ), although the spread in aortic stiffness is large ( $R^2 = 0.09$ ).

Figure 6.3 also shows that in three out of the four ruptured AAA patients a decrease in aortic stiffness was measured before the last US acquisition. Moreover, the aortic stiffness of the ruptured AAAs in the last measurement before rupture (red diamonds) was 0.96 kPa-m, 2.28 kPa-m, 1.55 kPa-m, and 1.07 kPa-m, which is relatively low compared to the mean aortic stiffness of the non-ruptured AAAs (2.21 kPa-m) in this diameter range (42 - 52 mm). However, this difference was not statistically significant ( $p = 0.15$ ) and sample size was limited.

The 99<sup>th</sup> percentile peak wall stress (PWS) is shown as function of the aortic diameter for all AAA patients in Figure 6.4. Although a considerable spread in wall stress is observed, a positive correlation between the maximum diameter and 99<sup>th</sup> percentile PWS is observed ( $\rho = 0.42$ ,  $p < 0.001$ ). Intuitively, the last measured PWS before rupture (red diamonds) should be high compared to the non-ruptured AAAs. However, current data do not support this hypothesis and shows PWS values which are comparable to the non-ruptured AAAs.

### Growth analysis

To analyze the relation between AAA growth and the evolution of the mechanical properties over time, the aortic stiffness and 99<sup>th</sup> percentile PWS were plotted for seven typical, non-ruptured AAA patients as a function of the maximum diameter in Figure 6.5 and Figure 6.6, respectively. Each connected group of data points represents an AAA patient.

Figures 6.5 and 6.6 show that the arterial stiffness and PWS varied considerable over time. It shows that the measured arterial stiffness changes in some cases more than 100% over time, while the PWS varied up to 55%.

Since the upcoming growth is not available for the last US measurement, these 70 measurements were excluded in further analysis. Combining all other datasets ( $n = 192$ ) from all included patients, revealed that in 17 cases an AAA growth rate of at least 2 mm in 3 months was observed between two consecutive follow-up intervals. The aortic stiffness and PWS values were compared between these rapid growing AAAs and the remaining stable or slow growing aneurysms.

In Figure 6.7 the differences in mechanical properties between the two groups are visualized in box-and-whisker plots. Results showed a median arterial stiffness with in-

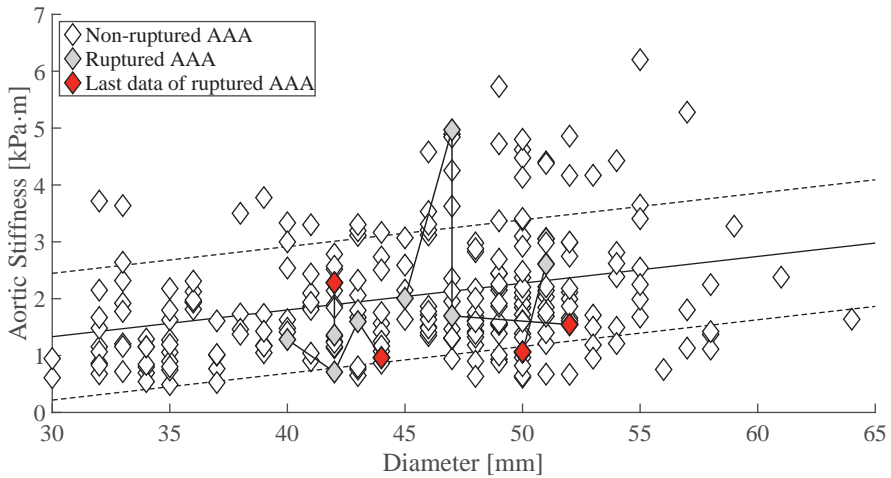


**Figure 6.3:** The aortic stiffness of the abdominal aortic aneurysm (AAA) wall as function of the maximum aortic diameter for all follow-up moments ( $N = 262$ ). The aortic stiffness for the non-ruptured AAAs are shown in *white diamonds*. The stiffness measurements of the four patients with an early rupture of the AAA are shown in *gray*, connected with *bold black lines* and the last stiffness measurement is indicated with a *red diamond*. The normal black line represent the regression line ( $R^2 = 0.09$ ,  $p < 0.001$ ), with its interquartile range indicated by the *black dotted line*.

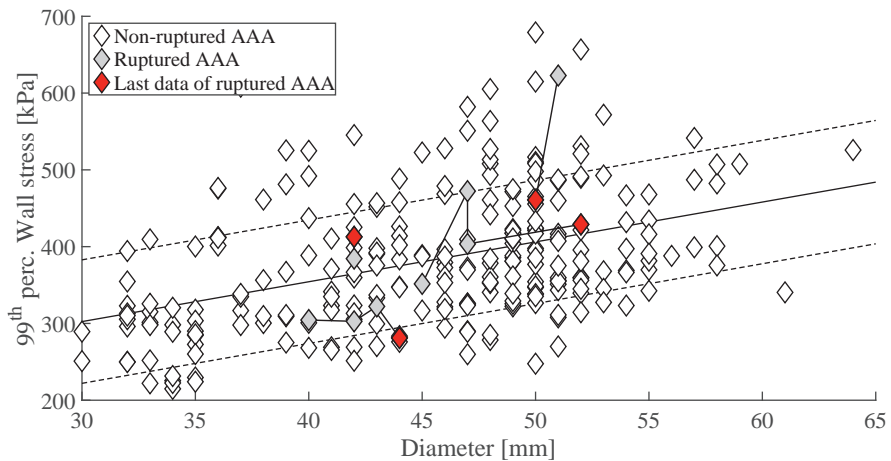


**Figure 6.4:** The 99<sup>th</sup> percentile peak wall stress (PWS) of the abdominal aortic aneurysm (AAA) wall as function of the maximum aortic diameter for all AAA datasets ( $N = 262$ ). The aortic PWS for the non-ruptured AAAs are shown (*white diamonds*) as well as the PWS values of the ruptured AAAs (*gray*). The *bold black line* connects the PWS of the AAA patients with a ruptured AAA for the different consecutive datasets, and the last PWS value is indicated in *red*. The black line represent a regression line ( $R^2 = 0.18$ ,  $p < 0.001$ ), with its interquartile range (*black dotted line*).

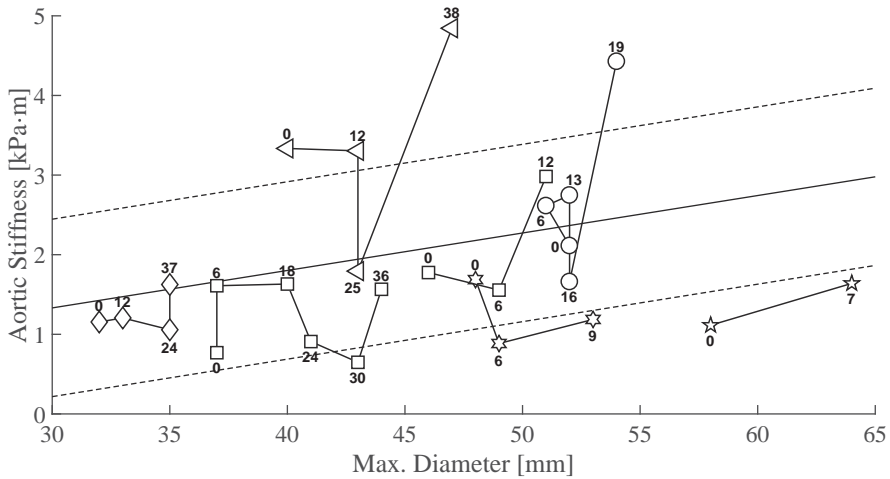


**Figure 6.5:** Aortic stiffness of non-ruptured abdominal aortic aneurysms (AAAs) over time and as function of the maximum diameter. Each AAA has a specific symbol with a number representing the amount of months after inclusion. Regression lines are based on the regression analysis shown in Figure 6.3

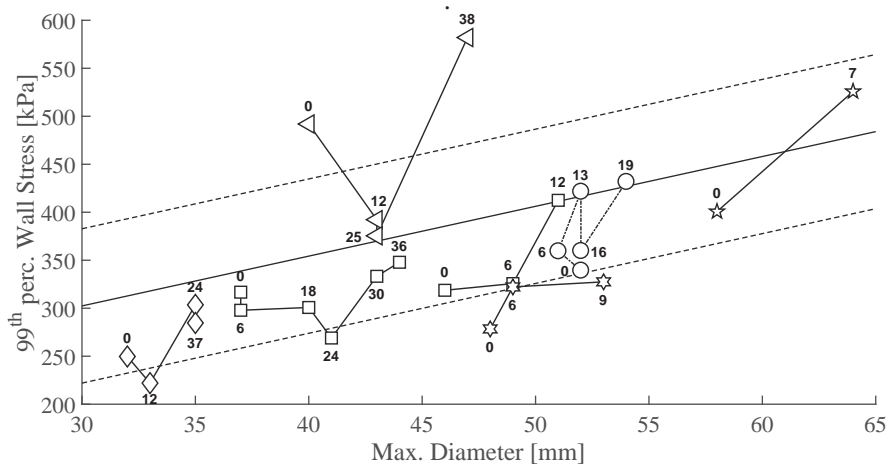


**Figure 6.6:** The 99<sup>th</sup> percentile peak wall stress (PWS) of seven non-ruptured abdominal aortic aneurysms (AAAs) over time and as function of the maximum diameter. Each AAA has a specific symbol with a number representing the amount of months after inclusion. The regression lines are based on regression analysis shown in Figure 6.4

terquartile range (IQR) of 1.3 (1.1 - 1.7) kPa·m before rapid growth of the AAA was observed, and a median stiffness of 1.8 (1.3 - 2.6) kPa·m before stable or slow growth of the aneurysms ( $p = 0.05$ ). No differences in the PWS were observed between the rapid and slow growing AAAs, i.e., a median PWS of 379 (IQR: 326 - 424) kPa and 370 (IQR: 313 - 432) kPa were measured for both groups, respectively ( $p = 0.60$ ).

Interestingly, a slightly lower arterial stiffness was measured before the onset of rapid AAA growth when compared to slow or no growth. However, to examine if this lower arterial stiffness could be used to predict upcoming growth, the change in arterial stiffness (before AAA growth was observed) is required. To calculate this change in aortic stiffness, the first US measurements of each patient was excluded for analysis since no preceding stiffness measurements were available. Results of the remaining datasets showed that in 8 out of the 12 consecutive datasets (67%) in the rapid growth group first a decrease in aortic stiffness was observed between two previous stiffness measurements. Furthermore, by analyzing only the follow-up intervals with at least 2.5 mm in 3 months, which is comparable with the current guidelines for surgical repair, i.e. rapid growth of 1 cm/year, a preceding decrease in arterial stiffness of 71% was observed (5 out of 7).

Finally, the absolute aortic stiffness and PWS of the AAA wall were compared with the subsequent AAA growth for different diameter groups. The results of this analysis are listed in Table 6.2 and Figure 6.8. Since none of the small AAAs revealed a growth rate of 2 mm in 3 months, the difference between slow and rapid growth for these AAA patients was set to 0.5 mm in 3 months. Figure 6.8 showed that the difference in stiffness between rapid and slow growing AAAs is predominantly visible in the moderate diameter group ( $p = 0.01$ ) and limited for the larger diameter group ( $p = 0.26$ ). For the small AAAs, no difference in aortic stiffness was noticed between the slow and rapid growing AAAs.

**Table 6.2:** Mechanical properties for the small, moderate, and large abdominal aortic aneurysms (AAAs). Each group is divided in slow and rapid growing AAAs. All values are reported as median with their interquartile range.

Variable:	Small AAAs		Moderate AAAs		Large AAAs	
	slow growth	rapid growth	slow growth	rapid growth	slow growth	rapid growth
Number US acquisitions [-]	34	4	87	11	50	6
AAA growth in 3 months [mm]	0 (0 - 0.2)	0.9 (0.7 - 1.0)	0.5 (0 - 1.0)	2.5 (2.1 - 3.0)	0.4 (0 - 1.0)	2.5 (2.0 - 2.5)
Aortic Stiffness [kPa·m]	1.2 (0.8 - 1.9)	1.0 (0.9 - 1.3)	1.8 (1.4 - 2.6)	1.3 (1.0 - 1.6)	2.0 (1.6 - 3.0)	1.7 (1.1 - 2.2)
99th perc. PWS [kPa]	302 (251 - 335)	304 (294 - 355)	375 (323 - 437)	361 (322 - 418)	404 (356 - 487)	404 (335 - 404)

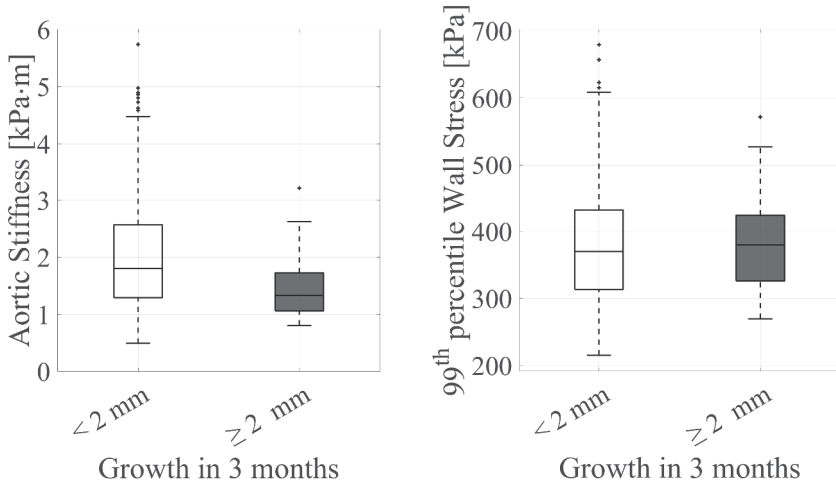


**Figure 6.7:** **Left:** Box-and-whiskers plots of the aortic stiffness as a function of the upcoming growth. One group represents stable or slow growth (< 2 mm in 3 months, in *white*), while the other represents rapid upcoming growth (≥ 2 mm in 3 months, in *dark gray*) of the AAA. **Right:** Box-and-whiskers of the 99<sup>th</sup> percentile peak wall stress for stable or slow growing (*white*), and for rapid growing (*dark gray*) AAAs.

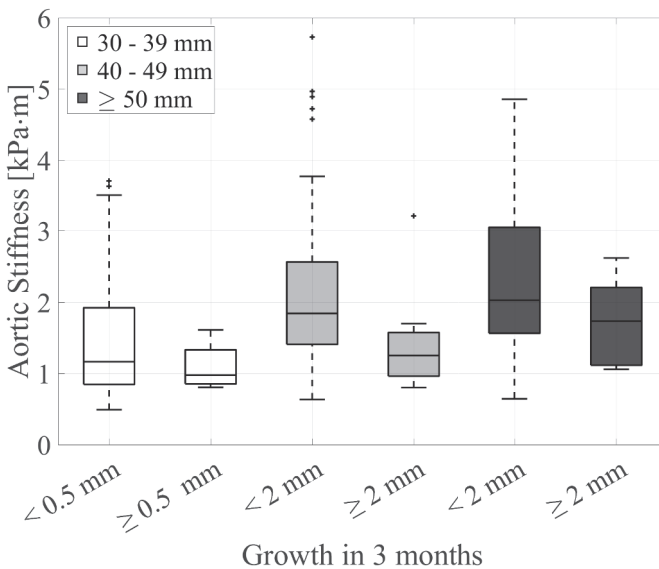


**Figure 6.8:** Box-and-whiskers plots of the aortic stiffness before the upcoming AAA growth for small (*white*), moderate (*gray*), and large (*dark gray*) AAAs. Each group is divided in stable or slow growing (*left*), and rapid growing AAAs (*right*).

## 6.4 Discussion

In this study, time-resolved 3D ultrasound data were acquired during regular follow-up intervals of AAA patients and used to assess the patient-specific stiffness of, and peak wall stress in the aortic wall. Monitoring aneurysm disease with these mechanical properties over time has the advantage to detect possible changes in aortic stiffness or peak stress even before a change in maximum aortic diameter can be observed. Follow-up of these mechanical properties provides opportunities to identify patients at risk, and by predicting possible growth of the AAA, the follow-up management could be personalized. Monitoring the expansion of the maximum diameter lacks sound scientific evidence and even misses spots of fast growth (Martufi et al., 2013). Hence, the fact that the timing of observations is based on the diameter itself is inadequate. Therefore, the mechanical properties were followed for a median period of 2 years in a group of AAA patients which covers the entire diameter range all off AAA patients in the outpatient follow-up. The two main findings of this study are:

1. Rapid growing AAAs have a lower arterial stiffness prior to AAA growth compared to slow growing AAAs. This difference in arterial stiffness is particularly observed in AAAs with a moderate to large size.
2. No significant difference in mechanical properties were obtained between the ruptured and non-ruptured AAAs in this study. Three out of four ruptured AAAs had a relatively low arterial stiffness before rupture, especially compared to non-ruptured AAAs, but the small sample number makes it impossible to draw any conclusions.

Prediction of AAA growth has the clinical advantage to guide in outpatient follow-up management. In the current study, lower arterial stiffnesses were observed for the rapidly growing AAAs, while overall the arterial stiffness increases as a function of the maximum AAA diameter. Rapid growing AAAs showed a 32%, and 14% decrease in median aortic stiffness compared to the AAAs with a low growth rate for respectively the moderate, and large AAAs (Figure 6.8). These findings are in accordance with the study by Wilson et al. (2003), which suggested that a 10% decrease in stiffness ( $E_p$ ) over time was associated with a 28% increase in AAA rupture risk compared with AAAs with no change in stiffness.

Furthermore, the current study also visualized a decrease in arterial stiffness before subsequent growth of the AAA. This phenomenon was observed in 67% of all patients that showed at least 2 mm growth in 3 months. This number increases further to 71% for all patients with at least a 3-monthly growth of 2.5 mm, which is comparable to current guidelines for surgical repair. This drop in arterial stiffness was also noticed when large absolute growth (instead of the growth rate) between two follow-up intervals was related to upcoming AAA growth. For all patients with at least 4 mm growth between two US measurements, 74% (14 out of 19 patients) revealed a preceding decrease in stiffness, and

this number increases to 83% (5 out of 6) for patients with at least 5 mm growth between two the follow-up intervals. A possible explanation for these findings might be that the AAA wall remodels before it is able to grow. Hence, the arterial stiffness is temporarily decreased as a consequence of the remodeling process. Using biomarkers this effect could be further examined (Lindholt et al., 2000; Hellenthal et al., 2012), however this was beyond the scope of current study.

Figure 6.6 shows the change in PWS over time for seven AAA patients. Overall, the PWS increases as function of the maximum AAA diameter, but for the individual patient it does not monotone increase and can fluctuate considerable. In a recent study by Stevens et al. (2017) the peak wall rupture risk index (PWRI) was followed over time for four AAA patients using CT data. A similar pattern was shown in this study, where the PWS overall increased with diameter but varies over time patient-specifically. Fluctuations in PWS or PWRI can be interpreted as adaptation (i.e. growth) of the aortic wall to reduce peak stresses in the AAA. An alternative explanation for these fluctuations might be that PWS should not be compared on a global scale, but locally. Local analysis of wall stress precludes that the PWS is obtained from different locations during follow-up intervals, and describes the stress behavior over time more reliably. However, this would require registration of the different datasets. This was not the goal of current research, and will be addressed in future studies.

In addition, four AAAs were included with a rupture of the AAA wall before current guidelines for surgical repair were achieved. The aortic stiffness and PWS of the last measurement before rupture were compared with non-ruptured AAAs. No statistical differences between both groups were observed, although in three cases the aortic stiffness was relatively low (Figure 6.3). This observation is in accordance with previous findings (rapid growing AAAs show lower aortic stiffness) and is in line with the study by Wilson et al. (1998). An elaborate comparison between the aortic stiffness of ruptured and non-ruptured AAAs will require more patient inclusions since the rupture incidence for patients under surveillance is relatively low (1 - 2%).

Interestingly, the 99<sup>th</sup> percentile wall stress was in the same range for the ruptured AAAs as it was for the non-ruptured AAAs (Figure 6.4). This is in contrast to the work by Fillinger et al. (2002) and Gasser et al. (2014), which showed that ruptured AAAs had in increased PWS. A possible explanation for this contra-dictionary finding is that PWS assessment may be underestimated. PWS is local parameter and regularly occurs in areas with high curvature. When a specific area with high curvature in the AAA geometry is missed because of the presence of bowel gas, calcifications in the aortic wall, or the reduced image quality (due to the depth of the AAA), the geometry could be less accurate, leading to an inaccurate prediction of the PWS. To overcome this issue, the image quality of the 3D US data could be improved by compounding multiple US acquisitions from different angles. However, this method will require first thorough verification to avoid stitching artefacts in the data.

One of the main limitations is the use of DICOM data in this study. DICOM data limit the precision of the 3D displacement estimates, and thereby the accuracy of the arterial



stiffness measurement. This constraint affects especially the displacement estimation of AAAs, which is a deep lying structure with limited compliance. Capturing the radio-frequency (RF) data before conversion into DICOM data could solve this issue and improve the displacement estimates.

Another limitation is the model complexity. Firstly, a Neo-Hookean model was used to describe the material behavior between patient-specific diastolic and systolic pressure. More complex material models (e.g., Holzapfel et al. (2000)) are available and describe the AAA behavior more reliably. However these models introduce more material parameters and thereby more uncertainties. Secondly, the intraluminal thrombus (ILT) was not included in the finite element model. Studies have shown that presence of ILT affect the strength of the AAA wall and ILT thickness might be associated with local AAA growth (Kazi et al., 2003; Martufi et al., 2016). Ultimately, including the patient-specific AAA wall thickness would be desirable since this will directly improve the arterial stiffness estimation and wall stress prediction. Unfortunately, none of the available non-invasive imaging modalities are currently able to measure the AAA wall thickness accurately.

In future research, a large multi-center clinical trial should be employed to study possible differences in mechanical properties (i.e., aortic stiffness and PWS) between ruptured and non-ruptured AAAs. Moreover, the ability to predict upcoming AAA growth should be investigated by following the aortic stiffness prospectively. Presented US-based characterization method might be an ideal methodology to perform this multi-center clinical trial, since it is easy implementable and only require a single 4D US acquisition and a brachial blood pressure measurement.

## 6.5 Conclusion

In conclusion, using the combination of time-resolved 3D ultrasound and biomechanical modeling, the patient-specific arterial stiffness and peak wall stress were assessed and followed over time in a longitudinal clinical study. Results revealed that rapid growing AAAs have a lower arterial stiffness prior to AAA growth, compared to slowly growing or stable AAAs. In addition, no differences in 99<sup>th</sup> percentile wall stress were observed between the slow and rapid growing AAAs. The lower arterial stiffness might be a predictive marker for upcoming AAA growth, and most certainly deserves further investigation.

# Reproducibility Assessment of US-Based Aortic Stiffness Quantification and Verification using Bi-axial Tensile Testing

This chapter is based on: Reproducibility Assessment of Ultrasound-Based Aortic Stiffness Quantification and Verification using Bi-axial Tensile Testing, **E.M.J. van Disseldorp**, M.H.M.H. van den Hoven, E.N. van de Vosse, M.R.H.M. van Sambeek, R.G.P. Lopata, *Submitted*, 2018;

## Abstract

**Background:** Current guidelines for abdominal aortic aneurysm (AAA) repair are primarily based on the maximum aortic diameter and its growth rate, but these methods lack robustness in decision making. Using time-resolved 3D ultrasound (4D US) additional risk estimators such as patient-specific peak wall stresses and wall stiffness can be measured non-invasively. In this study, **1)** the reproducibility of this US-based stiffness measurement is assessed *in vitro* and *in vivo*, and **2)** the method is verified using the gold standard: bi-axial tensile testing of the excised aortic tissue.

**Methods:** For the *in vitro* study, 4D US data were acquired in an idealized inflation experiment using porcine aortas ( $n = 7$ ). The full aortic geometry was automatically segmented, tracked over the cardiac cycle, and afterwards finite element analysis was performed by calibrating the finite element model to the measured US displacements to find the global aortic wall stiffness. For verification purposes, the porcine tissue was subjected to bi-axial tensile testing.

Secondly, four AAA patients were included and 4D US data were acquired before open aortic surgery was performed. Similar to the experimental approach, the 4D US data were analyzed using the iterative finite element approach. During surgery, aortic tissue was harvested and the resulting tissue specimens were analyzed using bi-axial tensile testing. Finally, reproducibility was quantified for both methods and the intraclass correlation (ICC) was assessed.

**Results:** A high reproducibility was observed for the wall stiffness measurements using 4D US, i.e., an ICC of 0.91 (95% CI: 0.78 - 0.98) for the porcine aortas and an ICC of 0.98 (95% CI: 0.84 - 1.00) for the AAA samples. Verification with bi-axial tensile testing revealed a good agreement for the inflation experiment (bias: 0.00 kPa·m; interquartile range (IQR): -0.04 - 0.02 kPa·m) and a moderate agreement for the AAA patients (bias: 0.61 kPa·m; IQR: -0.27 - 1.29) kPa·m), partially caused by the diseased state and inhomogeneities of the tissue.

**Conclusions:** The performance of aortic stiffness characterization using 4D US was assessed and verified using bi-axial tensile testing. Overall it revealed a high reproducibility and a moderate agreement with *ex vivo* mechanical testing. Future research should include more patient samples, to statistically assess the accuracy of the current *in vivo* method, which is not trivial due to the low number of open surgical interventions.

## 7.1 Introduction

An abdominal aortic aneurysm is a degenerative, localized dilation of the abdominal aorta which can eventually lead to a life-threatening hemorrhage when ruptured. Current guidelines for aortic surgery only include geometrical measures (Moll et al., 2011), however, several studies have shown that this method lacks robustness (Nicholls et al., 1998; Conway et al., 2001). As a consequence, over the last two decades several alternatives have been proposed for patient-specific AAA rupture risk assessment.

Wall stress analysis has been proposed and showed promising results in differentiating patients with ruptured and non-ruptured AAAs with similar maximum diameters (Fillinger et al., 2002; Venkatasubramaniam et al., 2004; Truijers et al., 2007; Gasser et al., 2014). These models require the patient-specific 3D geometry, arterial blood pressure, wall thickness, and the patient-specific material behavior. Since most of the wall stress studies used computed tomography (CT) to obtain the 3D AAA geometry, the material parameters to describe the AAA wall behavior were obtained from literature. The first wall stress studies mainly relied on material parameters obtained from uni-axial tensile test data of AAA tissue described by Raghavan et al. (1996). Later, in the work by Vande Geest et al. (2006b) and Polzer et al. (2013) bi-axial tensile tests were performed which described the anisotropic nature of the aortic tissue more accurately.

Mechanical characterization of AAA wall properties is not solely performed to provide input for patient-specific wall stress analysis, it can also be used as a measure for rupture risk on its own. In the first study by He and Roach (1994) it was shown that the amount of collagen fibers had increased in AAA tissue, whereas the amount of elastin and muscle cells was lower compared to healthy aortic tissue. In the studies by Wilson et al. (1998, 2003) a decrease in aortic compliance over time was measured for AAA patients using 2D ultrasound. In this study it was suggested that failure of compliance to decrease with size might be a marker for the onset of symptoms, such as above average growth of the aneurysm, or rupture. This assumption was strengthened by a tensile test study by Di Martino et al. (2006), which suggested that AAA rupture is associated with AAA weakening instead of stiffening. Later, *ex vivo* mechanical testing of AAA tissue was performed to examine the effect of presence of intraluminal thrombus on the wall strength of the AAA wall underneath (Tong et al., 2011, 2013), to assess the axial pre-stretch in AAAs and healthy tissue (Horný et al., 2011, 2014), and to capture the complete non-linear anisotropic behavior of the AAA wall to identify the material constants of the coefficients for constitutive models proposed (O'Leary et al., 2014; Pancheri et al., 2017).

Recently, we proposed an *in vivo* approach using time-resolved 3D (4D) ultrasound which can be used to perform patient-specific mechanical characterization of the aortic wall using finite element (FE) analysis in the pressure range available, by computing aortic wall stresses, and, by calibrating the 4D ultrasound (US) displacement field to the finite element output, estimating the wall stiffness (van Disseldorp et al., 2018). This method has

the advantage that it does not use radiation exposure, is relatively cheap, and can be easily implemented in a clinical work-flow. However, to rely on these wall stiffness measurements in a clinical setting, the reproducibility of this methodology still needs to be assessed as well as the method requires verification in terms of accuracy.

Verification experiments can be performed *ex vivo* using uni- or bi-axial tensile testing of aortic tissue. However, since the introduction of endovascular aneurysm repair (EVAR) in the early 90's (Parodi et al., 1991), EVAR has been widely used and is currently the preferred method of treatment for the majority of AAAs in follow-up (Chaikof et al., 2018). As a consequence, harvesting aortic tissue of patients in outpatient follow-up is challenging since the majority of patients are not subjected to open aortic surgery.

Alternatively, an idealized *in vitro* framework can be used to mimic the *in vivo* situation using porcine aortas (Mascarenhas et al., 2016). Similar to the AAA patient measurements, 4D US data can be acquired and analyzed by iterative finite element analysis, resulting in the porcine aortic stiffness. The advantage of current approach is that the porcine aortas are considered waste material, easy accessible, and can be used for bi-axial tensile testing (Lopata et al., 2014). Subsequently, the bi-axial stress-strain behavior can be used to validate the US-based stiffness measurement.

The purpose of this study is twofold. First, an *in vitro* experiment was designed and performed in which porcine aortas were mechanically inflated under physiological conditions in an idealized mock set-up loop. 4D US-based aortic stiffness was assessed in a controlled set-up, followed by bi-axial tensile testing for verification of the material properties found. Secondly, the reproducibility of both stiffness characterization methods was measured. Multiple heartbeats in the 4D US data were analyzed, whereas in the bi-axial tensile test experiments multiple aortic specimens were tested. In addition to the porcine aorta experiment, four AAA patients obtained from open surgeries were included to compare *in vivo* results.

## 7.2 Materials and Methods

### Experimental validation

A large part of the thorac-abdominal porcine aorta (length 12 - 20 cm) was used, originating from healthy young pigs ( $N = 7$ ) which were between 5 and 7 months of age and weighed between 100 and 120 kg. The porcine aortas were obtained from the local slaughterhouse and were considered a waste product. Directly after resection (< 6 hours), most of the excess fat and connective tissue was removed. The aortas were individually stored in a  $-20^{\circ}\text{C}$  freezer to preserve tissue degeneration awaiting experimental measurements (Stemper et al., 2007; O'Leary et al., 2014).

Prior to inflation and tensile testing experiments, each aorta was thawed slowly and remaining excess tissue was removed. Both ends were connected to cannulas, and side-

branches were securely closed with suture thread and tissue glue (Loctite superglue-3 PowerFlex, Henkel, Germany). Finally, the aortas were tested for leakage. When no further leakage was observed, each aorta was mounted in the mock set-up look with a longitudinal pre-stretch,  $\lambda_{zz}$  of 1.22 (Han and Fung, 1995). The setup is visualized in Figure 7.1.

The mock circulation set-up used was similar to the work in Mascarenhas et al. (2016), with the addition of a container surrounding the aorta. A 3D printed solid spine (Polyamide 12, Shapeways Inc., Eindhoven, the Netherlands) was positioned close to the dorsal side of the aorta. The presence of the spine will heavily influence the deformation pattern of the aorta and help mimicking the *in vivo* situation. The 3D geometry of the spine was obtained after segmentation of the abdominal part of the human spine in CT data using Mimics segmentation software (Mimics Research 17.0, Materialise, Leuven, Belgium).

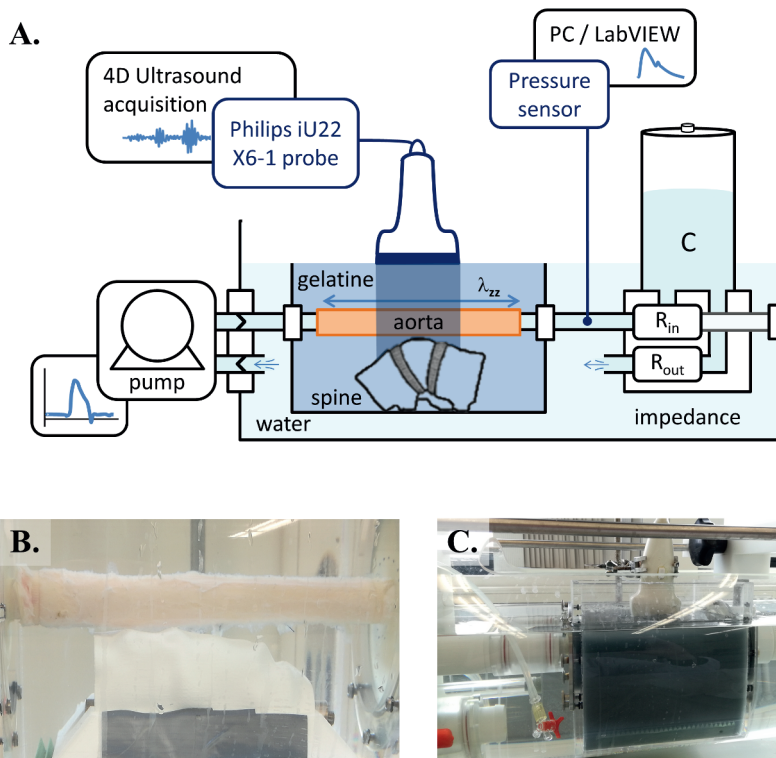


**Figure 7.1:** (A) Schematic overview of the mock loop used for the inflation tests. The aorta is mounted in the setup attached to two cannulas, positioned in a container filled with gelatin. The aorta is pressurized by pumping water from the basin into the aorta. Distal to the aorta a three-element Windkessel model is connected. Ultrasound data were recorded using a Philips iU22 scanner equipped with a 3D matrix probe. (B) Porcine aorta in the mock loop setup with the spine positioned at the dorsal side. (C) The aorta and spine surrounded by the gelatin solution. The gelatin is colored gray due to the addition of silicon carbide in the gelatin mixture.

After the spine and aorta were correctly positioned in the container, gelatin was added to mimic the surrounding tissue. A gelatin concentration of 8%wt was chosen since this results in a gelatin solution with an average Young's modulus of approximately 25 kPa (Hall et al., 1997). This Young's modulus is similar to that of surrounding subcutaneous adipose tissue (Geerligs et al., 2008). Although the mechanical properties of gelatin are comparable to the surrounding biological tissue, it does not have the same acoustical scattering properties as the actual tissue. Therefore 1%wt silicon carbide (SiC -400 Mesh, Sigma-Aldrich, Germany) was added to the gelatin mixture to achieve acoustic scattering in the gelatin, resulting in a speckle pattern in the US images. The gelatin mixture was heated to 60°C until all the gelatin was dissolved, and afterwards cooled down to 30°C whilst it kept being stirred. Finally, the gelatin was added to the aorta mock set-up. Inflation tests were performed after the gelatin had solidified.

Before inflation experiments, the water basin was filled with a saline solution of 0.9% which is similar to physiological concentrations. Afterwards, the aorta was inflated by pumping water from the basin into the aorta. Distal to the aorta a three-element Windkessel model was connected. This Windkessel model consist of a compliance (C) where the saline solution can be stored in a large container, and an inlet ( $R_{in}$ ) and outlet ( $R_{out}$ ) resistance. These Windkessel elements were adapted in order to obtain a physiological flow pulse in the aorta with a diastolic pressure of approximately 70 mmHg in diastole and 130 mmHg in systole. For more details on the hemodynamics part of the setup and protocol, we refer to Mascarenhas et al. (2016).

## Porcine data acquisition

4D US data were acquired during the inflation experiment. An example of the obtained US data is shown in Figure 7.2. A Philips iU22 scanner (Philips Medical Systems, Bothell, WA, USA) equipped with a matrix curved array probe (X6-1, center frequency = 3.5 MHz) was used for data acquisition. Multiple heart cycles were recorded with a volume rate of 8.1 - 10.3 Hz, while simultaneously measuring the intra-aortic pressure with a pressure sensor (St. Jude Medical, Saint Paul, MN, USA). It was ensured that at least five cardiac cycles were present in the US data.

The porcine US data were tracked over time to detect the diastolic and systolic phase of the cardiac cycle. Afterwards automatic segmentation and 3D displacement tracking were applied. The diastolic geometry of the porcine aorta (PA) was converted into a mesh with a generic wall thickness of 1.6 mm (Peña et al., 2015). Next, mechanical characterization was applied to predict the wall stiffness of these porcine aortas as described in van Disseldorp et al. (2018). Finally, the porcine aorta was removed from the gelatin solution and disconnected from the cannulas. The aorta was kept moist with PBS until bi-axial tensile testing was performed.

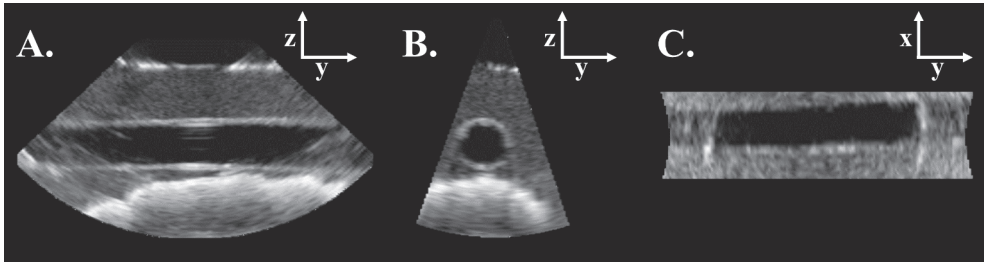


**Figure 7.2:** Example of the 3D ultrasound data of the porcine aorta, surrounded by the gelatin solution. (A) A longitudinal cross-section of the data is shown with the spine located at the dorsal side of the aorta. In (B) the corresponding transversal plane and in (C) the coronal plane are visualized.

### Patient population and tissue storage

In total 12 human specimens were obtained from four AAA patients (age: 70 - 83 years and max. diameter: 50 - 100 mm). Human samples were obtained during elective open surgery. All patients gave informed consent for both 4D US acquisition prior to surgery, and the use of tissue samples for biomechanical analysis post-surgery. This study was approved by the local ethics committee of the Catharina Hospital Eindhoven.

During open surgery, a specimen was resected in the longitudinal direction of the aorta with dimensions of approximately 40 by 20 mm. This tissue was stored in a container with phosphate buffered saline (PBS) solution and transported to the Eindhoven University of Technology. To prevent tissue deterioration while waiting for bi-axial tensile test analysis, the tissue was frozen at  $-80^{\circ}\text{C}$  in a 90% PBS and 10% dimethyl sulfoxide (DMSO) solution (Stemper et al., 2007).

### Ultrasound acquisition and analysis

4D US data of all AAA patients were acquired with a similar Philips iU22 scanner and the same X6-1 matrix probe as used in the experimental approach. The period between US imaging and the surgery ranged between 0 - 1 month. Volume data were acquired during breath-hold for 5 seconds in supine position with an acquisition rate of 3.2 - 4.4 Hz.

The 4D US data were imported in Matlab (2017a, Mathworks Inc., Natick, MA, USA) and converted into a Cartesian coordinate system. The spatial resolution varied from 0.5 - 0.6 mm in the axial, 1.1 - 1.3 mm in the elevational, and 1.0 - 1.2 mm in the lateral direction (Figure 7.3 left).

First, a longitudinal 2D slice in the middle of the AAA was selected and the aortic wall was segmented manually. A coarse-to-fine 2D displacement estimation algorithm (Lopata et al., 2009) was adapted for DICOM data and applied to identify the diastolic and systolic configuration of the AAA in the 3D US data. Subsequently, automatic segmentation was



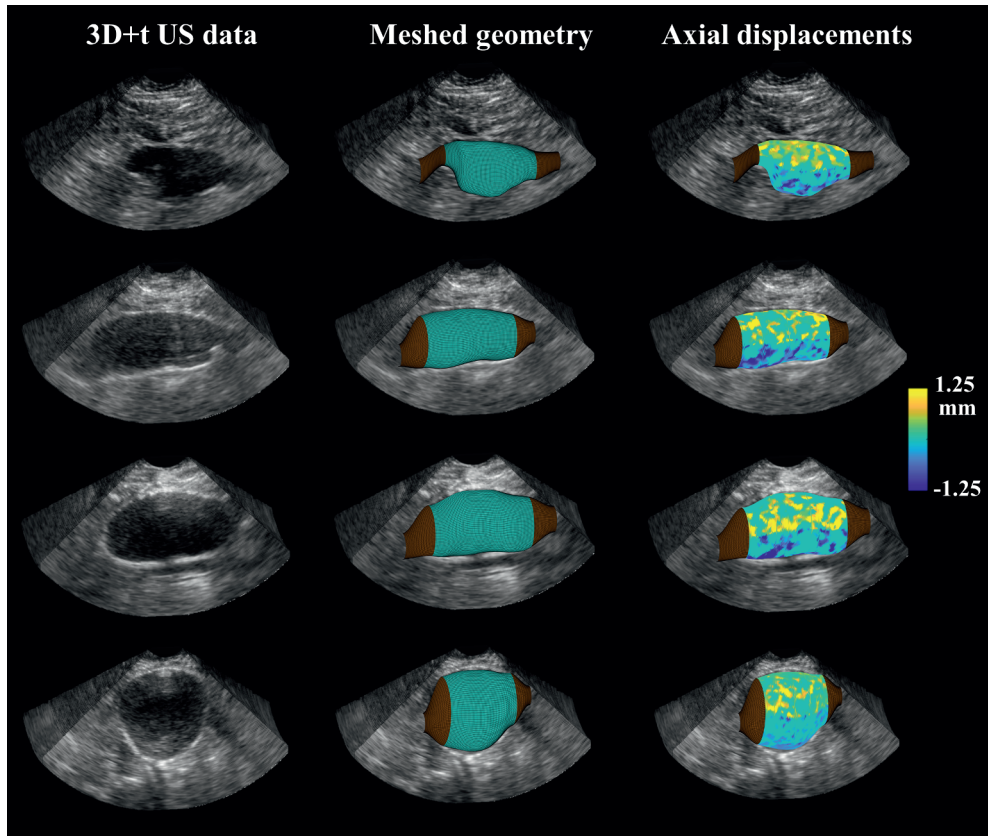


**Figure 7.3:** A cross-sectional view from the 3D ultrasound data of the four AAA patients (*left*). After automatic segmentation the geometry was meshed and used as input for finite element analysis (*middle*). The segmented geometry was used for 3D speckle tracking and the measured axial displacements (*right*) were used to calculate the subject specific aortic stiffness.

applied in the diastolic 3D geometry. Segmentation was first conducted in the 2D cross-sectional planes, followed by a 3D regularization step. For more detail on the segmentation approach, we refer to Chapter 5. The diastolic geometry was tracked over time using 3D speckle tracking (Lopata et al., 2011), followed by the FE-based mechanical characterization (van Disseldorp et al., 2018). In this calibration process the aortic wall stiffness (incremental shear modulus multiplied by the wall thickness) was adapted until the axial displacements in the finite element model were similar to the measured US displacements. The final axial US-displacements are visualized in Figure 7.3 right.

### Bi-axial tensile testing

Examples of the tissue samples, resected during surgery, are shown in Figure 7.4. The amount of tissue samples that were harvested from the resected AAA tissue varied between two and four samples. For the porcine aortas, in total five samples per specimen were cut from the aortic tissue at different locations. All tissue samples were obtained with a punch to ensure equal dimensions of 12 by 12 mm for each sample.

The samples were mounted in the bi-axial tensile testing device (CellScale, Waterloo, Canada) (Figure 7.5). It was ensured that the longitudinal and circumferential direction of the aortic tissue corresponded with the two directions of the tensile testing device. The tissue was connected to the device with a rake with five tines on each side (tine diameter: 305  $\mu\text{m}$ , tine spacing: 1.0 mm, puncture depth 1.9 mm), resulting in a bi-axial tensile testing area of 5.0 by 5.0 mm. Graphite particles were attached on the tissue and afterwards the tissue was placed in a bath filled with PBS at a temperature of 37 °Celsius corresponding to the physiological body temperature.

All specimens were pre-conditioned by applying ten equi-biaxial stretch cycles of 10% stretch with a stretch rate of 0.02  $\text{s}^{-1}$  (Okamoto et al., 2002). After each stretch cycle, a resting period of 5 seconds was applied. This resting period was applied to allow the aortic

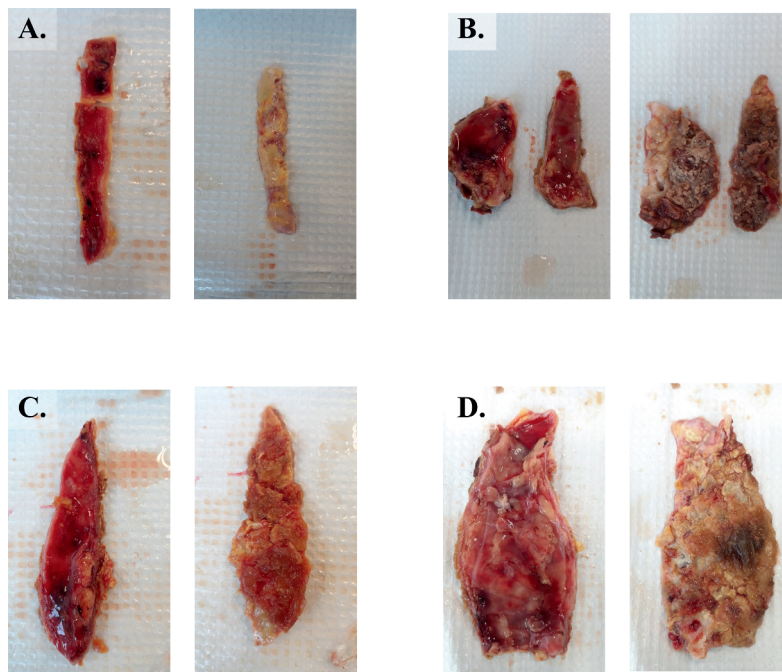


**Figure 7.4:** Human AAA tissue samples of the four patients included in this study. In all four cases, the adventitia side of the aorta is shown in the left image, while in the right image the internal intima side of the aortic tissue is shown.

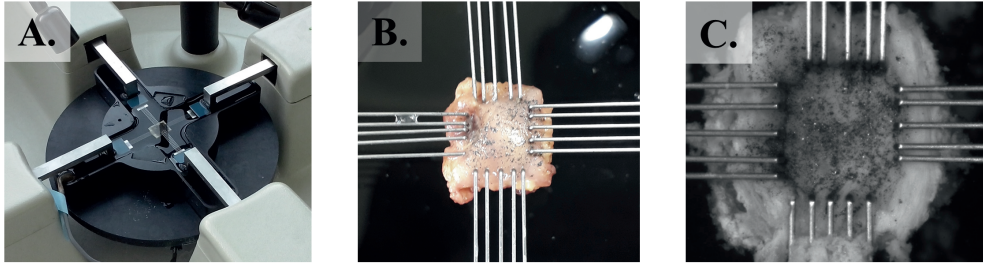


**Figure 7.5:** (A) Bi-axial tensile test device, with the AAA tissue sample mounted in the test setup with four rakes (B). (C) AAA tissue samples during tensile testing is visualized.

tissue to return to its initial configuration. Subsequently, in case of the porcine aortas, a longitudinal pre-stretch of  $\lambda_{zz} = 1.22$  was applied and kept constant for the remaining testing protocol (Han and Fung, 1995). For the human AAA specimens, the presence of longitudinal pre-stretch is unknown. In the work of Horný et al. (2011) it has been shown that the pre-stretch decreases with age and diameter in post-mortem specimens. The pre-stretch is approximately 1.3 in young aortas (20 - 30 years) and decreases to 1.0 in elderly people (70 - 90 years). Moreover, it is assumed that the longitudinal pre-stretch is negligible in aneurysms, due to the presence of calcifications and thrombus. For these reasons, no axial pre-stretch was applied to the AAA samples ( $\lambda_{zz} = 1.0$ ). After the pre-stretch was applied, the force on the rakes ( $F_{\text{rakes}}$ ) was set to zero.

Next, the tissue was stretched in the circumferential direction ( $\lambda_{\theta\theta}$ ) with increasing stretch cycles from 1.15 to 1.4 in steps of 0.05 at a stretch rate of  $0.02 \text{ s}^{-1}$ , and resting period of 5 seconds. During the entire testing experiment, both force and the distance between the rakes were recorded simultaneously with a frequency of 1 Hz for the porcine aortas and 5 Hz for the AAA specimens.

## Mechanical analysis

The force and displacement data were exported from the bi-axial tensile testing software (CellScale, Waterloo, Canada) into Matlab (2017a, Mathworks Inc., Natick, MA, USA). Similar to the US-based characterization method, an incompressible Neo-Hookean constitutive material behavior was assumed to describe the stress-strain curve for the stretch range between diastolic and systolic pressure. This material law accounts for large, linear deformations, is a valid linearization of the non-linear material behavior on the limited domain found *in vivo* and is given by Equation (7.1):

$$\boldsymbol{\sigma} = -p_0 \mathbf{I} + G(\mathbf{B} - \mathbf{I}) \quad (7.1)$$

with  $\boldsymbol{\sigma}$  the Cauchy stress tensor,  $p_0$  the Lagrange contribution to the hydrostatic stress that enforces incompressibility ( $-tr(\boldsymbol{\sigma})/3$ ),  $\mathbf{I}$  the identity matrix,  $G$  the shear modulus and  $\mathbf{B}$  the left Cauchy-Green deformation tensor. Since data is only available for a certain pressure range, not the total modulus  $G$ , but an incremental or tangential modulus,  $G_{TT}$ , will be estimated. Using this constitutive equation, the momentum and mass balance equations then read:

$$\begin{cases} \nabla \cdot \boldsymbol{\sigma} = -\nabla p + G \nabla \cdot (\mathbf{B} - \mathbf{I}) & = 0 \\ \det(\mathbf{F}) & = 1 \end{cases} \quad (7.2)$$

Note that the left Cauchy-Green deformation tensor  $\mathbf{B}$  is defined as  $\mathbf{B} = \mathbf{F} \cdot \mathbf{F}^T$ , and  $\mathbf{F}$  represents the deformation tensor obtained from the tensile test displacement data.

Since the force on the rakes ( $F_{rakes}$ ) was set to zero after the pre-stretch in the longitudinal direction ( $\lambda_{zz}$ ) was applied, the stress in the circumferential ( $\sigma_{\theta\theta}$ ) and radial ( $\sigma_{rr}$ ) direction can be derived using the constitutive law for Neo-Hookean materials (Equation Equation (7.1)). The circumferential and radial stresses now become:

$$\sigma_{\theta\theta} = -p_0 + G(\lambda_{\theta\theta}^2 - 1) \quad (7.3)$$

$$\sigma_{rr} = -p_0 + G\left(\frac{1}{\lambda_{\theta\theta}^2} - 1\right) \quad (7.4)$$

The hydrostatic pressure,  $p_0$ , can be eliminated in above mentioned Equation (7.3) by subtracting Equation (7.4) from Equation (7.3), which results in:

$$\sigma_{\theta\theta} - \sigma_{rr} = G\left(\lambda_{\theta\theta}^2 - \frac{1}{\lambda_{\theta\theta}^2}\right) \quad (7.5)$$

Since the stress in the out-of-plane direction of the applied stretch is negligible with respect to the applied direction, i.e.,  $\sigma_{rr} \ll \sigma_{\theta\theta}$ , plane stress ( $\sigma_{rr} = 0$ ) can be assumed and Equation (7.5) can be simplified to:

$$\sigma_{\theta\theta} = G\left(\lambda_{\theta\theta}^2 - \frac{1}{\lambda_{\theta\theta}^2}\right) \quad (7.6)$$

in which the circumferential stress is calculated by:

$$\sigma_{\theta\theta} = \frac{F_{rakes}}{A} = \frac{F_{rakes}}{w \cdot h(\lambda_{\theta\theta})} \quad (7.7)$$

with  $A$  the surface where the force  $F_{rakes}$  acts on, which is defined as the width of the

specimen ( $w$ ) multiplied by the thickness of the sample ( $h$ ). Since the material behavior was assumed incompressible (Equation (7.2)), the wall thickness can be directly related to circumferential stretch and the measured wall thickness at zero pressure ( $h_0$ ):

$$h(\lambda_{\theta\theta}) = \frac{h(0)}{\lambda_{\theta\theta}} \quad (7.8)$$

In general, a tensile test stretch cycle was selected in which the mean diastolic circumferential stress ( $\bar{\sigma}_{\theta\theta_{dia}}$ ) and systolic circumferential stress ( $\bar{\sigma}_{\theta\theta_{sys}}$ ) calculated from the US-based finite element models was present in the tensile stress-strain data. The circumferential diastolic and systolic stresses were used to match the US-based incremental modulus with that obtained from part of the stress-strain curve which corresponds with the *in vivo* loading.

Finally, the incremental shear modulus,  $G_{TT}$ , was calculated from a least-square fit in MATLAB, with the measured stretches, and calculated stresses on the given domain between the subject-specific diastolic to systolic pressures:

$$G_{TT} = \frac{\bar{\sigma}_{\theta\theta_{sys}} - \bar{\sigma}_{\theta\theta_{dia}}}{\lambda_{\theta\theta}^2 - \frac{1}{\lambda_{\theta\theta}^2}} \quad (7.9)$$

To calculate the wall stiffness, the incremental shear modulus,  $G_{TT}$ , was multiplied with the wall thickness at diastole using Equation (7.8).

## Reproducibility and verification

The reproducibility of the 4D US-based characterization method was tested by analysis of multiple heart cycles within one 4D US dataset for all AAA patients ( $N = 4$ ) and porcine aorta ( $N = 7$ ) datasets. The amount of heart cycles that were available in the US data varied between 2 and 4 for the AAA patients. In case of the porcine aortas, five heart cycles per aorta were analyzed resulting in a total of 35 stiffness measurements.

For the bi-axial tensile testing method, multiple tissue specimens were harvested from the resected AAA samples (Figure 7.4) and porcine aortas (Figure 7.1B). For the AAA samples, four tissue specimens of 12 mm by 12 mm could be obtained from the resected tissue. In case of the porcine aortas, aortic tissue was not the limited factor and in total five tissue samples were obtained from different locations of the aorta and mechanically tested.

To quantify the reproducibility of both the 4D US and bi-axial tensile testing method, the intra-class correlation coefficient (ICC) was calculated for the porcine aortas and the AAA patients, including its 95% confidence interval (CI). In general, ICC values lower than 0.5 indicate a poor reproducibility, ICC's between 0.50 and 0.75 indicate a moderate reproducibility, ICC's between 0.75 and 0.90 indicate a good reproducibility, while values larger than 0.90 indicate an excellent reliability (Koo and Li, 2016).

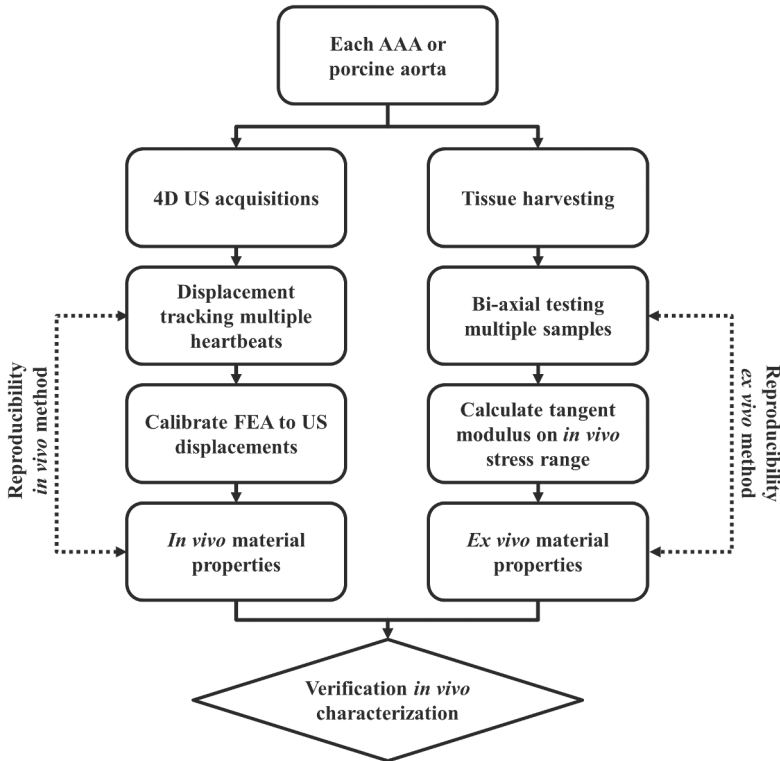


**Figure 7.6:** A graphical overview of the current method to test the reproducibility of the *in vivo* and *ex vivo* based mechanical characterization method. For each abdominal aortic aneurysm (AAA) and porcine aorta (PA) reproducibility of both methods is tested. Finally, mechanical parameters obtained from the *in vivo* method are verified using gold-standard: bi-axial tensile testing of the samples.

Finally, the agreement between both methods was assessed by the comparing the obtained wall stiffness for the *in vivo* and the *in vitro* cases. Bland-Altman analysis and pairwise comparison was performed to quantify a possible bias and the limits of agreement. A graphical overview of the data analysis workflow is found in Figure 7.6.

## 7.3 Results

### Porcine aortas

All 4D US datasets were analyzed. Visual inspection of the segmented geometry and the wall stress distribution did not reveal any artifacts or other complications. The measured diastolic and systolic pressure in the porcine aorta (PA) experiments varied between 61 - 73 mmHg and 120 - 130 mmHg, respectively. The porcine wall thickness at zero pressure ( $h_0$ ) was measured with a caliper and ranged between 1.75 - 2.35 mm for the different aortas.

**Table 7.1:** Wall stiffness of porcine aortas (PAs) in the physiological range. US indicates the stiffness predicted using ultrasound, and TT represents the wall stiffness from bi-axial tensile testing. S1 - S5 is an abbreviation for the sample number. All material properties are provided in kPa-m.

	PA 1		PA 2		PA 3		PA 4		PA 5		PA 6		PA 7	
	US	TT	US	TT	US	TT	US	TT	US	TT	US	TT	US	TT
<b>S1</b>	0.26	0.26	0.19	0.24	0.22	0.36	0.41	0.37	0.35	0.33	0.33	0.32	0.43	0.39
<b>S2</b>	0.26	0.27	0.19	0.25	0.22	0.35	0.38	0.32	0.34	0.31	0.30	0.42	0.35	0.37
<b>S3</b>	0.27	0.26	0.19	0.23	0.22	0.32	0.42	0.33	0.34	0.32	0.33	0.39	0.35	0.38
<b>S4</b>	0.25	0.27	0.19	0.22	0.22	0.31	0.49	0.38	0.34	0.32	0.39	0.33	0.36	0.38
<b>S5</b>	0.28	0.26	0.19	0.26	0.23	0.34	0.38	0.48	0.34	0.33	0.32	0.34	0.39	0.36

In Table 7.1 the wall stiffness is shown for the US-based method. This wall stiffness was obtained by multiplying the calibrated shear modulus from the iterative finite element process with the diastolic wall thickness (i.e., 1.6 mm). The ICC was calculated and revealed a good to excellent reproducibility (ICC = 0.91; 95% CI: 0.78 - 0.98). Although overall a high reproducibility is obtained using the 4D US method, inter-aorta reliability varies among the different samples. In porcine aorta 5 and 7 the spread is considerably higher compared to aorta 1 - 3.

For all seven porcine aortas, the median stress-strain behavior with its interquartile range (IQR) is visualized in Figure 7.7. In this graph, and for further analysis of the tensile test data, the 30% stretch cycle was used since this cycle covered the complete physiological loading conditions during the inflation experiments and revealed the least hysteresis. For each individual porcine aorta, the mean diastolic and systolic circumferential wall stresses were calculated from the five finite element model representing a separate heart cycle each. These mean circumferential wall stresses ranged between 40 - 64 kPa in diastole and 93 - 131 kPa in systole, respectively. The resulting incremental shear modulus for this stress range was converted into the wall stiffness and the corresponding values are reported in Table 7.1.

Similar to the inflation experiments the reproducibility varied between different porcine aortas (PAs). In PA 4 the aortic stiffness ranged between 0.32 - 0.48 kPa-m, while in PA 1 the variation with the different samples was only 0.01 kPa-m. Noticeable is that PA 4, the aorta with the lowest reproducibility in the tensile testing experiments, also revealed the poorest reliability in the 4D US measurement. Overall the ICC showed a moderate reproducibility with an ICC of 0.74 and a 95% confidence interval of 0.45 - 0.94.

### AAA samples

4D US data were acquired the day before surgery for two patients, while the other two patients underwent US acquisition less than a month before surgery. This intermediate time period was minimized to ensure that the *in vivo* measured wall stiffness was representative to the aortic tissue. The automatic segmented AAA geometry, the corresponding mesh, and

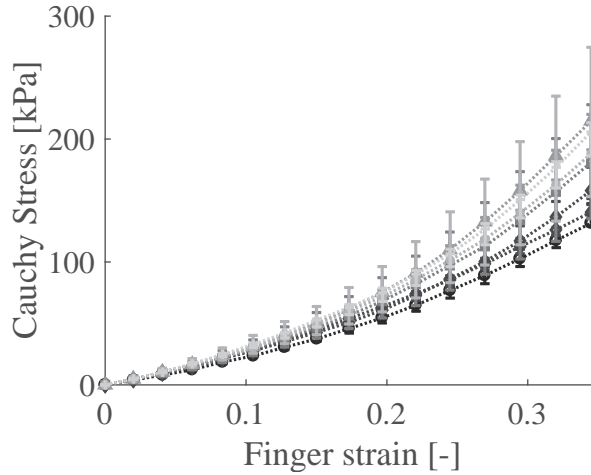


**Figure 7.7:** Median stress-strain curves for all seven porcine aortas (black to gray lines) for the 30% stretch cycle. The error bars represent the interquartile range (IQR).

the tracked axial displacement between diastole and systolic are shown in 7.3 right. The brachial pressures measured for patient AAA 1 - AAA 4 were: 79 - 132 mmHg, 92 - 143 mmHg, 88 - 127 mmHg, and 93 - 119 mmHg, respectively. The corresponding patient-specific wall stiffness values are listed in Table 7.2. For these aortas, only two heart cycles were captured in the 4D US data. Therefore, in these cases only two wall stiffness measurements were analyzed. Reproducibility was tested and resulted in an ICC of 0.98 (CI: 0.84 - 1.00).

Wall stiffness measurements revealed that AAA 2 and AAA 4 behave approximately three times stiffer compared to AAA 1 and AAA 3 (Table 7.2), and were statistically different ( $p = 0.002$ ). Moreover, the two AAAs with the highest aortic stiffness were also the AAAs which were obtained from the aneurysms with the largest diameter (AAA 2: 57 mm and AAA 4: 100 mm compared to AAA 1: 50 mm and AAA 3: 55 mm). Furthermore, the less stiff AAAs, AAA 1 and AAA 3, were subjected to aortic surgery due to rapid growth of the aneurysm,

**Table 7.2:** Wall stiffness of abdominal aortic aneurysms (AAAs) in the physiological range. US indicates the stiffness predicted using ultrasound, and TT represents the wall stiffness from bi-axial tensile testing. S1 - S4 is an abbreviation for the sample number.

	AAA 1		AAA 2		AAA 3		AAA 4	
	US	TT	US	TT	US	TT	US	TT
<b>S1</b>	0.91	1.04	3.10	2.36	0.86	1.52	3.50	2.10
<b>S2</b>	1.09	0.87	3.32	1.98	0.97	1.70	3.09	1.78
<b>S3</b>	1.20	0.98	3.03	NA	NA	1.80	NA	1.69
<b>S4</b>	1.43	1.04	3.37	NA	NA	1.51	NA	1.39

NA = not available



while in case of AAA 2 and AAA 4 the maximum diameter was the indication for surgery.

In total, four tissue specimens were mechanically tested from the each AAA tissue sample. The stress-strain behavior for the 40% stretch cycle is shown in Figure 7.8. The black dotted line with the red dots represent the part of the stress-strain curve which is representative for the *in vivo* circumferential stresses due to the presence of the aortic pressure. This part of the curve was used to calculate the patient-specific wall stiffness (listed in Table 7.2) together with the specific wall thickness ( $h_0 = 2.1 \pm 0.5$  mm). In Figure 7.8B, two out of four tissue specimens did not reach the circumferential stress domain which corresponds to the *in vivo* loading case, due to early ruptures in the AAA specimen. Therefore, these two samples were omitted in further analysis. The mean wall stiffness measured was: 0.98 kPa-m, 2.17 kPa-m, 1.63 kPa-m, and 1.74 kPa-m for patient AAA 1 - AAA 4 respectively. Similar to the US method, AAA 2 and 4 have a higher mean wall stiffness with tensile testing compared to the other two aneurysms. However, values

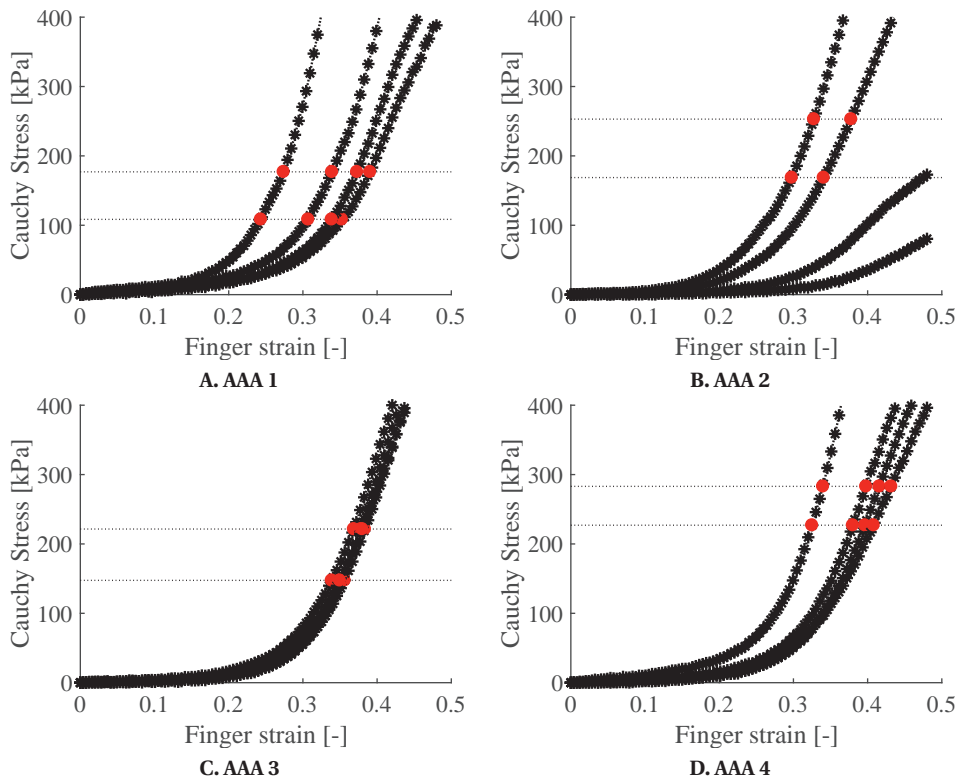


**Figure 7.8:** In (A) - (D) the stress-strain behavior of the four different AAA are visualized (Sub-figure numbering is similar to Figure 7.4). Each subfigure consist of four curves (black) representing the different tissue specimens obtained from the resected tissue. The red dots and the black dotted line shows the part of the stress-strain curve which represents the *in vivo* loading case during the 4D US acquisitions.

determined with both methods for AAA 3 and 4 were not statistically different ( $p = 0.88$ ). The ICC for the wall stiffness measurements using tensile testing was  $ICC = 0.81$  (CI: 0.34 - 0.99).

#### 4D US stiffness vs. bi-axial tensile testing

Both methods to quantify the aortic wall stiffness were compared using scatter and Bland-Altman plots for the porcine aortas (Figure 7.9A and Figure 7.9C) and for AAA patients in Figure 7.9B and Figure 7.9D. Both methods show overall a good agreement for the porcine aortas with a negligible median bias of  $-0.002$  (IQR:  $-0.04 - 0.02$ ) kPa·m. For the AAA patients, only four patients were included which limits an accurate comparison between tensile test and ultrasound. Taking this remark into account, Bland-Altman analysis revealed a median difference in absolute wall stiffness of  $0.61$  (IQR:  $-0.27 - 1.29$ ) kPa·m.

Moreover, a paired non-parametric Wilcoxon signed rank test was performed to test the difference in predicted wall stiffness using both methods. However, no significant differences were found between the 4D US method and the bi-axial tensile tests ( $p = 0.76$ ).

## 7.4 Discussion

In this study the aortic wall stiffness was characterized using a non-invasive 4D US-based method and afterwards measured using *ex vivo* bi-axial tensile testing. Reproducibility was assessed for both methods in an experimental controlled setup using porcine aortas and with patient AAA data. In addition, 4D US-based wall stiffness was compared with values obtained from bi-axial tensile testing and the differences were quantified. This study showed a high reproducibility for aortic wall stiffness measured using 4D US with an ICC of 0.91 for the porcine aortas and  $ICC = 0.98$  for the AAA patient data. Comparison with the gold standard bi-axial tensile testing revealed a good to excellent agreement for the experimental setup (bias of  $0.00$  kPa·m with IQR:  $-0.04 - 0.02$  kPa·m) and a moderate agreement for the AAA patients despite the limited number of patients included in this study.

AAA wall stiffness results are similar to those reported in Raghavan et al. (1996) where uni-axial tensile testing was used. Moreover, current results are in good agreement with the reproducibility study performed by Wilson et al. (2000) which compared using the intra- and inter-observer correlation of wall stiffness in a 2D, longitudinal, US plane. In this study a median incremental Young's modulus of  $3.1$  (IQR:  $2.1 - 4.6$ ) MPa was characterized with an inter-observer correlation ranging between  $0.62 - 0.82$ . This Young's modulus corresponds to a wall stiffness of  $2.07$  (IQR:  $1.40 - 3.07$ ) kPa·m with the assumption of a constant wall thickness of  $2$  mm. This is similar our current study which showed an overall median stiffness of  $2.23$  (IQR:  $1.03 - 3.21$ ) kPa·m.

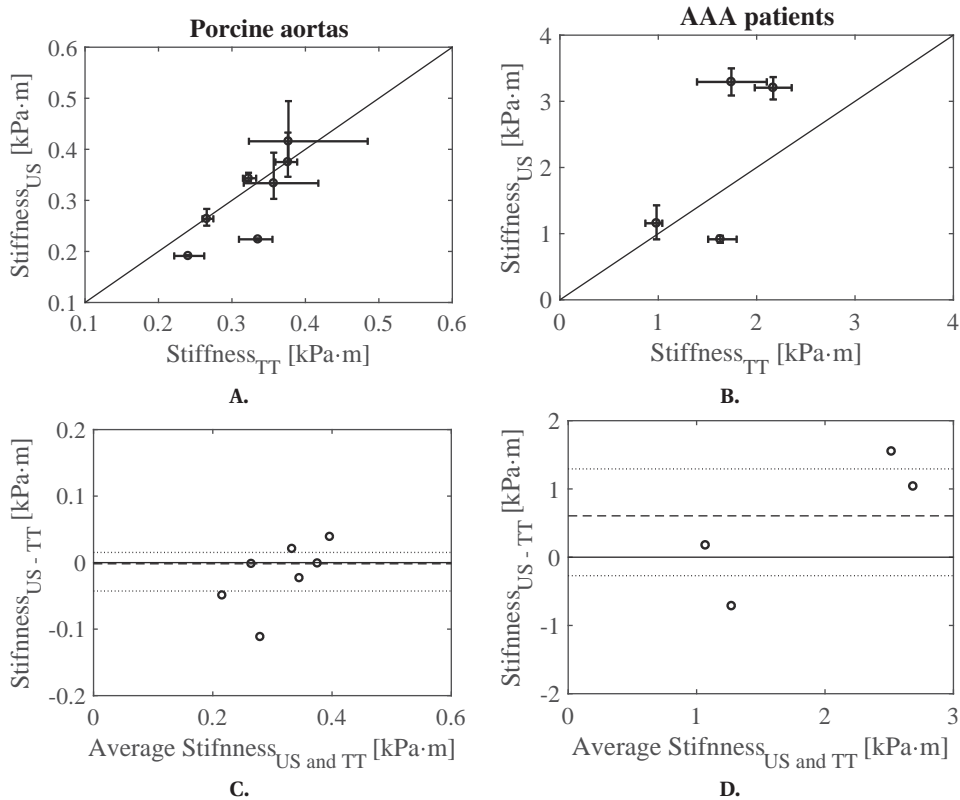


**Figure 7.9:** In (A) and (B) the wall stiffness measured with ultrasound (US) versus bi-axial tensile testing (TT) is shown for the porcine aortas and the AAA patients, respectively. The errorbars represent the complete range of the measured wall stiffness. Bland-Altman analysis was performed in (C) and (D), which showed a median difference of 0.00 kPa·m (interquartile range (IQR): -0.04 - 0.02 kPa·m) between both methods for the porcine aortas, and 0.61 kPa·m (IQR: -0.27 - 1.29 kPa·m) for the AAA patients. The line of equality was added as a visual aid (*solid black line*).

For the porcine aortas, a similar setup was used as previously described by Mascarenhas et al. (2016). The difference with the current experimental setup is that the aorta was surrounded by gelatin, and the addition of a spine at the dorsal side of the aorta. Moreover, not a 2D US probe with a high frame rate and radio-frequency output was used, but a low frame-rate 3D matrix array probe as used in current clinical practice. These improvements were made to improve the realism of the experiment and to mimic the *in vivo* patient measurements as closely as possible. In the studies by Kim and Baek (2011) and Mascarenhas et al. (2016) an incremental shear modulus,  $G_{\text{inc}}$  of  $240 \pm 39$  kPa was characterized. In the current study, a slightly lower incremental modulus of  $G_{\text{TT}} = 203$  (IQR: 140 - 226) kPa was obtained. This difference is most likely caused by a lower diastolic and systolic pressure during the inflation experiment in some of the porcine aortas.

Results revealed that the reproducibility in the 4D US method was higher compared to

the bi-axial tensile tests (Figure 7.9). An explanation for this observation could be the use of a constant wall thickness using the *in vivo* 4D US method, whereas in the bi-axial tensile tests the wall thickness of each specimen was properly measured. This wall thickness assessment was found to be very sensitive for errors. In order to reduce this error, the average value of three measurements was calculated. However, remaining errors in the wall thickness will directly affect the final wall stiffness. This variability in wall thickness was especially high in the AAA samples, due to the presence of thrombus at the inner layer of the tissue. Before tensile testing, this thrombus was removed from the tissue. However, due to calcifications in the tissue, and the different layers of thrombus, it was difficult to distinguish the intima from the outer thrombus layer (Tong et al., 2011).

Another explanation for the higher variability in the tensile test experiments might be that for these experiments a local wall stiffness was obtained, while in case of the US-based method, a global wall stiffness was estimated for the complete AAA. Local variation in aortic wall stiffness can be large in AAAs and might be due to the presence of calcifications, collagen remodeling in specific areas of the aneurysm, or by local variations in wall thickness (Raghavan et al., 2006; Gasser et al., 2012; Niestrawska et al., 2016). Ideally, measuring the patient-specific wall thickness *in vivo* and its spatial variability would increase the reliability of the wall stiffness estimation *in vivo* and improve the comparison with the *ex vivo* tensile test results. Unfortunately, none of the currently available imaging techniques can provide this information with sufficient accuracy.

Besides the comparison of both characterization methods and its reproducibility, another interesting finding in this study was that two of the four patients (AAA 1 and 3) who underwent aortic surgery due to rapid growth of the aneurysm had approximately a three times lower aortic wall stiffness using the US-based method compared to the other two AAAs. Although this comparison only includes four AAA patients, these findings correlate with the work of Wilson et al. (1998) and Di Martino et al. (2006), where ruptured AAAs were less stiff compare to non-growing AAAs.

The prior paragraph also takes us to the main limitation in this study, which was the limited number of AAA patients included in this study. Only patients undergoing open surgical AAA repair in an elective situation could be asked to participate in this study. Since the majority of the AAA patients are currently treated using endovascular aortic repair, inclusion of sufficient patients will be challenging in a single center study. An alternative might be to conduct post-mortem tissue samples of patients who recently underwent a 4D ultrasound acquisition of the AAA. However, ethical issues will make this approach less favorable.

Secondly, an incompressible Neo-Hookean material model was used in this study to describe the mechanical behavior of the aortic wall in the physiological range. This model is valid for linear-elastic isotropic materials subjected to large deformations. Aneurysm tissue is known to be highly anisotropic (Vande Geest et al., 2006b), which is currently not considered in our analysis. Moreover, the stress-strain curves in Figure 7.7 and Figure 7.8

reveal the well-known non-linear behavior of aortic and AAA tissue, which makes the analysis dependent on the pressure range *in vivo*. A non-linear isotropic material model of Raghavan and Vorp (2000) or a non-linear fiber-reinforced model of Holzapfel et al. (2000) can be used to describe the non-linear behavior. However, these material models include more material parameters, which results in higher parameter uncertainties when assessed patient-specifically *in vivo*.

Finally, in the current finite element simulations only the aortic wall was simulated while *in vivo*, and in the inflation experiments presented in this work, the AAA is surrounded by a spine and surrounding tissue. To improve current finite element simulations, these surrounding structures should be included in the model as well (Kwon et al., 2015; Farsad et al., 2015). These improvements will reduce the local errors between the model and the measured US displacements, and make the updated approach to calibrate the wall stiffness even more reliable. Although these additions could be directly be implemented in the model, this was beyond the scope of current study.

## 7.5 Conclusion

In this study, the performance of current 4D US-based characterization method was investigated and verified with bi-axial tensile testing. The aortic stiffness was assessed and results reveal a good to excellent reproducibility for the US-based method and a moderate reproducibility for the tensile tests. Comparison of both methods showed a good agreement for the porcine aortas in an idealized inflation experiment. AAA wall stiffness showed a similar trend, although, in order to perform an accurate comparison between both methods, more patients samples are required to provide a final verification of the techniques used.

# **Mechanical Characterization of Thoracic Aortic Aneurysms using 4D Ultrasound: In Vivo Findings and In Vitro Verification**

This chapter is based on: Mechanical Characterization of Thoracic Aortic Aneurysms using 4D Ultrasound: In Vivo Findings and In Vitro Verification, **E.M.J. van Disseldorp**, P.P.N. Kemper, J. Nijs, M.E.S.H Tan, F.N. van de Vosse, and R.G.P. Lopata, Submitted: 2018;

## Abstract

**Background:** An ascending thoracic aortic aneurysm (ATAA) is a life-threatening disease, due to the risk of dissection and rupture of the aorta. Nowadays the diameter is used as a criterion for risk estimation, however, biomechanical characteristics such as material properties and peak wall stresses could improve the patient-specific rupture risk assessment and thereby guide clinical decision making. In this study, the mechanical properties of the ATAA are characterized *in vivo* using 4D (3D+t) transesophageal ultrasound (US) imaging and iterative finite element analysis. The patient-specific material properties were verified by mechanically testing of the resected aortic tissue afterwards *ex vivo*.

**Methods:** The 4D US acquisitions were acquired peri-operatively, followed by automatic segmentation and cyclic deformation estimation using image registration. The cyclic deformation was input for an iterative finite element approach (FEA) where the displacements in the 3D FEA model were calibrated to the 3D+t US displacement field, resulting in a patient-specific incremental shear modulus. These moduli were compared to the bi-axial tensile testing results and those obtained with elastometry.

**Results:** The cyclic deformation of the ATAA showed reliable and representative displacements, resulting in a median incremental shear modulus of 200 kPa (IQR: 178 – 256 kPa) using FEA and using elastometry 161 kPa (IQR: 132 – 196 kPa). *Ex vivo* tensile testing of the aortic samples resulted in a median incremental modulus of 205 kPa (IQR: 145–274 kPa).

**Conclusions:** This study shows a minimally invasive approach to characterize the incremental mechanical properties of the ATAA wall *in vivo*, which is in agreement with the gold standard. In future studies, these material properties could be followed in time, to assess its relation with rupture and growth, and be compared to healthy subjects.

## 8.1 Introduction

A thoracic aortic aneurysm is an excessive localized enlargement of the thoracic aorta which has an incidence rate of 10.4 per 100.000 person-years, with two-thirds involving an ascending thoracic aorta aneurysm (ATAA) (Clouse et al., 1998). The main complication of ATAAs is rupture, which is frequently preceded by dissection of the aorta Chen et al. (1997). Thoracic dissection is a tear in the aortic wall intima, which causes the development of a false lumen within the media. This causes weakening of the aortic wall, leading to rapid growth, and finally rupture Chen et al. (1997). Hence, dissection involving an ATAA is a medical emergency and require urgent surgical repair.

The majority of ATAAs are asymptomatic and are often detected as an incidental finding on physical examination by various imaging modalities performed for other purposes Pande and Beckman (2013). The standard follow up involves measuring the diameter at regular intervals. The cut-off point for surgical intervention is 5.0 – 5.5 cm for ATAAs, which is set by large clinical trials Erbel et al. (2014). However, recent evidence has shown that 97% of dissected ATAAs had a pre-dissection diameter that would have not been eligible for elective surgery (< 5.5 cm) (Pape et al., 2007; Rylski et al., 2014). Furthermore, predicting in which patients the aortic root will dilate, is currently not possible. Therefore, there is a large demand for development of non-invasive clinical tools that not solely monitor geometrical changes but can also characterize the mechanical state of the aortic wall, i.e., wall stresses and mechanical properties, and their impact on growth (Fillinger et al., 2003; Pape et al., 2007; Rylski et al., 2014). Biomechanical factors such as peak wall stress have been shown to estimate risk of rupture better than the diameter criterion in abdominal aortic aneurysms (Fillinger et al., 2003). However, these biomechanical properties are currently not available for ATAAs.

Several groups investigated the mechanical properties of ATAA tissue *ex vivo* (Iliopoulos et al., 2009). Sokolis et al. (2012) showed that aneurysm formation had no effect on the strength of the ATAA tissue, but caused stiffening and distensibility reduction. In addition, Forsell et al. (2014) showed that patients with a bicuspid aortic valve revealed a higher macroscopic strength of the aneurysm compared to patients with a normal tricuspid aortic valve. Thereby, the stress in the wall of ATAAs has also been extensively studied. Beller et al. (2004) investigated the role of aortic root motion on wall stresses in the ATAA by assigning measured aortic root motion from angiograms as boundary condition in generic finite element analysis (FEA) models of the ATAA. It showed that both aortic root displacement and hypertension significantly increases the longitudinal stress in the ascending aorta. Hence, computational modeling or elastographic analysis should include the longitudinal stretch caused by aortic root motion. Trabelsi et al. (2015) estimated the material properties invasively by performing *ex vivo* inflation testing on patient-specific tissue samples of the ATAA. Next, patient-specific finite element analysis (FEA) was performed to obtain the local stresses in the aorta based on CT imaging data and the derived material properties.



However, in order to use the patient-specific material properties for risk analysis during clinical follow-up, the material properties have to be estimated non- or minimally invasively and not after abduction.

The mechanical properties of the aortic wall in other types of aortic aneurysms (mostly AAAs) have already been estimated non-invasively using pulse wave velocity (PWV) measurements (Blacher et al., 1999), pulse wave velocity imaging (PWVI) (Li et al., 2013), elastography (Damughatla et al., 2015; Fromageau et al., 2008) and inverse or iterative FEA (Flamini et al., 2015). In FEA, the wall deformation and wall stresses are calculated from prescribed material behavior and for the load given (i.e., the measured blood pressure). In iterative FEA the deformation is known, and the material behavior is estimated using aforementioned deformation and the blood pressure as input. An advantage of solving the inverse problem using FEA compared with the aforementioned techniques is that it simultaneously provides mechanical properties, estimates of the local wall stresses, and strains in the aneurysm (van Disseldorp et al., 2016b).

Many studies have used magnetic resonance imaging (MRI) and computed tomography (CT) to obtain patient-specific geometries of the AAAs and ATAAs (Borghi et al., 2006; Nathan et al., 2011; Trabelsi et al., 2015; Martin et al., 2015). However, the radiation exposure of CT and the high cost of MRI make these modalities not suited for routine screening. Ultrasound (US) is a promising alternative due to its low cost and high temporal resolution. A downside of US include lower contrast and resolution, but recently Kok et al. (2015), and van Disseldorp et al. (2016b), showed there was good similarity between the patient-specific geometry of AAAs obtained using US and CT, and its feasibility for US-based wall stress analysis. Not only will 4D (3D+t) US based FEA modelling approach yield biomechanical parameters of interest, it will also use a cost effective imaging modality, which uses no ionizing radiation, and can therefore be used for both monitoring and screening.

Estimating the cyclic deformation of the ATAA is challenging due to significant longitudinal motion and stretch caused by aortic root motion. Karatolios et al. (2013), and Wittek et al. (2016), recently investigated the cyclic deformation using 4D speckle tracking of US images for both the ascending thoracic aorta (using transthoracic 3D ultrasound) and the abdominal aortic aneurysm, revealing physiological values for wall motion and deformation.

The objective in this study was to characterize the mechanical properties of the ATAA non-invasively and verify the results *ex vivo* (Figure 8.1). A combination of 4D US motion estimation and US-based iterative solving of the inverse FEA problem was used to calculate the incremental mechanical properties *in vivo*. For the development of this technique and proof of principle, intra-operative transesophageal 4D ultrasound imaging was used, to determine the patient-specific aortic wall material properties prior to ATAA excision and graft placement. These estimates were compared to the properties obtained from *in vitro* bi-axial tensile testing of the corresponding ATAA tissue samples for verification.

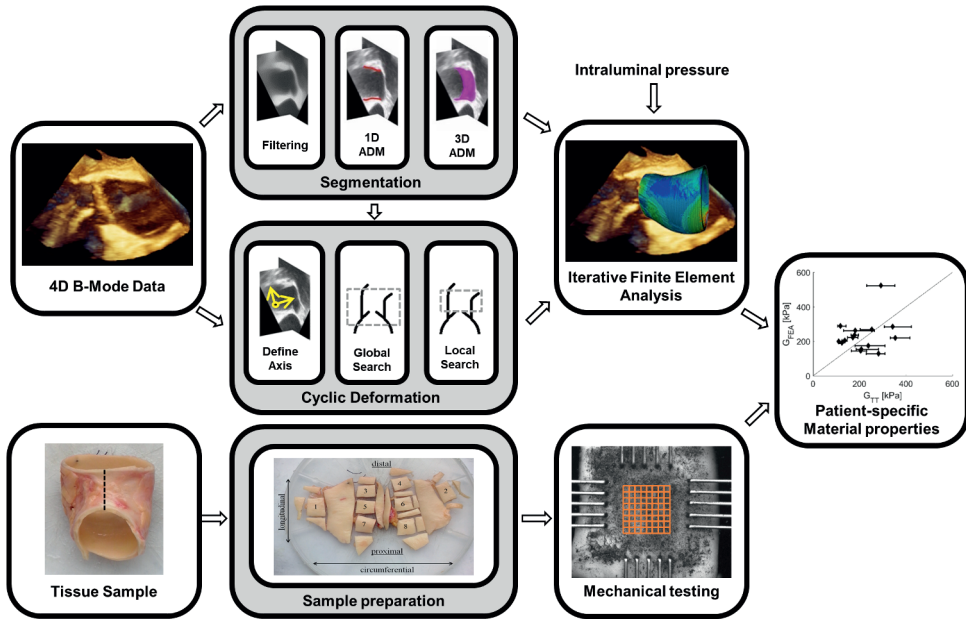


**Figure 8.1:** Schematic overview of the methodology. 4D B-Mode data is used for both the segmentation and estimation of the cyclic deformation (*top row*). Next, the measured intramural blood pressure, the estimated cyclic deformation, and the segmented geometry are used to solve the inverse problem (i.e. from deformation to mechanical properties) using iterative finite element analysis (FEA). Finally, the resulting patient-specific material property is compared to the values obtained with bi-axial tensile testing (*bottom row*).

## 8.2 Materials and Methods

### Study population

In this study, 23 patients (22/1 male/female) who underwent graft replacement were prospectively included. Eleven patients were enrolled in a study at the Catharina Hospital in Eindhoven (CZE) and 12 at the University Hospital in Brussels (UZB). This study was approved by the local ethical committees of both Eindhoven and Brussels, and all patients gave their informed consent. The age ranged between 44 and 72 years. The maximum diameter of the ATAA was measured using computed tomography (CT) and ranged between 37 – 69 mm. More patient-specific demographics are listed in Table 8.1.

### Data acquisition

US data were captured using a Philips IE33 or EPIQ Ultrasound System equipped with the same transducer, an X7-2t probe designed for transesophageal echocardiography (Philips

**Table 8.1:** Patient demographics involved in the study, for each analysis step

Demographics	Segmentation	Registration	FEA	Tensile testing
Number (-)	23	22	19	15
Gender (M/F)	22 / 1	21 / 1	18 / 1	15 / 0
Age (years)	44 - 72	44 - 72	44 - 66	44 - 66
Max. CT diameter supracoronaire ascendus (mm)	31 - 69	31 - 66	31 - 66	31 - 55
Max. CT diameter aortic root (mm)	37 - 58	37 - 58	37 - 58	37 - 58
Diastolic blood pressure (mmHg)	33 - 89	33 - 89	33 - 89	33 - 89
Systolic blood pressure (mmHg)	46 - 127	46 - 127	46 - 127	46 - 114

FEA = Finite element modeling

Medical Systems, Bothell, WA, USA). Image acquisition was performed peri-operatively and before the function of the heart was taken over by the cardiopulmonary bypass (Figure 8.2). These transesophageal US data were acquired as part of the routine clinical workflow during the surgery. For higher frame rate, ECG-triggered full volume data were acquired. These full volumes were only used for analysis when no stitching artifacts were present ( $n = 9$ ). When stitching artifacts were present, single volume, live 3D acquisitions were acquired and used for further analysis ( $n = 14$ ). Full volume acquisitions consisted of 20 – 33 time frames per heart cycle with a voxel size of  $0.58 \pm 0.11$  mm by  $0.69 \pm 0.13$  mm by  $0.68 \pm 0.14$  mm. The live acquisitions consisted of 7 – 20 time-frames per heart cycle with a voxel size of  $0.53 \pm 0.09$  mm by  $0.62 \pm 0.12$  mm by  $0.60 \pm 0.12$  mm in the axial, lateral, and elevational direction, respectively. The intramural pressure was measured during US acquisitions using an intravascular pressure needle in the ascending aorta.

### Tissue storage

The resected part of the thoracic aorta, was stored in a phosphate buffered saline (PBS) solution and transported to the Eindhoven University of Technology. To prevent tissue deterioration while awaiting biaxial tensile testing, the ATAA segments were frozen at -80 degrees Celsius in a 10% dimethyl sulfoxide (DMSO) and 90% phosphate buffered saline solution (PBS) solution (Stemper et al., 2007).

### Segmentation

The geometry of the ATAA was required for both FEA and aortic motion estimation. To reduce labor time and intra-user variability, aortic wall segmentation was performed automatically after manual initiation. Two points (i.e. proximal and distal) were selected at the centerline of the aorta in the longitudinal plane ( $d_a$ l-plane in Figure 8.3). The

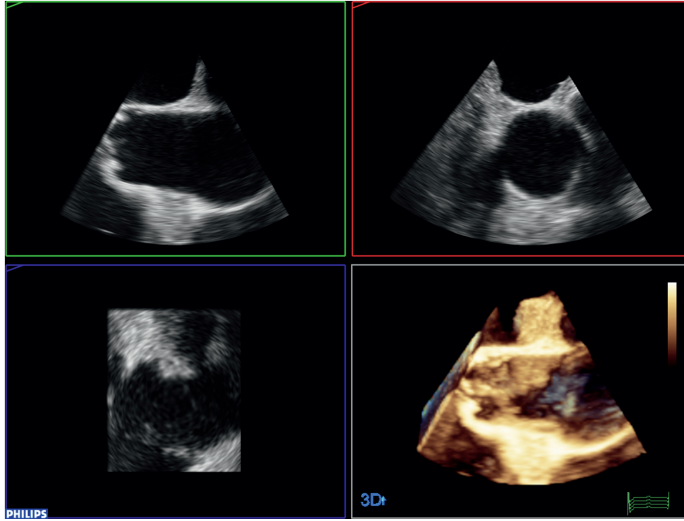


**Figure 8.2:** Example of a 3D transesophageal ultrasound acquisition of an ascending thoracic aortic aneurysm. Shown are a sagittal (*top, left*), transversal (*top, right*), and coronal (*bottom, left*) cross-section and a 3D volume render (*bottom, right*).

Euclidean shortening flow (ESF) filter, a well-known edge-preserving de-speckling filter, was used to reduce noise in the US data which could hinder the segmentation process (Alvarez et al., 1993). The segmentation was performed using active deformable models (ADMs) as introduced by Kass et al. (1988). The ADMs are deformed such that they are located at requested image features while minimizing an energy function. The total energy is given by:

$$E = s_1 E_{\text{in}} + s_2 E_{\text{edge}} + E_{\text{shape}} \quad (8.1)$$

with  $E_{\text{in}}$  and  $E_{\text{edge}}$  external energy terms based on respectively the image intensity and gradients,  $s_1$  and  $s_2$  weighting parameters (given in Table 8.2), and  $E_{\text{shape}}$  the internal energy of the shape of the segmentation.

The external energy was estimated using a Gaussian differentiator ( $\sigma = 0.7$ ) in the radial direction. Since the derivative is taken with respect to the vessel's centerline, the inner wall of the aorta is expressed as a positive value in  $E_{\text{edge}}$ , while the outer wall is expressed as a negative value. This ensures that the shape is contained within the aorta.

Wall – lumen contrast is larger for the part of the aortic wall where the wall's radial direction is normal to the US-beam. In these regions, the ATAA was segmented first using a 1D ADM approach, see Figure 8.3, starting from the centerline. The segmentation was performed by deforming the shape using a gradient descent method ( $k = 200$  iterations,  $\delta t = 1$  as step size), minimizing Equation 1, with an added initiation force term to reduce

dependency on the initial geometry (Xu and Prince, 1997). After this first segmentation, this method was repeated for the neighboring slices until the mean squared difference between the neighboring shapes becomes larger than a certain threshold (50 pixels).

The resulting contours were merged into a 3D membrane, which was used as initial shape for the 3D ADM approach. Furthermore, an initialization energy term ( $E_1$ ) was introduced, a Gaussian blurred version of the mask obtained during the 1D ADM step. Finally, the 3D geometry of the ATAA was obtained by minimizing:

$$E = s_1 E_{\text{in}} + s_2 E_{\text{edge}} + s_3 E_1 + E_{\text{shape}} \quad (8.2)$$

All parameters used are given in Table 8.2.

### Cyclic deformation

In the cyclic deformation of the ATAA, significant motion in the longitudinal direction was observed, i.e., parallel to the centerline of the ATAA (see Figure 8.4). Hence, 2D aortic expansion could not be tracked in-plane. Therefore, a multiscale registration approach was used, with the assumption that the cyclic motion and deformation of the ATAA segment within the limited field-of-view (FOV) could be approximated by an affine transformation. An affine parametrization was used in which the transformation matrix is described as a combination of a rotation, shear, scaling, and translation (Leermans and Jones, 2009).

The longitudinal axis was defined to be parallel to the centerline of the aorta (Figure 8.4A), which was obtained by manually rotating the B-mode data until the centerline was parallel to the y-axis. A region of interest closely surrounding the ATAA was chosen by expanding the segmentation results in radial direction (*see previous section*).

Registration was performed using the open source registration toolbox Elastix (Image Science Institute, UMC Utrecht, Utrecht, the Netherlands) in a two-step multi-resolution strategy, in which the longitudinal and circumferential stretch were estimated separately. In

**Table 8.2:** Parameters for the segmentation method

Parameter:	Value: [-]
$s_1$	0.125
$s_2$	20
$s_3$	-0.2
$\alpha$	1
$\beta$	3
$\delta t$	1
$\sigma$	0.7
$b$	0.9
$k$	200

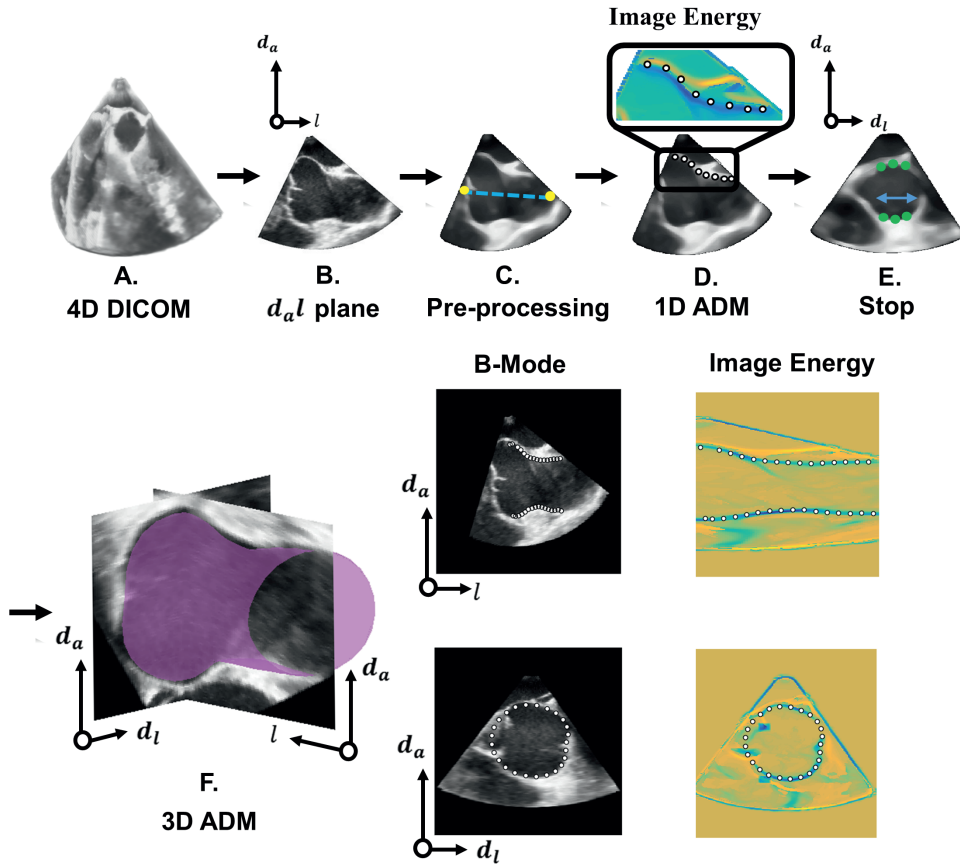


**Figure 8.3:** An overview of the segmentation process. (A) Initially, in the 4D DICOM data, a slice which contains the aorta was manually located (B). The automatic segmentation was initialized by selecting two points within the aortic segment. (C) Subsequently Euclidean Shortening flow (ESF) filtering was performed. (D) The 2D segmentation was applied by solving the minimization problem, i.e., the shape deforms such that the image energy is minimized while the internal energy of the shape prevents discontinuities. (E) This is repeated for neighboring slices until the deviation with the previous segmentation exceeded a set threshold. (F) The resulting geometry was used as initial geometry for the 3D active deformable model (ADM).

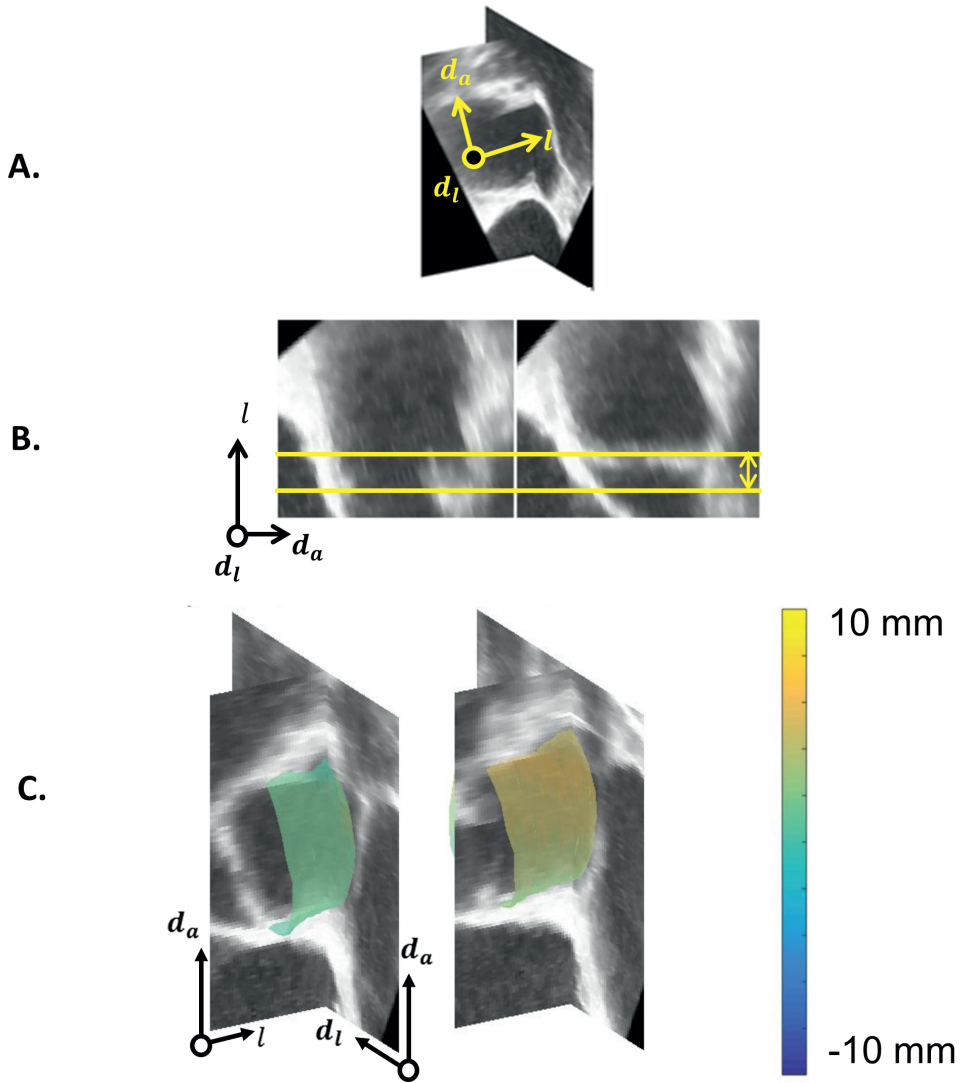


**Figure 8.4:** (A) Biplane image of an ascending thoracic aortic aneurysm and corresponding local coordinate system with the longitudinal axis ( $l$ ) parallel to the mean centerline, the diameter in lateral direction ( $d_l$ ) and the diameter in axial direction ( $d_a$ ). (B) The aortic root in diastole (left) and systole (right). (C) Significant motion in the longitudinal direction can be observed.

the first step, a larger region of interest (ROI) was used, including the heart, to estimate the longitudinal motion and stretch accurately. In the second step, the ROI was reduced such that the heart was excluded again, in order to estimate the circumferential stretch more accurately. Each step was performed at three resolution scales ( $\sigma = (1,4,8)$  voxels) using the adaptive stochastic gradient descent method (Klein et al., 2009). A normalized cross-correlation (NCC) function was used to calculate the similarity between two consecutive images, where high values of NCC ( $0.9 < \rho \leq 1$ ) correspond with a good similarity between the images. An Eulerian frame of reference was used to avoid error propagation. The motion estimation was performed by optimizing the transformation matrix such that it yielded the highest possible NCC. Visual inspection of the deformation revealed that the order of magnitude of the motion of the ATAA was in the order of 10 voxels, the rotation of the ATAA due to motion of the heart was  $10^\circ$ , while shearing and strain were in the order of 10% under physiological conditions. A total of 2000 iterations at every scale was sufficient to achieve convergence, which was defined as  $\text{NCC} < 0.001$  in the last 10 iterations.

### Iterative finite element analysis

The material properties were estimated by an iterative finite element approach (FEA) using Abaqus 6.14 (Dassault Systèmes, Paris, France). A mesh was created using the segmentation results, where the outer wall was interpolated, assuming a wall thickness of 2.4 mm in diastole. This value was chosen based on *ex vivo* wall thickness measurements at zero pressure (*see next section*), after correction for the longitudinal and circumferential pre-stretch. The aortic wall was modelled as an incompressible Neo-Hookean solid. The initial condition was obtained from the elastometry approach (*next section*). The ATAA wall was meshed with hybrid 8-node linear hexahedrons, while the presence of at least two elements in radial direction was ensured. The wall was fixated at the proximal side and fixed in the  $z$ -plane at the distal side.

To estimate the pressure-free geometry, the backward incremental method was applied (de Putter et al., 2007). After obtaining the pressure-free geometry, the proximal side was displaced with the estimated aortic root motion to simulate the *in vivo* longitudinal stretch. Subsequently, the patient-specific systolic pressure was applied to the inner surface of the aortic wall. Finally, the displacements of the aortic wall between the diastolic and systolic geometry were calculated from the FE model, and compared to the US displacement data.

Again a gradient descent method was used to optimize the incremental material property ( $G_{FEA}$ ) by minimizing the difference between the x-y-displacements in the FEA and the x-y-displacements derived from the US data (van Disseldorp et al., 2016b). An initial stepsize of 10 kPa was used. When the difference between the displacements from US data and FEA increases, the search direction changed and the step size was decreased by a factor 5. Convergence was obtained when the step size was smaller than 0.1.



## Elastometry

To verify the FEA results, a direct elastometry approach was used to estimate the material properties using a Neo-Hookean constitutive model and LaPlace's law as described in Lopata et al. (2014) and Mascarenhas et al. (2016). The deformation matrix ( $F_{total}$ ) that describes the stretching of the aorta in longitudinal motion due to the axial pre-stretch ( $\lambda_{zz_p}$ ) and cyclic deformation ( $\lambda_{zz_c}$ ), followed by inflation induced circumferential stretching ( $\lambda_{\theta\theta}$ ), is given by:

$$F_{total} = \begin{bmatrix} \frac{1}{\lambda_{\theta\theta} \sqrt{\lambda_{zz_p} \lambda_{zz_c}}} & 0 & 0 \\ 0 & \frac{\lambda_{\theta\theta}}{\sqrt{\lambda_{zz_p} \lambda_{zz_c}}} & 0 \\ 0 & 0 & \lambda_{zz_p} \lambda_{zz_c} \end{bmatrix} \quad (8.3)$$

The relationship between stretch and stress can be derived using the constitutive law for Neo-Hookean materials (Equation (7.1)), which leads to:

$$\sigma_{\theta\theta} = \frac{G_{ELASTO}}{\lambda_{zz_p} \lambda_{zz_c}} \left( \lambda_{\theta\theta}^2 - \frac{1}{\lambda_{\theta\theta}^2} \right) \quad (8.4)$$

The longitudinal stretching due to the aortic root motion ( $\lambda_{zz_c}$ ) occurs simultaneously with the circumferential stretching induced by the aortic inflation. Hence, the measured circumferential ( $\lambda_{\theta\theta_m}$ ) stretch is a combination of the true circumferential stretch ( $\lambda_{\theta\theta}$ ) and the cyclic longitudinal stretch ( $\lambda_{zz_c}$ ):

$$\lambda_{\theta\theta_m} = \frac{\lambda_{\theta\theta}}{\sqrt{\lambda_{zz_c}}} \quad (8.5)$$

Therefore, the constitutive Neo-Hookean law as function of the measured circumferential stress is obtained by substituting Equation (8.5) in Equation (8.4), which leads to:

$$\sigma_{\theta\theta} = \frac{G_{ELASTO}}{\lambda_{zz_p}} \left( \lambda_{\theta\theta_m}^2 - \frac{1}{\lambda_{\theta\theta_m}^2 \lambda_{zz_c}^2} \right) \quad (8.6)$$

Finally, the incremental shear modulus ( $G_{ELASTO}$ ) within the diastolic and systolic stress range was approximated using Equation (8.6), the measured stretches, and blood pressure.

## Bi-axial tensile testing

The ATAA segments were slowly thawed at room temperature, rinsed with PBS to wash out the DMSO and cleaned. The ATAA segments of all patients underwent cross-sectional 2D ultrasound in a water tank to determine the wall thickness at zero pressure. A linear array transducer (4-11 MHz) was placed perpendicular to the axis of the aorta. Using a

MyLAB70 ultrasound system (Esaote Europe, Maastricht, Netherlands), 2D raw ultrasound data were acquired (193 lines per frame), and discretized at a sample rate of 50MHz. The wall thickness was determined by manually selecting the inner and outer side of the aortic wall.

The aortic segment was cut open at the curvature minor, after which 4 samples were obtained at the curvature minor and 4 samples were obtained from the curvature major. The samples had an approximate area of 15 mm x 15 mm. The prepared samples were subjected to bi-axial tensile testing to obtain the material property as described by Lopata et al. (2014). The longitudinal and circumferential directions of the samples were aligned with the clamps of the biaxial tensile tester. Each bi-axial test was performed at 37°Celsius in PBS solution. Subsequently, the aortic samples were pre-conditioned and afterwards stretched in the circumferential direction in consecutive cycles of 0% to 50% strain, with a fixed longitudinal pre-stretch of 25%. This longitudinal pre-stretch was based on the averaged longitudinal pre-stretch measured before and after resecting of the aortic tissue. Finally, the image registration software of Labjoy (Cellscale, Waterloo, Canada) was used to obtain the displacement data by tracking the graphite particles.

The incremental shear modulus ( $G_{TT}$ ) was calculated for the patient-specific stress range, which were the diastolic and systolic circumferential stress from both the FEA and elastometry US-based methods (see Figure 8.7 for graphical interpretation). The Cauchy-stress was calculated by dividing the force at the rake by the cross-sectional area of the sample within the clamps. Finally,  $G_{TT}$  was estimated using a least squares parameter estimation algorithm in MATLAB (Mathworks, Natick, MA, USA) (Lopata et al., 2014).

## Data analysis

Manual segmentation and automatic segmentation were compared using the Dice coefficient or similarity index (SI). The SI is a measure for the percentile overlap between the two geometries, which is calculated by:

$$SI = \frac{2(P_{\text{auto}} \cap P_{\text{manual}})}{(P_{\text{auto}} + P_{\text{manual}})} \quad (8.7)$$

with  $P_{\text{auto}}$  and  $P_{\text{manual}}$  the number of pixels in the automatically and manually obtained geometry, respectively. Moreover, the mean absolute difference (MAD) was calculated as a measure for the local irregularities in the geometry. The mechanical properties calculated with iterative FEA, elastometry, and bi-axial tensile testing were compared with Bland-Altman analysis to quantify their bias and (limits of) agreement. The circumferential strains were verified by manual measurements based on segmentation of the diastolic and systolic ATAA geometry.

### 8.3 Results

#### Segmentation

In Figure 8.5A, three typical examples of transesophageal 4D ultrasound data of an ATAA geometry are shown. The SIs varied between 0.90 and 0.97 with a median of 0.93, which indicates that the segmented geometries are in good agreement to manual segmentation. The MAD, a measure for local irregularities, ranged between 0.9 - 2.4 mm. The manual and automatic segmented geometries with their SI and MAD for the abovementioned three geometries are shown in Figure 8.5B.

#### Cyclic deformation

One patient was excluded since the segmented geometry moved outside the field of view over the cardiac cycle, which inhibits correct calculation of the dynamic behavior of the ATAA. Before registration, the median longitudinal motion of the heart valves in the 4D US data was found to be 7.2 mm with an interquartile range (IQR) of 5.3 – 9.6 mm between patients. After correction, the median longitudinal motion was reduced by 81% to 1.6 mm (IQR: 0.7 – 1.9 mm). The estimated median longitudinal and circumferential strain after affine registration were respectively 17% (IQR: 8 – 27%) and 6% (IQR: 4 – 7%).

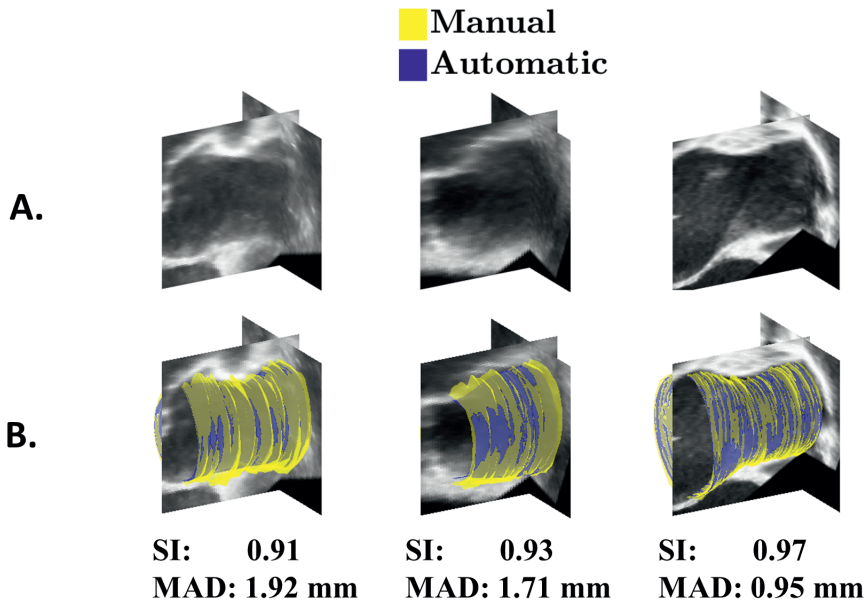


**Figure 8.5:** (A) Three examples of ultrasound images of an ascending thoracic aortic aneurysm (*top*). (B) The automatic (*blue*) and manually (*yellow*) segmented contours and corresponding similarity indices (SI) and mean absolute difference (MAD) values.

The comparison between the affine and circumferential stretch is visualized in Figure 8.6A. A mean difference of 0.9% was observed between the manual and affine derived circumferential strains.

### ***In vivo* mechanical characterization**

For 3 out of 22 patients, intraluminal pressure data were unavailable and were therefore excluded for mechanical characterization of the ATAA wall. For the remaining 19 patients the patient-specific incremental shear modulus was calculated with the iterative finite element model ( $G_{FEA}$ ) and elastometry ( $G_{ELASTO}$ ), shown in Figure 8.8A. The median  $G_{FEA}$  and  $G_{ELASTO}$  were respectively 200 kPa (IQR: 178 – 256 kPa) and 161 kPa (IQR: 132 – 196 kPa). In Figure 8.8B a Bland-Altman plot reveals a median difference of 34 kPa (IQR: 11 - 74 kPa) between  $G_{FEA}$  and  $G_{ELASTO}$ . Figure 8B also shows two outliers, where  $G_{ELASTO}$  is 29% higher and 35% lower, respectively, compared to the finite element method.

### ***In vitro* characterization using bi-axial tensile testing**

For 15 patients, ATAA tissue samples were available and mechanically tested using bi-axial tensile testing. The stress-strain curves of all aortic samples ( $n = 8$ ) of two ATAA patients are visualized in Figure 8.7. In Figure 8.7A, an example is shown of a patient with a small variety in stress-strain behavior between the different samples, resulting in similar predictions for  $G_{TT}$  (represented by the tangent of the red line). While in Figure 8.7B, an example is shown with a large dispersion in the stress-strain behavior between the different samples of the ATAA tissue.

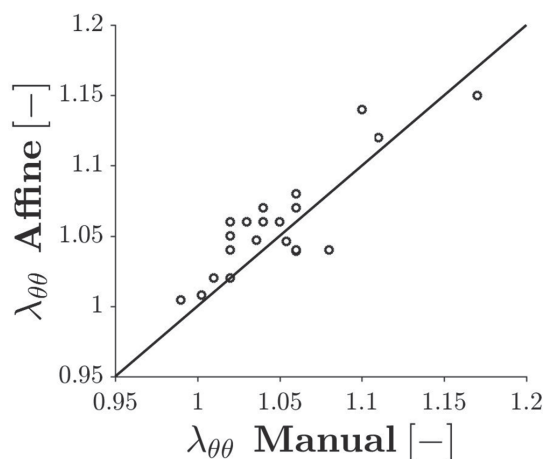


**Figure 8.6:** The circumferential stretch determined by affine registration as function of the manual derived circumferential stretch. The line of equality was added as a visual aid (*solid line*).

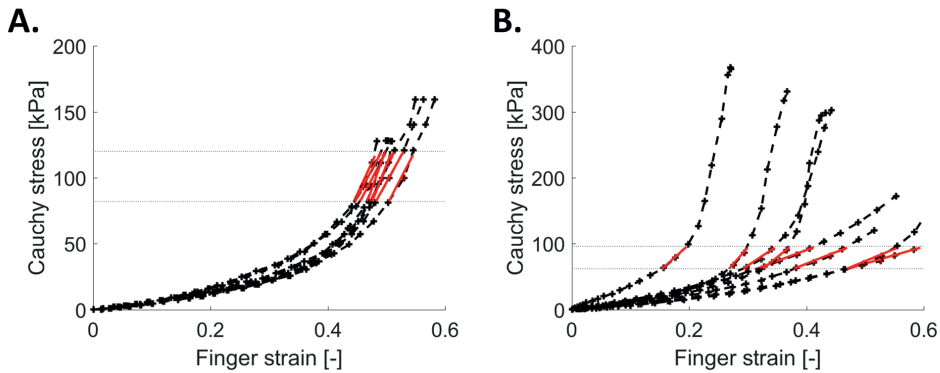


**Figure 8.7:** The stress-strain curves of two ATAA samples after mechanical bi-axial tensile testing. The black line represent the stress-strain curve for each sample ( $n=8$ ) while the red line shows the part of the stress-strain curve which is used to characterize the incremental shear modulus ( $G_{TT}$ ). (A) A sample with a low variety in ( $G_{TT}$ ), and (B) a sample with a large dispersion in the characterized modulus.

Finally, the *in vitro* incremental shear moduli were calculated for all ATAA patients and revealed a median of  $G_{TT} = 205$  kPa (IQR: 145 – 274 kPa). In Figure 8.8C and Figure 8.8D the patient-specific *in vivo*  $G_{FEA}$  is compared to  $G_{TT}$ . It shows a moderate agreement with a median difference of 51 kPa (IQR: -59 – 78 kPa). When  $G_{ELASTO}$  is compared to  $G_{TT}$  the bias between the two methods is reduced to a median difference of -36 kPa, as shown in Figure 8.8E and Figure 8.8F. However, the dispersion is considerable (IQR: -92 – 46 kPa).

## 8.4 Discussion

In this study, the estimation of the incremental mechanical properties of ATAAs was performed peri-operatively in a group of ATAA patients in two medical centers. The incremental shear modulus was estimated using an iterative FEA approach based on 4D ultrasound. Finally, the estimated material properties were verified with an elastometry approach and by *in vitro* bi-axial tensile testing.

The longitudinal motion of the ATAA, induced by contraction of the heart, was reduced by 81% in the multiscale registration step, which reduces errors caused by 2D out-of-plane motion and emphasizes the need for 3D US imaging when investigating ATAAs. Furthermore, the global deformation of the ATAA was estimated and verified. It yielded similar results for the longitudinal strain as found by Wittek et al. (2016) and Bell et al. (2014). The circumferential strain was similar to the manually determined circumferential strain except for a small bias of 0.9%. Hence, the global registration approach is able to capture the global cyclic deformation of the ATAA segments, thereby circumventing problems that would arise with block matching due to the lack of features in the longitudinal direction.

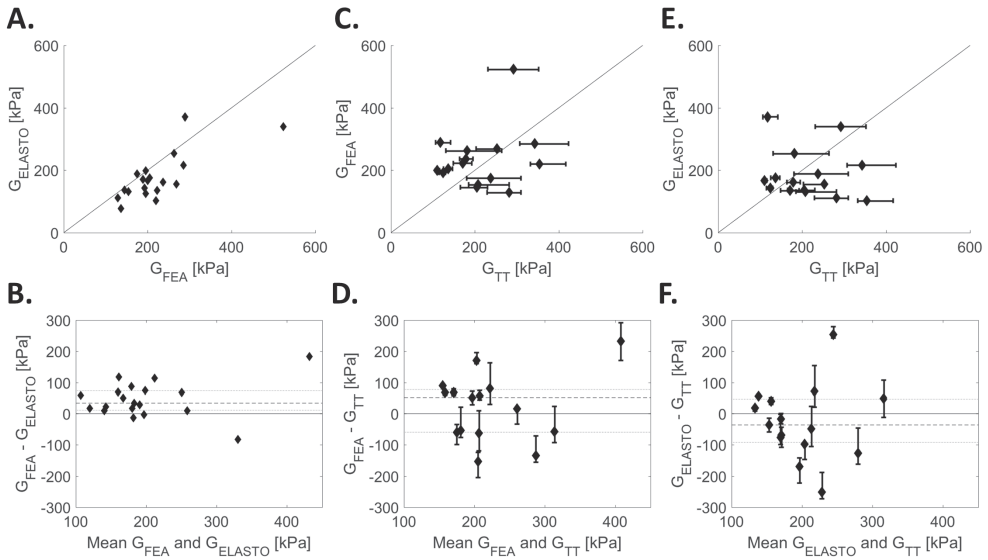


**Figure 8.8:** Scatter plots (*top row*) and Bland Altman plots (*bottom row*) for comparison of the incremental shear modulus ( $G$ ) estimates. **(A)** The patient-specific incremental shear moduli derived using finite element modelling ( $G_{FEA}$ ) and elastometry ( $G_{ELASTO}$ ). **(B)** Bland Altman plot shows a median difference of 34 kPa (interquartile range (IQR): 11 - 74 kPa) between  $G_{FEA}$  and  $G_{ELASTO}$ . **(C)** The patient-specific incremental shear moduli derived using finite element modeling ( $G_{FEA}$ ) and biaxial tensile testing ( $G_{TT}$ ), the error bars visualize the inter-quartile range. **(D)** Bland Altman plot shows a median difference of 51 kPa between  $G_{FEA}$  and  $G_{TT}$  with its IQR (-59 – 78 kPa). **(E)** The patient-specific incremental shear moduli derived using elastometry ( $G_{ELASTO}$ ) and bi-axial tensile testing ( $G_{TT}$ ). **(F)** Bland Altman plot shows a mean difference of -36 kPa (IQR: -92 – 46 kPa) between  $G_{ELASTO}$  and  $G_{TT}$ .

Moreover, transesophageal echocardiography B-mode data were used, in which the walls of the aorta are mostly a white edge/region without any distinguishable speckles due to the relatively low frequency used to gain sufficient penetration depth. This means that tracking of speckles will not be feasible in the longitudinal direction. Therefore, motion is hard to estimate locally using approaches like block matching techniques (Banerjee et al., 2015). Hence, a multiscale registration approach was used.

For clinical purposes and future large-scale studies, manual segmentation of all geometries is labor intensive and therefore not feasible. Therefore an automatic segmentation approach was implemented in this study to reduce user-bias and processing time. It showed similar results as obtained with manual segmentation and reduced the segmentation time from approximately 15 minutes to 1 minute.

The iterative FEA method yielded similar values compared to the elastometry approach, with a median difference of 34 kPa (IQR: 11 - 74 kPa). Differences could be explained due to

several assumptions in the elastometry approach, such as the cylindrical tube assumption, the use of LaPlace's law, and measurement uncertainties in geometry and aortic wall tracking. The estimated mechanical properties using the 4D ultrasound data were subsequently compared with the patient-specific tensile test results. Median differences of 51 and -36 kPa were observed between tensile testing and FEA results, and with respect to the elastometry characterization, respectively. However, a relatively large spread was found. This could be caused by inaccurate motion estimation due to the lack of RF data *in vivo*, which could lead to overestimation of the shear moduli *in vivo*.

Both the *in vivo* and *ex vitro* determined shear moduli were lower in comparison with values found by Azadani et al. (2013), who found a Young's Modulus in circumferential direction for healthy patients of 905 kPa. This corresponds to an incremental shear moduli ( $G_{inc}$ ) of 302 kPa when assuming an incompressible isotropic material. This difference is most likely caused by the relatively low diastolic and systolic aortic pressures in our study, since the US acquisitions were acquired during surgery (median mean arterial pressure: 69 mmHg, IQR: 59 – 72 mmHg). This may have led to a different part of the stress-strain curve that was analyzed. Furthermore, an inherent limitation of stress-matching is that the accuracy of  $G_{TT}$  is depended on defining an accurate stress range based on the patient-specific FEA. One might argue that stretch matching removes that uncertainty, however it is more susceptible for other inaccuracies involved with *ex vivo* tensile testing (e.g., hysteresis).

One of the limitations of 4D US is the relatively low frame rate in comparison with 2D US approaches. Furthermore, the use of DICOM instead of RF data limits the precision of the estimated displacement. The combination of a low frame-rate, artifacts, significant longitudinal motion of the aorta, and the lack of RF data made conventional speckle tracking of transesophageal US data not sufficiently robust for accurate motion tracking. Therefore, the cyclic deformation of the ATAA was approximated as an affine deformation. In reality, the 3D deformation field of the ATAA is more complex, which may have led to errors in the displacement estimation. In future studies, acquisition sequences leading to higher frame rate and the use of raw radiofrequency data should improve the displacement estimation and improve the accuracy of the motion and mechanical properties.

In this study, a Neo-Hookean material was used to describe the behavior of the aorta, which is acceptable within the limited pressure range between diastole and systole (See Figure 8.7). In future research, a more complex non-linear material model could be employed. A non-linear model could give information about the ratio between collagen and elastin, which is different in healthy and ATAA tissue. However, this would also lead to more parameters, which in turn will lead to higher model uncertainties. Moreover, future work could include a true inverse approach in which the stiffness matrix is directly calculated from the measured displacements, local stress analysis, and possibly fluid-structure interaction which might help to predict aneurysm growth or rupture (Duprey et al., 2016).

Despite these limitations, this study showed an *in vivo* approach to characterize the

mechanical properties of the ATAA wall non-invasively. In this study, transesophageal 4D US data was used since it was available peri-operatively without interfering with clinical workflow. However, the use of transthoracic US would allow to follow these material properties over time non-invasively. Finally, a longitudinal study should be performed in future to examine and assess a possible relation between mechanical properties and aneurysm growth and/or aortic root dilation.

## **8.5 Conclusion**

This study demonstrated the merit of an iterative FEA approach to estimate the patient-specific mechanical properties of the ATAA *in vivo* using 4D ultrasound, which was subsequently verified in an experimental setting. In future work, a comparison with healthy patients should be performed to investigate the feasibility to differentiate between high-risk and low-risk aneurysmal tissue prone for rupture.





CHAPTER 9

**General Discussion**

## 9.1 Motivation and main findings

In this thesis, mechanical characterization of abdominal aortic aneurysms (AAAs) has been developed, based on time-resolved 3D ultrasound (4D US). The advantage of using US as preferred image modality lie in its non-invasive and harmless nature, low cost, and high temporal resolution. Therefore, 4D US is accessible for a large cohort of patients, and an ideal modality to perform wall stress analysis during the regular AAA screening program. In addition, by using the available temporal data in the 4D US acquisition, not only the wall stress distribution could be assessed, but also the patient-specific aortic stiffness was successfully characterized. This method was verified using CT data for accurate geometry and wall stress comparison, and using *ex vivo* mechanical testing to verify the *in vivo* measured aortic stiffness. Finally, this method was employed in a longitudinal prospective clinical study of 3,5 years, where changes in wall stress and aortic stiffness were followed over time. The **main findings** of this thesis are:

- Ultrasound-based wall stress analysis can be performed accurately within the limited field-of-view that US provides, as long as both shoulders of the AAA are available for meshing. The aortic bifurcation is not necessarily needed for adequate wall stress quantification (**Chapter 2**).
- For aneurysms which exceed the US field-of-view, a fusion algorithm was developed to merge multi-perspective 3D US acquisitions. In addition, an automatic segmentation method was created to make the US segmentation process less labor intensive and more robust (**Chapter 5**).
- AAA geometries and wall stress distributions acquired using 4D US were verified using CT imaging and revealed good similarities (**Chapter 3 and 5**).
- A comparison study between AAA patients and age-matched volunteers showed that the AAA pathology causes an increase in aortic stiffness, already in an early stage of the disease, i.e., at small maximum diameters (**Chapter 4**). A similar pattern was observed for ascending thoracic aortic aneurysms (ATAAs) (**Chapter 8**).
- Peak wall stresses for volunteers and AAA patients showed a significant correlation with diameter. Moreover, AAA patients with peak stresses comparable to volunteers were observed while other patients with equivalent diameters revealed an increased peak wall stress (**Chapter 4 and 6**).
- Longitudinal analysis of the arterial stiffness revealed that rapid growing AAAs have a lower arterial stiffness before the onset of rapid AAA growth, when compared to AAAs with slow or no growth. (**Chapter 6**).

- Verification experiments were performed using bi-axial tensile testing and revealed moderate to good agreement in arterial stiffness between the *in vivo* and *ex vivo* measurements for both AAAs and ATAAs (**Chapter 7 and 8**).

In the following sections, the main findings and implications are evaluated. Furthermore, the limitations and future perspectives of this thesis will be discussed.

## 9.2 From evidence based to personalized medicine

Current clinical guidelines for AAA repair are based on large randomized controlled trials which are designed to predict the best population-based outcome (The UK Small Aneurysm Trial Participants, 1998; Lederle et al., 2002b). However, the best population-based solution is not necessarily the ideal treatment option for the individual patient. In AAA rupture risk management, this is reflected by early rupture in 2 - 10% of all AAAs in follow-up before current thresholds for repair are reached (Nicholls et al., 1998). On the other hand, approximately 25% of all patients with large, but stable AAA are currently subjected to surgical repair, which result in unnecessary surgical risks for the individual patient (Darling et al., 1977; Lederle et al., 2002a). Hence, in this thesis we want to move from population-based evidence towards a more personalized approach.

As stated before in this thesis, aneurysms will rupture if the aortic wall stress exceeds the mechanical strength of the AAA wall. Therefore, not the maximum aortic diameter, but the state of the aortic wall (i.e., wall stress and wall strength) should be monitored over time. Time-resolved 3D ultrasound (4D US) is therefore an ideal image modality which can be easily implemented in clinical workflow since it is non-invasive and easy applicable. 4D US can be acquired during regular outpatient follow-up, which only requires approximately 10 minutes of extra time. Therefore, in this thesis, we developed a method to characterize the mechanical state of the AAA wall based on 4D US.

Of course, US imaging has some challenges. First of all, image quality can be limited due to the presence of bowel gas, calcifications in the aortic wall, and the large depth of the AAA. In addition, the field-of-view (FOV) of US imaging is restricted due to physical constraints. To examine the effects of the limited FOV using 4D US imaging on the patient-specific wall stress distribution, a methodological study was executed in **Chapter 2**. Ten AAA patients with a variety of different AAA geometries were included and wall stress analysis was performed based on CT data. By systematically reducing the FOV, changes in the 99<sup>th</sup> percentile peak wall stress (PWS) were observed. Finally, the PWS at different locations in the original CT dataset were compared with the PWS in the reduced FOV which was comparable with a single 3D US acquisition. Results revealed that a limited field-of-view is not necessarily a concern, as long as both areas with high curvature ("shoulders" of the aneurysm) were included in the FOV of the US acquisition.

Since the FOV was not a limited factor for proper wall stress analysis, a first feasibility study was performed to characterize the mechanical properties using 4D US in **Chapter 3**. Forty patients with AAA geometries that fits in one single 4D US acquisition were enrolled, and subjected to 4D US imaging. Using a forward iterative finite element approach, the simulated wall displacements were matched with the measured US displacements resulting in the patient-specific wall stress distribution and mechanical properties. This was the first time that both wall stresses and mechanical properties were assessed simultaneously. Moreover, since US imaging was used to capture the AAA geometry, this method can be applied to the complete diameter range of patient in follow-up. This, in contrast to most previous CT-based wall stress studies, where only patients were included with diameters close to the threshold for surgery (Speelman et al., 2010; Gasser et al., 2014).

The 99<sup>th</sup> percentile PWS results were compared with the study by Speelman et al. (2008) and showed similar results for the overlapping diameter range. The main difference between both studies was that the AAA diameters ranged in our study between 27 and 52 mm whereas in Speelman's CT-work the AAAs ranged between 44 and 57 mm.

Moreover, for 7 out of the 40 AAA patients not only 4D US data were acquired, but also CT data were available. This data allowed direct comparison of the patient-specific aortic geometry and percentile wall stresses. A good to excellent similarity between both geometries was observed with similarity indices (i.e., Dice coefficients) between 0.90 and 0.96, which is in correspondence with a segmentation reproducibility study by Rouet et al. (2017). Wall stresses comparison showed that the 25<sup>th</sup> to 95<sup>th</sup> percentile wall stress were in agreement, while the 99<sup>th</sup> percentile PWS in the CT data exceed the US data by 5 - 58%. This is in contrast to the previous work by Kok et al. (2015) where the 99<sup>th</sup> percentile PWS was higher in the US data compared to the CT data. However, the overestimation of the 99<sup>th</sup> percentile wall stress in Kok et al. (2015) was caused by registration errors in the US data, whereas the difference in current study was most presumably induced by oversmoothing of the US geometry after manual segmentation. This result advocated for an automated segmentation approach to reduce smoothing artifacts, and to make the segmentation approach less labor intensive and more robust (Chapter 5).

Furthermore, the measured material properties in Chapter 3 were compared with the parameters of the well-established material model of Raghavan and Vorp (2000). Since *in vivo* only the mechanical behavior of the AAA wall at the physiological blood pressure range could be assessed, the material behavior was compared for this specific range. Results showed that 80% of the *in vivo* determined material properties were within the, *ex vivo* derived, 95% confidence interval.

First feasibility study revealed promising results, however, to prove the clinical value of the current model it should be able to distinguish between healthy and diseased aorta tissue. Therefore, arterial stiffness and the 99<sup>th</sup> percentile PWS were characterized for young individuals, age-matched individuals, and AAA patients in **Chapter 4**. In total, 30 volunteers (max. diameter 13 - 29 mm) and 65 AAA patients with AAA diameters ranging

from relatively small (31 - 39 mm) to large (50 - 63 mm) were included, and differences in mechanical properties and their relation to age, arterial pressure, diameter, and growth were assessed.

A significant increase in arterial stiffness was observed between the age-matched individuals and the patients with a relatively small AAAs, even after correcting for differences in mean arterial pressure and the effect of aging. This suggests that the AAA pathology causes stiffening of the aortic wall already in an early stage of the disease. As a consequence, following this arterial stiffness over time might help to predict possible formation and/or growth of the AAA, especially since the arterial stiffness further increases when the AAA pathology becomes more severe and the diameter enlarges.

Only a few studies compared the arterial stiffness between healthy volunteers and AAA patients. Li et al. (2013) used pulse wave velocity imaging (PWVI) to assess the arterial wall motion and reported average pulse wave velocities of 6.03 and 10.54 m/s for the normal and AAA subjects, respectively. This corresponds with an arterial stiffness of 0.26 and 1.57 kPa·m (Equation (1.5)), which is similar as observed in Chapter 4. The study of Derwich et al. (2016) did not focus on arterial stiffness, but characterized aortic strain between volunteers and AAA patients. Differences in mean circumferential strain were measured, and correspond to our findings by assuming similar physiological blood pressures in both volunteer and AAA group.

Moreover, the 99<sup>th</sup> percentile PWS was estimated for the young individuals, age-matched individuals, and AAA patients in Chapter 4, and revealed a significant correlation with the aortic diameter. Furthermore, AAA patients with PWS similar to age-matched volunteers were observed whereas other AAA patients with an equivalent maximum diameter had an increased PWS. An increased PWS has been associated with symptomatic and ruptured aneurysms (Fillinger et al., 2002; Truijers et al., 2007; Khosla et al., 2014) and revealed a higher sensitivity and specificity in rupture risk assessment compared to the maximum diameter (Fillinger et al., 2003; Gasser et al., 2014).

Next steps for the current research would be to follow these patients over time, to examine whether small AAAs with high PWS are more prone to rupture compared to large AAAs with relatively low PWS. In addition, it would be interesting to assess how the arterial stiffness evolves over time and their possible relation with AAA growth. A first longitudinal study on the biomechanical properties of AAA patients was discussed in Chapter 6.

Such a long-term study would require an automatic analysis platform. Consequently, in **Chapter 5** an automatic segmentation method was developed for 3D US data of AAA patients. In addition, based on the results in Chapter 2, a registration algorithm was developed to merge a proximal and a distal 3D US acquisition to include AAAs with a larger longitudinal length in our studies. In order to test the accuracy of this segmentation and registration algorithm, 40 AAA patients were included in this study for which both CT and US data were acquired. For 20 AAA patients, first registration of two multi-perspective 3D US datasets was required before final automatic segmentation was applied.

Good agreement was observed in AAA geometries (Figures 5.4 and 5.5) and wall stress distribution (Figures 5.6 and 5.7) between the 3D US and CT data. The median local mismatch between the AAA geometries was 4.6 mm, which is considerable, although in the same range as reported in previous studies (Rouet et al., 2010; Kok et al., 2015; Rouet et al., 2017). An advantage of proposed fusion algorithm is that high wall stress artifacts induced by manual registration (Kok et al., 2015) were precluded.

Improvement in segmentation and fusion of multiple 3D US data resulted in a robust and automated computer model which was able to assess the patient-specific arterial stiffness and PWS based on 3D US acquisitions with only limited user interaction. This opens the door for a longitudinal study to assess possible changes in arterial stiffness and PWS over time, and to study their relation to AAA growth and rupture.

Therefore, in **Chapter 6**, 70 AAA patients were followed during regular follow-up for a median period of 24 months. Besides the maximum AAA diameter, the aortic stiffness and PWS were regularly measured. In addition, mechanical properties of patients with a ruptured AAA ( $n = 4$ ) were compared with the non-ruptured AAAs ( $n = 66$ ).

First results of this longitudinal study revealed that most rapid growing AAAs have a lower arterial stiffness at the moment before AAA growth is observed compared to slow growing or stable AAAs. In addition, in 67% of all patients that exhibited rapid growth between two follow-up intervals, a preceding decrease in arterial stiffness was observed. This value increased up to 71% for all patients with at least 2.5 mm growth in 3 months, which is comparable with current guidelines for surgical repair (i.e. 1 cm/year). A possible explanation for this decrease in arterial stiffness might be that the AAA wall remodels before it is able (or starting) to grow. Hence, a decrease in arterial stiffness might be a requirement for this remodeling process. This finding is in accordance with findings by Wilson et al. (1998) and results in a later study by the same group (Wilson et al., 2003) which suggested that a decrease in aortic stiffness is associated with an increase in AAA rupture risk. However, more patient inclusions with a long period of follow-up are required to examine this possible relation between a reduced arterial stiffness and rapid subsequent growth further.

Longitudinal analysis of the 99<sup>th</sup> percentile PWS showed that PWS increases as function of the maximum diameter, but for the individual patient it does not increase in a monotone way and can fluctuate considerable over time (Chapter 6). In a comparable study by Stevens et al. (2017), four AAA patients were followed over time and the peak wall rupture risk index (PWRI) were assessed over time. Similar fluctuations in PWRI were observed, which might be induced by adaptation (i.e. growth) of the AAA wall to reduce asymmetry and areas with high curvature in the AAA geometry (Vorp et al., 1998). However, additional studies should be conducted to confirm these findings. This is also the case for the risk of rupture prediction, since the number of ruptured AAAs was too low to draw any conclusions.

Finally, verification experiments were performed in **Chapter 7**. Verification of the *in vivo* measured aortic stiffness is only rarely possible, since only AAA patients who undergo

open aortic surgery will be eligible to provide aortic tissue for bi-axial tensile testing. Therefore, an experimental setup using porcine aortas was developed to verify the US-measured aortic stiffness with *ex vivo* tensile testing. Results showed a good agreement for the experimental setup, and a moderate agreement for the four included AAA patients despite good reproducibility of the US measurements. The discrepancy in AAA stiffness between the *in vivo* and *ex vivo* measurement was partially caused by the diseased state of the AAA tissue which impeded adequate tensile testing. In addition, spatial variation in aortic stiffness is a known phenomenon in AAA tissue (Vande Geest et al., 2006b), which might cause differences between the global measured US aortic stiffness, and the local tensile testing estimates.

As an aside, the current characterization method was applied to ascending thoracic aortic aneurysms (ATAAs) in **Chapter 8**. ATAAs are subjected to large longitudinal motion induced by the contraction and motion of the heart. Transesophageal US was used, which results in images with little speckle or landmarks. Therefore, cyclic deformation estimation based on affine transformation was required. An advantage in this study was that all *in vivo* US-based measurements were accompanied with aortic tissue to mechanically test *ex vivo*. Agreement between both methods was observed, although for some patients substantial differences were found.

In summary, the first steps towards clinical applicability of personalized AAA wall characterization were made in this thesis. However, this research is not without limitations and these will be addressed in the next section.

### 9.3 Limitations

One of the limitations in this thesis is the relative low frame rate available (3 - 10 volumes/s) and the use of DICOM data. These factors limit the precision of the 3D motion estimation. Preferably, the radio-frequency (RF) data should be acquired before conversion into DICOM data. These raw RF data will improve the 3D displacement estimation and subsequently increase the accuracy of the aortic stiffness estimates (Lopata et al., 2011).

Ultimately, 3D US imaging using spherical waves instead of focused line-by-line 3D imaging would be a step forward, which will increase the frame rate tremendously (Provost et al., 2014; Papadacci et al., 2017). A disadvantage of the ultrafast imaging approach is the reduced image contrast. This issue might be solved by compounding of multiple 3D US acquisition from different positions and angles. Alternatively, a combination of both imaging schemes could be developed. In this approach, the AAA geometry could be imaged first with the highest resolution and contrast using focused 3D US imaging and then 2D or 3D ultrafast US imaging could be employed to measure wall displacements with the highest possible resolution.

A major limitation in the biomechanical modeling approach is the use of a uniform wall thickness over the complete AAA geometry. Several studies, and results in Chapter 7 have



indicated that AAA wall thickness varied between patients and within the individual AAA geometry (Thubrikar et al., 2001; Di Martino et al., 2006; Raghavan et al., 2006). In the study by Raghavan et al. (2006). It was shown that the wall thickness varied regionally within one AAA from 0.23 mm at the rupture site to 4.26 mm at a calcified site. This variation in wall thickness will have a direct and inevitable effect on the predicted peak wall stress and aortic stiffness. Unfortunately, none of the currently available imaging techniques can provide local wall thickness with sufficient accuracy yet. Intra-vascular ultrasound (IVUS) could solve this issue, although it would make the current technology proposed more invasive, which in turn limits the applicability for long-term follow-up studies.

Another limitation is the model complexity. In the current modeling approach solely the AAA wall is considered, while in most aneurysms intraluminal thrombus (ILT) is found between the flow lumen and the AAA wall, and the AAA is surrounded by different tissue types. The ILT could be incorporated in the biomechanical model, however thrombus segmentation in 3D US data is challenging due to the presence of different thrombus layers and often low contrast. Moreover, each thrombus layer has different elastic properties (Tong et al., 2011), which all will alter the echogenic properties of the ILT. Therefore, automatic segmentation of the ILT is challenging and will require improved US imaging techniques and sophisticated segmentation algorithms.

Furthermore, the biomechanical role of the ILT is still under debate. Studies have suggested that the presence of ILT may serve as a mechanical buffer and prevent the AAA from high aortic wall stresses and eventually rupture (Mower et al., 1997; Thubrikar et al., 2003; Li et al., 2008). On the other hand, studies indicated that the AAA walls covered with ILT had a lower wall thickness and revealed signs of inflammation, apoptosis of smooth muscle cells, and degradation of extracellular matrix (Vorp et al., 2001; Kazi et al., 2003). These studies suggested that localized hypoxia occurred when a thick layer of ILT was present, which consequently causes wall weakening. These possible effects of ILT could be studied with the presented biomechanical model once the thrombus is incorporated. However, this was beyond the scope of the current thesis.

In addition, a relatively simple Neo-Hookean constitutive material behavior was used to describe the mechanical behavior of the AAA wall. Although the AAA wall is known for its non-linear behavior (Vande Geest et al., 2006b), a Neo-Hookean material model was chosen to describe the stress-strain relation in this thesis since only a limited part of the stress-strain behavior of the AAA wall could be assessed *in vivo*. Furthermore, at the physiological pressure range the stress-strain relation of the aortic wall is predominantly linear. Consequently, an incremental shear modulus was characterized which was subsequently converted into the arterial stiffness. A non-linear material model (Raghavan and Vorp, 2000) or a more complex, an-isotropic, non-linear material model could be employed (e.g., Holzapfel et al. (2000) or Gasser et al. (2006)), however these models require more material parameters which will introduce higher parameter uncertainties when assessed *in vivo*. If the precision of the 3D US motion estimation will be increased in the future (by e.g.,

RF-capture or ultrafast US imaging), more structural and non-linearity parameters could be measured which could describe the AAA wall behavior more reliable. However, what will never change, is the fact that the physiological pressure range *in vivo* is approximately 60/90 mmHg in diastole to 110/140 mmHg in systole, which renders the characterization of the full non-linear behavior of the AAA wall to be highly unlikely.

## 9.4 Future model developments

Besides solutions to the aforementioned limitations, several additional improvements can be implemented in future research to assess the patient-specific mechanical behavior more reliable. In this section the most important model developments will be discussed.

First, the effects of surrounding structures and tissues are neglected and should be included. Especially the spine, which is located closely to the abdominal aorta and serves as a rigid boundary condition at the dorsal side of the aorta. When the aorta becomes aneurysmatic, the distance between the spine and aorta reduces, and this boundary effect become more predominantly present. The spine limits the pulsatile movement of the AAA, which consequently will result in an inhomogeneous displacement pattern (Farsad et al., 2015; Petterson et al., 2018). This displacement pattern is measured *in vivo* using 4D US, however not incorporated *in silico*. Subsequently, this will lead to a mismatch between the measured and simulated displacement fields. In the future, the location of the spine relative to the AAA could be indicated in the US data and introduced in the model using either a generic or patient-specific shape. This will reduce the discrepancies between the *in vivo* and model displacements, and improve both the PWS prediction and the arterial stiffness measurements.

Secondly, calcifications in the aortic wall are currently not considered in the biomechanical model. It is known that calcifications will significantly affect the local stiffness and strength of the AAA tissue (Buijs et al., 2013; Volokh and Aboudi, 2016), and increase the local peak wall stress (Speelman et al., 2007; Li et al., 2008). Calcifications will appear as bright regions in the US acquisition, and could possibly be segmented using dynamic thresholding. However, to include these calcifications in the model, accurate material properties (Marra et al., 2006) and a smooth transition between different material properties should be assured.

Besides a global aortic stiffness measurement presented in this thesis, a more regional stiffness map of the AAA could be examined and employed in future. A localized stiffness distribution might help to understand the mechanical alterations due to the AAA pathology (Chapters 4 and 6). In addition, the combination of a local aortic stiffness map together with a regional wall stress distribution can improve the identification of weak spots in the AAA wall by, e.g., calculating a local PWRI (Gasser et al., 2010), and finally identify regions in the AAA wall with a high risk of rupture.

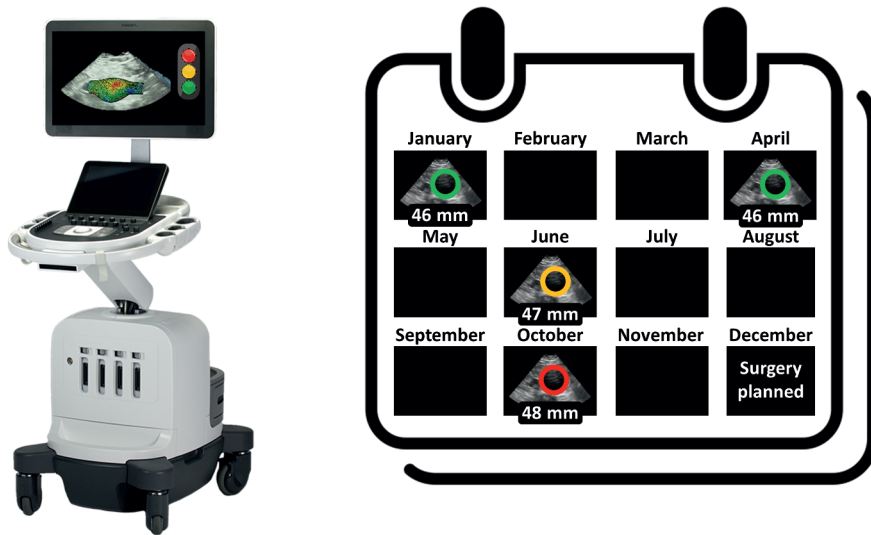


**Figure 9.1:** Future clinical perspective of current biomechanical model: **Left:** Implementation of the biomechanical model on a commercial US scanner which predict the patient-specific wall stress and arterial stiffness and report the outcome to the physician. **Right:** After large clinical trials the physician might not solely rely on the maximum diameter for surgical aortic repair, but also can take the mechanical state of the AAA wall into consideration.

## 9.5 Clinical perspective

In this thesis, the first steps were made to assess the patient-specific stiffness and peak wall stress of the AAA wall using a non-invasive image modality, which is easy accessible and implementable in clinical workflow. Results revealed that the methodology is able to distinguish between healthy and different stages of diseased aortic tissue (Chapter 4). Furthermore, in a prospective longitudinal study (Chapter 6), the peak wall stress and arterial stiffness were followed over time, and results hinted that rapid growth of the AAA is preceded by a lower arterial stiffness compared to stable or slow growing AAAs.

From a clinical perspective, the next step is to employ a large (500+ patients) prospective, single or multi-center study where the aortic stiffness and peak wall stress will be followed over a long period of time. A large patient group is required since aortic rupture is in present day a relatively rare phenomenon, and, to detect statistically significant differences in mechanical behavior between ruptured and non-ruptured AAAs. Moreover, this prospective study could be used to examine the relation between mechanical properties and AAA growth further.

Furthermore, if future research eventually reveals that AAA growth can be predicted by measuring arterial stiffness, personalized AAA follow-up management will become a reality (Moll et al., 2011). For example, a relatively small AAA which represent a sudden decrease in aortic stiffness, might need more frequent follow-up in the upcoming year. While on

the other hand, for a patient with a large yet stable AAA (in terms of diameter and arterial stiffness), a 3-monthly follow-up (according to current guidelines) is not necessary, and probably bi-yearly follow-up would be sufficient.

Finally, a randomized controlled trial (RCT) should be performed to prove the merit of this biomechanical modeling approach. In this RCT, the decision whether to perform aortic repair will be based on the maximum diameter in one group. In the other group, the physician will also be provided with the mechanical state of the aortic wall and should be able to freely decide whether to intervene or postpone surgery (Figure 9.1). Results of this RCT will demonstrate eventually the added clinical value of current methodology.

In Chapter 8 the method was applied to aneurysms in the ascending aorta. It was shown that characterization of the mechanical properties was feasible for this pathology. Hence, the current method is not only applicable to AAAs. In case of ascending thoracic aortic aneurysms (ATAAs), wall stress analysis and mechanical characterization could be used to monitor the state of the aortic wall. Additionally, a method using these mechanical parameters could be developed to predict dissection of the aorta (Thunes et al., 2018), which frequently precedes rupture of the ATAA.

Moreover, mechanical analysis of thoracic or abdominal aortic aneurysms is not limited to monitoring the deterioration of the arterial wall. It can also be used to predict the outcome of intervention. In case of abdominal aneurysms, the AAA geometry can be extracted from a pre-operative US acquisition, and could be extended with a stent-graft (Perrin et al., 2015). By simulating the post-operative situation, the aortic wall displacements could be compared with the pre-operative dataset to investigate the effect of the surgical intervention. Using this *in silico* stent-graft placement, the best position, size, and stent-graft type could be examined. Additionally, in the post-operative situation, a similar approach can be used to detect endoleaks before these are even visible with Doppler ultrasound.

## 9.6 General conclusion

In this thesis, an image-based, biomechanical modeling framework was developed which is able to assess the arterial stiffness and wall stress distribution of abdominal aortic aneurysms (AAAs) using time-resolved 3D ultrasound. Validation using CT-imaging shows good agreement in terms of geometry and wall stress distribution, which enabled opportunities to perform long-term patient and volunteer studies.

First studies revealed that the AAA pathology causes a significant increase in arterial stiffness, already in an early stage of the disease. In addition, first longitudinal analysis of these mechanical parameters hinted that before rapid AAA growth a lower arterial stiffness was observed, which stands in contrast to slow growing and stable AAAs. Future clinical trials should prove the predictive value of biomechanical modeling in AAA monitoring and rupture risk assessment. Nevertheless, using the US-based methodology presented, these studies can be executed easily and in a non-invasive and harmless manner.



# Bibliography

- Abbas, A., Hansrani, V., Sedgwick, N., Ghosh, J., and McCollum, C. N. (2014). 3d contrast enhanced ultrasound for detecting endoleak following endovascular aneurysm repair (EVAR). *European Journal of Vascular and Endovascular Surgery*, 47(5):487–492.
- Alvarez, L., Guichard, F., Lions, P.-L., and Morel, J.-M. (1993). Axioms and fundamental equations of image processing. *Archive for Rational Mechanics and Analysis*, 123(3):199–257.
- Ashton, H. A., Buxton, M. J., Day, N. E., Kim, L. G., Marteau, T. M., Scott, R. a. P., Thompson, S. G., Walker, N. M., and Multicentre Aneurysm Screening Study Group (2002). The Multicentre Aneurysm Screening Study (MASS) into the effect of abdominal aortic aneurysm screening on mortality in men: a randomised controlled trial. *Lancet (London, England)*, 360(9345):1531–1539.
- Azadani, A. N., Chitsaz, S., Mannion, A., Mookhoek, A., Wisneski, A., Guccione, J. M., Hope, M. D., Ge, L., and Tseng, E. E. (2013). Biomechanical Properties of Human Ascending Thoracic Aortic Aneurysms. *The Annals of Thoracic Surgery*, 96(1):50–58.
- Banerjee, J., Klink, C., Peters, E. D., Niessen, W. J., Moelker, A., and van Walsum, T. (2015). Fast and robust 3d ultrasound registration – Block and game theoretic matching. *Medical Image Analysis*, 20(1):173–183.
- Bartko, J. J. (1991). Measurement and Reliability: Statistical Thinking Considerations. *Schizophrenia Bulletin*, 17(3):483–489.
- Bell, V., Mitchell, W. A., Sigurðsson, S., Westenberg, J. J. M., Gotal, J. D., Torjesen, A. A., Aspelund, T., Launer, L. J., Roos, A. d., Gudnason, V., Harris, T. B., and Mitchell, G. F. (2014). Longitudinal and Circumferential Strain of the Proximal Aorta. *Journal of the American Heart Association*, 3(6):e001536.
- Beller, C. J., Labrosse, M. R., Thubrikar, M. J., and Robicsek, F. (2004). Role of Aortic Root Motion in the Pathogenesis of Aortic Dissection. *Circulation*, 109(6):763–769.

- Blacher, J., Asmar, R., Djane, S., London, G. M., and Safar, M. E. (1999). Aortic Pulse Wave Velocity as a Marker of Cardiovascular Risk in Hypertensive Patients. *Hypertension*, 33(5):1111–1117.
- Blankensteijn, J. D., de Jong, S. E. C. A., Prinssen, M., van der Ham, A. C., Buth, J., van Sterkenburg, S. M. M., Verhagen, H. J. M., Buskens, E., Grobbee, D. E., and Dutch Randomized Endovascular Aneurysm Management (DREAM) Trial Group (2005). Two-year outcomes after conventional or endovascular repair of abdominal aortic aneurysms. *The New England Journal of Medicine*, 352(23):2398–2405.
- Bodur, O., Grady, L., Stillman, A., Setser, R., Funka-Lea, G., and O'Donnell, T. (2007). Semi-automatic aortic aneurysm analysis. *Proceedings of SPIE - The International Society for Optical Engineering*, page 65111.
- Borghi, A., Wood, N. B., Mohiaddin, R. H., and Xu, X. Y. (2006). 3d geometric reconstruction of thoracic aortic aneurysms. *BioMedical Engineering OnLine*, 5:59.
- Bredahl, K., Sandholt, B., Lönn, L., Rouet, L., Ardon, R., Eiberg, J. P., and Sillesen, H. (2015). Three-dimensional ultrasound evaluation of small asymptomatic abdominal aortic aneurysms. *European Journal of Vascular and Endovascular Surgery: The Official Journal of the European Society for Vascular Surgery*, 49(3):289–296.
- Bredahl, K., Taudorf, M., Long, A., Lönn, L., Rouet, L., Ardon, R., Sillesen, H., and Eiberg, J. P. (2013). Three-dimensional ultrasound improves the accuracy of diameter measurement of the residual sac in EVAR patients. *European Journal of Vascular and Endovascular Surgery: The Official Journal of the European Society for Vascular Surgery*, 46(5):525–532.
- Breeuwer, M., Putter, S. d., Kose, U., Speelman, L., Visser, K., Gerritsen, F., Hoogeveen, R., Krams, R., Bosch, H. v. d., Buth, J., Gunther, T., Wolters, B., Dam, E. v., and Vosse, F. v. d. (2008). Towards patient-specific risk assessment of abdominal aortic aneurysm. *Medical & Biological Engineering & Computing*, 46(11):1085–1095.
- Budd, J. S., Finch, D. R., and Carter, P. G. (1989). A study of the mortality from ruptured abdominal aortic aneurysms in a district community. *European Journal of Vascular Surgery*, 3(4):351–354.
- Buijs, R. V. C., Willems, T. P., Tio, R. A., Boersma, H. H., Tielliu, I. F. J., Slart, R. H. J. A., and Zeebregts, C. J. (2013). Calcification as a Risk Factor for Rupture of Abdominal Aortic Aneurysm. *European Journal of Vascular and Endovascular Surgery*, 46(5):542–548.
- Chaikof, E. L., Dalman, R. L., Eskandari, M. K., Jackson, B. M., Lee, W. A., Mansour, M. A., Mastracci, T. M., Mell, M., Murad, M. H., Nguyen, L. L., Oderich, G. S., Patel, M. S., Schermerhorn, M. L., and Starnes, B. W. (2018). The Society for Vascular Surgery practice guidelines on the care of patients with an abdominal aortic aneurysm. *Journal of Vascular Surgery*, 67(1):2–77.e2.

- Chen, K., Varon, J., Wenker, O. C., Judge, D. K., Fromm, R. E., and Sternbach, G. L. (1997). Acute thoracic aortic dissection: the basics. *The Journal of Emergency Medicine*, 15(6):859–867.
- Clouse, W. D., John W. Hallett, J., Schaff, H. V., Gayari, M. M., Ilstrup, D. M., and Iii, L. J. M. (1998). Improved Prognosis of Thoracic Aortic Aneurysms: A Population-Based Study. *JAMA*, 280(22):1926–1929.
- Conlisk, N., Forsythe, R. O., Hollis, L., Doyle, B. J., McBride, O. M. B., Robson, J. M. J., Wang, C., Gray, C. D., Semple, S. I. K., MacGillivray, T., van Beek, E. J. R., Newby, D. E., and Hoskins, P. R. (2017). Exploring the Biological and Mechanical Properties of Abdominal Aortic Aneurysms Using USPIO MRI and Peak Tissue Stress: A Combined Clinical and Finite Element Study. *Journal of Cardiovascular Translational Research*, 10(5-6):489–498.
- Conway, K. P., Byrne, J., Townsend, M., and Lane, I. F. (2001). Prognosis of patients turned down for conventional abdominal aortic aneurysm repair in the endovascular and sonographic era: Szilagyi revisited? *Journal of Vascular Surgery*, 33(4):752–757.
- Damughatla, A. R., Raterman, B., Sharkey-Toppen, T., Jin, N., Simonetti, O. P., White, R. D., and Kolipaka, A. (2015). Quantification of aortic stiffness using MR elastography and its comparison to MRI-based pulse wave velocity. *Journal of magnetic resonance imaging: JMRI*, 41(1):44–51.
- Darling, R. C. (1970). Ruptured arteriosclerotic abdominal aortic aneurysms: A pathologic and clinical study. *The American Journal of Surgery*, 119(4):397–401.
- Darling, R. C., Messina, C. R., Brewster, D. C., and Ottinger, L. W. (1977). Autopsy study of unoperated abdominal aortic aneurysms. The case for early resection. *Circulation*, 56(3 Suppl):II161–164.
- De Bruin, J. L., Baas, A. F., Buth, J., Prinssen, M., Verhoeven, E. L., Cuypers, P. W., van Sambeek, M. R., Balm, R., Grobbee, D. E., and Blankensteijn, J. D. (2010). Long-Term Outcome of Open or Endovascular Repair of Abdominal Aortic Aneurysm. *New England Journal of Medicine*, 362(20):1881–1889.
- de Putter, S., Wolters, B. J. B. M., Rutten, M. C. M., Breeuwer, M., Gerritsen, F. A., and van de Vosse, F. N. (2007). Patient-specific initial wall stress in abdominal aortic aneurysms with a backward incremental method. *Journal of Biomechanics*, 40(5):1081–1090.
- Derwich, W., Wittek, A., Pfister, K., Nelson, K., Bereiter-Hahn, J., Fritzen, C. P., Blase, C., and Schmitz-Rixen, T. (2016). High Resolution Strain Analysis Comparing Aorta and Abdominal Aortic Aneurysm with Real Time Three Dimensional Speckle Tracking Ultrasound. *European Journal of Vascular and Endovascular Surgery*, 51(2):187–193.



- Di Martino, E. S., Bohra, A., Vande Geest, J. P., Gupta, N., Makaroun, M. S., and Vorp, D. A. (2006). Biomechanical properties of ruptured versus electively repaired abdominal aortic aneurysm wall tissue. *Journal of Vascular Surgery*, 43(3):570–576.
- Dubost, C., Allary, M., and Oeconomos, N. (1952). Resection of an aneurysm of the abdominal aorta: Reestablishment of the Continuity by a Preserved Human Arterial Graft, with Result After Five Months. *A.M.A. Archives of Surgery*, 64(3):405–408.
- Duprey, A., Trabelsi, O., Vola, M., Favre, J.-P., and Avril, S. (2016). Biaxial rupture properties of ascending thoracic aortic aneurysms. *Acta Biomaterialia*, 42:273–285.
- Duquette, A. A., Jodoin, P.-M., Bouchot, O., and Lalande, A. (2012). 3d segmentation of abdominal aorta from CT-scan and MR images. *Computerized Medical Imaging and Graphics*, 36(4):294–303.
- Elger, D. F., Blacketter, D. M., Budwig, R. S., and Johansen, K. H. (1996). The influence of shape on the stresses in model abdominal aortic aneurysms. *Journal of Biomechanical Engineering*, 118(3):326–332.
- Epstein, D. M., Sculpher, M. J., Manca, A., Michaels, J., Thompson, S. G., Brown, L. C., Powell, J. T., Buxton, M. J., and Greenhalgh, R. M. (2008). Modelling the long-term cost-effectiveness of endovascular or open repair for abdominal aortic aneurysm. *BJS*, 95(2):183–190.
- Erbel, R., Aboyans, V., Boileau, C., Bossone, E., Bartolomeo, R. D., Eggebrecht, H., Evangelista, A., Falk, V., Frank, H., Gaemperli, O., Grabenwöger, M., Haverich, A., Jung, B., Manolis, A. J., Meijboom, F., Nienaber, C. A., Roffi, M., Rousseau, H., Sechtem, U., Sirnes, P. A., Allmen, R. S. v., Vrints, C. J. M., and ESC Committee for Practice Guidelines (2014). 2014 ESC Guidelines on the diagnosis and treatment of aortic diseases: Document covering acute and chronic aortic diseases of the thoracic and abdominal aorta of the adult. The Task Force for the Diagnosis and Treatment of Aortic Diseases of the European Society of Cardiology (ESC). *European Heart Journal*, 35(41):2873–2926.
- Erhart, P., Hyhlik-Dürr, A., Geisbüsch, P., Kotelis, D., Müller-Eschner, M., Gasser, T. C., von Tengg-Kobligh, H., and Böckler, D. (2015). Finite Element Analysis in Asymptomatic, Symptomatic, and Ruptured Abdominal Aortic Aneurysms: In Search of New Rupture Risk Predictors. *European Journal of Vascular and Endovascular Surgery*, 49(3):239–245.
- Farotto, D., Segers, P., Meuris, B., Vander Sloten, J., and Famaey, N. (2018). The role of biomechanics in aortic aneurysm management: requirements, open problems and future prospects. *Journal of the Mechanical Behavior of Biomedical Materials*, 77:295–307.

- Farsad, M., Zeinali-Davarani, S., Choi, J., and Baek, S. (2015). Computational Growth and Remodeling of Abdominal Aortic Aneurysms Constrained by the Spine. *Journal of Biomechanical Engineering*, 137(9).
- Fillinger, M. F., Marra, S. P., Raghavan, M. L., and Kennedy, F. E. (2003). Prediction of rupture risk in abdominal aortic aneurysm during observation: Wall stress versus diameter. *Journal of Vascular Surgery*, 37(4):724–732.
- Fillinger, M. F., Raghavan, M. L., Marra, S. P., Cronenwett, J. L., and Kennedy, F. E. (2002). In vivo analysis of mechanical wall stress and abdominal aortic aneurysm rupture risk. *Journal of Vascular Surgery*, 36(3):589–597.
- Flamini, V., Creane, A. P., Kerskens, C. M., and Lally, C. (2015). Imaging and finite element analysis: A methodology for non-invasive characterization of aortic tissue. *Medical Engineering & Physics*, 37(1):48–54.
- Forsell, C., Björck, H. M., Eriksson, P., Franco-Cereceda, A., and Gasser, T. C. (2014). Biomechanical properties of the thoracic aneurysmal wall: differences between bicuspid aortic valve and tricuspid aortic valve patients. *The Annals of Thoracic Surgery*, 98(1):65–71.
- Fromageau, J., Lerouge, S., Maurice, R. L., Soulez, G., and Cloutier, G. (2008). Noninvasive vascular ultrasound elastography applied to the characterization of experimental aneurysms and follow-up after endovascular repair. *Physics in Medicine & Biology*, 53(22):64–75.
- Ganten, M.-K., Krautter, U., von Tengg-Kobligk, H., Böckler, D., Schumacher, H., Stiller, W., Delorme, S., Kauczor, H.-U., Kauffmann, G. W., and Bock, M. (2008). Quantification of aortic distensibility in abdominal aortic aneurysm using ECG-gated multi-detector computed tomography. *European Radiology*, 18(5):966–973.
- Gasser, T. C., Auer, M., Labruto, F., Swedenborg, J., and Roy, J. (2010). Biomechanical Rupture Risk Assessment of Abdominal Aortic Aneurysms: Model Complexity versus Predictability of Finite Element Simulations. *European Journal of Vascular and Endovascular Surgery*, 40(2):176–185.
- Gasser, T. C., Gallinetti, S., Xing, X., Forsell, C., Swedenborg, J., and Roy, J. (2012). Spatial orientation of collagen fibers in the abdominal aortic aneurysm's wall and its relation to wall mechanics. *Acta Biomaterialia*, 8(8):3091–3103.
- Gasser, T. C., Nchimi, A., Swedenborg, J., Roy, J., Sakalihasan, N., Böckler, D., and Hyhlik-Dürr, A. (2014). A Novel Strategy to Translate the Biomechanical Rupture Risk of Abdominal Aortic Aneurysms to their Equivalent Diameter Risk: Method and Retrospective Validation. *European Journal of Vascular and Endovascular Surgery*, 47(3):288–295.

- Gasser, T. C., Ogden, R. W., and Holzapfel, G. A. (2006). Hyperelastic modelling of arterial layers with distributed collagen fibre orientations. *Journal of the Royal Society Interface*, 3(6):15–35.
- Geerligs, M., Peters, G. W. M., Ackermans, P. A. J., Oomens, C. W. J., and Baaijens, F. P. T. (2008). Linear viscoelastic behavior of subcutaneous adipose tissue. *Biorheology*, 45(6):677–688.
- Greenhalgh, R. M., Brown, L. C., Kwong, G. P. S., Powell, J. T., Thompson, S. G., and EVAR trial participants (2004). Comparison of endovascular aneurysm repair with open repair in patients with abdominal aortic aneurysm (EVAR trial 1), 30-day operative mortality results: randomised controlled trial. *Lancet (London, England)*, 364(9437):843–848.
- Hall, T. J., Bilgen, M., Insana, M. F., and Krouskop, T. A. (1997). Phantom materials for elastography. *IEEE Transactions on Ultrasonics, Ferroelectrics, and Frequency Control*, 44(6):1355–1365.
- Han, H.-C. and Fung, Y.-C. (1995). Longitudinal strain of canine and porcine aortas. *Journal of Biomechanics*, 28(5):637–641.
- He, C. M. and Roach, M. R. (1994). The composition and mechanical properties of abdominal aortic aneurysms. *Journal of Vascular Surgery*, 20(1):6–13.
- Hellenthal, F. A. M. V. I., Pulinx, B., Welten, R. J. T. J., Teijink, J. A. W., van Dieijen-Visser, M. P., Wodzig, W. K. W. H., and Schurink, G. W. H. (2012). Circulating biomarkers and abdominal aortic aneurysm size. *The Journal of surgical research*, 176(2):672–678.
- Heng, M. S., Fagan, M. J., Collier, J. W., Desai, G., McCollum, P. T., and Chetter, I. C. (2008). Peak wall stress measurement in elective and acute abdominal aortic aneurysms. *Journal of Vascular Surgery*, 47(1):17–22.
- Holzapfel, G. A., Gasser, T. C., and Ogden, R. W. (2000). A New Constitutive Framework for Arterial Wall Mechanics and a Comparative Study of Material Models. *Journal of elasticity and the physical science of solids*, 61(1):1–48.
- Horný, L., Adamek, T., Gultova, E., Zitny, R., Vesely, J., Chlup, H., and Konvickova, S. (2011). Correlations between age, prestrain, diameter and atherosclerosis in the male abdominal aorta. *Journal of the Mechanical Behavior of Biomedical Materials*, 4(8):2128–2132.
- Horný, L., Netušil, M., and Voňavková, T. (2014). Axial prestretch and circumferential distensibility in biomechanics of abdominal aorta. *Biomechanics and Modeling in Mechanobiology*, 13(4):783–799.
- Hua, J. and Mower, W. R. (2001). Simple geometric characteristics fail to reliably predict abdominal aortic aneurysm wall stresses. *Journal of Vascular Surgery*, 34(2):308–315.

- Iliopoulos, D. C., Kritharis, E. P., Giagini, A. T., Papadodima, S. A., and Sokolis, D. P. (2009). Ascending thoracic aortic aneurysms are associated with compositional remodeling and vessel stiffening but not weakening in age-matched subjects. *The Journal of Thoracic and Cardiovascular Surgery*, 137(1):101–109.
- Johnston, K. W., Rutherford, R. B., Tilson, M. D., Shah, D. M., Hollier, L., and Stanley, J. C. (1991). Suggested standards for reporting on arterial aneurysms. *Journal of Vascular Surgery*, 13(3):452–458.
- Karatolios, K., Wittek, A., Nwe, T. H., Bihari, P., Shelke, A., Josef, D., Schmitz-Rixen, T., Geks, J., Maisch, B., Blase, C., Moosdorf, R., and Vogt, S. (2013). Method for Aortic Wall Strain Measurement With Three-Dimensional Ultrasound Speckle Tracking and Fitted Finite Element Analysis. *The Annals of Thoracic Surgery*, 96(5):1664–1671.
- Kass, M., Witkin, A., and Terzopoulos, D. (1988). Snakes: Active contour models. *International Journal of Computer Vision*, 1(4):321–331.
- Kauffmann, C., Tang, A., Dugas, A., Therasse, r., Oliva, V., and Soulez, G. (2011). Clinical validation of a software for quantitative follow-up of abdominal aortic aneurysm maximal diameter and growth by CT angiography. *European Journal of Radiology*, 77(3):502–508.
- Kauffmann, C., Tang, A., Therasse, E., Giroux, M.-F., Elkouri, S., Melanson, P., Melanson, B., Oliva, V. L., and Soulez, G. (2012). Measurements and detection of abdominal aortic aneurysm growth: Accuracy and reproducibility of a segmentation software. *European Journal of Radiology*, 81(8):1688–1694.
- Kazi, M., Thyberg, J., Religa, P., Roy, J., Eriksson, P., Hedin, U., and Swedenborg, J. (2003). Influence of intraluminal thrombus on structural and cellular composition of abdominal aortic aneurysm wall. *Journal of Vascular Surgery*, 38(6):1283–1292.
- Khosla, S., Morris, D. R., Moxon, J. V., Walker, P. J., Gasser, T. C., and Golledge, J. (2014). Meta-analysis of peak wall stress in ruptured, symptomatic and intact abdominal aortic aneurysms. *The British Journal of Surgery*, 101(11):1350–1357.
- Kim, J. and Baek, S. (2011). Circumferential variations of mechanical behavior of the porcine thoracic aorta during the inflation test. *Journal of Biomechanics*, 44(10):1941–1947.
- Klein, S., Pluim, J. P. W., Staring, M., and Viergever, M. A. (2009). Adaptive Stochastic Gradient Descent Optimisation for Image Registration. *International Journal of Computer Vision*, 81(3):227.
- Kok, A. M., Nguyen, V. L., Speelman, L., Brands, P. J., Schurink, G.-W. H., van de Vosse, F. N., and Lopata, R. G. P. (2015). Feasibility of wall stress analysis of abdominal aortic aneurysms using three-dimensional ultrasound. *Journal of Vascular Surgery*, 61(5):1175–1184.

- Kolipaka, A., Illapani, V. S. P., Kenyhercz, W., Dowell, J. D., Go, M. R., Starr, J. E., Vaccaro, P. S., and White, R. D. (2016). Quantification of abdominal aortic aneurysm stiffness using magnetic resonance elastography and its comparison to aneurysm diameter. *Journal of Vascular Surgery*, 64(4):966–974.
- Koo, T. K. and Li, M. Y. (2016). A Guideline of Selecting and Reporting Intraclass Correlation Coefficients for Reliability Research. *Journal of Chiropractic Medicine*, 15(2):155–163.
- Kwon, S. T., Burek, W., Dupay, A. C., Farsad, M., Baek, S., Park, E.-A., and Lee, W. (2015). Interaction of expanding abdominal aortic aneurysm with surrounding tissue: Retrospective CT image studies. *Journal of nature and science*, 1(8):e150.
- Lederle, F. A., Freischlag, J. A., Kyriakides, T. C., Padberg, F. T., Matsumura, J. S., Kohler, T. R., Lin, P. H., Jean-Claude, J. M., Cikrit, D. F., Swanson, K. M., Peduzzi, P. N., and Open Versus Endovascular Repair (OVER) Veterans Affairs Cooperative Study Group (2009). Outcomes following endovascular vs open repair of abdominal aortic aneurysm: a randomized trial. *JAMA*, 302(14):1535–1542.
- Lederle, F. A., Johnson, G. R., Wilson, S. E., Ballard, D. J., William D. Jordan, J., Blebea, J., Littooy, F. N., Freischlag, J. A., Bandyk, D., Rapp, J. H., Salam, A. A., and Investigators, f. t. V. A. C. S. . (2002a). Rupture Rate of Large Abdominal Aortic Aneurysms in Patients Refusing or Unfit for Elective Repair. *JAMA*, 287(22):2968–2972.
- Lederle, F. A., Johnson, G. R., Wilson, S. E., Chute, E. P., Littooy, F. N., Bandyk, D., Krupski, W. C., Barone, G. W., Acher, C. W., and Ballard, D. J. (1997). Prevalence and associations of abdominal aortic aneurysm detected through screening. Aneurysm Detection and Management (ADAM) Veterans Affairs Cooperative Study Group. *Annals of Internal Medicine*, 126(6):441–449.
- Lederle, F. A., Wilson, S. E., Johnson, G. R., Reinke, D. B., Littooy, F. N., Acher, C. W., Ballard, D. J., Messina, L. M., Gordon, I. L., Chute, E. P., Krupski, W. C., Busuttil, S. J., Barone, G. W., Sparks, S., Graham, L. M., Rapp, J. H., Makaroun, M. S., Moneta, G. L., Cambria, R. A., Makhoul, R. G., Eton, D., Ansel, H. J., Freischlag, J. A., Bandyk, D., and Aneurysm Detection and Management Veterans Affairs Cooperative Study Group (2002b). Immediate repair compared with surveillance of small abdominal aortic aneurysms. *The New England Journal of Medicine*, 346(19):1437–1444.
- Leermans, A. and Jones, D. (2009). The B-matrix must be rotated when correcting for subject motion in DTI data. *Magnetic Resonance in Medicine*, 61:1336–49.
- Li, R. X., Luo, J., Balaram, S. K., Chaudhry, F. A., Shahmirzadi, D., and Konofagou, E. E. (2013). Pulse wave imaging in normal, hypertensive and aneurysmal human aortas in vivo: a feasibility study. *Physics in Medicine and Biology*, 58(13):4549–4562.

- Li, Z.-Y., Sadat, U., U-King-Im, J., Tang, T. Y., Bowden, D. J., Hayes, P. D., and Gillard, J. H. (2010). Association between aneurysm shoulder stress and abdominal aortic aneurysm expansion: a longitudinal follow-up study. *Circulation*, 122(18):1815–1822.
- Li, Z.-Y., U-King-Im, J., Tang, T. Y., Soh, E., See, T. C., and Gillard, J. H. (2008). Impact of calcification and intraluminal thrombus on the computed wall stresses of abdominal aortic aneurysm. *Journal of Vascular Surgery*, 47(5):928–935.
- Lindholt, J. S., Vammen, S., Fastang, H., Henneberg, E. W., and Heickendorff, L. (2000). The plasma level of matrix metalloproteinase 9 may predict the natural history of small abdominal aortic aneurysms. A preliminary study. *European journal of vascular and endovascular surgery: the official journal of the European Society for Vascular Surgery*, 20(3):281–285.
- Long, A., Rouet, L., Debreuve, A., Ardon, R., Barbe, C., Becquemin, J. P., and Allaire, E. (2013). Abdominal Aortic Aneurysm Imaging with 3-D Ultrasound: 3-D-Based Maximum Diameter Measurement and Volume Quantification. *Ultrasound in Medicine & Biology*, 39(8):1325–1336.
- Lopata, R. G. P., Nillesen, M. M., Hansen, H. H. G., Gerrits, I. H., Thijssen, J. M., and de Korte, C. L. (2009). Performance Evaluation of Methods for Two-Dimensional Displacement and Strain Estimation Using Ultrasound Radio Frequency Data. *Ultrasound in Medicine & Biology*, 35(5):796–812.
- Lopata, R. G. P., Nillesen, M. M., Thijssen, J. M., Kapusta, L., and de Korte, C. L. (2011). Three-Dimensional Cardiac Strain Imaging in Healthy Children Using RF-Data. *Ultrasound in Medicine & Biology*, 37(9):1399–1408.
- Lopata, R. G. P., Peters, M. F. J., Nijs, J., Oomens, C. W. J., Rutten, M. C. M., and van de Vosse, F. N. (2014). Vascular Elastography: A Validation Study. *Ultrasound in Medicine & Biology*, 40(8):1882–1895.
- Marra, S. P., Daghlian, C. P., Fillinger, M. F., and Kennedy, F. E. (2006). Elemental composition, morphology and mechanical properties of calcified deposits obtained from abdominal aortic aneurysms. *Acta Biomaterialia*, 2(5):515–520.
- Martin, C., Sun, W., and Elefteriades, J. (2015). Patient-specific finite element analysis of ascending aorta aneurysms. *American Journal of Physiology-Heart and Circulatory Physiology*, 308(10):1306–1316.
- Martufi, G., Auer, M., Roy, J., Swedenborg, J., Sakalihan, N., Panuccio, G., and Gasser, T. C. (2013). Multidimensional growth measurements of abdominal aortic aneurysms. *Journal of vascular surgery*, 58(3):748–755.

- Martufi, G., Lindquist Liljeqvist, M., Sakalihasan, N., Panuccio, G., Hultgren, R., Roy, J., and Gasser, T. C. (2016). Local Diameter, Wall Stress, and Thrombus Thickness Influence the Local Growth of Abdominal Aortic Aneurysms. *Journal of Endovascular Therapy: An Official Journal of the International Society of Endovascular Specialists*, 23(6):957–966.
- Mascarenhas, E. J. S., Peters, M. F. J., Nijs, J., Rutten, M. C. M., van de Vosse, F. N., and Lopata, R. G. P. (2016). Assessment of mechanical properties of porcine aortas under physiological loading conditions using vascular elastography. *Journal of the Mechanical Behavior of Biomedical Materials*, 59(Supplement C):185–196.
- Merkx, M. a. G., van 't Veer, M., Speelman, L., Breeuwer, M., Buth, J., and van de Vosse, F. N. (2009). Importance of initial stress for abdominal aortic aneurysm wall motion: dynamic MRI validated finite element analysis. *Journal of Biomechanics*, 42(14):2369–2373.
- Moll, F. L., Powell, J. T., Fraedrich, G., Verzini, F., Haulon, S., Waltham, M., van Herwaarden, J. A., Holt, P. J. E., van Keulen, J. W., Rantner, B., Schlösser, F. J. V., Setacci, F., and Ricco, J. B. (2011). Management of Abdominal Aortic Aneurysms Clinical Practice Guidelines of the European Society for Vascular Surgery. *European Journal of Vascular and Endovascular Surgery*, 41(Supplement 1):S1–S58.
- Mower, W. R., Quiñones, W. J., and Gambhir, S. S. (1997). Effect of intraluminal thrombus on abdominal aortic aneurysm wall stress. *Journal of Vascular Surgery*, 26(4):602–608.
- Nathan, D. P., Xu, C., Gorman, J. H., Fairman, R. M., Bavaria, J. E., Gorman, R. C., Chandran, K. B., and Jackson, B. M. (2011). Pathogenesis of Acute Aortic Dissection: A Finite Element Stress Analysis. *The Annals of Thoracic Surgery*, 91(2):458–463.
- Nicholls, S. C., Gardner, J. B., Meissner, M. H., and Johansen, K. H. (1998). Rupture in small abdominal aortic aneurysms. *Journal of Vascular Surgery*, 28(5):884–888.
- Niestrawska, J. A., Viertler, C., Regitnig, P., Cohnert, T. U., Sommer, G., and Holzapfel, G. A. (2016). Microstructure and mechanics of healthy and aneurysmatic abdominal aortas: experimental analysis and modelling. *Journal of the Royal Society, Interface*, 13(124).
- Nillesen, M. M., Lopata, R. G. P., Gerrits, I. H., Kapusta, L., Huisman, H. J., Thijssen, J. M., and de Korte, C. L. (2007). Segmentation of the heart muscle in 3-D pediatric echocardiographic images. *Ultrasound in Medicine & Biology*, 33(9):1453–1462.
- Okamoto, R. J., Wagenseil, J. E., DeLong, W. R., Peterson, S. J., Kouchoukos, N. T., and Sundt, T. M. (2002). Mechanical properties of dilated human ascending aorta. *Annals of Biomedical Engineering*, 30(5):624–635.
- Olabarriaga, S. D., Breeuwer, M., and Niessen, W. J. (2004a). Multi-scale Statistical Grey Value Modelling for Thrombus Segmentation from CTA. In *Medical Image Computing*

- and *Computer-Assisted Intervention – MICCAI 2004*, Lecture Notes in Computer Science, pages 467–474. Springer, Berlin, Heidelberg.
- Olabbariaga, S. D., Breeuwer, M., and Niessen, W. J. (2004b). Segmentation of Abdominal Aortic Aneurysms with a Non-parametric Appearance Model. In *Computer Vision and Mathematical Methods in Medical and Biomedical Image Analysis*, Lecture Notes in Computer Science, pages 257–268. Springer, Berlin, Heidelberg.
- O’Leary, S. A., Doyle, B. J., and McGloughlin, T. M. (2014). The impact of long term freezing on the mechanical properties of porcine aortic tissue. *Journal of the Mechanical Behavior of Biomedical Materials*, 37:165–173.
- O’Leary, S. A., Healey, D. A., Kavanagh, E. G., Walsh, M. T., McGloughlin, T. M., and Doyle, B. J. (2014). The biaxial biomechanical behavior of abdominal aortic aneurysm tissue. *Annals of Biomedical Engineering*, 42(12):2440–2450.
- Pancheri, F. Q., Peattie, R. A., Reddy, N. D., Ahamed, T., Lin, W., Ouellette, T. D., Iafrati, M. D., and Luis Dorfmann, A. (2017). Histology and Biaxial Mechanical Behavior of Abdominal Aortic Aneurysm Tissue Samples. *Journal of Biomechanical Engineering*, 139(3).
- Pande, R. L. and Beckman, J. A. (2013). Chapter 37 - Pathophysiology, Epidemiology, and Prognosis of Aortic Aneurysms. In *Vascular Medicine: A Companion to Braunwald’s Heart Disease (Second Edition)*, pages 457–470. W.B. Saunders, Philadelphia.
- Papadacci, C., Bunting, E. A., and Konofagou, E. E. (2017). 3d Quasi-Static Ultrasound Elastography With Plane Wave In Vivo. *IEEE transactions on medical imaging*, 36(2):357–365.
- Pape, L. A., Tsai, T. T., Isselbacher, E. M., Oh, J. K., O’Gara, P. T., Evangelista, A., Fattori, R., Meinhardt, G., Trimarchi, S., Bossone, E., Suzuki, T., Cooper, J. V., Froehlich, J. B., Nienaber, C. A., and Eagle, K. A. (2007). Aortic Diameter 5.5 cm Is Not a Good Predictor of Type A Aortic Dissection: Observations From the International Registry of Acute Aortic Dissection (IRAD). *Circulation*, 116(10):1120–1127.
- Parodi, J. C., Palmaz, J. C., and Barone, H. D. (1991). Transfemoral intraluminal graft implantation for abdominal aortic aneurysms. *Annals of Vascular Surgery*, 5(6):491–499.
- Parr, A., Jayaratne, C., Buttner, P., and Golledge, J. (2011). Comparison of volume and diameter measurement in assessing small abdominal aortic aneurysm expansion examined using computed tomographic angiography. *European Journal of Radiology*, 79(1):42–47.
- Peña, J. A., Martínez, M. A., and Peña, E. (2015). Layer-specific residual deformations and uniaxial and biaxial mechanical properties of thoracic porcine aorta. *Journal of the Mechanical Behavior of Biomedical Materials*, 50:55–69.



- Perona, P. and Malik, J. (1990). Scale-space and edge detection using anisotropic diffusion. *IEEE Transactions on Pattern Analysis and Machine Intelligence*, 12(7):629–639.
- Perrin, D., Badel, P., Orgéas, L., Geindreau, C., Dumenil, A., Albertini, J.-N., and Avril, S. (2015). Patient-specific numerical simulation of stent-graft deployment: Validation on three clinical cases. *Journal of Biomechanics*, 48(10):1868–1875.
- Petterson, N. J., Disseldorp, E. M. J. v., Sambeek, M. R. H. M. v., Vosse, F. N. v. d., and Lopata, R. G. P. (2018). Influence of surrounding tissue on US-based 3d mechanical characterization of abdominal aortic aneurysms. *Journal of Biomechanics*, Submitted.
- Pleumeekers, H. J. C. M., Hoes, A. W., van der Does, E., van Urk, H., Hofman, A., de Jong, P. T. V. M., and Grobbee, D. E. (1995). Aneurysms of the Abdominal Aorta in Older Adults The Rotterdam Study. *American Journal of Epidemiology*, 142(12):1291–1299.
- Polzer, S. and Gasser, T. C. (2015). Biomechanical rupture risk assessment of abdominal aortic aneurysms based on a novel probabilistic rupture risk index. *Journal of the Royal Society, Interface*, 12(113):20150852.
- Polzer, S., Gasser, T. C., Bursa, J., Staffa, R., Vlachovsky, R., Man, V., and Skacel, P. (2013). Importance of material model in wall stress prediction in abdominal aortic aneurysms. *Medical Engineering & Physics*, 35(9):1282–1289.
- Polzer, S., Gasser, T. C., Swedenborg, J., and Bursa, J. (2011). The Impact of Intraluminal Thrombus Failure on the Mechanical Stress in the Wall of Abdominal Aortic Aneurysms. *European Journal of Vascular and Endovascular Surgery*, 41(4):467–473.
- Powell, M. J. D. (1964). An efficient method for finding the minimum of a function of several variables without calculating derivatives. *The Computer Journal*, 7(2):155–162.
- Prinssen, M., Verhoeven, E. L., Buth, J., Cuypers, P. W., van Sambeek, M. R., Balm, R., Buskens, E., Grobbee, D. E., and Blankensteijn, J. D. (2004). A Randomized Trial Comparing Conventional and Endovascular Repair of Abdominal Aortic Aneurysms. *New England Journal of Medicine*, 351(16):1607–1618.
- Provost, J., Papadacci, C., Arango, J. E., Imbault, M., Fink, M., Gennisson, J.-L., Tanter, M., and Pernot, M. (2014). 3d ultrafast ultrasound imaging in vivo. *Physics in Medicine and Biology*, 59(19):L1–L13.
- Raaz, U., Zöllner, A. M., Schellinger, I. N., Toh, R., Nakagami, F., Brandt, M., Emrich, F. C., Kayama, Y., Eken, S., Adam, M., Maegdefessel, L., Hertel, T., Deng, A., Jagger, A., Buerke, M., Dalman, R. L., Spin, J. M., Kuhl, E., and Tsao, P. S. (2015). Segmental aortic stiffening contributes to experimental abdominal aortic aneurysm development. *Circulation*, 131(20):1783–1795.

- Raghavan, M. L., Kratzberg, J., Castro de Tolosa, E. M., Hanaoka, M. M., Walker, P., and da Silva, E. S. (2006). Regional distribution of wall thickness and failure properties of human abdominal aortic aneurysm. *Journal of Biomechanics*, 39(16):3010–3016.
- Raghavan, M. L. and Vorp, D. A. (2000). Toward a biomechanical tool to evaluate rupture potential of abdominal aortic aneurysm: identification of a finite strain constitutive model and evaluation of its applicability. *Journal of Biomechanics*, 33(4):475–482.
- Raghavan, M. L., Vorp, D. A., Federle, M. P., Makaroun, M. S., and Webster, M. W. (2000). Wall stress distribution on three-dimensionally reconstructed models of human abdominal aortic aneurysm. *Journal of Vascular Surgery*, 31(4):760–769.
- Raghavan, M. L., Webster, M. W., and Vorp, D. A. (1996). Ex vivo biomechanical behavior of abdominal aortic aneurysm: Assessment using a new mathematical model. *Annals of Biomedical Engineering*, 24(5):573–582.
- Reed, W. W., Hallett, J. W., Damiano, M. A., and Ballard, D. J. (1997). Learning from the last ultrasound. A population-based study of patients with abdominal aortic aneurysm. *Archives of Internal Medicine*, 157(18):2064–2068.
- Reimerink, J. J., van der Laan, M. J., Koelemay, M. J., Balm, R., and Legemate, D. A. (2013). Systematic review and meta-analysis of population-based mortality from ruptured abdominal aortic aneurysm. *The British Journal of Surgery*, 100(11):1405–1413.
- Renapurkar, R. D., Setser, R. M., O'Donnell, T. P., Egger, J., Lieber, M. L., Desai, M. Y., Stillman, A. E., Schoenhagen, P., and Flamm, S. D. (2012). Aortic volume as an indicator of disease progression in patients with untreated infrarenal abdominal aneurysm. *European Journal of Radiology*, 81(2):e87–93.
- Rote, G. (1991). Computing the minimum Hausdorff distance between two point sets on a line under translation. *Information Processing Letters*, 38(3):123–127.
- Rouet, L., Ardon, R., Rouet, J. M., Mory, B., Dufour, C., and Long, A. (2010). Semi-automatic abdominal aortic aneurysms geometry assessment based on 3d ultrasound. In *2010 IEEE International Ultrasonics Symposium*, pages 201–204.
- Rouet, L., Mory, B., Attia, E., Bredahl, K., Long, A., and Ardon, R. (2017). A minimally interactive and reproducible method for abdominal aortic aneurysm quantification in 3d ultrasound and computed tomography with implicit template deformations. *Computerized Medical Imaging and Graphics*, 58:75–85.
- Rylski, B., Branchetti, E., Bavaria, J. E., Vallabhajosyula, P., Szeto, W. Y., Milewski, R. K., and Desai, N. D. (2014). Modeling of predissection aortic size in acute type A dissection: More than 90% fail to meet the guidelines for elective ascending replacement. *The Journal of Thoracic and Cardiovascular Surgery*, 148(3):944–948.

- Sacks, M. S. and Chuong, C. J. (1998). Orthotropic mechanical properties of chemically treated bovine pericardium. *Annals of biomedical engineering*, 26(5):892–902.
- Schermerhorn, M. (2009). A 66-Year-Old Man With an Abdominal Aortic Aneurysm: Review of Screening and Treatment. *JAMA*, 302(18):2015–2022.
- Scott, R. A., Tisi, P. V., Ashton, H. A., and Allen, D. R. (1998). Abdominal aortic aneurysm rupture rates: a 7-year follow-up of the entire abdominal aortic aneurysm population detected by screening. *Journal of Vascular Surgery*, 28(1):124–128.
- Scott, R. A., Wilson, N. M., Ashton, H. A., and Kay, D. N. (1995). Influence of screening on the incidence of ruptured abdominal aortic aneurysm: 5-year results of a randomized controlled study. *The British Journal of Surgery*, 82(8):1066–1070.
- Si, H. (2015). Tetgen, a delaunay-based quality tetrahedral mesh generator. *ACM Transactions on Mathematical Software*, 41(2):11:1–11:36.
- Sidloff, D., Stather, P., Dattani, N., Bown, M., Thompson, J., Sayers, R., and Choke, E. (2014). Aneurysm Global Epidemiology Study: Public Health Measures Can Further Reduce Abdominal Aortic Aneurysm Mortality. *Circulation*, 129(7):747–753.
- Singh, K., Bønaa, K. H., Jacobsen, B. K., Bjørk, L., and Solberg, S. (2001). Prevalence of and risk factors for abdominal aortic aneurysms in a population-based study : The Tromsø Study. *American Journal of Epidemiology*, 154(3):236–244.
- Sokolis, D. P., Kritharis, E. P., Giagini, A. T., Lampropoulos, K. M., Papadodima, S. A., and Iliopoulos, D. C. (2012). Biomechanical response of ascending thoracic aortic aneurysms: association with structural remodelling. *Computer Methods in Biomechanics and Biomedical Engineering*, 15(3):231–248.
- Sonesson, B., Sandgren, T., and Länne, T. (1999). Abdominal Aortic Aneurysm Wall Mechanics and their Relation to Risk of Rupture. *European Journal of Vascular and Endovascular Surgery*, 18(6):487–493.
- Speelman, L., Bohra, A., Bosboom, E. M. H., Schurink, G. W. H., van de Vosse, F. N., Makaorun, M. S., and Vorp, D. A. (2007). Effects of wall calcifications in patient-specific wall stress analyses of abdominal aortic aneurysms. *Journal of Biomechanical Engineering*, 129(1):105–109.
- Speelman, L., Bosboom, E. M. H., Schurink, G. W. H., Hellenthal, F. A. M. V. I., Buth, J., Breeuwer, M., Jacobs, M. J., and van de Vosse, F. N. (2008). Patient-Specific AAA Wall Stress Analysis: 99-Percentile Versus Peak Stress. *European Journal of Vascular and Endovascular Surgery*, 36(6):668–676.

- Speelman, L., Hellenthal, F. A., Pulinx, B., Bosboom, E. M. H., Breeuwer, M., van Sambeek, M. R., van de Vosse, F. N., Jacobs, M. J., Wodzig, W. K. W. H., and Schurink, G. W. H. (2010). The influence of wall stress on AAA growth and biomarkers. *European journal of vascular and endovascular surgery : the official journal of the European Society for Vascular Surgery*, 39(4):410–416.
- Stemper, B. D., Yoganandan, N., Stineman, M. R., Gennarelli, T. A., Baisden, J. L., and Pintar, F. A. (2007). Mechanics of Fresh, Refrigerated, and Frozen Arterial Tissue. *Journal of Surgical Research*, 139(2):236–242.
- Stevens, R. R. F., Grytsan, A., Biasetti, J., Roy, J., Lindquist Liljeqvist, M., and Gasser, T. C. (2017). Biomechanical changes during abdominal aortic aneurysm growth. *PloS One*, 12(11).
- Stringfellow, M. M., Lawrence, P. F., and Stringfellow, R. G. (1987). The influence of aorta-aneurysm geometry upon stress in the aneurysm wall. *Journal of Surgical Research*, 42(4):425–433.
- The UK Small Aneurysm Trial Participants (1998). Mortality results for randomised controlled trial of early elective surgery or ultrasonographic surveillance for small abdominal aortic aneurysms. *The Lancet*, 352(9141):1649–1655.
- The United Kingdom EVAR Trial Investigators (2010). Endovascular versus Open Repair of Abdominal Aortic Aneurysm. *New England Journal of Medicine*, 362(20):1863–1871.
- Thubrikar, M. J., Labrosse, M., Robicsek, F., Al-Soudi, J., and Fowler, B. (2001). Mechanical properties of abdominal aortic aneurysm wall. *Journal of Medical Engineering & Technology*, 25(4):133–142.
- Thubrikar, M. J., Robicsek, F., Labrosse, M., Chervenkov, V., and Fowler, B. L. (2003). Effect of thrombus on abdominal aortic aneurysm wall dilation and stress. *The Journal of Cardiovascular Surgery*, 44(1):67–77.
- Thunes, J. R., Phillippi, J. A., Gleason, T. G., Vorp, D. A., and Maiti, S. (2018). Structural modeling reveals microstructure-strength relationship for human ascending thoracic aorta. *Journal of Biomechanics*, 71:84–93.
- Tong, J., Cohnert, T., Regitnig, P., and Holzzapfel, G. A. (2011). Effects of Age on the Elastic Properties of the Intraluminal Thrombus and the Thrombus-covered Wall in Abdominal Aortic Aneurysms: Biaxial Extension Behaviour and Material Modelling. *European Journal of Vascular and Endovascular Surgery*, 42(2):207–219.
- Tong, J., Schriefl, A. J., Cohnert, T., and Holzzapfel, G. A. (2013). Gender differences in biomechanical properties, thrombus age, mass fraction and clinical factors of abdominal

- aortic aneurysms. *European Journal of Vascular and Endovascular Surgery: The Official Journal of the European Society for Vascular Surgery*, 45(4):364–372.
- Trabelsi, O., Davis, F. M., Rodriguez-Matas, J. F., Duprey, A., and Avril, S. (2015). Patient specific stress and rupture analysis of ascending thoracic aneurysms. *Journal of Biomechanics*, 48(10):1836–1843.
- Truijers, M., Pol, J. A., Schultzekool, L. J., van Sterkenburg, S. M., Fillinger, M. F., and Blankensteijn, J. D. (2007). Wall stress analysis in small asymptomatic, symptomatic and ruptured abdominal aortic aneurysms. *European Journal of Vascular and Endovascular Surgery*, 33(4):401–407.
- Valentine, R. J., DeCaprio, J. D., Castillo, J. M., Modrall, J. G., Jackson, M. R., and Clagett, G. P. (2000). Watchful waiting in cases of small abdominal aortic aneurysms— appropriate for all patients? *Journal of Vascular Surgery*, 32(3):441–450.
- van Disseldorp, E. M. J., Hobelman, K. H., Petterson, N. J., van de Vosse, F. N., van Sambeek, M. R. H. M., and Lopata, R. G. P. (2016a). Influence of limited field-of-view on wall stress analysis in abdominal aortic aneurysms. *Journal of Biomechanics*, 49(12):2405–2412.
- van Disseldorp, E. M. J., Petterson, N. J., Rutten, M. C. M., van de Vosse, F. N., van Sambeek, M. R. H. M., and Lopata, R. G. P. (2016b). Patient Specific Wall Stress Analysis and Mechanical Characterization of Abdominal Aortic Aneurysms Using 4d Ultrasound. *European Journal of Vascular and Endovascular Surgery*, 52(5):635–642.
- van Disseldorp, E. M. J., Petterson, N. J., van de Vosse, F. N., van Sambeek, M. R. H. M., and Lopata, R. G. P. (2018). Quantification of aortic stiffness and wall stress in healthy volunteers and abdominal aortic aneurysm patients using time-resolved 3d ultrasound: a comparison study. *European Heart Journal Cardiovascular Imaging*.
- van 't Veer, M., Buth, J., Merckx, M., Tonino, P., van den Bosch, H., Pijls, N., and van de Vosse, F. (2008). Biomechanical properties of abdominal aortic aneurysms assessed by simultaneously measured pressure and volume changes in humans. *Journal of Vascular Surgery*, 48(6):1401–1407.
- Vande Geest, J. P., Di Martino, E. S., Bohra, A., Makaroun, M. S., and Vorp, D. A. (2006a). A biomechanics-based rupture potential index for abdominal aortic aneurysm risk assessment: demonstrative application. *Annals of the New York Academy of Sciences*, 1085:11–21.
- Vande Geest, J. P., Sacks, M. S., and Vorp, D. A. (2006b). The effects of aneurysm on the biaxial mechanical behavior of human abdominal aorta. *Journal of Biomechanics*, 39(7):1324–1334.

- Vappou, J., Luo, J., and Konofagou, E. E. (2010). Pulse Wave Imaging for Noninvasive and Quantitative Measurement of Arterial Stiffness In Vivo. *American Journal of Hypertension*, 23(4):393–398.
- Venkatasubramaniam, A. K., Fagan, M. J., Mehta, T., Mylankal, K. J., Ray, B., Kuhan, G., Chetter, I. C., and McCollum, P. T. (2004). A Comparative Study of Aortic Wall Stress Using Finite Element Analysis for Ruptured and Non-ruptured Abdominal Aortic Aneurysms. *European Journal of Vascular and Endovascular Surgery*, 28(2):168–176.
- Vidakovic, R., Feringa, H. H. H., Kuiper, R. J., Karagiannis, S. E., Schouten, O., Dunkelgrun, M., Hoeks, S. E., Bom, N., Bax, J. J., Neskovic, A. N., and Poldermans, D. (2007). Comparison With Computed Tomography of Two Ultrasound Devices for Diagnosis of Abdominal Aortic Aneurysm. *The American Journal of Cardiology*, 100(12):1786–1791.
- Vidakovic, R., Schouten, O., Feringa, H. H. H., Dunkelgrun, M., Karagiannis, S. E., Merks, E., Bosch, J., Bom, N., Neskovic, A. N., Bax, J. J., and Poldermans, D. (2006). Abdominal Aortic Aneurysm Screening Using Non-imaging Hand-held Ultrasound Volume Scanner – A Pilot Study. *European Journal of Vascular and Endovascular Surgery*, 32(6):615–619.
- Volodos, N. L., Karpovich, I. P., Troyan, V. I., Kalashnikova YuV, n., Shekhanin, V. E., Ternyuk, N. E., Neoneta, A. S., Ustinov, N. I., and Yakovenko, L. F. (1991). Clinical experience of the use of self-fixing synthetic prostheses for remote endoprosthetics of the thoracic and the abdominal aorta and iliac arteries through the femoral artery and as intraoperative endoprosthesis for aorta reconstruction. *VASA. Supplementum*, 33:93–95.
- Volokh, K. Y. and Aboudi, J. (2016). Aneurysm strength can decrease under calcification. *Journal of the Mechanical Behavior of Biomedical Materials*, 57:164–174.
- Vorp, D. A. (2007). Biomechanics of abdominal aortic aneurysm. *Journal of Biomechanics*, 40(9):1887–1902.
- Vorp, D. A., Lee, P. C., Wang, D. H., Makaroun, M. S., Nemoto, E. M., Ogawa, S., and Webster, M. W. (2001). Association of intraluminal thrombus in abdominal aortic aneurysm with local hypoxia and wall weakening. *Journal of Vascular Surgery*, 34(2):291–299.
- Vorp, D. A., Raghavan, M., and Webster, M. W. (1998). Mechanical wall stress in abdominal aortic aneurysm: Influence of diameter and asymmetry. *Journal of Vascular Surgery*, 27(4):632–639.
- Wilson, K., Bradbury, A., Whyman, M., Hoskins, P., Lee, A., Fowkes, G., McCollum, P., and Vaughan Ruckley, C. (1998). Relationship between abdominal aortic aneurysm wall compliance and clinical outcome: a preliminary analysis. *European Journal of Vascular and Endovascular Surgery*, 15(6):472–477.

- Wilson, K., MacCallum, H., Wilkinson, I. B., Hoskins, P. R., Lee, A. J., and Bradbury, A. W. (2001). Comparison of Brachial Artery Pressure and Derived Central Pressure in the Measurement of Abdominal Aortic Aneurysm Distensibility. *European Journal of Vascular and Endovascular Surgery*, 22(4):355–360.
- Wilson, K. A., Hoskins, P. R., Lee, A. J., Fowkes, F. G., Ruckley, C. V., and Bradbury, A. W. (2000). Ultrasonic measurement of abdominal aortic aneurysm wall compliance: a reproducibility study. *Journal of Vascular Surgery*, 31(3):507–513.
- Wilson, K. A., Lee, A. J., Lee, A. J., Hoskins, P. R., Fowkes, F. G. R., Ruckley, C. V., and Bradbury, A. W. (2003). The relationship between aortic wall distensibility and rupture of infrarenal abdominal aortic aneurysm. *Journal of Vascular Surgery*, 37(1):112–117.
- Wittek, A., Derwich, W., Karatolios, K., Fritzen, C. P., Vogt, S., Schmitz-Rixen, T., and Blase, C. (2016). A finite element updating approach for identification of the anisotropic hyperelastic properties of normal and diseased aortic walls from 4d ultrasound strain imaging. *Journal of the Mechanical Behavior of Biomedical Materials*, 58(Supplement C):122–138.
- Wittek, A., Karatolios, K., Bihari, P., Schmitz-Rixen, T., Moosdorf, R., Vogt, S., and Blase, C. (2013). In vivo determination of elastic properties of the human aorta based on 4d ultrasound data. *Journal of the Mechanical Behavior of Biomedical Materials*, 27:167–183.
- Xu, C. and Prince, J. L. (1997). Gradient vector flow: a new external force for snakes. In *Proceedings of IEEE Computer Society Conference on Computer Vision and Pattern Recognition*, pages 66–71.
- Yeoh, O. H. (1993). Some Forms of the Strain Energy Function for Rubber. *Rubber Chemistry and Technology*, 66(5):754–771.

# Dankwoord

Op de voorkant van dit proefschrift staat slechts één naam, maar dit proefschrift is tot stand gekomen dankzij de bijdrage en steun van veel verschillende mensen. Daarom zou ik in dit dankwoord graag een aantal mensen willen bedanken.

Allereerst gaat mijn dank uit mijn beide promotoren, prof. dr. **Marc van Sambeek** en prof. dr. ir. **Frans van de Vosse**, en mijn co-promotor dr. ir. **Richard Lopata**. Ik heb jullie begeleiding vanuit verschillende invalshoeken altijd ontzettend gewaardeerd en dit zorgde ervoor dat ik de afgelopen 4 jaar met veel plezier aan mijn promotieonderzoek heb gewerkt. Beste **Marc**, bedankt voor het vertrouwen dat je in me had en de vrijheid waarmee jij mij onderzoek liet doen binnen het ziekenhuis en de TU/e. Jouw klinische en kritische blik hebben mij geholpen om dit mooie resultaat te bereiken en om nooit de klinische relevantie uit het oog te verliezen.

Beste **Frans**, ondanks dat we elkaar niet heel frequent spraken, was jouw bijdrage altijd ontzettend waardevol. Ik ben blij dat ik mijn promotie bij jou in de CVB groep kon doen en kijk met veel plezier terug op onze jaarlijkse groepsuitjes.

Beste **Richard**, het is inmiddels 7 jaar geleden dat ik bij jou binnenliep als bachelor student op zoek naar een interessant maar vooral veelzijdig bachelor project. Dankzij jouw enthousiasme en begeleiding ben ik nooit meer weggegaan en daar heb ik geen seconde spijt van gehad. Jij hebt mij in de afgelopen jaren gevormd van bachelor student naar volwaardig wetenschapper, en daar ben ik je ontzettend dankbaar voor! Daarnaast heb ik altijd genoten van de gezelligheid binnen de PULS/e groep en de congresreizen. Of we nu aan de kippensoep zaten in Taiwan, aan het barbecueën waren in de PULS/e villa in Tours, of gewoon even één biertje gingen pakken tijdens de donderdagmiddag borrel, er was naast werk altijd tijd voor ontspanning. Ik kijk hier met heel veel plezier op terug en ik hoop dat we dit in de toekomst nog steeds kunnen blijven doen.

I would like to thank the members of the defense committee, prof. dr. **Christian Gasser**, prof. dr. ir. **Patrick Segers**, prof. dr. **Jan Blankensteijn**, and prof. dr. ir. **Marc Geers** for reviewing my dissertation and participating in the defense ceremony.



Veel dank ben ik verschuldigd aan de vaatlaboranten van het Catharina Ziekenhuis voor het belangeloos maken van de vele honderden echo's voor mijn promotie. Beste **Anja, Jolien, Lisanne, Olga** en **Yvonne**, zonder jullie hulp was het nooit mogelijk geweest om zoveel patiënten voor een lange tijd te volgen. Daarnaast heb ik jullie interesse in mijn onderzoek altijd ontzettend gewaardeerd. Bedankt hiervoor!

Ik wil graag alle mensen van de vaatclub binnen het Catharina Ziekenhuis bedanken. Als onderzoeker vanuit de TU/e voelde ik me direct thuis bij jullie in de groep en vond ik het interessant maar vooral ook erg leuk om een keer mee te gaan naar de Vaatdagen. In het bijzonder wil ik graag bedanken: prof. dr. **Joep Teijink** en dr. **Philippe Cuypers** voor jullie medewerking aan mijn onderzoek, en **Nicole Verhofstad** voor al je hulp bij het opstellen van verschillende onderzoeksprotocollen. Daarnaast wil ik graag alle **collega onderzoekers** uit de onderzoekskelder en later de onderzoekszolder bedanken voor het uitleggen van de vele klinische termen, maar vooral ook voor de gezelligheid tijdens het werk.

Ik waardeer het enorm dat ik de afgelopen jaren nauw heb kunnen samenwerken op dit aneurysmaproject met vriend en collega **Niels Petterson**. Beste Niels, of eigenlijk moet ik zeggen: beste PetterMesh<sup>®</sup>, behalve met veel plezier, hebben we de afgelopen jaren ook goed kunnen samenwerken. Jouw systematische aanpak en analytische skills zorgde ervoor dat complexe problemen eigenlijk geen problemen waren, maar meer gezien moesten worden als uitdagingen. Bedankt voor al je hulp en goede ideeën. Ik weet zeker dat jij over een jaar ook met een mooi proefschrift in je handen zal staan!

Tijdens mijn promotie heb ik verschillende bachelor en master studenten mogen begeleiden. Ik wil jullie allemaal bedanken voor jullie interesse, ideeën en bijdrage aan dit onderzoek. In het bijzonder wil ik de masterstudenten **Julia, Paul** en **Marcel** bedanken. Mede dankzij jullie hulp zijn drie hoofdstukken uit dit proefschrift tot stand gekomen. Inmiddels zijn jullie alle drie al aan een toffe baan begonnen en hopelijk komen we elkaar snel nog eens tegen.

Naast werken aan dit proefschrift was er de afgelopen jaren ook genoeg tijd voor plezier en ontspanning. Dit is ontzettend belangrijk om daarna weer met frisse moed aan het werk te gaan. Ik kan er niet omheen om dan allereerst mijn kantoorgenoten uit kamer 4.11 op de TU/e te bedanken. Beste **Eline, Janine, Jibbe, Joerik, Kujtim, Louis, Louise, Maarten, Marloes, Nicole, Niels, Rob, Roel, Stefan** en **Ümit**, ik heb ontzettend genoten van het plezier en de gezelligheid die wij hadden in het kantoor! De humor en grappen die vaak op het randje van toelaatbaar waren (en soms misschien een beetje erover), de lunch gesprekken over zoveel mogelijk onzin en de gezellige kantooruitjes (die soms nog wel eens wat vertraging opliepen) zullen mij nog lang bijblijven. Echter is kantoor 4.11 niet compleet zonder de mannen uit de HIR. **Kujtim** en **Niels**, waar zou het kantoor zijn

zonder deze exceptionele regio? Jullie hebben aan Joerik een waardige vervanger! Ook wil ik graag **Ashley, Laura, Mathieu, Nicole, Pim** en **Willeke** bedanken voor alle gezellige koffiekwartiertjes en leuke borrels. Ik voel me vereerd dat ik de afgelopen jaren met zoveel vrienden om me heen heb mogen werken.

Beste **Mathieu** en **Siem**, heren van de Raad van Advies, collegae ciderbrouwers, leden van HSV de Klamme Hengel, maar vandaag vooral mijn paranimfen. Fijn dat jullie vandaag aan mijn zijde willen staan. Of het nu een Bourgondische avond, jonge bokkenweekend, of een middag pattelulle in Roosendaal is, met jullie erbij wordt het altijd een feest. Laten we er vanavond ook een mooi feest van maken!

Beste middelbare school vrienden, mede Polengangers en vaste bezoekers van café Het Buitenbeentje, bedanken voor alle gezellige avonden die we tot nu toe hebben gehad. **Adriaan, Christian, Enzo, Geert, Lennart, Luc** en **Sebastiaan**, of we elkaar nu vaak of weinig zien, jullie zijn vrienden voor het leven. Ik hoop dat we nog vaak oud en nieuw in een Oost-Europese stad vieren.

Daarnaast wil ik mijn schoonfamilie bedanken. Beste **Willem, Jeanne, Jeroen, Nadja, Suzan** en **Ferry**, ik voel me thuis als ik bij jullie ben. Bedankt voor jullie oprechte interesse in mijn onderzoek en fijn dat jullie er vandaag bij zijn.

Lieve **pap** en **mam**, ik ben ontzettend blij met de onvoorwaardelijke steun en liefde die jullie mij geven. Mede dankzij jullie vertouwen in mij is dit proefschrift tot stand gekomen. Lieve **Luuk** en **Hannah** en lieve **Hannah** en **Nick**, ik ben trots dat jullie mijn (schoon)broer en (schoon)zus zijn! Bij jullie is het altijd fijn thuiskomen.

Tenslotte wil ik de belangrijkste persoon in mijn leven bedanken. Lieve **Evi**, jouw liefde en steun hebben er voor gezorgd dat dit proefschrift nu af is. Ik kijk uit om een ontzettend mooie toekomst samen met jou te beleven. Ik hou van je!

Emiel van Disseldorp  
November 2018



# Curriculum vitae

Emiel M.J. van Disseldorp was born on the 8<sup>th</sup> of July 1990, in Tilburg, the Netherlands. He grew up in Berkel-Enschot, and attended secondary school (VWO) at the Theresialyceum in Tilburg, where he graduated in 2008. In the same year he started studying Biomedical Engineering at the Eindhoven University of Technology, where he obtained his Bachelor's degree in 2012. Afterwards, he continued his Master Medical Engineering in the Cardiovascular Biomechanics Group of prof. Frans van de Vosse. During his Master's degree, he performed an internship at the New Zealand ICT Innovation Institute in Christchurch, New Zealand, where he worked on the development of a computational model to gain more insights in Alzheimer's disease. For his Master's thesis, he studied the mechanical behavior of ascending thoracic aortic aneurysms (ATAAs) using finite element analysis. This research was in close collaboration with the department of Cardiothoracic Surgery at the Catharina Hospital, and the department of Cardiovascular Connective Tissue Disease at the University Hospital Brussels. He graduated in 2014 with the distinction 'with great appreciation'.

In September 2014, he started as a PhD candidate in both the Catharina Hospital and the Eindhoven University of Technology, with the focus on mechanical characterization of abdominal aortic aneurysms (AAAs) using three dimensional ultrasound. During his PhD, he received the student award of the European Society of Biomechanics (ESB), and the young investigator award of the European Federation of Ultrasound Societies in Medicine and Biology (EFSUMB). The results of this PhD research are presented in this dissertation.



# List of publications

## Journal publications

**E.M.J. van Disseldorp**, M.H.M.H. van den Hoven, F.N. van de Vosse, M.R.H.M. van Sambeek, R.G.P. Lopata, Reproducibility Assessment of Ultrasound-Based Aortic Stiffness Quantification and Verification using Bi-axial Tensile Testing, Submitted: *Journal of Mechanical Behaviour of Biomedical Materials*, 2018;

**E.M.J. van Disseldorp**, P.P.N. Kemper, J. Nijs, M.E.S.H. Tan, F.N. van de Vosse, R.G.P. Lopata, Mechanical Characterization of Thoracic Aortic Aneurysms using 4D Ultrasound: In Vivo Findings and In Vitro Verification, Submitted: *Journal of Mechanical Behaviour of Biomedical Materials*, 2018;

N.J. Petterson, **E.M.J. van Disseldorp**, M.R.H.M. van Sambeek, F.N. van de Vosse, R.G.P. Lopata, Influence of surrounding tissue on US-based 3D mechanical characterization of abdominal aortic aneurysms, In revision: *Journal of Biomechanics*, 2018;

**E.M.J. van Disseldorp**, J.J. van Dronkelaar, J.P.W. Pluim, F.N. van de Vosse, M.R.H.M. van Sambeek, R.G.P. Lopata, Wall Stress Analysis using Multi-Perspective 3D Ultrasound Imaging of Large Abdominal Aortic Aneurysms, In revision: *European Journal of Vascular and Endovascular Surgery*, 2018;

**E.M.J. van Disseldorp**, N.J. Petterson, F.N. van de Vosse, M.R.H.M. van Sambeek, R.G.P. Lopata, Quantification of Aortic Stiffness and Wall Stress in Healthy Volunteers and Abdominal Aortic Aneurysm Patients using Time-Resolved 3D Ultrasound: a Comparison Study, In: *European Heart Journal: Cardiovascular Imaging*, 2018; [Epub ahead of print]

**E.M.J. van Disseldorp**, N.J. Petterson, M.C.M. Rutten, F.N. van de Vosse, M.R.H.M. van Sambeek, R.G.P. Lopata, Patient-specific wall stress analysis and mechanical characterization of abdominal aortic aneurysms using 4D ultrasound, In: *European Journal of Vascular and Endovascular Surgery*, 2016; 52(5): pp. 636-642.

**E.M.J. van Disseldorp**, K.H. Hobelman, N.J. Petterson, F.N. van de Vosse, M.R.H.M. van Sambeek, R.G.P. Lopata, Influence of limited field-of-view on wall stress analysis in abdominal aortic aneurysms, In: *Journal of Biomechanics*, 2016; 49(12): pp. 2405-2412.

S. Quicken, W.P. Donders, **E.M.J. van Disseldorp**, K. Gashi, B.M. Mees, F.N. van de Vosse, R.G.P. Lopata, T. Delhaas, W. Huberts, Application of an Adaptive Polynomial Chaos Expansion on Computationally Expensive Three-Dimensional Cardiovascular Models for Uncertainty Quantification and Sensitivity Analysis, In: *Journal of Biomechanical Engineering*, 2016; 138(12): pp. 1-11.

L.N.M. Gommans, A.T. Smid, M.R.M. Scheltinga, F.A.M. Brooijmans, **E.M.J. van Disseldorp**, F.T.P.M. van der Linden, K. Meijer, J.A.W. Teijink, Altered joint kinematics and increased electromyographic muscle activity during walking in patients with intermittent claudication, In: *Journal of Vascular Surgery*, 2016; 63(3): pp. 664-672.

K. Dormanns, **E.M.J. van Disseldorp**, R.G. Brown, T. David, Neurovascular coupling and the influence of luminal agonists via the endothelium, In: *Journal of Theoretical Biology*, 2015; 364: pp. 49-70.

## Conference contributions

**E.M.J. van Disseldorp**, N.J. Petterson, F.N. van de Vosse, M.R.H.M. van Sambeek, and R.G.P. Lopata, Longitudinal Study of the Mechanical Properties of Abdominal Aortic Aneurysms: The First Results, *IEEE International Ultrasound Symposium*, Oct 2018, Kobe, Japan, Oral presentation.

**E.M.J. van Disseldorp**, N.J. Petterson, F.N. van de Vosse, M.R.H.M. van Sambeek, and R.G.P. Lopata, Modelling of Large Abdominal Aortic Aneurysms using Multi-Perspective 3D Ultrasound, *World Congress of Biomechanics*, July 2018, Dublin, Ireland, Poster presentation.

**E.M.J. van Disseldorp**, N.J. Petterson, F.N. van de Vosse, M.R.H.M. van Sambeek, and R.G.P. Lopata, In-vivo mechanical characterization of abdominal aortic aneurysms and healthy aortas using 4D ultrasound: A comparison study, *IEEE International Ultrasound Symposium*, Sept 2017, Washington, DC, USA, Oral presentation, rewarded with a **Travel Award**.

**E.M.J. van Disseldorp**, N.J. Petterson, F.N. van de Vosse, M.R.H.M. van Sambeek, and R.G.P. Lopata, Mechanical characterization of abdominal aortic aneurysms and Healthy Aortas using 4D ultrasound, *European Conference of Biomechanics*, June 2017, Sevilla, Spain, Oral presentation, rewarded with a **Travel Award**.

**E.M.J. van Disseldorp**, N.J. Petterson, F.N. van de Vosse, M.R.H.M. van Sambeek, and R.G.P. Lopata, Patient-specific mechanical characterization of abdominal aortic aneurysms and healthy aortas using 4D ultrasound: An in vivo comparison study, *Summer Biomechanics, Bioengineering and Biotransport Conference*, June 2017, Tucson, AZ, USA, Oral presentation.

**E.M.J. van Disseldorp**, N.J. Petterson, F.N. van de Vosse, M.R.H.M. van Sambeek, and R.G.P. Lopata, Patient-Specific Mechanical Characterization of Abdominal Aortic Aneurysms and Healthy Volunteers Using 4D Ultrasound, *Biomechanics in Vascular Biology and Cardiovascular Disease*, April 2017, Rotterdam, the Netherlands, Oral presentation.

**E.M.J. van Disseldorp**, N.J. Petterson, F.N. van de Vosse, M.R.H.M. van Sambeek, and R.G.P. Lopata, Patient-Specific Mechanical Characterization of Abdominal Aortic Aneurysms using 4D Ultrasound, *EUROSON 2016, European Federation of Societies for Ultrasound in Medicine and Biology*, Oct 2016, Leipzig, Germany, Oral presentation, rewarded with the **Young Investigator Award**.

**E.M.J. van Disseldorp**, J.J. van Dronkelaar, J.P.W. Pluim F.N. van de Vosse, M.R.H.M. van Sambeek, and R.G.P. Lopata, Automatic segmentation and registration of abdominal aortic aneurysms using 3D ultrasound, *IEEE International Ultrasound Symposium*, Sept 2016, Tours, France, Oral presentation.

P.P.N. Kemper, **E.M.J. van Disseldorp**, J. Nijs, M.E.S.H. Tan, F.N. van de Vosse, R.G.P. Lopata, Mechanical characterization of ascending thoracic aortic aneurysms using ultrasound, *IEEE International Ultrasound Symposium*, Sept 2016, Tours, France, Oral presentation.

**E.M.J. van Disseldorp**, N.J. Petterson, F.N. van de Vosse, M.C.M. Rutten, M.R.H.M. van Sambeek, and R.G.P. Lopata, Wall stress analysis and mechanical characterization of abdominal aortic aneurysms using 4D ultrasound, *European Congress of Biomechanics* July 2016, Lyon, France, Oral presentation, rewarded with the **Student Award**.

**E.M.J. van Disseldorp**, N.J. Petterson, M.C.M. Rutten, F.N. van de Vosse, M.R.H.M. van Sambeek, and R.G.P. Lopata, Wall stress analysis and mechanical characterization of abdominal aortic aneurysms using 4D ultrasound, *IEEE International Ultrasound Symposium*, Oct 2015, Taipei, Taiwan, Oral presentation.



**E.M.J. van Disseldorp**, N.J. Petterson, M.C.M. Rutten, F.N. van de Vosse, M.R.H.M. van Sambeek, and R.G.P. Lopata, Patient-specific wall stress analysis and mechanical characterization of abdominal aortic aneurysms using 4D ultrasound, *Artimino Ultrasound Conference*, June 2015, Helsingborg, Sweden, Oral presentation.

**E.M.J. van Disseldorp**, J. Nijs, M.E.S.H. Tan, F.N. van de Vosse, R.G.P. Lopata, Mechanical characterization of ascending thoracic aortic aneurysms using 4D ultrasound, *Computational Methods on Biomechanics and Biomedical Engineering*, Dec 2014, Amsterdam, the Netherlands, Oral presentation.

**E.M.J. van Disseldorp**, J. Nijs, M.E.S.H. Tan, F.N. van de Vosse, R.G.P. Lopata, Mechanical characterization of ascending thoracic aortic aneurysms using 4D ultrasound, *International Tissue Elasticity Conference*, Sept 2014, Salt Lake City, UT, USA, Oral presentation.



